UNIVERSITY OF CALIFORNIA SAN DIEGO

The *GNAQ*-oncogenic signaling network: Targeting FAK and its synthetic lethal interactome as a precision therapeutic approach against uveal melanoma

A dissertation submitted in partial satisfaction of the

requirements for the degree Doctor of Philosophy

in

Biomedical Sciences

by

Nadia Arang

Committee in charge:

Professor J. Silvio Gutkind, Chair
Professor Joan Heller Brown
Professor Tracy Handel
Professor Matthew Hangauer
Professor Alexandra Newton

2022

The Dissertation of Nadia Arang is approved, and it is acceptable in quality and form for publication on microfilm and electronically

University of California San Diego

2022

DEDICATION

This thesis is dedicated to my family, friends, and mentors throughout my academic career, for their continual support and guidance.

TABLE OF CONTENTS

LIST OF FIGURES

ACKNOWLEDGEMENTS

I am immensely grateful to my PhD advisor Dr. J. Silvio Gutkind for his mentorship, dedication, and guidance throughout my PhD to guide me towards becoming a better scientist. His strength and tenacity inspire me and all those around him to strive to make breakthrough discoveries, regardless of topic. I am also very thankful to my thesis committee, Dr. Joan Heller Brown, Dr. Tracy Handel, Dr. Matthew Hangauer, and Dr. Alexandra Newton, for their support, guidance, and advice throughout the development of my dissertation.

I am deeply thankful to the support of my friends inside and out of the BMS program for making me a better person. I look forward to the future adventures we will share and for reminiscing on the memories we've made together.

Finally, and most importantly, I am immeasurably grateful to my family, without whose support, I would not have been able to accomplish a fraction of what I did during my PhD. I am thankful every day, for their impactful presence in my life.

Chapter 1, in part, has been accepted for publication of the material in "G Protein-Coupled receptors and heterotrimeric G proteins as cancer drivers", in *FEBS Letters*, 2020. Arang, Nadia; Gutkind, J Silvio. The dissertation author was the primary investigator and author of this paper.

Chapter 2, in full, has been accepted for publication of the material in "A Platform of Synthetic Lethal Gene Interaction Networks Reveals that the GNAQ Uveal Melanoma Oncogene Controls the Hippo Pathway through FAK", in *Cancer Cell*, 2019. Feng, Xiaodong; Arang, Nadia; Rigiracciolo, Damiano Cosimo; Lee, Joo Sang; Yeerna, Huwate; Wang, Zhiyong; Lubrano, Simone; Kishore, Ayush; Pachter, Jonathan; Konig, Gabriele M; Maggiolini, Marcello; Kostenis,

Evi, Schlaepfer, David D; Tamayo, Pablo; Chen, Qianming; Ruppin, Eytan; Gutkind, J Silvio. The dissertation author was the primary investigator and author of this paper.

Chapter 3, in full, is under review for publication of the material in "Whole genome CRISPR screening identifies PI3K/AKT as a downstream component of the oncogenic GNAQ-FAK signaling circuitry" in the *Journal of Biological Sciences*. Arang, Nadia; Lubrano, Simone; Rigiracciolo, Damiano Cosimo; Nachmanson, Daniela; Mali, Prashant; Harismendy, Olivier; Gutkind, J Silvio. The dissertation author was the primary investigator and author of this paper.

Chapter 4 in full, is currently being prepared for submission for publication of the material in "High throughput chemogenetic drug screening reveals kinase-driven therapeutic vulnerabilities in *GNAQ*-mutant uveal melanoma". Arang, Nadia; Ceribelli, Michele; Rigiracciolo, Damiano Cosimo; Lubrano, Simone; Saddawi-Konefka, Robert; Wang, Zhiyong; Kim, Daewhan; Molinolo, Alfredo; Coma, Silvia; Pachter, Jon; Yang, Jing; Swaney, Danielle L; Krogan, Nevan J; Alessi, Dario; Thomas, Craig; Gutkind, J Silvio. The dissertation author was the primary investigator and author of this paper.

Chapter 5, in part, has been accepted for publication of the material in "G Protein-Coupled receptors and heterotrimeric G proteins as cancer drivers", in *FEBS Letters*, 2020. Arang, Nadia; Gutkind, J Silvio. The dissertation author was the primary investigator and author of this paper.

VITA

University of Washington
B.S. – Microbiology, 2014

University of California San Diego
Ph.D., Biomedical Sciences, 2022

FELLOWSHIPS

National Science Foundation Graduate Research Fellowship
NSF Grant number: DGE- 1650112
Funding period: (9/15/2018-6/15/2022)

UCSD Pharmacological Sciences T32
NIH Grant number: 5T32GM007752
Funding period: (7/1/2017 – 6/20/2018)

David Goeddell Endowned Fellowship
Funding period: 9/30/2016-6/30/2017

PUBLICATIONS

2022

Valentin NH, Ma N, **Arang N**, Prakash A, DiBerto JF, Knight KM, Ghosh S, Olsen RHJ, Roth BL, Gutkind JSG, Vaidehi N, Campbell SL, and Dohlman HG. Non-catalytic functions of the catalytic glutamine in G proteins. In revision.

Arang N, Lubrano S, Rigiracciolo DR, Nachmanson D, Mali P, Harismendy O, Gutkind JS. Whole genome CRISPR screening identifies PI3K/AKT as a major downstream component of the oncogenic GNAQ-FAK signaling circuitry. In revision.

Arang N, Ceribelli M, Rigiracciolo DR, Lubrano S, Saddawi-Konefka R, Kim D, Wang Z, Molinolo A, Coma S, Pachter J, Yang J, Swaney DL, Krogan NJ, Alessi D, Thomas C, Gutkind JS. High throughput chemogenetic drug screening reveals systems vulnerabilities in the druggable landscape of GNAQ-mutant uveal melanoma. In preparation.

Vijayan K, **Arang N**, Wei L, Morrison R, Geiger R, Parks KR, Lewis AJ, Mast FD, Douglass AN, Kain HS, Aitchison JD, Johnson JS, Aderem A, Kaushansky A. A Genome-wide CRISPR-Cas9 Screen Identifies Host Factors Essential for Optimal Plasmodium Liver Stage Development. *Cell Chemical Biology.* 2022 Jun 18;S2451-9456(22)00205-7. PMID: 35738280.

Rigiracciolo DC, Nohata N, Lappano R, Cirillo F, Talia M, Adame-Garcia SR, **Arang N**, Lubrano S, De Francesco EM, Belfiore A, Gutkind JS, Maggiolini M. Focal Adhesion Kinase (FAK)-Hippo/YAP transduction signaling mediates the stimulatory effects exerted by S100A8/A9-RAGE system in triple-negative breast cancer (TNBC). Journal of Experimental and Clinical Cancer Research. 2022 Jun 3;41(1):193. PMID: 35655319.

2021

Nagao RJ, Marcu R, Shin YJ, Lih D, Xue J, **Arang N**, Wei L, Akilesh S, Kaushansky A, Himmelfarb J, Zheng Y. Cyclosporine Induces Fenestra-Associated Injury in Human Renal Microvessels In Vitro. *ACS Biomaterials Science and Engineering*. 2022 Jan 10;8(1):196-207. Epub 2021 Dec 19. PMID: 34927415.

Ando T, **Arang N**, Wang Z, Costea DE, Feng X, Goto Y, Izumi H, Gilardi M, Ando K, Gutkind JS. EGFR Regulates the Hippo pathway by promoting the tyrosine phosphorylation of MOB1. *Communications Biology*. 2021 Nov 1;4(1):1237. PMID: 34725466.

Ramms DJ, Raimondi F, **Arang N**, Herberg FW, Taylor SS, Gutkind JS. Gαs-Protein Kinase A (PKA) Pathway Signalopathies: The Emerging Genetic Landscape and Therapeutic Potential of Human Diseases Driven by Aberrant Gαs-PKA Signaling. *Pharmacological Reviews*. 2021 Oct;73(4):155-197. PMID: 34663687.

Paradis J*, Acosta M*, Saddawi-Konefka R, Kishore A, Lubrano S, Gomes F, **Arang N**, Tiago M, Coma S, Wu X, Ford K, Mali P, Pachter J, Sato T, Aplin A, Gutkind JS. Synthetic Lethal Screens Reveal Co-Targeting FAK and MEK as a Multimodal Precision Therapy for GNAQ-Driven Uveal Melanoma. *Clinical Cancer Research*. 2021 Jun 1;27(11):3190-3200. PMID: 33568347.

2020

Arang N, Gutkind JS. G Protein-Coupled receptors and heterotrimeric G proteins as cancer drivers. *FEBS Letters*. 2020 Dec;594(24):4201-4232. PMID: 33270228.

Goto Y, Ando T, Izumi H, Feng X, **Arang N**, Gilardi M, Wang Z, Ando K, Gutkind JS. Muscarinic receptors promote castration-resistant growth of prostate cancer through a FAK-YAP signaling axis. Oncogene. 2020 May;39(20):4014-4027. doi: 10.1038/s41388-020-1272-x. Epub 2020 Mar 23. PMID: 32205868.

Kain H, Glennon E, Vijayan K, **Arang N**, Douglass AN, Fortin CL, Zuch M, Lewis AJ, Whiteside SL, Dudgeon DR, Johnson JS, Aderem A, Stevens KR, Kaushansky A. Liver stage malaria infection is controlled by host regulators of lipid peroxidation. *Cell Death and Differentiation,* 27,1 (2020): 44–54. PMID: 31065106.

2019

Inoue A*, Raimondi F*, Kadji FMN, Singh G, Kishi T, Uwamizu A, Ono Y, Shinjo Y, Ishida S, **Arang N**, Kawakami K, Gutkind JS, Aoki J, Russell RB. Illuminating G-Protein-Coupling Selectivity of GPCRs. *Cell*, 177,7 (2019): 1933–1947.e25. PMID: 31160049.

Bandekar SJ, **Arang N**, Tang BA, Tully ES, Barton BL, Li S, Gutkind JS, Tesmer JJG. Structure of the C-terminal Guanine Exchange Factor Module of Trio in an Autoinhibited Conformation Reveals its Oncogenic Potential. *Science Signaling* vol. 12,569 (2019): eaav2449. PMID: 30783010.

Feng X[#], **Arang N**[#], Rigiracciolo DC, Lee JS, Yeerna H, Wang Z, Lubrano S, Kishore A, Pachter J, Kostenis E, Schlaepfer DD, Tamayo P, Chen Q, Ruppin E, Gutkind JS. A Platform of Synthetic Lethal Gene Interaction Networks Reveals that the GNAQ Uveal Melanoma Oncogene Controls the Hippo Pathway through FAK. [#]***Authors contributed equally***. *Cancer Cell* vol. 35,3 (2019): 457-472.e5. PMID: 30773340.

Glennon EKK, Austin LS, **Arang N**, Kain H, Mast FD, Aitchison JD, Kappe SHI, Kaushansky A. Alterations in Phosphorylation of hepatocyte Ribosomal Protein S6 controls *Plasmodium* Liver Stage Infection. *Cell Reports* vol. 26,12 (2019): 3391-3399.e4. PMID: 30893610.

2017

Arang N, Kain H, Glennon E, Bello T, Dudgeon DR, Walter ENF, Gujral TS, Kaushansky A. Identifying host regulators and inhibitors of liver stage malaria infection using kinase activity profiles. *Nature Communications* vol. 8,1, (2017): 1232. PMID: 29089541

2015

Kaushansky A, Douglass AN, **Arang N**, Vigdorovich V, Dambrauskas N, Kain HS, Austin LS, Sather DN, Kappe SHI. Malaria parasites target the hepatocyte receptor EphA2 for successful host infection. *Science* vol. 350,6264 (2015): 1089-92. PMID: 26612952.

Douglass AN, Kain HS, Abdullahi M, **Arang N**, Austin LS, Mikolajczak SA, Billman ZP, Hume JC, Murphy SC, Kappe SHI, Kaushansky A. Host-based prophylaxis successfully targets liver stage malaria parasites. *Molecular Therapy* vol. 23,5 (2015): 857-865. PMID: 25648263.

Kaushansky A, Austin LS, Mikolajczak SA, Lo FY, Miller JL, Douglass AN, **Arang N**, Vaughan AM, Gardner MJ, Kappe SHI. Susceptibility to *Plasmodium yoelii* pre-erythrocytic infection in BALB/c sub-strains is determined at the point of hepatocyte invasion. *Infection and Immunity* vol. 83,1 (2015): 39-47. PMID: 25312960.

2014

Harupa A, Sack B, Lakshmanan V, **Arang N**, Douglass AN, Oliver B, Stuart AB, Sather DN, Lindner SE, Hybiske K, Torii M, Kappe SHI. SSP3 is a novel *Plasmodium yoelii* sporozoite surface protein with a role in gliding motility. *Infection and Immunity* vol. 82,11 (2014): 4643-53. PMID: 25156733.

ABSTRACT OF THE DISSERTATION

The GNAQ-oncogenic signaling network: Targeting FAK and its synthetic lethal interactome as a precision therapeutic approach against uveal melanoma

by

Nadia Arang

Doctor of Philosophy in Biomedical Sciences

University of California San Diego, 2022

Professor J. Silvio Gutkind Chair

Hotspot activating mutations in GNAQ/GNA11, encoding Gαq proteins, are driver oncogenes in uveal melanoma (UM), the primary cancer of the eye in adults, with limited additional aberrancies. However, there are few effective therapies available for UM and metastatic UM (mUM) patients, posing a critical need for novel therapeutic strategies against UM and mUM. Here, we have focused our efforts on dissecting Gαq-regulated signaling circuitries towards a better understanding of how Gαq promotes aberrant cell growth when activated, and to identify which Gαq-regulated signaling events can serve as actionable therapeutic targets for the treatment of UM. Using the convergence of bioinformatic, genetic and biochemical investigation, we uncovered a molecular framework poising Focal Adhesion Kinase (FAK) as a central mediator of oncogenic Gαq-regulated signaling, and as a controller of YAP through a mechanism suppressing the Hippo kinase cascade. We show that FAK inhibitors (FAKi) suppress YAP activation *in vivo* and halt UM growth, exposing a signaling vulnerability that can be targeted for UM treatment. Further interrogation into Gαq/FAK-regulated signaling mechanisms demonstrates that in addition to YAP, FAK controls PI3K/AKT signaling, and that UM cells require PI3K/AKT signaling for survival. These findings establish a novel link between Gαq-driven signaling and the stimulation of PI3K, and the aberrant activation of signaling networks underlying the growth and survival of UM. Finally, through a high-throughput, chemogenetic drug screen we profile the druggable landscape of UM and identified PKC inhibitors (PKCi) as a class targeting UM-specific vulnerabilities. Of note, we identified one compound with the highest preferential activity against UM. We investigated the mechanism of action of this compound, revealing a unique activity profile inhibiting PKC and PKC-related kinases, priming it to target cell-essential pathways that drive tumor growth in UM. Further work demonstrated that the combination of PKCi and FAKi synergistically inhibit UM growth and promote cytotoxic cell death in vitro and in preclinical xenograft and metastatic mouse models representing an exciting and highly translatable therapeutic strategy against UM. Collectively, the data presented here provides a wealth of information that can be readily translated to fill the lack of precision therapies against UM.

CHAPTER 1: Introduction—G Protein-Coupled receptors and heterotrimeric G proteins as cancer drivers

1.1 G protein and GPCRs as signal transducers

G proteins and G protein coupled receptors (GPCRs) represent the largest family of cell surface receptors, with over 800 GPCRs and 35 G protein subunits involved in transduction of diverse signaling cascades(1-3). GPCRs are characterized by a distinct 7-transmembrane domain structure with an extracellular amino terminus and an intracellular carboxyl terminus, and by their ability to couple to heterotrimeric G proteins, comprised of α, β, and γ subunits, which activate a diverse array of downstream signaling pathways(1). These receptors play key roles in many cellular and physiological functions, including in neurotransmission, cardiac response and blood pressure regulation, vision, olfaction, tissue development and immune regulation(2,4).

The human GPCR superfamily can be phylogenetically grouped into 5 subfamilies based on distinct structural features— Class A (rhodopsin), Class B1 (secretin), Class B2 (adhesion), Class C (glutamate), and Class F (frizzled/taste2)(1). Most GPCRs activate one or multiple Gα proteins, which are subdivided into 4 major families: Gαi, Gα12, Gαs, and Gαq, with each family activating a distinct repertoire of signaling mechanisms(4). GPCR activation is initiated by the binding of an agonist ligand to the extracellular domain of the receptor which induces a rapid conformational change in the extracellular and intracellular loops of the receptor(5). This transition into the active conformation of the receptor results in coupling to the heterotrimeric G proteins and triggers the exchange of GTP for GDP on the Gα subunit, promoting its dissociation from Gβγ dimers. Both Gα-GTP bound and Gβγ subunit complexes then stimulate downstream signaling cascades, including the rapid generation of multiple second messengers by modulating the activity of ion channels, phospholipases, phosphodiesterases, and adenylyl cyclases(2). These second messenger generating systems and their downstream regulated kinases cascades are

responsible for most of the rapid physiological responses elicited by GPCRs(6-12). In tandem to these processes, Regulators of G protein Signaling (RGS) proteins enhance the GTPase activity of the Gα subunit, enabling the reassociation of the Gα and Gβγ subunits into a bound heterotrimeric G protein, and returning the protein complex to a GDP-bound inactive state(5). Moreover, arrestins are recruited to activated GPCRs to promote receptor endocytosis and can participate in downstream signaling as scaffolds for signaling complexes, and as molecular rheostats of G protein-driven signal transduction(13). This model of GPCR function has been improved over the recent years to encompass various classes of ligands, including agonists, partial agonist, inverse agonists and allosteric modulators, and the detailed structure features of the corresponding GPCR conformations that can be stabilized upon binding(14).

As GPCRs and their associated G proteins are involved in a diverse array of signal transduction pathways and cellular processes, dysregulation in either can have significant impacts on cellular behaviour and the initiation of pathogenic processes. This is highlighted by large body of drugs in the market targeting GPCRs. Indeed, 34% of all FDA approved drugs currently on the market target GPCRs directly or indirectly(15-17). This chapter will summarize the growing body of information establishing GPCRs as drivers of cancer and their roles in cancer initiation and progression.

1.2 Historical perspective

The earliest evidence suggesting a role for GPCRs in tumorigenesis stems from work demonstrating that expression of a GPCR encoded by the *mas* oncogene (*MAS1* gene), had the ability to transform and induce foci formation in NIH3T3 fibroblasts, as well as develop tumors in nude mice(18). This pivotal work was novel in contrast to the many known oncogenes at the time, most of which were discovered based on the transforming activity of oncogenic viruses. These findings were reinforced by the observation that ectopic expression of the 5HT1c serotonin receptor (*HTR1C*) led to transformation of NIH3T3 cells(19). However, in both cases the receptors

did not harbour any identifiable mutations, contrasting with most viral and human oncogenes, and these observations were not widely appreciated. Subsequent studies examining the transforming potential of GPCRs led to the discovery that coupling specificity and excess ligand availability were key determinants of the oncogenic activity of wild type GPCRs. Specifically, overexpression alone of muscarinic cholinergic receptors (CHRMs), which span across Gα-coupling subtypes, was found to be insufficient to transform NIH3T3 cells. However, in the presence of the agonist carbachol foci were readily induced for Gαq-coupled CHRMs, thereby establishing that wild-type GPCRs can act as agonist-dependent oncogenes based on their G protein coupling capacity(20). The α1B-adrenergnic receptor (*ADRA1B*) was found to behave similarly by inducing neoplastic transformation when ectopically expressed in NIH3T3 cells, and triggering formation of foci in an agonist-dependent manner(21). However, mutation of this receptor eliminated agonist dependency of receptor activation, rendering it constitutively active, thus raising the possibility that mutations may be a mechanism to enhance the oncogenic potential of GPCRs.

1.3 The mutation spectrum of GPCRs in cancer

As massive advances in the field of cancer genomics have transformed our understanding of oncogenesis and drivers of cancer, GPCRs and G proteins have emerged as candidate drivers. The generation of vast cancer sequencing resources including The Cancer Genome Atlas (TCGA), and the Catalogue of Somatic Mutations in Cancer (COSMIC) have revealed that GPCRs and G proteins are collectively mutated in roughly 20% of all cancers, spanning across numerous tumor types(22-25). The biological function and consequence of many of these mutations are as of yet largely unknown, highlighting the previously underappreciated role that GPCRs and G proteins play in tumor biology. Despite this, there is emerging work underscoring the cancer relevance of mutated GPCRs. Recent cross-cancer analysis of GPCR mutation patterns in human malignancies has revealed that gastrointestinal (GI) cancers harbour the highest number of mutated GPCRs and G proteins, irrespective of the mutational load of these

cancers(26). This is coupled with the recent finding that a significant portion of mutated GPCRs couple to Gαs and Gαi/o, more specifically, an enrichment of activating mutants of Gαs-coupled receptors, and deleterious (inactivating) mutants of Gαi/o-coupled receptors(27). Together, these mutation patterns converge on the oncogenic impact of elevated adenylyl cyclase activity and production of cAMP, which is stimulated by Gαs and inhibited by Gαi/o, suggesting a prominent role for enhanced cAMP signalling in cancer. The cAMP signaling network is involved in different aspects of tumorigenesis, and these findings establish a functional link between the mutation patterns in GPCRs and their candidate role as cell-context specific oncodrivers, with emphasis on GI cancers, including colorectal, stomach, and pancreatic adenocarcinomas.

Broken down phylogenetically, the adhesion and glutamate GPCR are the first and second most highly mutated families of GPCRs in cancer; however, their role in cancer is not well defined(22). Adhesion GPCRs (aGPCRs) are named as such due to the extended extracellular N terminus containing structural domains such as thrombospondin repeats, and leucine-rich-repeats (LRRs), which participate in a variety of protein-protein interactions and can mediate adhesion to cellular matrix proteins(28). The aGPCR subfamily is widely mutated among cancer types in TCGA and a number of aGPCRs are involved in angiogenesis, metastasis, and other critical components of cancer initiation and progression(29,30) (Fig 1.1). Among them, GPR98 (*ADGRV1*) is the most frequently mutated GPCR across all cancer types. In particular *ADGRV1* is mutated in roughly 45% of skin cutaneous melanoma, and is the longest GPCR by amino acid length; however, not much is known regarding its functional impact(26). *ADGRE5*, also known as CD97, was the first aGPCR to be linked to cancer, as its expression was found to be a sensitive marker of dedifferentiation in thyroid carcinomas(31,32). While *ADGRE5* expression was nearly absent in normal thyrocytes, its levels increased in correlation with thyroid tumor stage(31,32). Its over-expression has since been identified in several other cancer types including pancreatic, gallbladder, and esophageal carcinomas, and is linked to metastatic aggressiveness in gastric,

colorectal cancers, and particularly in glioblastoma(33). Glioblastoma in particular, is known to develop extensive intratumoral hypoxia, and GPR133 (*ADGRD1*) has been implicated to be critical for glioblastoma growth under hypoxic conditions(34). Interestingly, targeting of the dopamine receptor *DRD2* has shown to be a highly promising drug target for the treatment of glioblastoma(35,36).

Glutamate receptors, which bind glutamate as their ligand have primarily been studied for their roles in the central nervous system but are becoming increasingly implicated in cancer, including squamous non-small cell lung cancer, and adenocarcinomas among others(37,38). In one case, a GPCR-targeted mutation analysis of melanomas revealed that *GPR98* (mentioned above) and *GRM3*, a metabotropic glutamate receptor, were the most frequently mutated genes(39). Expression of patient-derived *GRM3* mutants in melanoma cell lines significantly increased anchorage-independent cell proliferation, as well as cell migration *in vitro* and *in vivo* metastatic rate(39). Similarly, ectopic expression of *GRM1 and GRM5* have been found to induce spontaneous formation of melanoma in transgenic mouse models suggesting a role for GRMs in driving melanoma initiation(40-42). Other metabolite-binding GPCRs, such as the lactate and succinate-binding *GPR81* and *GPR91*, play a significant role in tumor promotion through both autocrine and paracrine mechanisms that contribute to control tumor energetic dynamics. *GPR81* has been found to be significantly upregulated in numerous cancer types and to be a crucial driver of tumor growth and metastasis with further roles modulating the tumor microenvironment in angiogenesis and immune evasion(43,44). Similarly, *GPR91* has significant roles in modulation of the tumor-immune microenvironment, as well as angiogenesis, together with its role in cellular metabolism(45-47).

One of the most prominent GPCRs implicated in neoplastic growth is the Thyroid-stimulating hormone (TSH) receptor (*TSHR*). TSHR is coupled primarily to Gαs and to a lesser extent Gαq, and is a key regulator of thyroid cell function, growth and hormone metabolism(48). Mutations in *TSHR* have been found to lead to numerous thyroid diseases, including hyper- and hypo-

thyroidism and hyperfunctioning thyroid adenomas(49). Strikingly, activating mutations in *TSHR* are the predominant cause of solitary toxic thyroid adenomas, accounting for roughly 60-80% of all cases, and in roughly 30% of thyroid adenomas among other cancers(50,51). Aligned with this, activating mutations in *GNAS* and *TSHR* are commonly found in differentiated thyroid carcinomas(50,52,53).

Another seven-transmembrane receptor frequently mutated in cancer is Smoothened (*SMO*), which drives activation of the transcription factor GLI(54,55). SMO is negatively regulated by the twelve-transmembrane receptor patched (PTCH); however, this inhibition is relieved upon binding of PTCH to hedgehog family members, including sonic hedgehog (SHH)(54). Mutations that result in the activation of the PTCH-SMO-SHH signaling axis have been found to drive sporadic basal cell carcinomas (BCCs)(56,57). As of yet, the potential role of G proteins in the signalling capacity of SMO have not been fully clarified(55). Studies have found that in some cell contexts, $G\alpha i$ and $G\alpha 12$ are involved in activation of the pathway; however, the dependency of SMO on G protein coupling for its roles in cancer initiation and progression is not well understood and requires further investigation(58-60).

The Frizzled family of seven-transmembrane receptors are also heavily involved in cancer, as transducers of the Wnt signaling cascade(61). Wnt signaling can drive the activation of several transcriptional networks, primarily β-catenin and has been described to play a role in numerous cancer types, with emphasis in colorectal cancer(61,62). Indeed, the Frizzled family of GPCRs is collectively mutated in >15% of colon adenocarcinomas in TCGA. There is mounting evidence supporting the G protein coupling of Frizzleds as a critical component of the Wnt signaling pathway(63-65). For example, inhibition of $G\alpha o$ and $G\alpha q$ has been found to disrupt Wnt-mediated stabilization of β-catenin and teratocarcinoma stem-cell differentiation(64,66). Future work will likely expand the current view of G protein regulated Wnt signaling in cancer initiation and progression

In contrast to the pro-tumorigenic role of many GPCRs, GPCR-driven signaling has in some cases, been shown to play a tumor suppressive role, highlighting the complexity and the cell-context dependency of these signaling events. This is highly aligned with tumor suppressive roles for G proteins in certain contexts as well. For example, inactivation of Gα13 signaling, either by inactivating mutations in the Gα13-coupled Sphingosine-1-phosphate receptor 2 (*S1PR2*), or in Gα13 itself have both been identified to enhance tumor progression in diffuse large B cell lymphoma(67). In another case, inactivating polymorphisms in the melanocortin 1 receptor (*MC1R*) have been found to promote melanoma through an ultraviolet radiation independent mechanism(68) (Fig 1.1). Moreover, the Kisspeptin receptor (*KISS1R*) has been widely implicated as a metastatic suppressor in numerous cancer types(69,70). Similarly, GPR68 has been found to be a metastatic suppressor in prostate cancer and was found to be significantly downregulated in metastatic tumors(71,72). Finally, *ADGRB1*-3 are silenced or mutated in numerous cancer types(25). Of note, *ADGRB1*, also known as BAI1, has been found to have potent antiangiogenic and antitumorigenic functions, particularly in brain tumors(73). Strikingly, BAI1 has been shown to prevent MDM2-mediated p53 degradation, and BAI1 loss leads to a significant decrease in p53 levels(74). The protective effect of BAI1 on p53 degradation is a remarkable illustration of the diverse roles that GPCRs can play in tumorigenesis (Fig 1.1).

Despite the large number of mutations in GPCRs across cancers, the functional consequence of most of these mutations have not been widely studied. Moreover, the contribution of increased gene length to the higher number of mutations complicates the prediction of cancer-driving mutations. Coupled with this, most of the mutations are not isolated to hotspot residues, further hindering efforts to predict their signaling and cellular impact and potential role in cancer. As a result, it has been difficult to predict which mutations in GPCRs have cancer-driving effects as compared to passenger mutations with little functional impact. Structure-function analyses of

mutations in GPCRs have begun to shed light on these observations and a new framework of the functional impact of GPCR mutations is emerging. Projection of cancer-related mutations for TSHR, for example, have revealed an accumulation of mutations clustered at the cytoplasmic tail of helix 6, suggesting that in the absence of a physical hotspot mutation, structural motif hotspots may be more prevalent manifestations of cancer-associated GPCR mutations(22). Indeed, our recent pan-cancer analysis of functional somatic mutations in gene families has demonstrated significant enrichment of mutations in a handful of highly conserved regions of GPCRs that regulate GPCR function and activation. These include mutations localized to the DRY motif, which mediates the inactive conformation of class A GPCRs, with particular emphasis on recurrent mutations in DRY arginine, in addition to the NPxxY motif, both of which are critical regulators of GPCR activation. Mutations in these positions show statistically significant mutual exclusivity between motifs, as well as with activating hotspot mutations in the Gα subunit further supporting the functional significance of these structure-based predictions(27). DRY arginine mutations are also mutually exclusive with many common mutant oncogenes that are downstream of GPCR-mediated signaling cascades, including *AKT* E17K, *PI3K* E545K and *JAK2* V617F(27). The unanticipatedly high frequency of mutations in GPCRs coupled with absence of clearly identifiable hotspot mutations highlight the complex and previously underappreciated role of GPCR signalling in cancer, which can now be clarified building on novel computational biology pipelines enabling structure-function predictions and the analysis of the impact of cancer-associated mutations in GPCRs.

1.4 Mutations in G proteins in cancer

Despite continuously emerging work on the functional impact of GPCRs in cancer, the complexity of expression and mutation patterns among cancer types remain a challenge towards their identification as cancer-specific drivers. In contrast, the presence of hotspot mutations in G

proteins have enabled them to be clearly defined as cancer drivers in specific cancer types. Here we will summarize the role of G proteins in cancer and as cancer drivers.

1.4.1 Signaling through Gαq G proteins: The GNAQ oncogenes

The Gαq family of heterotrimeric subunits, encoded by *GNAQ*, *GNA11*, *GNA14* and *GNA15*, and their coupled receptors, are responsible for transducing many of the mitogenic signals initiated by growth factors acting on GPCRs(4,75). Members of the Gαq family activate phospholipase-Cβ (*PLCB1-4*), which cleaves PIP_2 into diacyglycerol and inositol 1,4,5 triphosphate. Generation of these second messengers triggers the mobilization of cytosolic calcium and all together, elicit the activation of numerous downstream signaling events via regulated kinases and transcriptional networks(8-11). Mutation of the Gαq subunit into a GTPase defective, constitutively active conformation (Q209L and G207T) was originally modelled based on previous studies examining mutations in the *ras* oncogene(76). These Gαq mutants induced malignant transformation in NIH3T3 cells and were found to be tumorigenic in nude mice(76).

Since this original discovery, aberrant Gαq activity has been found to be involved in diverse pathological conditions including congenital hemangiomas, leptomeningeal melanocytic lesions, Sturge Weber syndrome, and recent cancer sequencing efforts revealed that activating mutations in Gαq or Gα11, predominantly at Q209, are collectively found in >90% of uveal melanoma (UM) where they act as driver oncogenes(77-81) (Fig 1.2). The Gαq family is also mutated in roughly 10% of skin cutaneous melanomas (Fig 1.2). UM is the primary cancer of the eye in adults, affecting roughly 2500 patients in the US each year(82). Nearly 5% of UM patients who lack mutation in Gαq or Gα11, possess mutually exclusive activating mutations in other levels of the Gαq pathway, including in *CYSLTR2*, a Gαq-coupled GPCR, or *PLCB4*, a downstream effector of Gαq, firmly establishing hyper-activation of the Gαq-pathway as the oncogenic driver

of UM(83,84). UM caused by mutation and hyperactivation of CYSLTR2 remains one of the most striking examples of a GPCR-driven cancer type to date(85).

Studies investigating the mechanisms by which aberrant Gαq signaling drives tumorigenesis have revealed that compared to the transient stimulation of second messengers and mitogenic kinases after canonical Gαq stimulation, mutant Gαq requires a protein-protein interaction with the Rho-specific guanine nucleotide exchange factor (GEF) TRIO in order to sustain persistent signaling(86). In *in vivo* UM models, knockdown of TRIO phenocopies reduction of Gαq expression based on cell proliferation assays, tumorigenic potential as well as activation of JNK, p38 and AP-1-mediated transcription(86). Remarkably, this signaling circuitry was independent of PLCβ, the best-known target of Gαq and led to the activation of YAP, a transcriptional co-activator regulated by the Hippo pathway. The Hippo pathway is a tumor suppressive pathway, broadly involved in cell proliferation and organ size control, and has been found to be frequently altered in cancer(87). In UM, YAP activity was demonstrated to be necessary for tumor growth and proliferation(88,89).

Mutations in Gαq/11 at residue R183, the second most commonly mutated site in *GNAQ* have been found to cause Sturge-Weber Syndrome, a neurocutaneous disorder characterized by facial port-wine stains and ipsilateral occipital leptomeningeal angiomas, and are also sometimes found in UM patients(80) (Fig 1.2, 1.3). Similar to Q209, R183 is located in the GTP-binding region of Gαq, whereby mutation interferes with the intrinsic GTPase activity and increases signaling activity; however, R183 mutants possess significantly lower signaling potential than that of Q209 mutants. Activating Gαq mutants have also been associated with congenital hemangiomas, and frequently found in a subset of other melanocytic neoplasms, including blue nevi, nevi of Ota, and primary melanocytic tumors of the central nervous system(79,81).

Gαq has also been found to play diverse roles in the immune system, where Gαq has been implicated to have a tumor suppressive role. Loss of *GNAQ* expression enhances both B and T cell proliferation *in vivo* and survival *in vitro*(91-93). Strikingly, alteration of the Gαq pathway by loss of Gαq expression or recurrent loss of function (LOF) mutations at T96S or Y101, are found in roughly 25% of natural killer/T cell lymphoma (NKTCL), a malignant and highly aggressive subtype of non-Hodgkin's lymphoma(94). Consistent with the impact of Gαq loss in other immune cells, NK-specific knockout of Gαq in mice imparted an intrinsic survival advantage of NK cells as compared to wild type NK cells. Moreover, expression of WT Gαq in Gαq-low NK cell lines promoted apoptosis, which could be ablated by concomitant expression of T96S Gαq suggesting T96S Gαq acts as a dominant negative mutant to promote NK cell tumorigenicity(94). The proclivity of R183 and Q209 hotspot mutations in Gαq to solid tumors compared to the incidence of T96 and Y101 in hematopoietic malignancies suggests a complex relationship between the oncogenic or tumor suppressive function of these mutations and the cell context in which they originate, highlighting the complex molecular events underlying Gαq-driven oncogenic signaling.

1.5 Figures

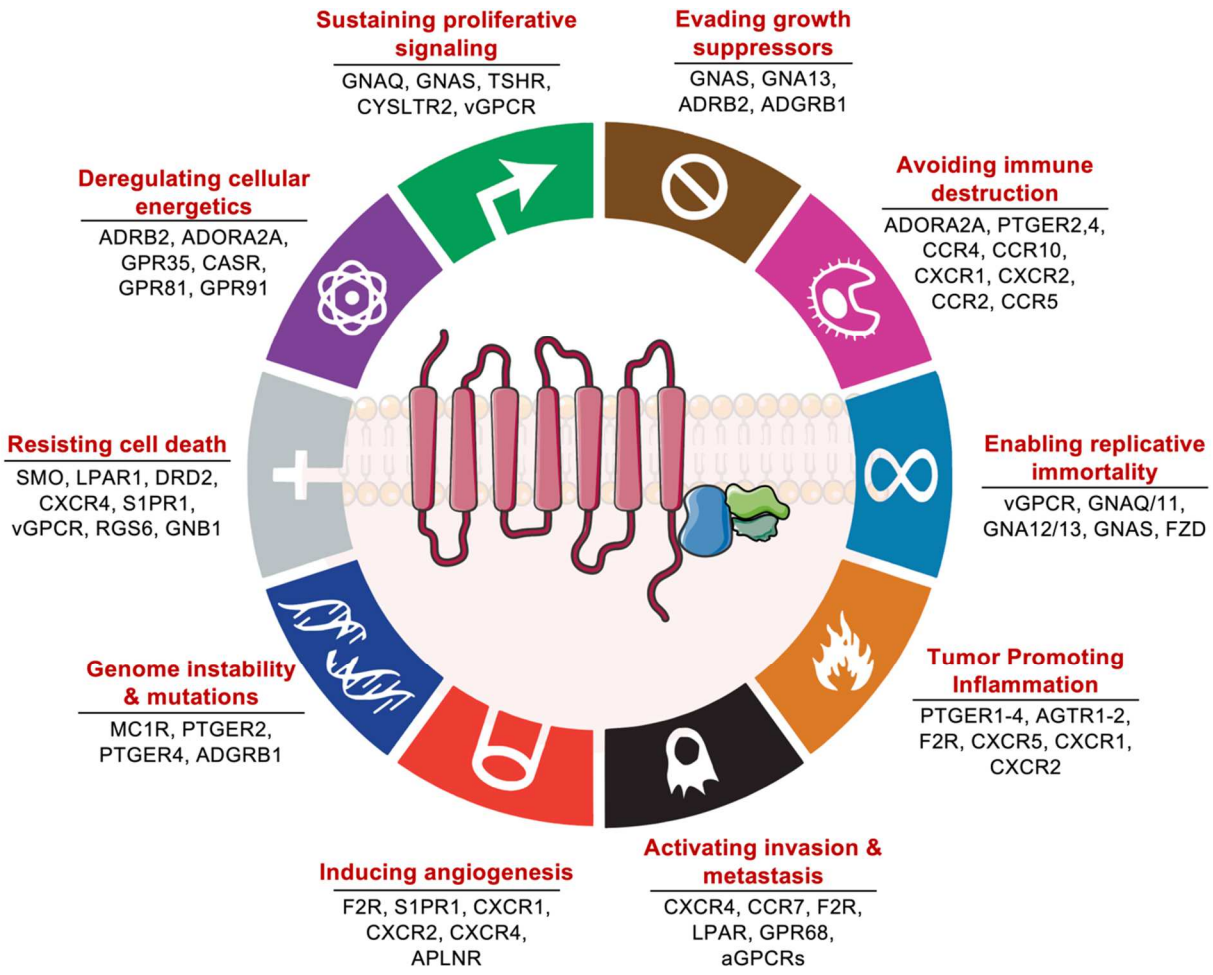

Figure 1.1 The roles of GPCRs and heterotrimeric G Proteins in the Hallmarks of Cancer

Highlighted are representative G proteins and GPCRs with well-established roles as drivers of each cancer promoting hallmark. The centrality of GPCR signalling to cellular processes within and outside the tumour microenvironment through dysregulated oncocrine signalling networks promotes the development and progression of cancer. GPCRs are in labelled in black, heterotrimeric G proteins are in blue, and signalling regulators (RGS and β-arrestin) are in purple. Refer to the text for details on each gene. Figure adapted from Hanahan and Weinberg [[22]] and modified from SMART (Servier Medical Art), licensed under a Creative Common Attribution 3.0 Generic License.

	TCGA PanCancer Atlas Studies	Abbreviation	Study size	G Protein Family Mutation Frequencies											
				Gαq (n=4)		Gα12 (n=2)		Gαs (n=2)		Gαi/o (n=8)		Gβ (n=5)		Gγ (n=12)	
				%	#	%	#	%	#	%	#	%	#	%	#
CNS	Glioblastoma multiforme	GBM	397	0.76	3	0.50	2	1.01	4	1.76	7	0.50	2	1.01	4
	Brain Lower Grade Glioma	LGG	512	0.78	4	0.00	0	0.39	2	1.37	7	0.39	2	0.20	1
Head and Neck	Head and Neck squamous cell carcinoma	HNSC	515	1.75	9	0.19	1	3.30	17	3.50	18	3.11	16	1.17	6
Endocrine	Thyroid carcinoma	THCA	490	0.00	0	0.00	0	1.22	6	0.20	1	0.00	0	0.41	2
	Adrenocortical carcinoma	ACC	91	0.00	0	0.00	0	6.59	6	2.20	2	2.20	2	0.00	0
	Pheochromocytoma and Paraganglioma	PCPG	178	0.00	0	0.00	0	0.00	0	0.00	0	0.00	0	0.00	0
	Thymoma	THYM	123	0.00	0	0.00	0	0.00	0	0.00	0	0.81	1	0.00	0
Lung	Lung adenocarcinoma	LUAD	566	1.94	11	1.24	7	4.77	27	4.77	27	2.83	16	4.06	23
	Lung squamous cell carcinoma	LUSC	484	2.27	11	1.45	7	3.10	15	5.37	26	2.69	13	1.86	9
Breast	Breast invasive carcinoma	BRCA	1066	1.22	13	0.56	6	1.03	11	1.69	18	1.03	11	0.28	3
Gastrointestinal	Esophageal carcinoma	ESCA	182	1.10	2	0.00	0	5.49	10	2.20	4	1.10	2	1.10	2
	Stomach adenocarcinoma	STAD	436	4.13	18	1.61	7	5.96	26	8.49	37	3.67	16	6.19	27
	Colon adenocarcinoma	COAD	534	5.06	27	2.06	11	5.24	28	7.68	41	5.62	30	4.31	23
	Cholangiocarcinoma	CHOL	36	2.78	1	2.78	1	0.00	0	0.00	0	0.00	0	0.00	0
	Pancreatic adenocarcinoma	PAAD	179	1.12	2	0.00	0	5.03	9	1.12	2	1.68	3	0.00	0
	Liver hepatocellular carcinoma	LIHC	366	1.09	4	1.09	4	1.64	6	3.28	12	2.19	8	0.55	2
Genito-urinary	Bladder Urothelial Carcinoma	BLCA	410	2.20	9	3.66	15	3.41	14	6.34	26	3.90	16	2.93	12
	Kidney Chromophobe	KICH	65	0.00	0	0.00	0	0.00	0	1.54	1	1.54	1	0.00	0
	Kidney renal clear cell carcinoma	KIRC	402	0.50	2	1.00	4	0.75	3	1.49	6	1.24	5	0.50	2
	Kidney renal papillary cell carcinoma	KIRP	276	0.36	1	0.72	2	1.09	3	2.90	8	0.72	2	0.72	2
Reproductive	Cervical squamous cell carcinoma and endocervical adenocarcinoma	CESC	291	3.44	10	1.37	4	4.81	14	5.50	16	3.09	9	0.69	2
	Uterine Corpus Endometrial Carcinoma	UCEC	517	8.12	42	6.00	31	9.67	50	14.12	73	8.90	46	7.35	38
	Uterine Carcinosarcoma	UCS	57	1.75	1	0.00	0	3.51	2	3.51	2	1.75	1	0.00	0
	Ovarian serous cystadenocarcinoma	OV	523	1.34	7	0.38	2	1.91	10	1.72	9	0.96	5	0.38	2
	Prostate adenocarcinoma	PRAD	494	0.20	1	0.40	2	0.20	1	1.82	9	0.81	4	0.40	2
	Testicular Germ Cell Tumors	TGCT	145	0.69	1	0.00	0	0.69	1	0.69	1	0.00	0	0.00	0
Melanoma	Skin Cutaneous Melanoma	SKCM	440	10.68	47	1.14	5	7.73	34	12.50	55	8.86	39	3.64	16
	Uveal Melanoma	UVM	80	92.50	74	0.00	0	0.00	0	0.00	0	3.75	3	0.00	0
Hematological	Diffuse Large B-cell Lymphoma	DLBC	41	0.00	0	7.32	3	0.00	0	0.00	0	0.00	0	0.00	0
	Acute Myeloid Leukemia	LAML	200	1.00	2	0.00	0	0.50	1	0.50	1	1.00	2	0.50	1
Other	Mesothelioma	MESO	86	0.00	0	0.00	0	2.33	2	1.16	1	0.00	0	1.16	1
	Sarcoma	SARC	255	0.39	1	0.00	0	1.57	4	1.96	5	0.78	2	0.39	1
		Cumulative	10437	2.90	303	1.09	114	2.93	306	3.98	415	2.46	257	1.73	181

Figure 1.2 Mutation frequencies of G protein families in patients across TCGA PanCancer Atlas studies

Frequencies (left column) and number (right column) of patients carrying a mutation in one or more G proteins in each indicated family. Cumulative mutation frequencies and absolute number of patients carrying a mutation in one or more G proteins in each indicated family across all 10,437 patients in all studies are listed in the last row. Number of G proteins considered in each family are listed with each family name. The data shown here are based upon data generated by the TCGA Research Network. All data was downloaded from cBio Portal(95,96).

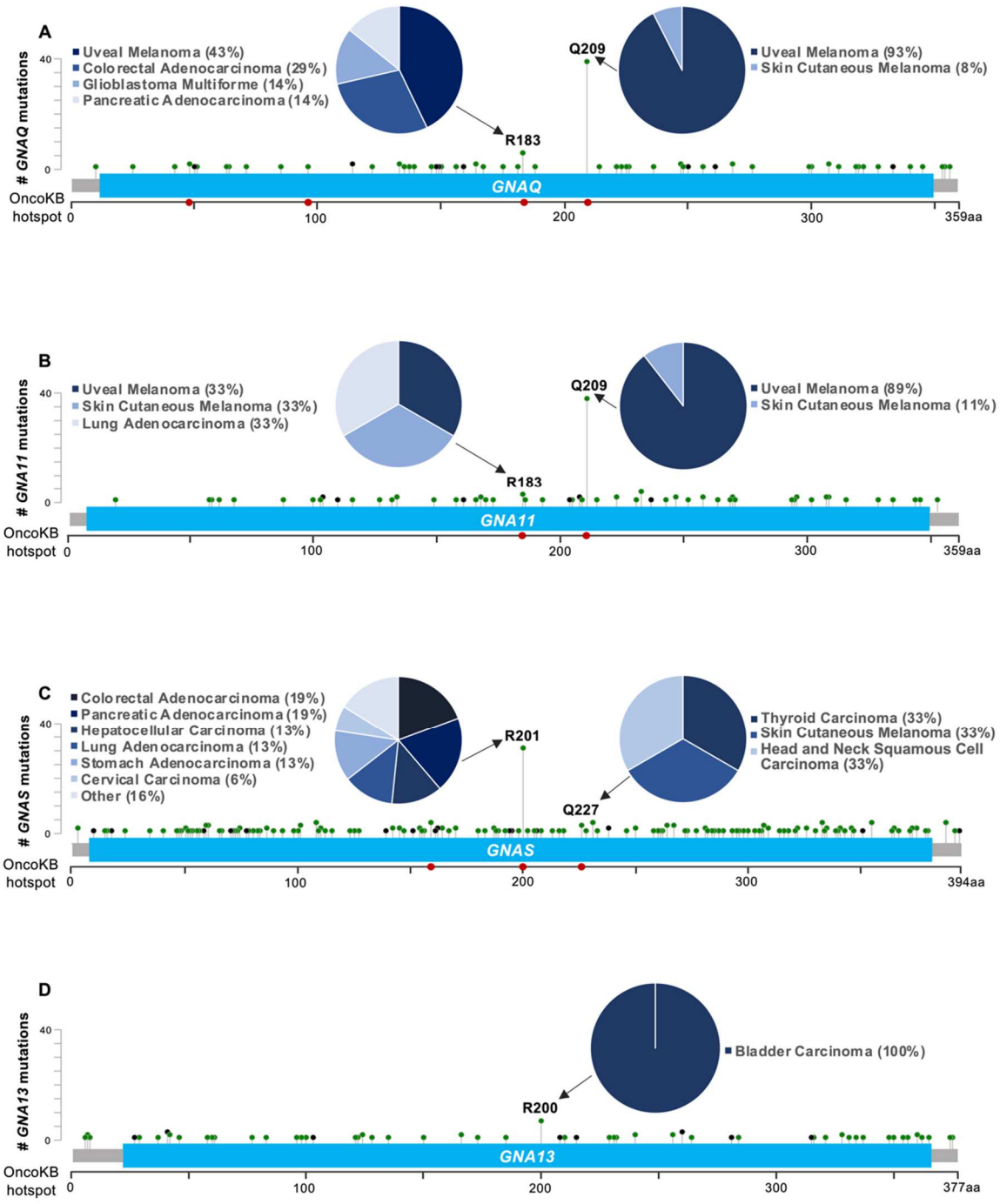

Figure 1.3 G Protein Mutation Distributions Across TCGA PanCancer Studies

Lollipop plot depicting the mutation spectrum of A) *GNAQ*, B) *GNA11*, C) *GNAS*, and D) *GNA13* across TCGA PanCancer studies. Missense mutations are depicted in green, and truncating mutations are depicted in black along the gene body. OncoKB annotated hotspot mutations are depicted in red below each gene. Pie charts represent distribution of cancer types where selected hotspots have been found. The data shown here are based upon data generated by the TCGA Research Network. All data was downloaded from cBio Portal(95,96).

1.6 Acknowledgements

Chapter 1, in part, has been accepted for publication of the material in “G Protein-Coupled receptors and heterotrimeric G proteins as cancer drivers”, in *FEBS Letters*, 2020. Arang, Nadia; Gutkind, J Silvio. The dissertation author was the primary investigator and author of this paper.

1.7 References

1. Fredriksson, R., Lagerstrom, M. C., Lundin, L. G., and Schioth, H. B. (2003) The G-protein-coupled receptors in the human genome form five main families. Phylogenetic analysis, paralogon groups, and fingerprints. *Mol Pharmacol* **63**, 1256-1272
2. Pierce, K. L., Premont, R. T., and Lefkowitz, R. J. (2002) Seven-transmembrane receptors. *Nat Rev Mol Cell Biol* **3**, 639-650
3. Milligan, G., and Kostenis, E. (2006) Heterotrimeric G-proteins: a short history. *Br J Pharmacol* **147 Suppl 1**, S46-55
4. Dorsam, R. T., and Gutkind, J. S. (2007) G-protein-coupled receptors and cancer. *Nature reviews. Cancer* **7**, 79-94
5. Rosenbaum, D. M., Rasmussen, S. G., and Kobilka, B. K. (2009) The structure and function of G-protein-coupled receptors. *Nature* **459**, 356-363
6. Sassone-Corsi, P. (2012) The cyclic AMP pathway. *Cold Spring Harbor perspectives in biology* **4**
7. Howe, A. K. (2011) Cross-talk between calcium and protein kinase A in the regulation of cell migration. *Curr Opin Cell Biol* **23**, 554-561
8. Prevarskaya, N., Skryma, R., and Shuba, Y. (2011) Calcium in tumour metastasis: new roles for known actors. *Nat Rev Cancer* **11**, 609-618
9. Griner, E. M., and Kazanietz, M. G. (2007) Protein kinase C and other diacylglycerol effectors in cancer. *Nat Rev Cancer* **7**, 281-294
10. Newton, A. C. (2010) Protein kinase C: poised to signal. *Am J Physiol Endocrinol Metab* **298**, E395-402
11. Rozengurt, E. (2007) Mitogenic signaling pathways induced by G protein-coupled receptors. *J Cell Physiol* **213**, 589-602
12. Gutkind, J. S. (1998) The pathways connecting G protein-coupled receptors to the nucleus through divergent mitogen-activated protein kinase cascades. *J Biol Chem* **273**, 1839-1842
13. Gutkind, J. S., and Kostenis, E. (2018) Arrestins as rheostats of GPCR signalling. *Nat Rev Mol Cell Biol* **19**, 615-616
14. Weis, W. I., and Kobilka, B. K. (2018) The Molecular Basis of G Protein-Coupled Receptor Activation. *Annual review of biochemistry* **87**, 897-919
15. Hauser, A. S., Chavali, S., Masuho, I., Jahn, L. J., Martemyanov, K. A., Gloriam, D. E., and Babu, M. M. (2018) Pharmacogenomics of GPCR Drug Targets. *Cell* **172**, 41-54 e19
16. Santos, R., Ursu, O., Gaulton, A., Bento, A. P., Donadi, R. S., Bologa, C. G., Karlsson, A., Al-Lazikani, B., Hersey, A., Oprea, T. I., and Overington, J. P. (2017) A comprehensive map of molecular drug targets. *Nat Rev Drug Discov* **16**, 19-34

17. Hauser, A. S., Attwood, M. M., Rask-Andersen, M., Schioth, H. B., and Gloriam, D. E. (2017) Trends in GPCR drug discovery: new agents, targets and indications. *Nat Rev Drug Discov* **16**, 829-842
18. Young, D., Waitches, G., Birchmeier, C., Fasano, O., and Wigler, M. (1986) Isolation and characterization of a new cellular oncogene encoding a protein with multiple potential transmembrane domains. *Cell* **45**, 711-719
19. Julius, D., Livelli, T. J., Jessell, T. M., and Axel, R. (1989) Ectopic expression of the serotonin 1c receptor and the triggering of malignant transformation. *Science* **244**, 1057-1062
20. Gutkind, J. S., Novotny, E. A., Brann, M. R., and Robbins, K. C. (1991) Muscarinic acetylcholine receptor subtypes as agonist-dependent oncogenes. *Proc Natl Acad Sci U S A* **88**, 4703-4707
21. Allen, L. F., Lefkowitz, R. J., Caron, M. G., and Cotecchia, S. (1991) G-protein-coupled receptor genes as protooncogenes: constitutively activating mutation of the alpha 1B-adrenergic receptor enhances mitogenesis and tumorigenicity. *Proc Natl Acad Sci U S A* **88**, 11354-11358
22. O'Hayre, M., Vazquez-Prado, J., Kufareva, I., Stawiski, E. W., Handel, T. M., Seshagiri, S., and Gutkind, J. S. (2013) The emerging mutational landscape of G proteins and G-protein-coupled receptors in cancer. *Nat Rev Cancer* **13**, 412-424
23. Cancer Genome Atlas Research, N., Weinstein, J. N., Collisson, E. A., Mills, G. B., Shaw, K. R., Ozenberger, B. A., Ellrott, K., Shmulevich, I., Sander, C., and Stuart, J. M. (2013) The Cancer Genome Atlas Pan-Cancer analysis project. *Nat Genet* **45**, 1113-1120
24. Tate, J. G., Bamford, S., Jubb, H. C., Sondka, Z., Beare, D. M., Bindal, N., Boutselakis, H., Cole, C. G., Creatore, C., Dawson, E., Fish, P., Harsha, B., Hathaway, C., Jupe, S. C., Kok, C. Y., Noble, K., Ponting, L., Ramshaw, C. C., Rye, C. E., Speedy, H. E., Stefancsik, R., Thompson, S. L., Wang, S., Ward, S., Campbell, P. J., and Forbes, S. A. (2019) COSMIC: the Catalogue Of Somatic Mutations In Cancer. *Nucleic Acids Res* **47**, D941-D947
25. Kan, Z., Jaiswal, B. S., Stinson, J., Janakiraman, V., Bhatt, D., Stern, H. M., Yue, P., Haverty, P. M., Bourgon, R., Zheng, J., Moorhead, M., Chaudhuri, S., Tomsho, L. P., Peters, B. A., Pujara, K., Cordes, S., Davis, D. P., Carlton, V. E., Yuan, W., Li, L., Wang, W., Eigenbrot, C., Kaminker, J. S., Eberhard, D. A., Waring, P., Schuster, S. C., Modrusan, Z., Zhang, Z., Stokoe, D., de Sauvage, F. J., Faham, M., and Seshagiri, S. (2010) Diverse somatic mutation patterns and pathway alterations in human cancers. *Nature* **466**, 869-873
26. Wu, V., Yeerna, H., Nohata, N., Chiou, J., Harismendy, O., Raimondi, F., Inoue, A., Russell, R. B., Tamayo, P., and Gutkind, J. S. (2019) Illuminating the Onco-GPCRome: Novel G protein-coupled receptor-driven oncocrine networks and targets for cancer immunotherapy. *J Biol Chem* **294**, 11062-11086
27. Raimondi, F., Inoue, A., Kadji, F. M. N., Shuai, N., Gonzalez, J. C., Singh, G., de la Vega, A. A., Sotillo, R., Fischer, B., Aoki, J., Gutkind, J. S., and Russell, R. B. (2019) Rare, functional, somatic variants in gene families linked to cancer genes: GPCR signaling as a paradigm. *Oncogene* **38**, 6491-6506
28. Bjarnadottir, T. K., Fredriksson, R., and Schioth, H. B. (2007) The adhesion GPCRs: a unique family of G protein-coupled receptors with important roles in both central and peripheral tissues. *Cell Mol Life Sci* **64**, 2104-2119
29. Gad, A. A., and Balenga, N. (2020) The Emerging Role of Adhesion GPCRs in Cancer. *ACS Pharmacol Transl Sci* **3**, 29-42
30. Aust, G., Zhu, D., Van Meir, E. G., and Xu, L. (2016) Adhesion GPCRs in Tumorigenesis. *Handb Exp Pharmacol* **234**, 369-396

31. Hoang-Vu, C., Bull, K., Schwarz, I., Krause, G., Schmutzler, C., Aust, G., Kohrle, J., and Dralle, H. (1999) Regulation of CD97 protein in thyroid carcinoma. *The Journal of clinical endocrinology and metabolism* **84**, 1104-1109
32. Aust, G., Eichler, W., Laue, S., Lehmann, I., Heldin, N. E., Lotz, O., Scherbaum, W. A., Dralle, H., and Hoang-Vu, C. (1997) CD97: a dedifferentiation marker in human thyroid carcinomas. *Cancer Res* **57**, 1798-1806
33. Aust, G., Steinert, M., Schutz, A., Boltze, C., Wahlbuhl, M., Hamann, J., and Wobus, M. (2002) CD97, but not its closely related EGF-TM7 family member EMR2, is expressed on gastric, pancreatic, and esophageal carcinomas. *Am J Clin Pathol* **118**, 699-707
34. Bayin, N. S., Frenster, J. D., Kane, J. R., Rubenstein, J., Modrek, A. S., Baitalmal, R., Dolgalev, I., Rudzenski, K., Scarabottolo, L., Crespi, D., Redaelli, L., Snuderl, M., Golfinos, J. G., Doyle, W., Pacione, D., Parker, E. C., Chi, A. S., Heguy, A., MacNeil, D. J., Shohdy, N., Zagzag, D., and Placantonakis, D. G. (2016) GPR133 (ADGRD1), an adhesion G-protein-coupled receptor, is necessary for glioblastoma growth. *Oncogenesis* **5**, e263
35. Arrillaga-Romany, I., Chi, A. S., Allen, J. E., Oster, W., Wen, P. Y., and Batchelor, T. T. (2017) A phase 2 study of the first imipridone ONC201, a selective DRD2 antagonist for oncology, administered every three weeks in recurrent glioblastoma. *Oncotarget* **8**, 79298-79304
36. Kline, C. L. B., Ralff, M. D., Lulla, A. R., Wagner, J. M., Abbosh, P. H., Dicker, D. T., Allen, J. E., and El-Deiry, W. S. (2018) Role of Dopamine Receptors in the Anticancer Activity of ONC201. *Neoplasia* **20**, 80-91
37. Teh, J., and Chen, S. (2012) mGlu Receptors and Cancerous Growth. *Wiley Interdiscip Rev Membr Transp Signal* **1**, 211-220
38. Stepulak, A., Luksch, H., Gebhardt, C., Uckermann, O., Marzahn, J., Sifringer, M., Rzeski, W., Staufner, C., Brocke, K. S., Turski, L., and Ikonomidou, C. (2009) Expression of glutamate receptor subunits in human cancers. *Histochem Cell Biol* **132**, 435-445
39. Prickett, T. D., Wei, X., Cardenas-Navia, I., Teer, J. K., Lin, J. C., Walia, V., Gartner, J., Jiang, J., Cherukuri, P. F., Molinolo, A., Davies, M. A., Gershenwald, J. E., Stemke-Hale, K., Rosenberg, S. A., Margulies, E. H., and Samuels, Y. (2011) Exon capture analysis of G protein-coupled receptors identifies activating mutations in GRM3 in melanoma. *Nat Genet* **43**, 1119-1126
40. Pollock, P. M., Cohen-Solal, K., Sood, R., Namkoong, J., Martino, J. J., Koganti, A., Zhu, H., Robbins, C., Makalowska, I., Shin, S. S., Marin, Y., Roberts, K. G., Yudt, L. M., Chen, A., Cheng, J., Incao, A., Pinkett, H. W., Graham, C. L., Dunn, K., Crespo-Carbone, S. M., Mackason, K. R., Ryan, K. B., Sinsimer, D., Goydos, J., Reuhl, K. R., Eckhaus, M., Meltzer, P. S., Pavan, W. J., Trent, J. M., and Chen, S. (2003) Melanoma mouse model implicates metabotropic glutamate signaling in melanocytic neoplasia. *Nat Genet* **34**, 108-112
41. Choi, K. Y., Chang, K., Pickel, J. M., Badger, J. D., 2nd, and Roche, K. W. (2011) Expression of the metabotropic glutamate receptor 5 (mGluR5) induces melanoma in transgenic mice. *Proc Natl Acad Sci U S A* **108**, 15219-15224
42. Shin, S. S., Namkoong, J., Wall, B. A., Gleason, R., Lee, H. J., and Chen, S. (2008) Oncogenic activities of metabotropic glutamate receptor 1 (Grm1) in melanocyte transformation. *Pigment Cell Melanoma Res* **21**, 368-378
43. Brown, T. P., and Ganapathy, V. (2020) Lactate/GPR81 signaling and proton motive force in cancer: Role in angiogenesis, immune escape, nutrition, and Warburg phenomenon. *Pharmacology & therapeutics* **206**, 107451
44. Roland, C. L., Arumugam, T., Deng, D., Liu, S. H., Philip, B., Gomez, S., Burns, W. R., Ramachandran, V., Wang, H., Cruz-Monserrate, Z., and Logsdon, C. D. (2014) Cell surface lactate receptor GPR81 is crucial for cancer cell survival. *Cancer Res* **74**, 5301-5310

45. Mu, X., Zhao, T., Xu, C., Shi, W., Geng, B., Shen, J., Zhang, C., Pan, J., Yang, J., Hu, S., Lv, Y., Wen, H., and You, Q. (2017) Oncometabolite succinate promotes angiogenesis by upregulating VEGF expression through GPR91-mediated STAT3 and ERK activation. *Oncotarget* **8**, 13174-13185
46. Ryan, D. G., Murphy, M. P., Frezza, C., Prag, H. A., Chouchani, E. T., O'Neill, L. A., and Mills, E. L. (2019) Coupling Krebs cycle metabolites to signalling in immunity and cancer. *Nat Metab* **1**, 16-33
47. Wu, J. Y., Huang, T. W., Hsieh, Y. T., Wang, Y. F., Yen, C. C., Lee, G. L., Yeh, C. C., Peng, Y. J., Kuo, Y. Y., Wen, H. T., Lin, H. C., Hsiao, C. W., Wu, K. K., Kung, H. J., Hsu, Y. J., and Kuo, C. C. (2020) Cancer-Derived Succinate Promotes Macrophage Polarization and Cancer Metastasis via Succinate Receptor. *Mol Cell* **77**, 213-227 e215
48. Kleinau, G., Neumann, S., Gruters, A., Krude, H., and Biebermann, H. (2013) Novel insights on thyroid-stimulating hormone receptor signal transduction. *Endocr Rev* **34**, 691-724
49. Parma, J., Duprez, L., Van Sande, J., Cochaux, P., Gervy, C., Mockel, J., Dumont, J., and Vassart, G. (1993) Somatic mutations in the thyrotropin receptor gene cause hyperfunctioning thyroid adenomas *Nature* **365**, 649-651
50. Rodien, P., Ho, S. C., Vlaeminck, V., Vassart, G., and Costagliola, S. (2003) Activating mutations of TSH receptor. *Ann Endocrinol (Paris)* **64**, 12-16
51. Kleinau, G., and Biebermann, H. (2014) Constitutive activities in the thyrotropin receptor: regulation and significance. *Adv Pharmacol* **70**, 81-119
52. Russo, D., Arturi, F., Schlumberger, M., Caillou, B., Monier, R., Filetti, S., and Suarez, H. G. (1995) Activating mutations of the TSH receptor in differentiated thyroid carcinomas. *Oncogene* **11**, 1907-1911
53. Tong, G. X., Mody, K., Wang, Z., Hamele-Bena, D., Nikiforova, M. N., and Nikiforov, Y. E. (2015) Mutations of TSHR and TP53 Genes in an Aggressive Clear Cell Follicular Carcinoma of the Thyroid. *Endocr Pathol* **26**, 315-319
54. Lee, R. T., Zhao, Z., and Ingham, P. W. (2016) Hedgehog signalling. *Development* **143**, 367-372
55. Lum, L., and Beachy, P. A. (2004) The Hedgehog response network: sensors, switches, and routers. *Science* **304**, 1755-1759
56. Iglesias-Bartolome, R., Torres, D., Marone, R., Feng, X., Martin, D., Simaan, M., Chen, M., Weinstein, L. S., Taylor, S. S., Molinolo, A. A., and Gutkind, J. S. (2015) Inactivation of a Galpha(s)-PKA tumour suppressor pathway in skin stem cells initiates basal-cell carcinogenesis. *Nature cell biology* **17**, 793-803
57. Xie, J., Murone, M., Luoh, S. M., Ryan, A., Gu, Q., Zhang, C., Bonifas, J. M., Lam, C. W., Hynes, M., Goddard, A., Rosenthal, A., Epstein, E. H., Jr., and de Sauvage, F. J. (1998) Activating Smoothened mutations in sporadic basal-cell carcinoma. *Nature* **391**, 90-92
58. Kasai, K., Takahashi, M., Osumi, N., Sinnarajah, S., Takeo, T., Ikeda, H., Kehrl, J. H., Itoh, G., and Arnheiter, H. (2004) The G12 family of heterotrimeric G proteins and Rho GTPase mediate Sonic hedgehog signalling. *Genes Cells* **9**, 49-58
59. Riobo, N. A., Saucy, B., Dilizio, C., and Manning, D. R. (2006) Activation of heterotrimeric G proteins by Smoothened. *Proc Natl Acad Sci U S A* **103**, 12607-12612
60. Villanueva, H., Visbal, A. P., Obeid, N. F., Ta, A. Q., Faruki, A. A., Wu, M. F., Hilsenbeck, S. G., Shaw, C. A., Yu, P., Plummer, N. W., Birnbaumer, L., and Lewis, M. T. (2015) An essential role for Galpha(i2) in Smoothened-stimulated epithelial cell proliferation in the mammary gland. *Science signaling* **8**, ra92
61. Nusse, R., and Clevers, H. (2017) Wnt/beta-Catenin Signaling, Disease, and Emerging Therapeutic Modalities. *Cell* **169**, 985-999
62. Segditsas, S., and Tomlinson, I. (2006) Colorectal cancer and genetic alterations in the Wnt pathway. *Oncogene* **25**, 7531-7537

63. Schulte, G., and Wright, S. C. (2018) Frizzleds as GPCRs - More Conventional Than We Thought! *Trends Pharmacol Sci* **39**, 828-842
64. Liu, X., Rubin, J. S., and Kimmel, A. R. (2005) Rapid, Wnt-induced changes in GSK3beta associations that regulate beta-catenin stabilization are mediated by Galpha proteins. *Curr Biol* **15**, 1989-1997
65. Arthofer, E., Hot, B., Petersen, J., Strakova, K., Jager, S., Grundmann, M., Kostenis, E., Gutkind, J. S., and Schulte, G. (2016) WNT Stimulation Dissociates a Frizzled 4 Inactive-State Complex with Galpha12/13. *Mol Pharmacol* **90**, 447-459
66. Liu, T., Liu, X., Wang, H., Moon, R. T., and Malbon, C. C. (1999) Activation of rat frizzled-1 promotes Wnt signaling and differentiation of mouse F9 teratocarcinoma cells via pathways that require Galpha(q) and Galpha(o) function. *J Biol Chem* **274**, 33539-33544
67. Green, J. A., Suzuki, K., Cho, B., Willison, L. D., Palmer, D., Allen, C. D., Schmidt, T. H., Xu, Y., Proia, R. L., Coughlin, S. R., and Cyster, J. G. (2011) The sphingosine 1-phosphate receptor S1P(2) maintains the homeostasis of germinal center B cells and promotes niche confinement. *Nat Immunol* **12**, 672-680
68. Mitra, D., Luo, X., Morgan, A., Wang, J., Hoang, M. P., Lo, J., Guerrero, C. R., Lennerz, J. K., Mihm, M. C., Wargo, J. A., Robinson, K. C., Devi, S. P., Vanover, J. C., D'Orazio, J. A., McMahon, M., Bosenberg, M. W., Haigis, K. M., Haber, D. A., Wang, Y., and Fisher, D. E. (2012) An ultraviolet-radiation-independent pathway to melanoma carcinogenesis in the red hair/fair skin background. *Nature* **491**, 449-453
69. Lee, J. H., Miele, M. E., Hicks, D. J., Phillips, K. K., Trent, J. M., Weissman, B. E., and Welch, D. R. (1996) KiSS-1, a novel human malignant melanoma metastasis-suppressor gene. *J Natl Cancer Inst* **88**, 1731-1737
70. Ohtaki, T., Shintani, Y., Honda, S., Matsumoto, H., Hori, A., Kanehashi, K., Terao, Y., Kumano, S., Takatsu, Y., Masuda, Y., Ishibashi, Y., Watanabe, T., Asada, M., Yamada, T., Suenaga, M., Kitada, C., Usuki, S., Kurokawa, T., Onda, H., Nishimura, O., and Fujino, M. (2001) Metastasis suppressor gene KiSS-1 encodes peptide ligand of a G-protein-coupled receptor. *Nature* **411**, 613-617
71. Singh, L. S., Berk, M., Oates, R., Zhao, Z., Tan, H., Jiang, Y., Zhou, A., Kirmani, K., Steinmetz, R., Lindner, D., and Xu, Y. (2007) Ovarian cancer G protein-coupled receptor 1, a new metastasis suppressor gene in prostate cancer. *J Natl Cancer Inst* **99**, 1313-1327
72. LaTulippe, E., Satagopan, J., Smith, A., Scher, H., Scardino, P., Reuter, V., and Gerald, W. L. (2002) Comprehensive gene expression analysis of prostate cancer reveals distinct transcriptional programs associated with metastatic disease. *Cancer Res* **62**, 4499-4506
73. Zhu, D., Hunter, S. B., Vertino, P. M., and Van Meir, E. G. (2011) Overexpression of MBD2 in glioblastoma maintains epigenetic silencing and inhibits the antiangiogenic function of the tumor suppressor gene BAI1. *Cancer Res* **71**, 5859-5870
74. Zhu, D., Osuka, S., Zhang, Z., Reichert, Z. R., Yang, L., Kanemura, Y., Jiang, Y., You, S., Zhang, H., Devi, N. S., Bhattacharya, D., Takano, S., Gillespie, G. Y., Macdonald, T., Tan, C., Nishikawa, R., Nelson, W. G., Olson, J. J., and Van Meir, E. G. (2018) BAI1 Suppresses Medulloblastoma Formation by Protecting p53 from Mdm2-Mediated Degradation. *Cancer Cell* **33**, 1004-1016 e1005
75. van Biesen, T., Luttrell, L. M., Hawes, B. E., and Lefkowitz, R. J. (1996) Mitogenic signaling via G protein-coupled receptors. *Endocr Rev* **17**, 698-714
76. Kalinec, G., Nazarali, A. J., Hermouet, S., Xu, N., and Gutkind, J. S. (1992) Mutated alpha subunit of the Gq protein induces malignant transformation in NIH 3T3 cells. *Mol Cell Biol* **12**, 4687-4693
77. Van Raamsdonk, C. D., Bezrookove, V., Green, G., Bauer, J., Gaugler, L., O'Brien, J. M., Simpson, E. M., Barsh, G. S., and Bastian, B. C. (2009) Frequent somatic mutations of GNAQ in uveal melanoma and blue naevi. *Nature* **457**, 599-602

78. Van Raamsdonk, C. D., Griewank, K. G., Crosby, M. B., Garrido, M. C., Vemula, S., Wiesner, T., Obenauf, A. C., Wackernagel, W., Green, G., Bouvier, N., Sozen, M. M., Baimukanova, G., Roy, R., Heguy, A., Dolgalev, I., Khanin, R., Busam, K., Speicher, M. R., O'Brien, J., and Bastian, B. C. (2010) Mutations in GNA11 in uveal melanoma. *The New England journal of medicine* **363**, 2191-2199
79. Ayturk, U. M., Couto, J. A., Hann, S., Mulliken, J. B., Williams, K. L., Huang, A. Y., Fishman, S. J., Boyd, T. K., Kozakewich, H. P., Bischoff, J., Greene, A. K., and Warman, M. L. (2016) Somatic Activating Mutations in GNAQ and GNA11 Are Associated with Congenital Hemangioma. *Am J Hum Genet* **98**, 789-795
80. Shirley, M. D., Tang, H., Gallione, C. J., Baugher, J. D., Frelin, L. P., Cohen, B., North, P. E., Marchuk, D. A., Comi, A. M., and Pevsner, J. (2013) Sturge-Weber syndrome and port-wine stains caused by somatic mutation in GNAQ. *The New England journal of medicine* **368**, 1971-1979
81. Kusters-Vandevelde, H. V., van Engen-van Grunsven, I. A., Kusters, B., van Dijk, M. R., Groenen, P. J., Wesseling, P., and Blokx, W. A. (2010) Improved discrimination of melanotic schwannoma from melanocytic lesions by combined morphological and GNAQ mutational analysis. *Acta Neuropathol* **120**, 755-764
82. Helgadottir, H., and Höiom, V. (2016) The genetics of uveal melanoma: current insights. in *Appl Clin Genet*. pp 147-155
83. Robertson, A. G., Shih, J., Yau, C., Gibb, E. A., Oba, J., Mungall, K. L., Hess, J. M., Uzunangelov, V., Walter, V., Danilova, L., Lichtenberg, T. M., Kucherlapati, M., Kimes, P. K., Tang, M., Penson, A., Babur, O., Akbani, R., Bristow, C. A., Hoadley, K. A., Iype, L., Chang, M. T., Network, T. R., Cherniack, A. D., Benz, C., Mills, G. B., Verhaak, R. G. W., Griewank, K. G., Felau, I., Zenklusen, J. C., Gershenwald, J. E., Schoenfield, L., Lazar, A. J., Abdel-Rahman, M. H., Roman-Roman, S., Stern, M. H., Cebulla, C. M., Williams, M. D., Jager, M. J., Coupland, S. E., Esmaeli, B., Kandoth, C., and Woodman, S. E. (2017) Integrative Analysis Identifies Four Molecular and Clinical Subsets in Uveal Melanoma. *Cancer Cell* **32**, 204-220 e215
84. Johansson, P., Aoude, L. G., Wadt, K., Glasson, W. J., Warrier, S. K., Hewitt, A. W., Kiilgaard, J. F., Heegaard, S., Isaacs, T., Franchina, M., Ingvar, C., Vermeulen, T., Whitehead, K. J., Schmidt, C. W., Palmer, J. M., Symmons, J., Gerdes, A. M., Jonsson, G., and Hayward, N. K. (2016) Deep sequencing of uveal melanoma identifies a recurrent mutation in PLCB4. *Oncotarget* **7**, 4624-4631
85. Moore, A. R., Ceraudo, E., Sher, J. J., Guan, Y., Shoushtari, A. N., Chang, M. T., Zhang, J. Q., Walczak, E. G., Kazmi, M. A., Taylor, B. S., Huber, T., Chi, P., Sakmar, T. P., and Chen, Y. (2016) Recurrent activating mutations of G-protein-coupled receptor CYSLTR2 in uveal melanoma. *Nature Genetics* **48**, 675-680
86. Vaque, J. P., Dorsam, R. T., Feng, X., Iglesias-Bartolome, R., Forsthoefel, D. J., Chen, Q., Debant, A., Seeger, M. A., Ksander, B. R., Teramoto, H., and Gutkind, J. S. (2013) A genome-wide RNAi screen reveals a Trio-regulated Rho GTPase circuitry transducing mitogenic signals initiated by G protein-coupled receptors. *Molecular cell* **49**, 94-108
87. Pan, D. (2010) The hippo signaling pathway in development and cancer. *Dev Cell* **19**, 491-505
88. Feng, X., Degese, M. S., Iglesias-Bartolome, R., Vaque, J. P., Molinolo, A. A., Rodrigues, M., Zaidi, M. R., Ksander, B. R., Merlino, G., Sodhi, A., Chen, Q., and Gutkind, J. S. (2014) Hippo-independent activation of YAP by the GNAQ uveal melanoma oncogene through a trio-regulated rho GTPase signaling circuitry. *Cancer Cell* **25**, 831-845
89. Yu, F. X., Luo, J., Mo, J. S., Liu, G., Kim, Y. C., Meng, Z., Zhao, L., Peyman, G., Ouyang, H., Jiang, W., Zhao, J., Chen, X., Zhang, L., Wang, C. Y., Bastian, B. C., Zhang, K., and Guan, K. L. (2014) Mutant Gq/11 promote uveal melanoma tumorigenesis by activating YAP. *Cancer Cell* **25**, 822-830

90. Misra, R. S., Shi, G., Moreno-Garcia, M. E., Thankappan, A., Tighe, M., Mousseau, B., Kusser, K., Becker-Herman, S., Hudkins, K. L., Dunn, R., Kehry, M. R., Migone, T. S., Marshak-Rothstein, A., Simon, M., Randall, T. D., Alpers, C. E., Liggitt, D., Rawlings, D. J., and Lund, F. E. (2010) G alpha q-containing G proteins regulate B cell selection and survival and are required to prevent B cell-dependent autoimmunity. *J Exp Med* **207**, 1775-1789
91. He, Y., Yuan, X., Li, Y., Zhong, C., Liu, Y., Qian, H., Xuan, J., Duan, L., and Shi, G. (2018) Loss of Galphaq impairs regulatory B-cell function. *Arthritis Res Ther* **20**, 186
92. Wang, D., Zhang, Y., He, Y., Li, Y., Lund, F. E., and Shi, G. (2014) The deficiency of Galphaq leads to enhanced T-cell survival. *Immunology and cell biology* **92**, 781-790
93. Li, Z., Zhang, X., Xue, W., Zhang, Y., Li, C., Song, Y., Mei, M., Lu, L., Wang, Y., Zhou, Z., Jin, M., Bian, Y., Zhang, L., Wang, X., Li, L., Li, X., Fu, X., Sun, Z., Wu, J., Nan, F., Chang, Y., Yan, J., Yu, H., Feng, X., Wang, G., Zhang, D., Fu, X., Zhang, Y., Young, K. H., Li, W., and Zhang, M. (2019) Recurrent GNAQ mutation encoding T96S in natural killer/T cell lymphoma. *Nature communications* **10**, 4209
94. Cerami, E., Gao, J., Dogrusoz, U., Gross, B. E., Sumer, S. O., Aksoy, B. A., Jacobsen, A., Byrne, C. J., Heuer, M. L., Larsson, E., Antipin, Y., Reva, B., Goldberg, A. P., Sander, C., and Schultz, N. (2012) The cBio cancer genomics portal: an open platform for exploring multidimensional cancer genomics data. *Cancer Discov* **2**, 401-404
95. Gao, J., Aksoy, B. A., Dogrusoz, U., Dresdner, G., Gross, B., Sumer, S. O., Sun, Y., Jacobsen, A., Sinha, R., Larsson, E., Cerami, E., Sander, C., and Schultz, N. (2013) Integrative analysis of complex cancer genomics and clinical profiles using the cBioPortal. *Science signaling* **6**, pl1

CHAPTER 2: A Platform of Synthetic Lethal Gene Interaction Networks Reveals that the GNAQ Uveal Melanoma Oncogene Controls the Hippo Pathway through FAK

2.1 Introduction

Recent advances in omics technologies have enabled the sequencing and characterization of cancers to an unprecedented depth, revealing mechanisms of growth and molecular drivers of disease. Bioinformatics analyses of these data have demonstrated a large heterogeneity in genetic drivers, highlighting complex biological networks towards the identification of therapeutic targets. These large-scale genomics efforts have revealed a small set of cancers that are driven by only a select number of mutational events. One such cancer, uveal melanoma (UM), is characterized by a gain of function mutations in the heterotrimeric G protein, Gαq. A hotspot mutation in *GNAQ* or in *GNA11* result in encoding constitutively active Gαq proteins rendering them as driver oncogenes in approximately 93% of UM (77,78). Another ~4% of UM harbor activating mutations in *CYSLTR2*, a Gαq-linked G protein coupled receptor (GPCR) (85) firmly establishing UM as a Gαq-driven malignancy.

Aberrant activity of G proteins and GPCRs have been frequently associated with an oncogenic state and promotion of tumorigenesis (4,22). However, the precise molecular mechanisms by which prolonged Gαq signaling controls cancer cell growth are still under investigation. We and others have previously shown that these mechanisms are in part due to unique signaling circuitries that lead to the activation of YAP, a transcriptional co-activator regulated by the Hippo pathway. In turn, YAP activation is necessary for UM growth (88,89). As a key downstream target of the tumor suppressive Hippo signaling cascade, YAP is over-activated in multiple cancers (97,98). Despite this, pharmacological targeting of YAP or the Hippo pathway has been challenging. Verteporfin, an ophthalmological drug, inhibits YAP-TEAD interaction, which is the major transcriptional factor regulated by YAP, in UM (88,89) with some anecdotal clinical success (99,100). However, the potential for verteporfin as a therapeutic has

been hindered by its high systemic toxicities after prolonged use (101,102). Currently, no effective therapeutic targets are available for UM, and no specific YAP inhibitors are currently in clinical use (97). A more complete understanding of Hippo/YAP-regulating mechanisms in cancer could identify urgently needed therapeutic opportunities to inhibit YAP-dependent tumors, including UM.

The highly distinctive and well-defined genetic landscape of UM provides a unique opportunity for the application of unbiased bioinformatics approaches to investigate the precise molecular mechanisms by which prolonged Gαq signaling controls cancer cell growth, and how these pathways can be targeted for precision therapies of Gαq-driven pathophysiologies.

2.2 Results

2.2.1 A bioinformatics pipeline identifies PTK2 as a druggable candidate synthetic lethal gene with GNAQ.

To identify the specific vulnerabilities of *GNAQ*-driven tumors, we adapted our recently established bioinformatics pipeline that Identifies clinically relevant Synthetic Lethal Interactions (termed ISLE, (103)). We denote a sample with mutations in or amplification of *GNAQ*, *GNA11*, or *CYSLTR2* as $G\alpha q^{+}$, while a sample without any of these genetic alterations as $G\alpha q^{-}$. Adapting the rationale of the ISLE pipeline to our aim here, a candidate gene was determined to be a synthetic lethal (and thus a druggable vulnerability) of $G\alpha q^{+}$ tumors if it satisfies the following four conditions (Fig 2.1A): (i) molecular condition: $G\alpha q^{+}$ tumor should differentially overexpress the candidate gene *vs* $G\alpha q^{-}$ samples, (ii) clinical condition: Overexpression of the candidate gene should be associated with poor survival of patients with $G\alpha q^{+}$ tumors, (iii) phenotypic condition: The candidate gene is significantly more essential in $G\alpha q^{+}$ than in $G\alpha q^{-}$ cell lines, (iv) druggable condition: Targeting the candidate gene products with inhibitors is significantly more

effective in Gαq$^+$ than in Gαq$^-$ cell lines, i.e. Gαq$^+$ cell lines are more sensitive to cell growth inhibition by the candidate inhibitors than Gαq$^-$ cell lines.

Our analysis therefore proceeded along four steps. First, taking advantage of the publicly available Cancer Genome Atlas (TCGA) (23) data, we extracted genes that are differentially overexpressed in Gαq$^+$ UM (>96%). Since there are not sufficient UM Gαq$^-$ samples, we used Gαq$^-$ skin cutaneous melanoma (SKCM) samples as a control. Indeed, we observed significant overlap in the overexpressed genes in Gαq$^+$ UM and Gαq$^+$ SKCM samples (hypergeometric $p<4.83\ e^{-199}$, see STAR Methods) compared to Gαq$^-$ SKCM samples, justifying the use of Gαq$^-$ SKCM samples as a control for Gαq$^+$ UM. We excluded genes overexpressed in UM compared to SKCM irrespective of Gαq status to control for cancer type-specific differential expression. Second, among the genes that pass the first filter, we identified those whose expression correlates with poor prognosis of UM patients. Third, we further selected those genes from *in vitro* functional screens that show significantly higher essentiality (or drug response) in Gαq$^+$ cancer cell lines following the standard procedure to determine cancer cell dependency (104). Lastly, we selected only those genes that are druggable, i.e. targets of known cancer drugs (Fig 2.1A). We performed cell viability assays after siRNA mediated gene inhibition, confirming the vulnerabilities of our predicted hits in Gαq$^+$ cells (Fig 2.1B). This four step Gαq$^+$ synthetic lethal (SL) identification process results in 7 predicted SL genes, which play roles in multiple biological processes, including cell growth, cell survival, lipid metabolism regulation, cell cycle control and the processing of class I MHC peptide, all of which reduced cell growth when knocked down. Among them, the top predicted gene, *PTK2*, encoding Focal Adhesion Kinase (FAK), reduced cell viability almost 60% after inhibition using *PTK2* specific siRNA knockdown (Fig 2.1B).

PTK2 is not mutated in UM, a disease that is characterized by mutations, primarily mutually-exclusive activating mutations in *GNAQ*, *GNA11* and *CYSLTR2*, and mutually exclusive mutations in genes encoding two RNA splicing factors, *EIF1AX* and *SF3B1*, or a deubiquitinase

BAP1, as depicted in (Fig 2.1C) (77,78,83,85). Instead, statistically significant gain of chromosome 8q (83), including *PTK2* and *MYC*, occurs in UM. Interestingly, *PTK2* and *MYC* are amplified in 18% of UM cases (TCGA), and 38% of UM cases also exhibit *PTK2* mRNA upregulation independent of amplification (Fig 2.1C). In total 56% of UM cases have *PTK2* gene amplification or mRNA upregulation (Fig 2.1C). Interestingly, we found that expression of *PTK2* is significantly correlated with reduced overall patient survival (Fig 2.1D). Strikingly, a pan-cancer analysis of alteration frequency of *PTK2* reveals that UM has the highest alteration frequency among all available TCGA solid tumor cohorts (Fig S2.1A). We next tested the sensitivity of five representative UM cell lines, 92.1, OMM1.3, OMM1.5, Mel270, and Mel202, all of which harbor *GNAQ* mutations, to FAK inhibition using VS-4718, an orally-bioavailable FAK inhibitor (FAKi) (105), using the SKCM cell line SK-MEK-28 (*BRAF* mutant) as a control. *In vitro*, UM cell lines demonstrate a dose-dependent sensitivity to FAK inhibition with an EC_{50} of around 1 μM (Fig 2.1E). Similar results were obtained with PF562771, a chemically distinct FAKi (Fig S2.1B). Instead, the SK-MEK-28 cell line was largely insensitive to FAKi, with an EC_{50}>10 μM for VS-4718 (Fig 2.1E). siRNA knockdown of FAK reduced cell viability in two representative UM cells nearly as potently as G□q (encoded by *GNAQ*) knock down (Fig S2.1C, D, E and F). Gαq knock down reduced the accumulation of FAK in its active, tyrosine 397 phosphorylated form (pY397-FAK) (105) (Fig S2.1D), while FAK knock down reduced total FAK and pY397-FAK protein levels, as expected (Fig S2.1E). FAKi inhibited FAK rapidly (Fig S2.1F and S2.1G), and resulted in UM apoptosis as judged by the accumulation of cleaved PARP (Fig 2.1F). We further assessed whether inhibition of FAK impacted the oncogenic potential of UM cells by measuring their clonogenic capacity in semisolid media and found that FAKi nearly abolished the colony formation ability of UM cells (Fig 2.1G). Together, these findings support that FAK may be required for *GNAQ*-driven UM cell proliferation, survival, and clonogenic growth, thereby representing a potential therapeutic target for the treatment of UM.

2.2.2 The canonical Gαq signaling pathway is dispensable but a TRIO-RhoA non-canonical signaling mechanism is evident for FAK activation.

We next sought to investigate the mechanism by which Gαq controls FAK. To understand the impact of *GNAQ* mutation on FAK activation, we express an HA-tagged activated G□q mutant, Gαq-Q209L (HA-GαqQL), observed in UM and an empty vector control in human embryonic kidney 293 (HEK293) cells. Immunoblotting against total and phosphorylated forms of FAK revealed that phosphorylation of FAK at Y397 was significantly increased after expression of GαqQL (Fig 2.2A). We next took advantage of a previously established synthetic Gαq-coupled GPCR (Gαq-DREADD) that can be activated by a synthetic ligand, Clozapine N-oxide (CNO) (86,106). We stimulated Gαq-DREADD expressing HEK293 cells with CNO over a time course and found increasingly elevated levels of pY397 FAK in response to CNO (Fig 2.2B). In UM cells, G□q knockdown by siRNA or inhibition by FR900359 (FR), a potent Gαq inhibitor (107), diminished FAK and ERK activation (Fig 2.2C and Fig S2.1D). Consistent with these data, Gαq inhibition with FR in UM cells and SKCM cells showed inhibition of cell proliferation only in UM cells (Fig 2.2D). These results support the notion that FAK acts downstream from the G□q in UM. However, it is unclear which of the multiple Gαq or Gαq coupled receptor-initiated signaling pathways are responsible for regulating FAK activation.

PLCβ-dependent second messenger activation is among the best-known downstream events stimulated by Gαq (9,108), and is considered to be the canonical Gαq signaling pathway, causing transient ERK activation (86). Inhibition of PLCβ by the use of a small-molecule PLC inhibitor (U73122) abolished the ERK activation, as we previously reported (86), but did not have an impact on the activation of FAK (Fig 2.2E). Similarly, inhibition of PKC blocked ERK activation but not FAK in UM cells (Fig 2.2F), indicating that FAK may be activated independently of PLCβ. As Gαq activation of the AP1 and YAP transcriptional programs involves the stimulation of the TRIO guanine nucleotide exchange factor (GEF) for Rho

GTPases (86,88), we next asked if this non-canonical Gαq signaling pathway is involved in FAK activation by Gαq. Knockdown of TRIO or RhoA prevented the activation of FAK by Gαq-DREADD in HEK293 cells and Gαq in UM cells (Fig 2.2G and 2.2H). In line with these findings, knockdown of Rac1 had no impact on FAK activation (Fig 2.2G). Further analysis showed that blocking actin polymerization by inhibiting ROCK or actomyosin contraction by Y-27632 (109,110) and blebbistatin (111), respectively, repressed FAK activation by Gαq-DREADD in HEK293 cells and Gαq in UM cells (Fig 2.2I and 2.2J). Together, these findings suggest that Gαq stimulates FAK independently of PLCβ and PKC, but instead through a non-canonical TRIO-dependent pathway resulting in RhoA activation and consequent cytoskeletal changes and actomyosin-initiated cell contraction and signaling (Fig 2.2K).

2.2.3 FAK inhibition represses the transcriptional activity of YAP.

FAK is at the intersection of multiple signaling pathways that promote cancer progression (105), but it is not clear which downstream targets of FAK play a critical role in UM. As an approach to identify key downstream targets of the Gαq-FAK signaling axis, we performed transcriptomic RNA-sequencing on UM cells treated with FAKi, and performed Gene Set Enrichment Analysis (GSEA) (112) to characterize the transcriptional effects of inhibiting Gαq and FAK at the pathway level using over 10,000 gene sets from the MSigDB (Molecular Signatures Database), including two sub-collections of oncogenic signatures and hallmark gene sets that we added to the database (113). In spite of this large collection of transcriptional regulated genes, only 20 oncogenic signature gene sets were significantly repressed and 5 were activated by FAKi in UM cells (Fig 2.3A and S2.2A). These include the downregulation of genes described as stimulated by KRAS and EGFR and cytokines such as IL21 and IL15, consistent with the likely role in the activation of growth promoting pathways by FAK (105). FAKi also reduced the expression of genes repressed by JAK2, p53, and BMI, suggesting that FAK inhibition may trigger a p53-response and stimulate BMI and JAK2, all of which may contribute to FAK-dependent cell growth

and warrant further investigation. One intriguing observation was that FAKi treatment resulted in a significant downregulation of YAP-signature genes (114) (Fig 2.3A-D and S2.2A and S2.2B). The involvement of Hippo/YAP signaling in cancer progression as well as previous work demonstrating the key role of YAP signaling in uveal melanoma (88,89,115) led us to pursue this specific gene signature. To validate these findings, we performed qPCR for the classical YAP-target genes *CTGF* and *CYR61* in UM cells and found significant reduction in the presence of FAKi and knockdown of FAK or Gαq (Fig 2.3E and S2.2C and S2.2D). We also found that FAKi clearly diminished YAP nuclear accumulation through quantification of anti-YAP staining and western blot analysis of nuclear and cytoplasmic cellular fractions (Fig 2.3F and 2.3G and S2.2E). We further confirmed the functional impact of FAKi and FAK knock down on YAP by performing YAP/TAZ luciferase reporter assays, and using Gαq inhibition and knock down as a control (Fig 2.3H-2.3K, see Fig S2.1D and S2.1E for knock down validation). Interestingly, inhibition of Gαq or FAK or siRNA-mediated FAK knockdown repressed YAP phosphorylation on tyrosine 357 (Y357) and increased phosphorylation on serine 127 (S127), which is one of the main repressive targets of Hippo signaling (87) (Fig 2.3I and 2.3K). We recapitulated these findings in heterologous systems, using HEK293 cells expressing Gαq-DREADD stimulated with CNO and HEK293 cells expressing GαqQL. In both cases, FAK inhibition or knockdown reduced YAP pY357 and increased pS127, and reduced mRNA levels of YAP targets and YAP activity measured by luciferase reporter assay (Fig S2.3A-E), similar to UM cells. Inhibition of SRC in UM cells had no impact on YAP activity, measured by YAP/TAZ luciferase reporter assay, and failed to promote changes in YAP phosphorylation status (Fig 2.3J and 2.3K). Together, these results suggest that Gαq and FAK regulate YAP activation in UM, and that this process is likely independent of SRC.

2.2.4 FAK regulates YAP activation through YAP tyrosine phosphorylation and inhibition of Hippo core kinases.

We sought to further investigate the impact of FAK on YAP activity and found that overexpression of FAK in HEK293 cells leads to a significant increase of YAP activity (Fig 2.4A). It is well-established that YAP activity and stability is tightly controlled by its phosphorylation on a number of residues (97,98). To define the phosphorylation state of YAP in the context of aberrant Gαq signaling, we expressed GαqQL and active FAK in HEK293 cells. Overexpression of GαqQL or FAK led to increased YAP protein level, diminished YAP pS127, and increased YAP pY357 (Fig 2.4B and 2.4C).

Regarding the changes in YAP pS127 levels, we hypothesized that FAK may also repress inhibitory signals to YAP from the Hippo pathway through direct phosphorylation on the core kinases of the Hippo pathway. In the canonical Hippo pathway, MST1/2 kinases bound to their regulatory protein SAV1 to activate the LATS1/2 kinases (collectively referred to as LATS) as part of a complex with MOB1A/B. LATS in turn phosphorylates YAP (or in certain cells TAZ) at multiple serine residues, including S127, leading to YAP inactivation by cytoplasmic retention and subsequent degradation (87,97,98). By a systematic analysis of the tyrosine phosphorylation status of each Hippo core kinase cascade component after co-transfection with FAK, we found only MOB1A to be tyrosine phosphorylated, as judged by its detection with anti-phosphotyrosine antibodies in tagged MOB1A immune precipitates (Fig 2.4D). MOB1 plays a critical regulatory role in the Hippo signaling cascade by transferring the upstream signal from the kinase complex of MST1/SAV1 to LATS (116). Consistent with our findings, scanning through large phosphoprotein databases (PhosphoSitePlus® PTM Resource), we found that Y26 on MOB1A/B is conserved among mammals, and that this particular residue is phosphorylated in numerous high-throughput phosphoproteomic datasets (n=161) (Fig S2.4A). To interrogate the functional impact of this phosphorylation on MOB1, we transfected HEK293 cells with HA-MOB1 and

performed anti-HA and anti-pY immunoprecipitation (IP) assays. We found that an anti-pY26 MOB1 antibody recognized MOB1 only when co-transfected with FAK, which was abolished upon mutation of Y26 on MOB1 to Y26F (Fig 2.4E and 2.4F), thus serving as a specificity control. We further verified that FAK was able to directly phosphorylate MOB1 on its Y26 by *in vitro* kinase reaction using purified recombinant proteins (Fig S2.4B). When exploring the consequences of this post translational modification in the assembly of Hippo kinase complexes, we found that phosphorylation on Y26-MOB1 by FAK dissociates the MOB1/LATS complex (Fig 2.4E). Strikingly, mutation of Y26 of MOB1 to Y26F rescued FAK-induced dissociation from LATS1 (Fig 2.4F) and abolished YAP activation by FAK (Fig S2.4C). Together, these data suggest that FAK regulates MOB1 Y26 phosphorylation, resulting in the dissociation of the functional MOB1/LATS complex, preventing Hippo-dependent inhibition of YAP and thereby promoting YAP activity.

2.2.5 FAK inhibition results in increased MOB1/LATS association and signaling and reduced YAP protein stability in UM.

To study the effect of FAK inhibition on the Hippo pathway in UM cells, we examined the phosphorylation status of key Hippo pathway components after treated with FAKi. We observed an increase of pS127-YAP, p909-LATS1, p1079-LATS1, a dose-dependent decrease in pY26 MOB1, and in line with our previous data, enhanced MOB1/LATS interaction (Fig 2.5A and 2.5B, and S5A). In contrast, the MOB1-Y26F mutant demonstrated constitutively strong interaction with LATS independent of FAKi treatment (Fig S2.5B and S2.5C). Expression of MOB1-Y26F in UM cells phenocopied FAKi treatment as it diminished cell proliferation that could not be further reduced by FAKi (Fig S2.5D). Of interest, however, we did not observe an increase in p-MST1 in response to FAK inhibition (Fig 2.5A), nor a change in phosphorylation of MOB1 at T35, the main target of MST1 on MOB1 (116) with FAKi or knockdown of FAK (Fig S2.5B and S2.5C). This suggests that in UM, FAK regulates the link between LATS1 and YAP through MOB1, acting downstream from MST1 rather than controlling MST1 (Hippo) activity. In conjunction, we found

FAK was able to phosphorylate YAP at Y357 *in vitro* (Fig S2.5E), a post-translational modification that has been shown to regulate YAP stability and activity (117,118), and, aligned with this finding, that FAK inhibition also caused diminished phosphorylation of Y357-YAP in UM cells (Fig 2.5A). Indeed, we confirmed that long-term (up to 36 hours) FAK inhibition caused YAP protein downregulation (Fig 2.5C). Furthermore, LATS1/2 knockdown was sufficient to rescue from the growth inhibition by FAKi in UM cells (Fig 2.5D), supporting that YAP signaling plays a key role in growth promotion downstream from FAK in UM cells. Altogether, our data suggest that FAK drives UM cell growth through promotion of YAP activity by coordinating the previously described F-actin-mediated release of YAP from AMOT, which enhances the pool of cytosolic YAP and enables its nuclear translocation (88), with the release of the inhibitory Hippo kinase cascade through the FAK-mediated phosphorylation of MOB1 and the concomitant tyrosine phosphorylation and stabilization of YAP (Fig 2.5E).

2.2.6 FAK represents a therapeutic target in UM.

We next tested the potential of FAK inhibition for UM treatment. For these studies, we first used lentiviral-delivered Cas9-sg*PTK2* to knockout (KO) *PTK2* in UM cells (Fig 2.6A). Most UM cells did not survive after genome editing of *PTK2* (not shown), only mass cultures of Mel270 targeted for *PTK2* grew in culture after puromycin selection, displaying nearly abolished FAK protein levels (Fig 2.6A). Re-expression of FAK under control of a doxycycline-inducible promoter was sufficient to rescue cell viability in UM cells in which FAK expression was reduced (Fig S2.6). We observed that *PTK2* KO cells developed only very small tumors (Fig 2.6B), suggesting that FAK activation is important for UM tumor growth *in vivo*. These observations further support the therapeutic potential of targeting FAK for UM. While there are multiple FAKi under clinical evaluation (105), VS-4718, chosen for our studies, was specifically designed for oral administration. We found that VS-4718 treatment reduces both UM tumor size and cell proliferation in two different UM tumor models (Fig 2.6C-2.6F). We observed clearly increased cytoplasmic retention of YAP in VS-4718

treated tumors, consistent with our previous findings that FAK controls YAP-activity in UM cells (Fig 2.6G and 2.6H). These results suggest that the pharmacological inhibition of FAK may represent a viable therapeutic approach for the treatment of patients with UM harboring increased YAP activity.

2.3 Discussion

The generation of massive quantities of genomic, epigenomic and proteomic data has greatly enhanced our understanding of oncogenesis and cancer as a cellular state. The development of bioinformatics pipelines to predict nodes of connectivity between transcriptional and signaling networks can expedite efforts to identify and exploit molecular vulnerabilities for the treatment of cancer. We thus hypothesized that focusing on a cancer type specifically driven by few activating (Gαq) mutations may serve as a good testbed for studying such an approach, harnessing a SL-based integrated bioinformatics analysis to uncover potential oncogenic signaling mechanisms controlled by Gαq and target them. In this study, we demonstrate that FAK acts as a critical oncogenic signaling node in UM—mediating Gαq-driven regulation of the Hippo/YAP pathway and enabling the promotion of an oncogenic state. We provide evidence that FAK destabilizes interactions between key core Hippo pathway members thereby activating YAP in an MST1 (Hippo)-independent manner. Furthermore, we show that the oncogenic activity of FAK in UM is targetable by clinically relevant therapeutic agents.

The transformative potential of Gαq signaling was established in the early 1990s (20,76) however, the precise signaling events by which Gαq and its linked receptors transduce sustained proliferative signals is not yet well defined. This is due in part to the large number of second messenger generating systems and signaling events that can be perturbed upon Gαq activation. The activation of these second messenger systems and their direct targets, including ion channels and kinases such as PKC, CAMKs and MAPK, are responsible for most of the rapid physiological responses elicited by GPCRs (6-11,119). Recent studies have identified additional members of

this network for UM, highlighting the role of GEFs such as RasGRP3 in MAPK activation (120). Despite this link, therapeutic strategies targeting MAPKs have yet to be successful. Clinical trials demonstrated that MEK inhibition with selumetinib or trametinib, as single agents or in combination with Dacarbazine, has little impact on the overall survival of UM patients (121,122). This suggests that although MEK/MAPK networks activated by PLCβ may contribute to UM initiation, they may not be critical for the maintenance of tumorigenic potential in UM.

Contrary to the transient nature of signal transmission through PLCβ, genome-wide RNAi screens revealed that the signaling events driven by Gαq that result in aberrant cell proliferation depends on highly specific protein-protein interactions, rather than solely on diffusible second-messenger systems. Specifically, prior systems biology approaches have identified the RhoGEF TRIO as critical for activating Gαq-driven AP-1-regulated transcriptional networks independently of PLCβ to achieve sustained stimulation of proliferative pathways (86). Further work has shown that this pathway converges in the activation of YAP and that YAP activation is critical for oncogenic potential of UM (88,89,123). The Hippo/YAP cascade is a key growth-regulating pathway in normal cellular physiology (97,98,124). Unsurprisingly, dysregulation of the Hippo pathway is seen frequently in cancer; however, its core components are rarely mutated (97,125). Rather, external pressures from upstream oncogenes typically drive YAP-dependent cell proliferation. Identifying the key molecular players that facilitate oncogenic signaling through Hippo/YAP pathway may also uncover potential network vulnerabilities. Interestingly, inhibition of PLCβ does not impact the activation of YAP after Gαq stimulation (88). Together, these findings suggest that the canonical Gαq-PLCβ-MAPK signaling axis may be critical for tumor initiation rather than tumor maintenance and that opportunities for intervention may lie within the distinct signaling circuitry transduced through TRIO.

FAK is a non-receptor tyrosine kinase whose role as a downstream target of Gαq has been well established by biochemical studies (126); however, the contribution of FAK as a mediator of oncogenic Gαq signaling has not been previously explored. Our finding that FAK is

rapidly activated by Gαq-linked GPCRs and the oncogenic mutant Gαq through TRIO and RhoA, rather than PLCβ prompted us to focus on the possibility that FAK may represent an integral component of the non-canonical pathway by which Gαq regulates aberrant cell growth. We found that inhibition of FAK was sufficient to reduce UM cell proliferation and, if prolonged, to trigger apoptotic cell death. This response was unanticipated as FAK inhibitors often have limited activity in most cancers as single agents but instead synergize with cytotoxic agents, as we have shown for ovarian cancer that overexpresses FAK as a typical example (105). We hypothesized that as compared to other cancer types with FAK overexpression, the compounding impact of *PTK2* copy number gain and overexpression together with Gαq-driven FAK activity in UM creates a unique cellular state that may be highly dependent on the activity of FAK and therefore highly sensitive to FAK inhibition. This convergence of computational predictions, biochemical, and genetic information enabled the discovery of the therapeutic potential of inhibiting FAK for UM treatment.

FAK has been recently linked to YAP activity in mechanotransduction and in the coordination of cell proliferation and differentiation in mouse incisors during development (127,128). However, the underlying cell-context specific and developmental mechanisms are still not fully understood. We provide evidence that in UM the role of FAK converges on promoting YAP activity through the tandem inhibition of Hippo pathway signals by phosphorylation of Y26 of MOB1 and Y357 of YAP. In the case of YAP phosphorylation, these observations extend prior studies indicating the role of JAK2 and SRC in Y357 phosphorylation (117,118). However, downstream from FAK, we observed both tyrosine-phosphorylated YAP and a decrease in pS127 YAP, the latter a direct target of the Hippo signaling pathway. In this regard, there is increasing evidence suggesting that Hippo signaling is tightly regulated by the assembly and dissociation of key signaling complexes. Our interrogation of these complexes in response to FAK activation led to the finding that FAK phosphorylates MOB1 on Y26, resulting in the disassembly of the MOB1/LATS complex and disruption of the Hippo pathway downstream from MST1, effectively rewiring the molecular mechanisms controlling YAP activity. Mutation of Y26 of MOB1 is sufficient

to abolish the effect of FAK. Whereas further work may be required to establish the structural basis for this inhibition, as well as alternative FAK-driven pathways in mechanotransduction and development, our findings support that disruption of the MOB1/LATS signaling complex by FAK is a key regulatory step resulting in YAP activation by Gαq. Ultimately, this mechanism may coordinate the Gαq-induced increase in cytosolic free YAP, which is mediated by Rho-induced actin polymerization (88), with Hippo kinase cascade inhibition through the FAK-mediated phosphorylation of MOB1, resulting in the YAP-dependent UM cell growth.

The current lack of effective treatments for primary or metastatic UM leaves a large therapeutic gap for patients and clinicians underscoring an urgent need for the identification of additional pharmacological targets for therapeutic intervention. As YAP-targeting strategies have remained elusive thus far, the success of FAK inhibition in our *in vivo* models in the context of previously established success and safety of FAK inhibitors in human clinical trials highlight the translational potential of our findings and establish FAK as a therapeutic target for the treatment of UM. Towards this end, the application of systems-level and bioinformatics investigation will be a powerful strategy to identify precision treatment options for UM and a myriad of Gαq-driven diseases.

2.4 Figures

Figure 2.1 Bioinformatics analysis reveals FAK as critical for UM progression.

(A) Pipeline to discover druggable therapeutic targets in UM: molecular screen, survival screen, *in vitro* screen and druggable screen. (B) Summary of the final 7 gene hits. Molecular, clinical, phenotypic, and synthetic lethal (SL) scores were calculated as in (Lee et al., 2018). Cell viability was assessed *in vitro* in UM cells (OMM1.3) following siRNA-mediated inhibition of each gene (cell viability normalized to OMM1.3 treated with non-targeting siRNA, siRNA-*GNAQ* used as positive control, mean, n=3). (C) Oncoprint depicting the genomic landscape of TCGA UM cohort (83) downloaded from cBioPortal (96). Each bar represents one sample and their respective gene mutation or expression status. Percentage of gene alterations (in blue) and MutSig (in orange) or Gistic Q value (in purple) is listed on the right. (D) Kaplan-Meier plot depicting overall survival for UM patients stratified against *PTK2* expression in their tumors. *PTK2*-High and *PTK2*-Low groups are defined as top and bottom 50% of *PTK2* expression. p value=0.002. (E) UM cell lines (Mel270, 92.1, OMM1.3, OMM1.5 and MEL202 with *GNAQ* active mutation) cell viability assay after treatment with 1 μM FAK inhibitor (VS-4718), SKCM cells (SK-MEL-28) served as control. Data are the percent viability normalized to vehicle treatment (mean ± SEM, n = 3). (F) Immunoblot of OMM1.3 cells showing pY397-FAK after treatment with VS-4718 (1 μM) (left) and cleaved PARP in response to 36 hr VS-4718 (1-10 μM) treatment (right). (G) Representative images (left) and quantification (right) of colony formation assay of OMM1.3 cells with VS-4718 treatment in semisolid media (i, mean ± SEM, n = 3; ***, p<0.001, DMSO treatment as control). See also Figure S1.

A

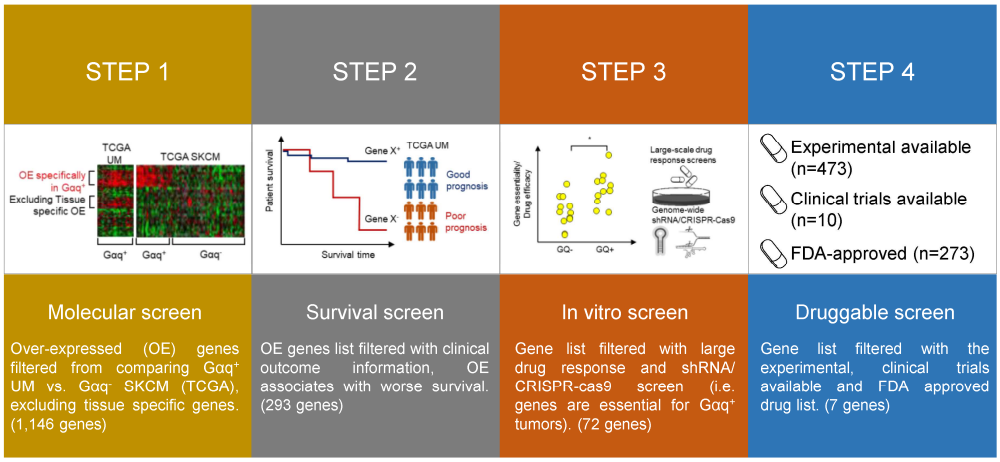

B

Genes	Molecular	Clinical	Phenotypic	SL-score	Viability %
PTK2	1.05E-09	1.71E-03	8.62E-03	0.94	40.35
MGLL	6.62E-04	1.87E-02	6.01E-03	0.78	75.57
AKT1	8.71E-03	1.29E-02	2.21E-02	0.64	39.16
SIRT1	6.20E-04	9.29E-02	3.55E-02	0.53	66.38
MTHFD1	4.42E-02	4.43E-03	3.50E-02	0.50	61.64
CDK1	8.14E-03	9.20E-03	7.12E-02	0.50	35.99
PSMB5	3.93E-02	9.97E-04	4.36E-01	0.36	64.76
GNAQ					26.06

C

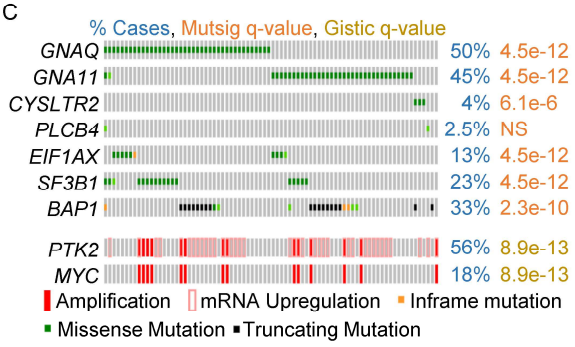

D

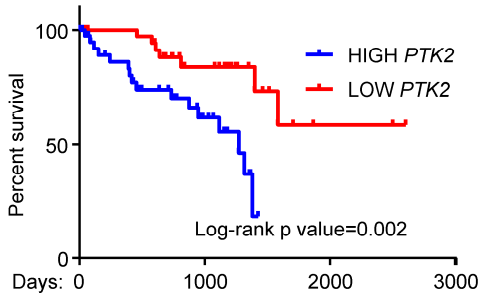

E

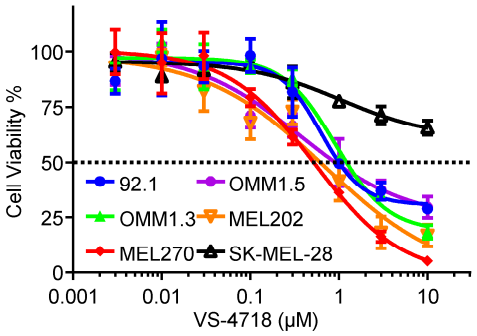

F

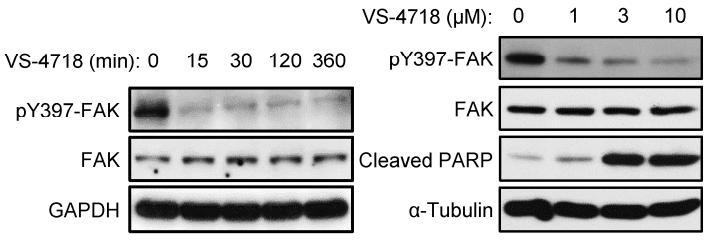

G

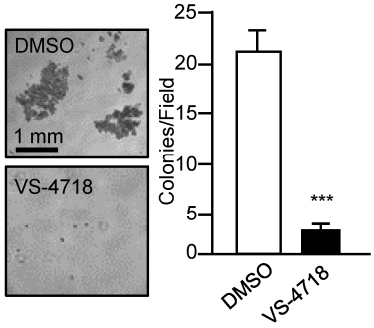

Figure 2.2 Gαq regulates FAK activation through a non-canonical TRIO/RhoA-mediated signaling circuitry.

(A) Immunoblot depicting phosphorylation of FAK after transfection with HA-GαqQL and control expression vectors in HEK293 cells. (B) Immunoblot showing FAK phosphorylation in Gαq-DREADD expressing HEK293 cells stimulated with CNO (1 μM) over a time course analysis. (C) Immunoblot depicting FAK and ERK phosphorylation after 2 hr FR (1 μM) treatment in OMM1.3 cells. (D) UM cell viability assay after 72 hr treatment with FR, SK-MEL-28 *BRAF* SKCM served as control, percent viability is normalized to vehicle treatment (mean ± SEM, n = 3). (E) Immunoblot showing phosphorylation of ERK and FAK after stimulation of Gαq-DREADD expressing HEK293 cells with CNO (1 μM) at 5 min in combination with 1 hr U73122 (1 μM) pre-treatment. (F) Immunoblot showing phosphorylation of ERK and FAK during a time course of treatment with GF109203X (1 μM) in OMM1.3 cells. (G) Immunoblot showing FAK phosphorylation in Gαq-DREADD expressing HEK293 cells after 5 min of CNO stimulation (1 μM) in combination with siRNA mediated TRIO, RhoA or Rac1 knockdown (top), and immunoblot to show efficiency of siRNA mediated TRIO, RhoA or Rac1 knockdown (bottom). (H) Immunoblot showing FAK phosphorylation after siRNA mediated RhoA knockdown in OMM1.3 cells. (I) Immunoblot showing FAK phosphorylation in Gαq-DREADD expressing HEK293 cells after 5 min of CNO stimulation (1 μM) in combination with 1 hr Y-27632 (10 μM) pre-treatment (top), and in combination with 1 hr blebbistatin (20 μM) pre-treatment (bottom). (J) Immunoblot showing FAK phosphorylation during a time course of treatment with Y-27632 (top) and blebbistatin (bottom) in OMM1.3 cells. (K) Cartoon depicting the non-canonical signaling pathway regulating FAK activation by Gαq. G protein βγ subunits are depicted in addition to Gαq. DAG, diacylglycerol; MLC, myosin light chain.

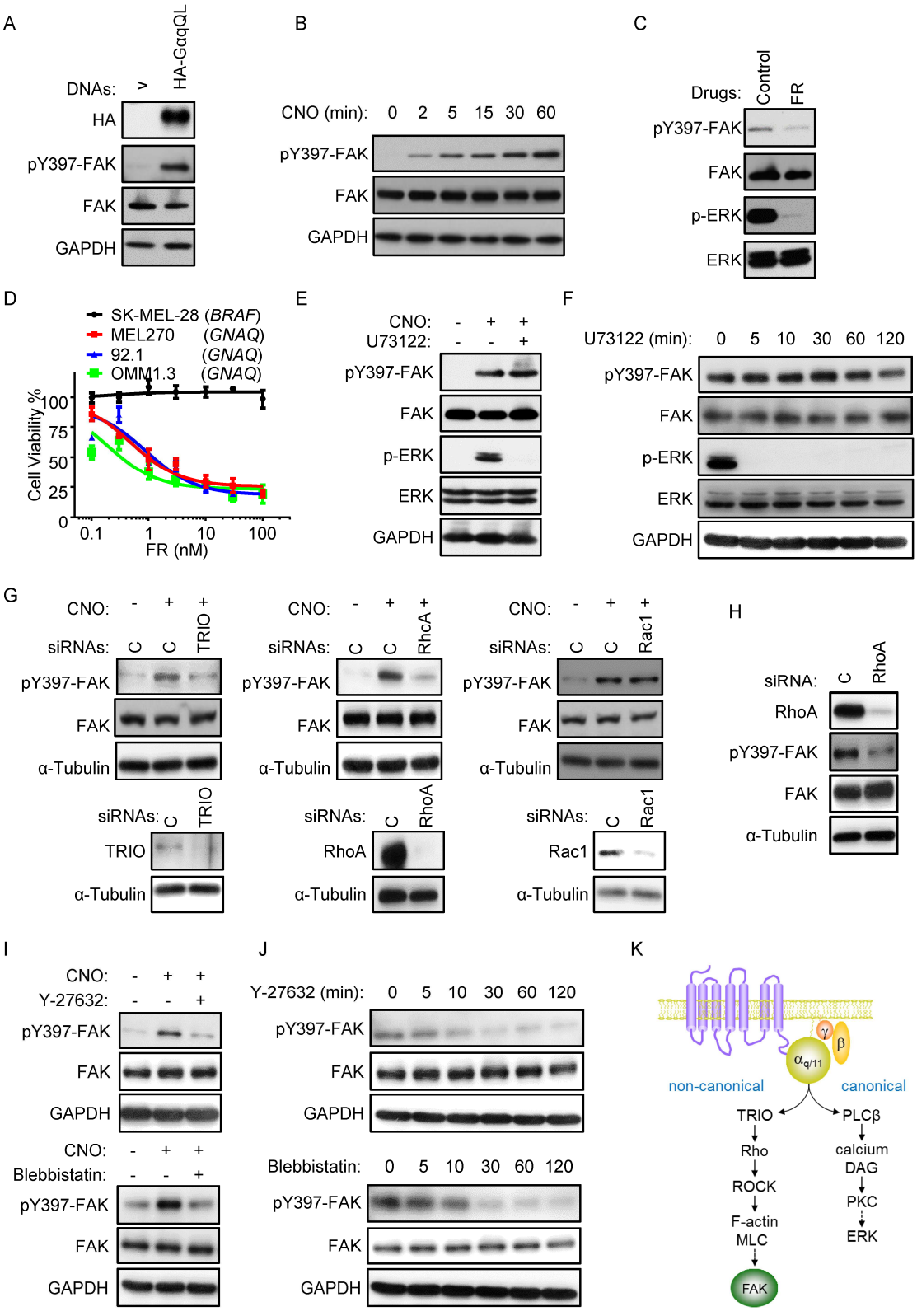
A
DNAs: > HA-GαqQL
HA
pY397-FAK
FAK
GAPDH
B
CNO (min): 0 2 5 15 30 60
pY397-FAK
FAK
GAPDH
C
Drugs: Control FR
pY397-FAK
FAK
p-ERK
ERK
D
SK-MEL-28 (BRAF)
MEL270 (GNAQ)
92.1 (GNAQ)
OMM1.3 (GNAQ)
Cell Viability %
100
75
50
25
0
0.1 1 10 100
FR (nM)
E
CNO: - + +
U73122: - - +
pY397-FAK
FAK
p-ERK
ERK
GAPDH
F
U73122 (min): 0 5 10 30 60 120
pY397-FAK
FAK
p-ERK
ERK
GAPDH
G
CNO: - + +
siRNAs: C C TRIO
pY397-FAK
FAK
α-Tubulin
siRNAs: C TRIO
TRIO
α-Tubulin
CNO: - + +
siRNAs: C C RhoA
pY397-FAK
FAK
α-Tubulin
siRNAs: C RhoA
RhoA
α-Tubulin
CNO: - + +
siRNAs: C C Rac1
pY397-FAK
FAK
α-Tubulin
siRNAs: C Rac1
Rac1
α-Tubulin
H
siRNA: C RhoA
RhoA
pY397-FAK
FAK
α-Tubulin
I
CNO: - + +
Y-27632: - - +
pY397-FAK
FAK
GAPDH
CNO: - + +
Blebbistatin: - - +
pY397-FAK
FAK
GAPDH
J
Y-27632 (min): 0 5 10 30 60 120
pY397-FAK
FAK
GAPDH
Blebbistatin: 0 5 10 30 60 120
pY397-FAK
FAK
GAPDH
K
γ
β
αq/11
non-canonical
canonical
TRIO
Rho
ROCK
F-actin
MLC
FAK
PLCβ
calcium
DAG
PKC
ERK

Figure 2.3 FAK inhibition regulates the Hippo-YAP pathway in UM.

(A) The top 10 down-regulated oncogenic signatures gene sets of OMM1.3 cells treated with VS-4718 (1 μM, 2 hr, vehicle treatment as control). (B) Heatmap depicting the most down-regulated genes by VS-4718 treatment (as A), *=YAP signature genes. (C) mRNA expression level of YAP signature genes from RNA-seq data (mean ± SEM, n = 3). (D) Enrichment plot for YAP Conserved Signature gene set (GSEA, http://software.broadinstitute.org/gsea/index.jsp). (E) mRNA expression of *CTGF* and *CYR61* measured by qPCR in OMM1.3 cells after 2 hr VS-4718 treatment (1 μM, vehicle treatment as control, mean ± SEM, n = 3). (F) Immunofluorescent staining of endogenous YAP (green) and Hoeschst staining for nuclear DNA (blue) in OMM1.3 cells after 4 hr VS-4718 (1 μM) treatment, vehicle treatment as control. (G) Immunoblot showing YAP nuclear and cytoplasmic localization after 2 hr VS-4718 (1 μM) treatment in OMM1.3 cells, using lamin A/C and α-tubulin as nuclear and cytoplasmic markers, respectively. (H) YAP/TAZ Luciferase reporter assay after siRNA mediated FAK and G□q knockdown in OMM1.3 cells (mean ± SEM, n = 3). (I) Immunoblot showing YAP phosphorylation after siRNA mediated FAK knockdown in OMM1.3 cells. (J) YAP/TAZ Luciferase reporter assay after 2 hr treatment with FR, VS-4718 or Dasatinib (all used at 1 μM) in OMM1.3 cells (mean ± SEM, n = 3). (K) Immunoblot showing YAP phosphorylation after 2 hr FR (1 μM), VS-4718 (1 μM) or Dasatinib (1 μM) treatment in OMM1.3 cells. (In all cases, **, $p<0.01$; ***, $p<0.001$). See also Figures S2.2 and S2.3.

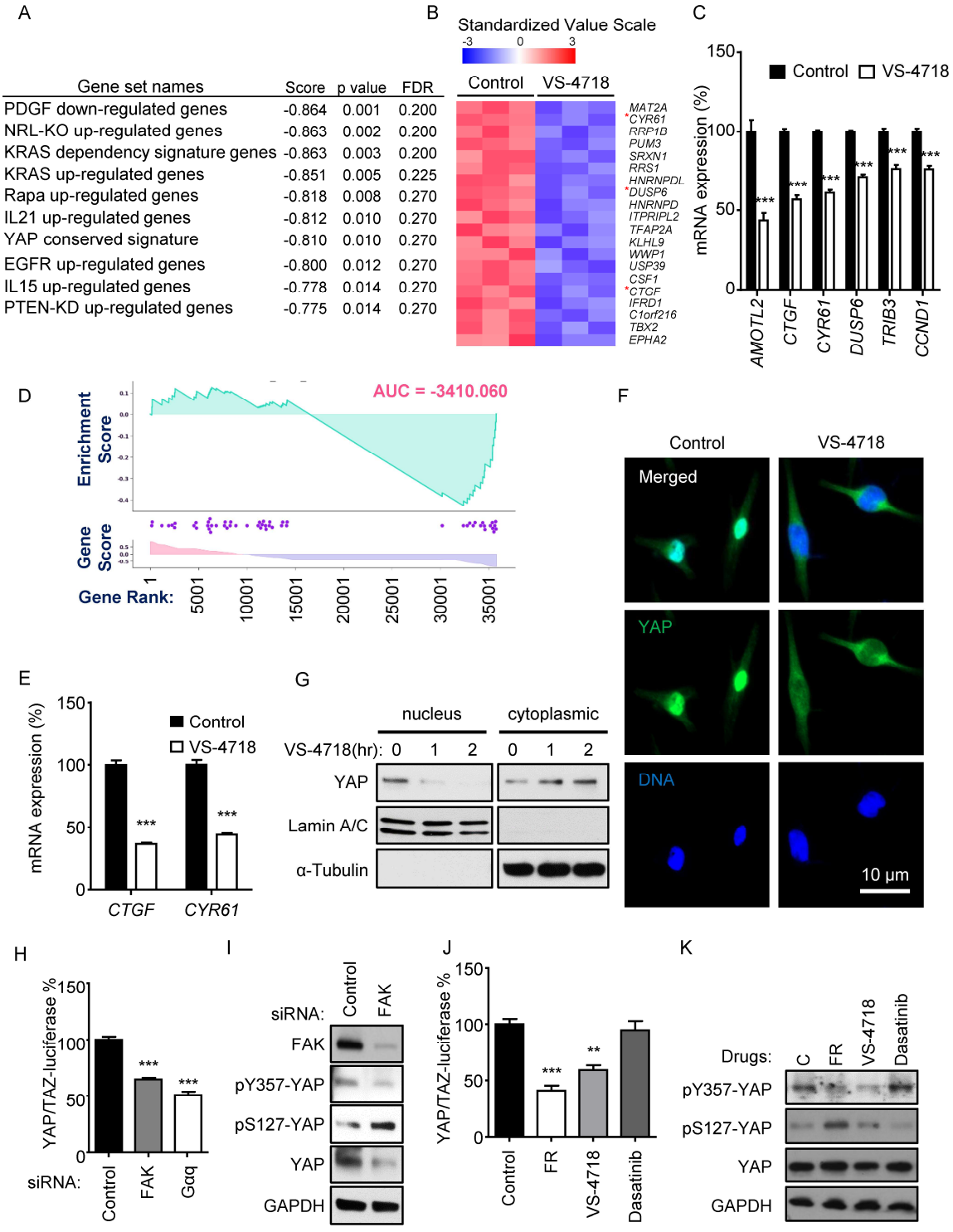
A
Gene set names Score p value FDR
PDGF down-regulated genes -0.864 0.001 0.200
NRL-KO up-regulated genes -0.863 0.002 0.200
KRAS dependency signature genes -0.863 0.003 0.200
KRAS up-regulated genes -0.851 0.005 0.225
Rapa up-regulated genes -0.818 0.008 0.270
IL21 up-regulated genes -0.812 0.010 0.270
YAP conserved signature -0.810 0.010 0.270
EGFR up-regulated genes -0.800 0.012 0.270
IL15 up-regulated genes -0.778 0.014 0.270
PTEN-KD up-regulated genes -0.775 0.014 0.270
B
Standardized Value Scale
-3 0 3
Control VS-4718
MAT2A
CYR61
RRP1B
PUM3
SRXN1
RRS1
HNRNPDL
DUSP6
HNRNPD
ITPRIPL2
TFAP2A
KLHL9
WWP1
USP39
CSF1
CTGF
IFRD1
C1orf216
TBX2
EPHA2
C
Control VS-4718
mRNA expression (%)
150
100
50
0
AMOTL2 CTGF CYR61 DUSP6 TRIB3 CCND1
D
AUC = -3410.060
Enrichment Score
Gene Score
Gene Rank: 1 5001 10001 15001 20001 25001 30001 35001
E
Control
VS-4718
mRNA expression (%)
150
100
50
0
CTGF CYR61
F
Control VS-4718
Merged
YAP
DNA
10 μm
G
nucleus cytoplasmic
VS-4718(hr): 0 1 2 0 1 2
YAP
Lamin A/C
α-Tubulin
H
YAP/TAZ-luciferase %
150
100
50
0
siRNA: Control FAK Gαq
I
siRNA: Control FAK
FAK
pY357-YAP
pS127-YAP
YAP
GAPDH
J
YAP/TAZ-luciferase %
150
100
50
0
Control FR VS-4718 Dasatinib
K
Drugs: C FR VS-4718 Dasatinib
pY357-YAP
pS127-YAP
YAP
GAPDH

Figure 2.4 FAK regulates YAP activation through MOB-Y26 phosphorylation, disrupting the core Hippo kinase signaling pathway.

(A) YAP/TAZ Luciferase reporter assay after transient transfection of FAK and control expression vectors in HEK293 cells (mean ± SEM, n = 3; ***, p<0.001). (B) Immunoblot showing phosphorylation status of YAP after transfection of HA-GαqQL and control expression vectors in HEK293 cells. (C) Immunoblot showing phosphorylation status of YAP after transfection of FAK and control expression vectors in HEK293 cells. (D) Immunoblot against phospho-tyrosine after immunoprecipitation (IP) of tagged Hippo signaling core components (myc-MST1, flag-SAV1, flag-LATS1 or HA-MOB1) transfected with or without FAK in HEK293 cells. Total cell lysates (input) and IP by the indicated antibodies are shown. Western blot for FAK and each of the epitope tags are also shown. (E) Immunoblot showing phosphorylation of MOB1 and association with MST1 and LATS1 after HA or pY immunoprecipitation (IP) in HEK293 cells transfected with or without FAK and wildtype HA-MOB1. (F) Immunoblot showing phosphorylation of MOB1 and association with MST1 and LATS1 after HA or pY immunoprecipitation in HEK293 cells transfected with or without FAK and mutant HA- Y26F-MOB1. See also Figure S2.4.

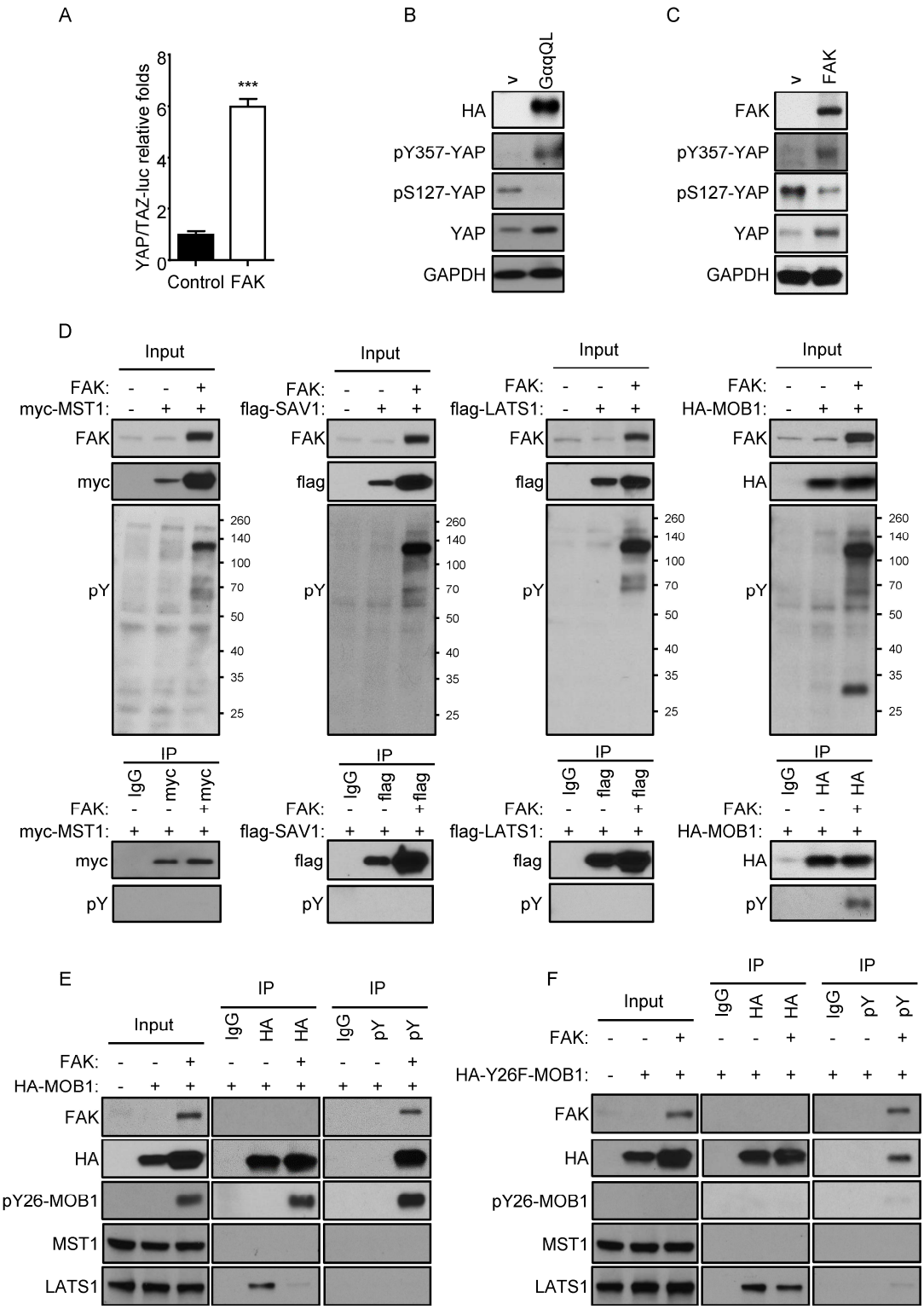
A
YAP/TAZ-luc relative folds
***
Control FAK
B
v
GαqQL
HA
pY357-YAP
pS127-YAP
YAP
GAPDH
C
v
FAK
FAK
pY357-YAP
pS127-YAP
YAP
GAPDH
D
Input
IP
FAK:
myc-MST1:
flag-SAV1:
flag-LATS1:
HA-MOB1:
IgG
myc
flag
HA
pY
E
Input
IP
FAK:
HA-MOB1:
pY26-MOB1
MST1
LATS1
F
Input
IP
FAK:
HA-Y26F-MOB1:
pY26-MOB1
MST1
LATS1

Figure 2.5 Inhibition of FAK causes YAP inhibition in UM by unleashing Hippo pathway signaling, and inducing inhibitory YAP phosphorylation and degradation.

(A) Immunoblot of total and phosphorylated core Hippo pathway members in OMM1.3 cells after 1 μM VS-4718 treatment for 0, 1 and 2 hours. (B) Immunoblot showing the association of MOB1 with LATS1 after HA or pY immunoprecipitation of OMM1.3 cells transfected with HA-MOB1 with or without 1 hr VS-4718 treatment. (C) Immunoblot showing levels of total YAP over a time course of 1 μM VS-4718 treatment in OMM1.3 cells. (D) Immunoblot showing levels of LATS1/2 after knockdown in OMM1.3 cells (top) and cell viability assay of OMM1.3 cells with LATS1/2 knockdown in combination with VS-4718 treatment (bottom, mean ± SEM, n = 3; **, $p<0.01$, ***, $p<0.001$, ns; not significant). (E) Cartoon depicting the signaling pathway by which FAK mediates YAP activation downstream from constitutively active Gαq mutant in UM. See text for details. See also Figure S2.5.

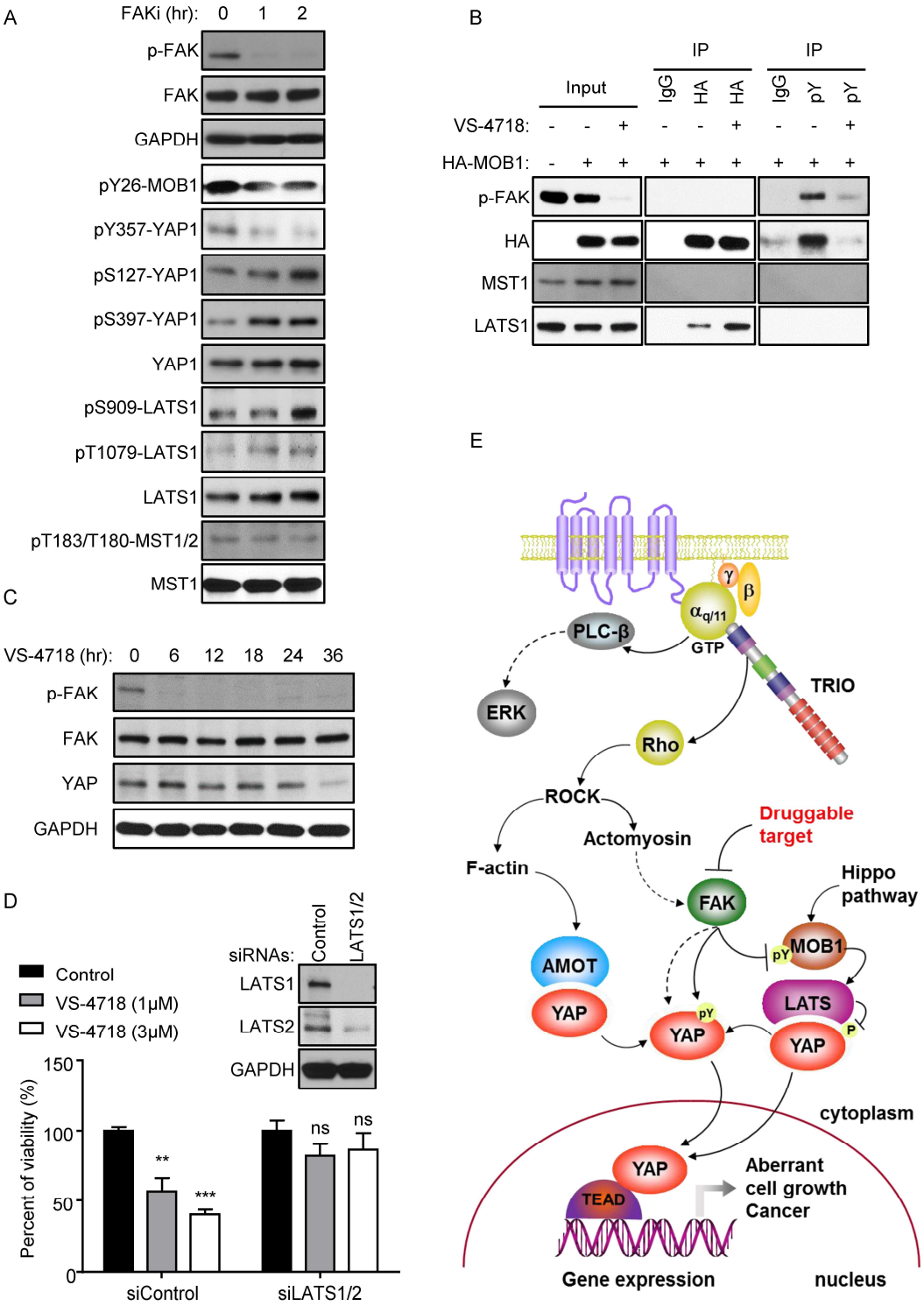
A
FAKi (hr): 0 1 2
p-FAK
FAK
GAPDH
pY26-MOB1
pY357-YAP1
pS127-YAP1
pS397-YAP1
YAP1
pS909-LATS1
pT1079-LATS1
LATS1
pT183/T180-MST1/2
MST1
B
Input
IP
IgG
HA
HA
IP
IgG
pY
pY
VS-4718: - - + - - + - - +
HA-MOB1: - + + + + + + + +
p-FAK
HA
MST1
LATS1
C
VS-4718 (hr): 0 6 12 18 24 36
p-FAK
FAK
YAP
GAPDH
D
Control
VS-4718 (1μM)
VS-4718 (3μM)
siRNAs: Control LATS1/2
LATS1
LATS2
GAPDH
Percent of viability (%)
150
100
50
0
**
***
ns
ns
siControl
siLATS1/2
E
γ
β
αq/11
PLC-β
GTP
TRIO
ERK
Rho
ROCK
Actomyosin
Druggable target
F-actin
Hippo pathway
FAK
AMOT
YAP
MOB1
pY
LATS
P
YAP
pY
YAP
cytoplasm
YAP
TEAD
Aberrant cell growth Cancer
Gene expression
nucleus

Figure 2.6 FAKi in UM inhibits YAP-dependent UM tumor growth.

(A) Immunoblot showing CRISPR/Cas9-mediated *PTK2* knockout in Mel270 cells (wildtype as control). (B) Tumor volume of *PTK2* knockout Mel270 cells *in vivo* (wildtype as control) at the end of the study (mean ± SEM, n = 4) (left) and hematoxylin and eosin (H&E)-stained sections of representative tumors from each group (right). (C) Tumor volume of Mel270 cells *in vivo* with or without VS-4718 treatment at the end of the study (mean ± SEM, n = 8) (left) and hematoxylin and eosin (H&E)-stained sections of representative tumors from each group (right). (D) Ki67 immunohistochemistry staining in Mel270 tumors with or without VS-4718 treatment. (E) Tumor volume of OMM1.3 cells *in vivo* with or without VS-4718 treatment at the end of the study (mean ± SEM, n = 4) (left) and hematoxylin and eosin (H&E)-stained sections of representative tumors from each group (right). (F) Ki67 immunohistochemistry staining of OMM1.3 tumors with or without VS-4718 treatment. (G) Representative YAP immunohistochemistry staining of Mel270 tumors with or without VS-4718 treatment. (H) Quantification of Figure 2.6G, showing fraction of cells with nuclear YAP localization (mean ± SEM, n = 3). In all cases ***, $p<0.001$. See also Figure S2.6.

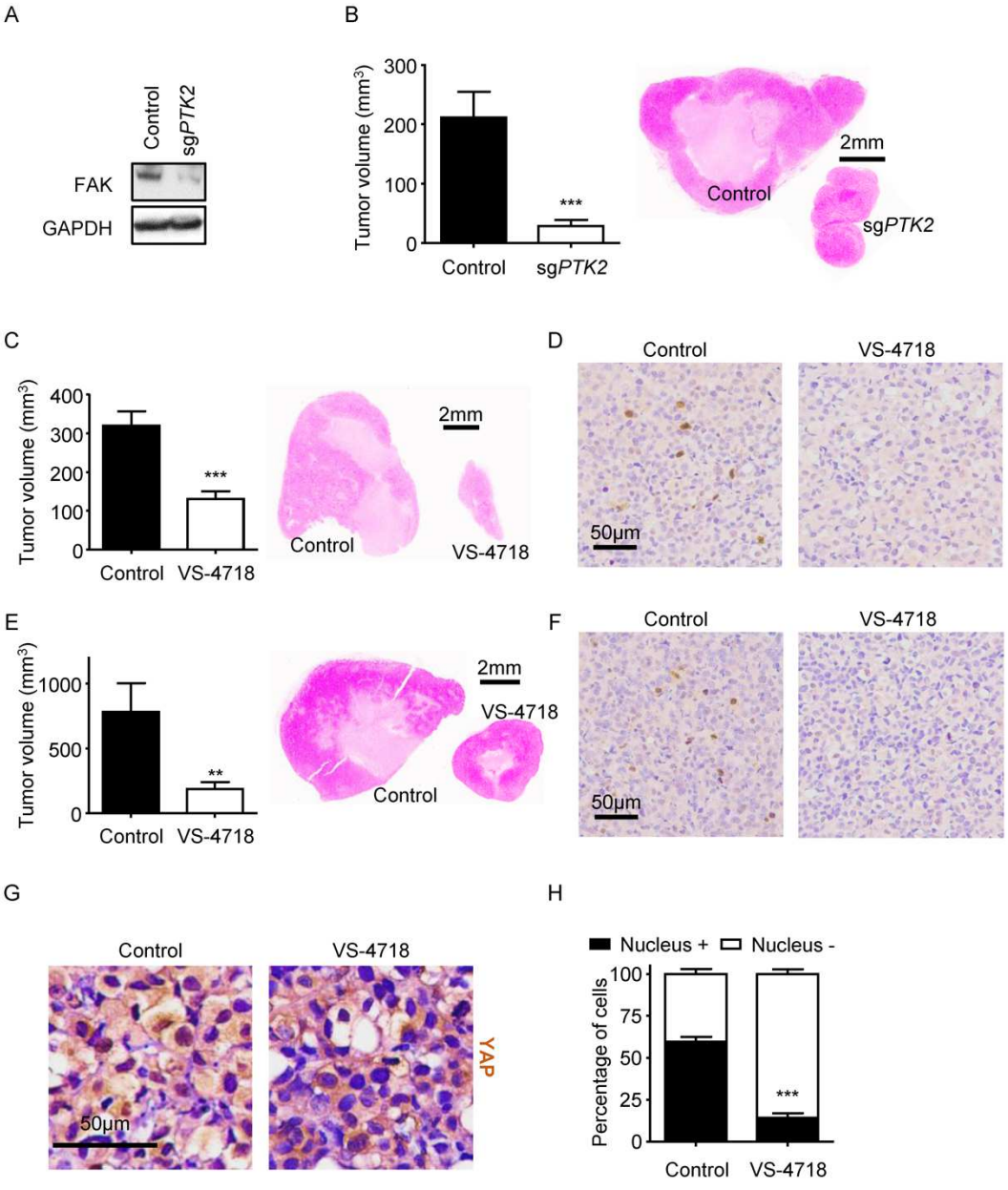
A
Control
sgPTK2
FAK
GAPDH
B
Tumor volume (mm3)
300
200
100
0
***
Control
sgPTK2
2mm
Control
sgPTK2
C
Tumor volume (mm3)
400
300
200
100
0
***
Control
VS-4718
2mm
Control
VS-4718
D
Control
VS-4718
50μm
E
Tumor volume (mm3)
1000
500
0
**
Control
VS-4718
2mm
VS-4718
Control
F
Control
VS-4718
50μm
G
Control
VS-4718
50μm
YAP
H
Nucleus +
Nucleus -
Percentage of cells
100
75
50
25
0
***
Control
VS-4718

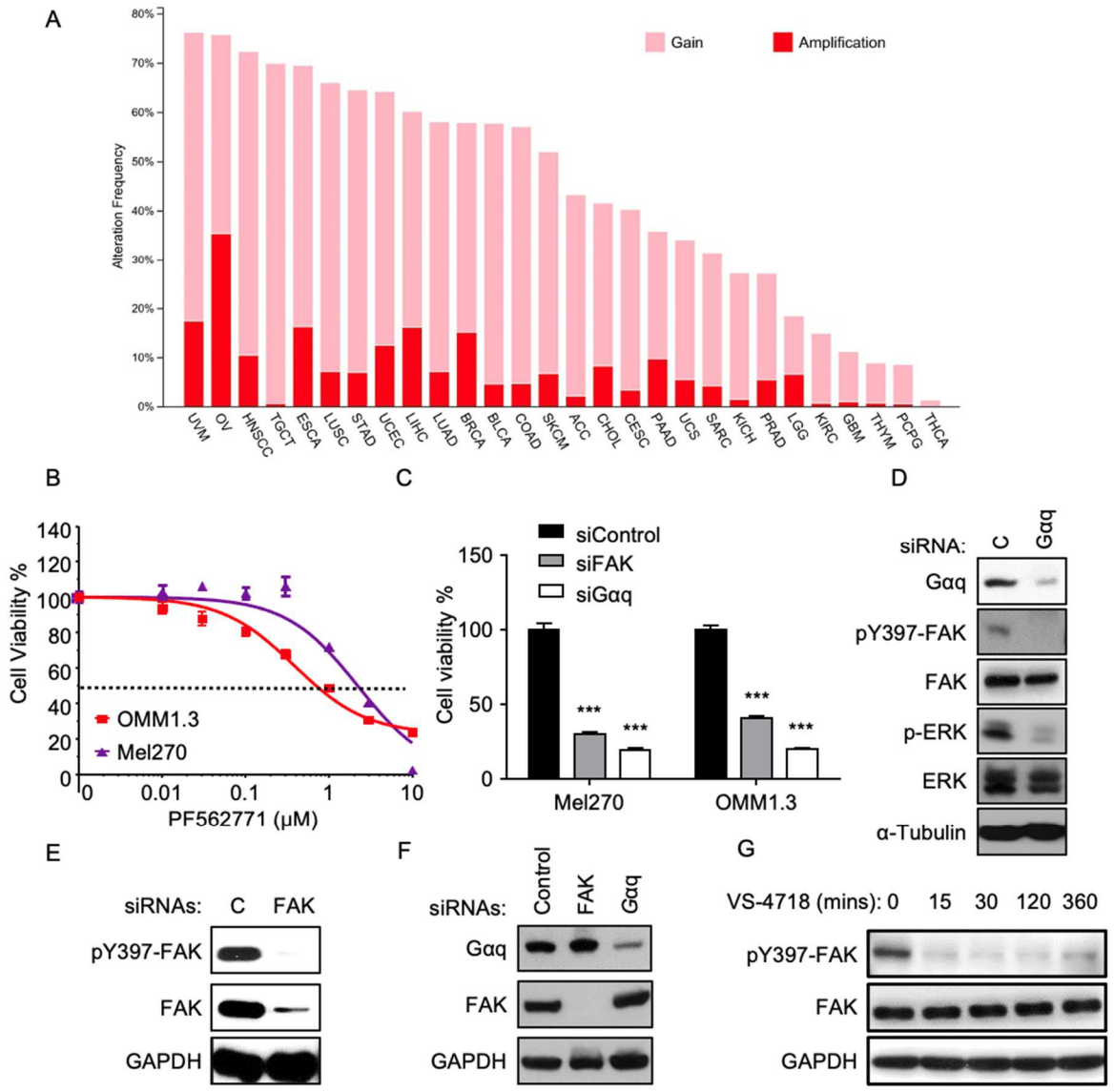

Figure S2.1

(A) Pan-cancer analysis of FAK alteration frequency. Data on genomic alterations (copy number gain and amplification) were downloaded from each indicated TCGA cancer cohort from cBioPortal (Gao et al., 2013). (B) Cell viability assay in UM cell lines (OMM1.3 and Mel270) after treatment with PF562771 (FAK inhibitor), percent viability is normalized to vehicle treatment (mean ± SEM, n = 3). (C) Mel270 and OMM1.3 cell viability in response to siRNA mediated FAK and Gαq knockdown (mean ± SEM, n = 3). (D) Immunoblot of siRNA mediated Gαq knockdown in OMM1.3 cells, and impact on FAK and ERK activation status. (E) Immunoblot showing total and phosphorylated FAK after siRNA mediated FAK knockdown in OMM1.3 cells. (F) Immunoblot showing levels of Gαq and FAK after siRNA mediated FAK and Gαq knockdown in Mel270 cells. (G) Immunoblot showing impact on FAK phosphorylation after a timecourse of 1μM VS-4718 treatment in Mel270 cells. In all cases *** $p<0.001$.

A

Oncogenic signatures gene set	Oncogenic signatures gene set (original name)	Score	0.95 MoE	p value	FDR
PDGF down-regulated genes	PDGF_UP.V1_DN	-0.864	0.184	0.001	0.200
NRL-KO up-regulated genes	NRL_DN.V1_UP	-0.863	0.173	0.002	0.200
KRAS dependency signature genes	SINGH_KRAS_DEPENDENCY_SIGNATURE_	-0.863	0.184	0.003	0.200
KRAS up-regulated genes	KRAS.300_UP.V1_UP	-0.851	0.172	0.005	0.225
Rapa up-regulated genes	MTOR_UP.N4.V1_UP	-0.818	0.164	0.008	0.270
IL21 up-regulated genes	IL21_UP.V1_UP	-0.812	0.170	0.010	0.270
YAP conserved signature genes	CORDENONSI_YAP_CONSERVED_SIGNATURE	-0.810	0.180	0.010	0.270
EGFR up-regulated genes	EGFR_UP.V1_UP	-0.800	0.179	0.012	0.270
IL15 up-regulated genes	IL15_UP.V1_UP	-0.778	0.166	0.014	0.270
PTEN-KD up-regulated genes	PTEN_DN.V2_UP	-0.775	0.175	0.014	0.270
RAD001 down-regulated genes	MTOR_UP.V1_DN	-0.736	0.183	0.019	0.318
E2F3 up-regulated genes	E2F3_UP.V1_UP	-0.721	0.158	0.023	0.336
JAK2-KD down-regulated genes	JAK2_DN.V1_DN	-0.718	0.178	0.024	0.336
BMI1-KD up-regulated genes	BMI1_DN_MEL18_DN.V1_UP	-0.716	0.168	0.025	0.336
P53-KD up-regulated genes	P53_DN.V2_UP	-0.710	0.180	0.029	0.360
BRCA1-KD up-regulated genes	BRCA1_DN.V1_DN	-0.686	0.156	0.033	0.388
Up-regulated genes in astroglia cells	CAHOY_ASTROGLIAL	-0.682	0.147	0.035	0.388
KRAS up-regulated genes	KRAS.50_UP.V1_UP	-0.659	0.164	0.043	0.440
TGFB1 down-regulated genes	TGFB_UP.V1_DN	-0.653	0.152	0.045	0.440
Late serum down-regulated genes	CSR_LATE_UP.V1_DN	-0.651	0.184	0.047	0.440

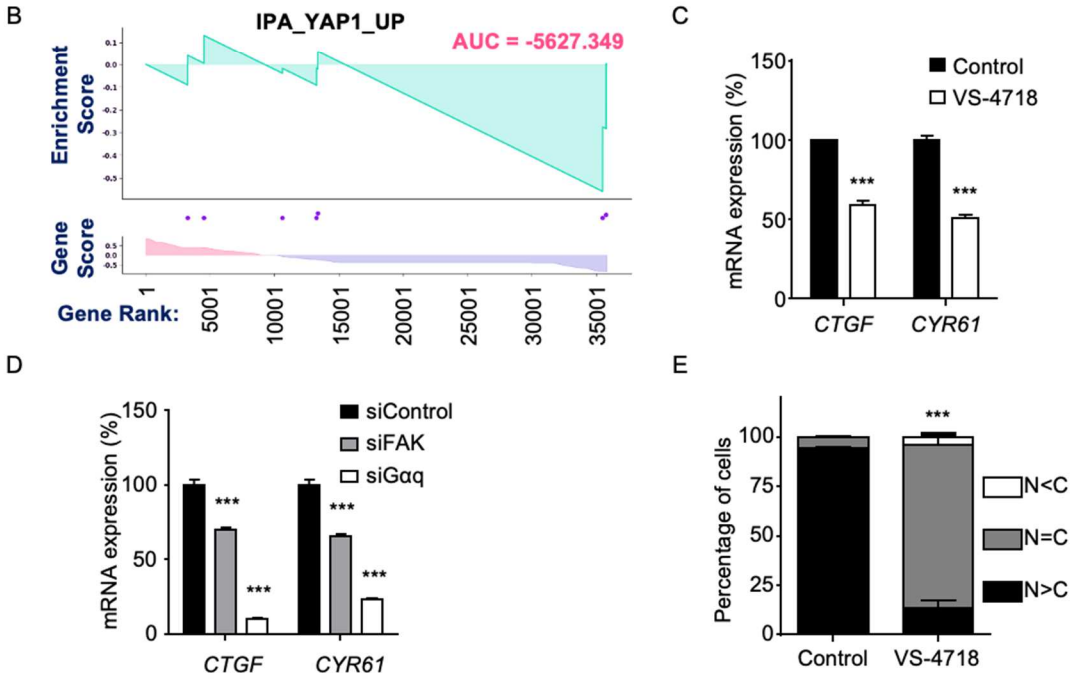

Figure S2.2

(A) The top 20 down-regulated oncogenic signatures gene sets from RNA-seq analysis of OMM1.3 cells treated with VS-4718 (1μM, 2 hr, vehicle treatment as control, with original gene set names). (B) Enrichment plot for IPA YAP1 upregulate gene set. (GSEA, http://software.broadinstitute.org/gsea/index.jsp). (C) mRNA expression of *CTGF* and *CYR61* measured by qPCR in Mel270 cells after 2 hr, 1 μM VS-4718 treatment (vehicle treatment as control, mean ± SEM, n = 3). (D) mRNA expression of *CTGF* and *CYR61* measured by qPCR after siRNA mediated knockdown of FAK and Gαq in Mel270 cells (mean ± SEM, n = 3). (E) Nuclear and cytoplasmic YAP quantification from Figure 3F, cytoplasm (C) and nucleus (N) (mean ± SEM, n = 3). In all cases *** p<0.001.

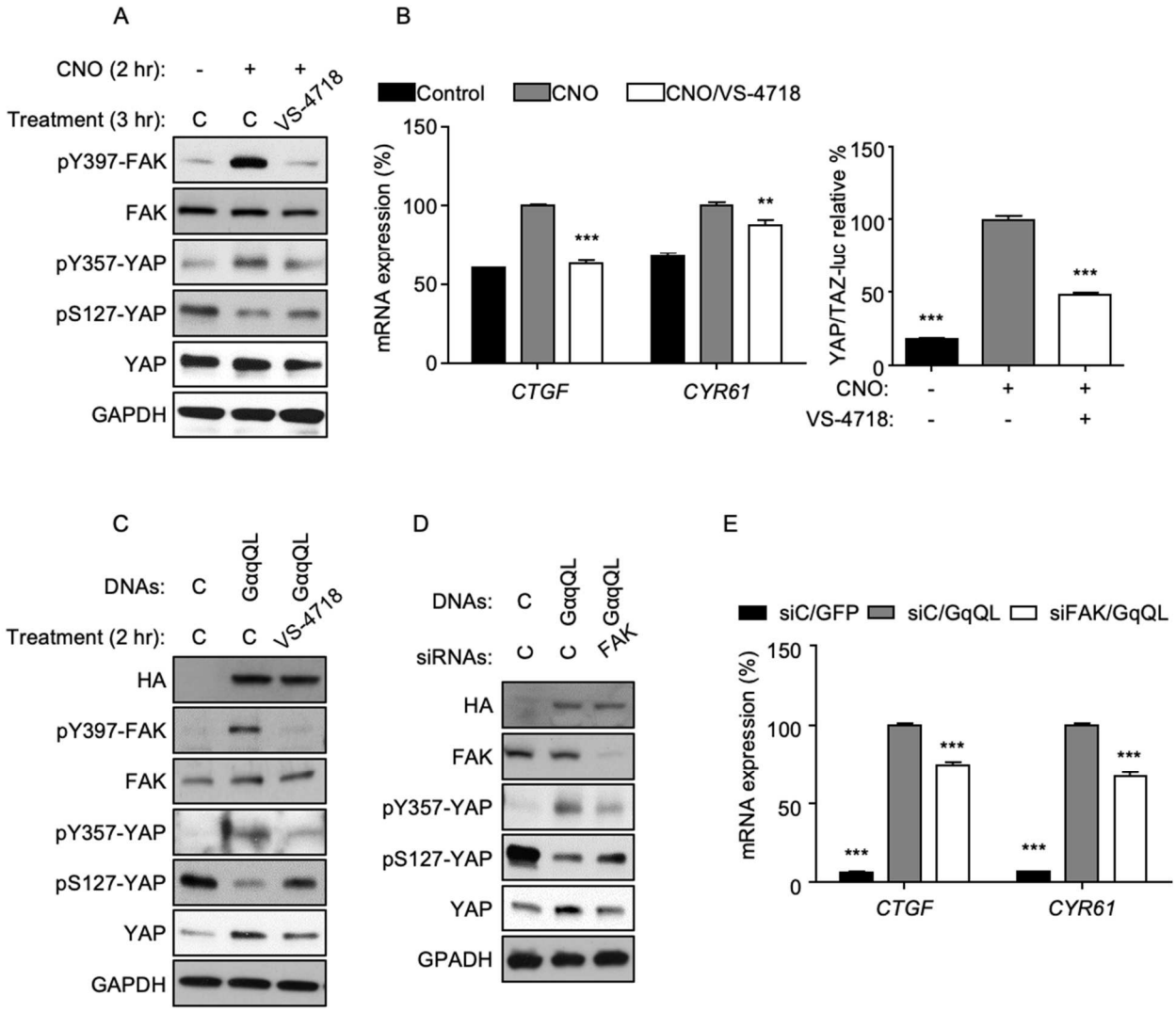

Figure S2.3

(A) Immunoblot showing phosphorylation of YAP after stimulation of Gαq-DREADD expressing HEK293 cells with 1μM CNO in combination with 1 μM VS-4718 treatment. (B) mRNA expression of *CTGF* and *CYR61* measured by qPCR (mean ± SEM, n = 3), and YAP/TAZ Luciferase reporter assay measuring YAP activity (mean ± SEM, n = 3) with the same treatment in the same cells as A. (C) Immunoblot showing phosphorylation of YAP after transient transfection of GαqQL and control expression vectors in HEK293 cells in combination with 1μM VS-4718 treatment. (D) Immunoblot showing phosphorylation of YAP after transient transfection of GαqQL and control expression vectors in HEK293 cells in combination with siRNA mediated FAK knockdown. (E) mRNA expression of *CTGF* and *CYR61* measured by qPCR with the same treatment in the same cells as D (mean ± SEM, n = 3). In all cases ** $p<0.01$; *** $p<0.001$.

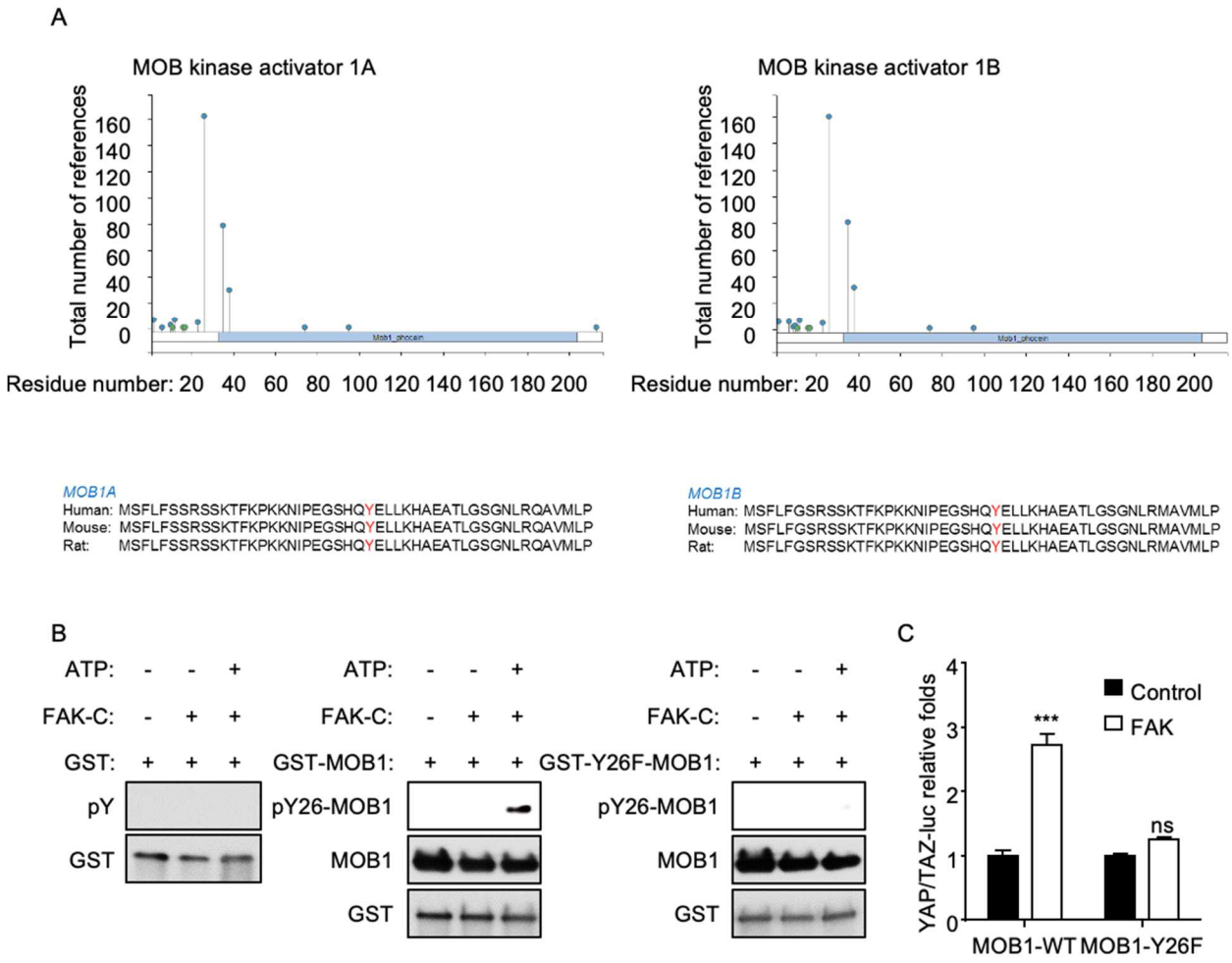

Figure S2.4

MOB1A and MOB1B phosphorylation sites from PhophoSitePlus (Cell Signaling Technology, https://www.phosphosite.org, top), and amino acid sequence of MOB1A and MOB1B from human, mouse and rat including tyrosine 26 (Y, red) site (bottom). (B) Y26 phosphorylation of GST-MOB1 or GST-Y26F-MOB1 (GST used as control) after in vitro kinase reaction using active recombinant human FAK (catalytic domain, FAK-C). (C) YAP/TAZ Luciferase reporter assay after transient transfection of HA-MOB1 or HA-MOB-Y26F, with or without FAK transfection in HEK293 cells (mean ± SEM, n = 3; *** $p<0.001$; ns: not significant).

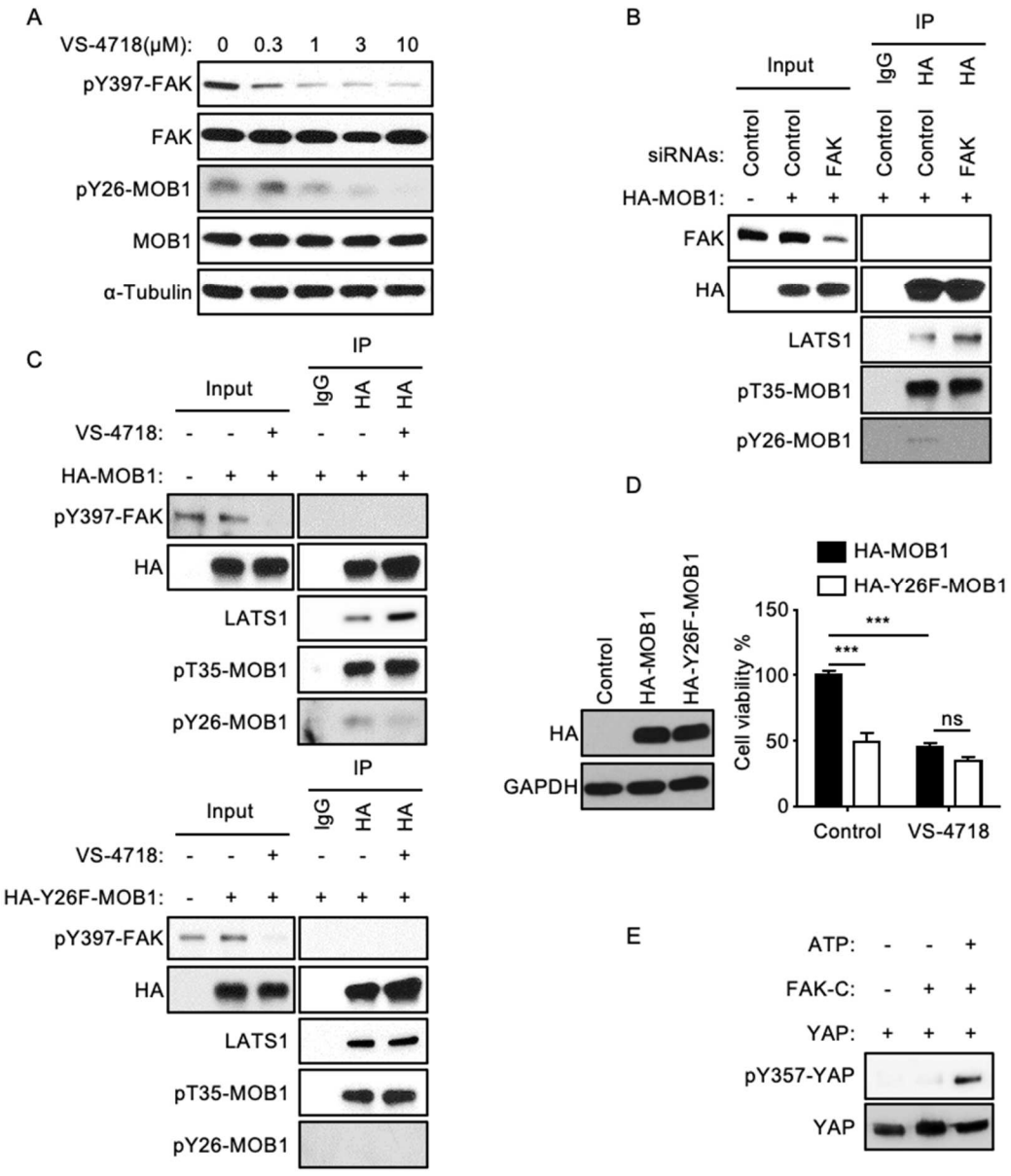

Figure S2.5

(A) Immunoblot showing pY397-FAK and pY26-MOB1 with 2 hr treatment of VS-4718 at different doses in OMM1.3 cells (0-10 μM). (B) Immunoblot showing phosphorylation of HA-MOB1 and association with LATS1 after HA immunoprecipitation in OMM1.3 cells with siRNA mediated FAK knockdown. (C) Immunoblot showing phosphorylation of HA-MOB1 or HA-MOB1-Y26F and association with LATS1 after HA immunoprecipitation in OMM1.3 cells with or without VS-4718 treatment (1 μM, 2 hr). (D) Immunoblot showing HA-MOB1 and HA-Y26F-MOB1 expression in OMM1.3 (left), HA-Y26F-MOB1 expressing OMM1.3 cells phenocopy the effect of VS-4718 treatment in HA-MOB1 expressing OMM1.3 cells measured by cell viability assay (right, mean ± SEM, n = 3; *** $p<0.001$; ns: not significant). (E) Immunoblot showing YAP phosphorylation after *in vitro* kinase reaction with active recombinant human FAK (catalytic domain, FAK-C).

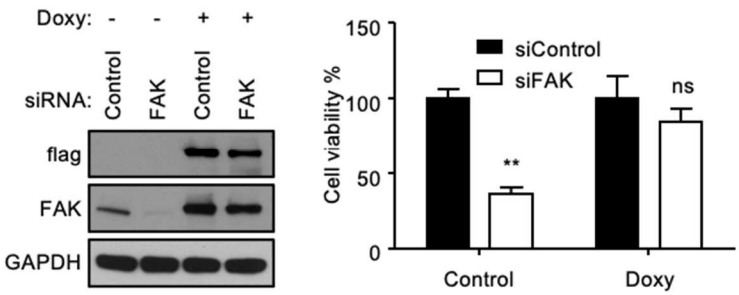

Figure S2.6

Immunoblot showing siRNA mediated FAK knockdown and doxycycline-induced FAK re-expression in OMM1.3 cells (left). Impact of siRNA mediated knockdown and doxycycline-induced FAK re-expression in OMM1.3 cells as measured by cell viability assay (right, mean ± SEM, n = 3; ** $p < 0.01$; ns: not significant).

2.5 Materials and Methods

RESOURCES

REAGENT or RESOURCE	SOURCE	IDENTIFIER
Antibodies		
YAP	Cell Signaling Technology, MA	14074
pS127-YAP	Cell Signaling Technology, MA	4911
pS909-LATS1	Cell Signaling Technology, MA	9157
pT1079-LATS1	Cell Signaling Technology, MA	8654
LATS1	Cell Signaling Technology, MA	3477
p-MST1/MST2	Cell Signaling Technology, MA	3681
MST1	Cell Signaling Technology, MA	3682
GAPDH(14C10)	Cell Signaling Technology, MA	2118
α-Tubulin	Cell Signaling Technology, MA	3873
pY	Cell Signaling Technology, MA	9411
HA-tag-HRP	Cell Signaling Technology, MA	2999
HA-tag	Cell Signaling Technology, MA	3724
myc-tag	Cell Signaling Technology, MA	2278
pY397-FAK	Cell Signaling Technology, MA	8556
FAK	Cell Signaling Technology, MA	3285
cleaved PARP	Cell Signaling Technology, MA	9541
p-ERK1/2	Cell Signaling Technology, MA	4370
ERK1/2	Cell Signaling Technology, MA	4696
MOB1	Cell Signaling Technology, MA	13730
pT35-MOB1	Cell Signaling Technology, MA	8699
Gαq(E-17)	Santa Cruz Biotech., CA	sc-393
FAK(C-20)	Santa Cruz Biotech., CA	sc-558

RhoA	Cell Signaling Technology, MA	2117
TRIO(H120)	Santa Cruz Biotech., CA	sc-28564
Rac1	BD Biosciences, CA	610651
pY357-YAP	Abcam, MA	ab62751
LATS2	Bethyl Laboratories, TX	A300-479A
pY26-MOB1A	Signalway Antibody, MA	12878
flag-tag-HRP	Sigma-Aldrich, MO	A8592
Ki67	DAKO, CA	M724029-2
Bacterial strains		
DH5alpha Competent E. coli	BioPioneer, CA	GACC-96
Stbl3 Competent E. coli	Thermo Fisher	C737303
siRNAs		
Non-targeting	Dharmacon, CO	D-001810-0X
Gαq	Sigma-Aldrich, MO	SASI_Hs01_00231793
FAK	Thermo Fisher, MA	s11485
AKT1	Thermo Fisher, MA	s659
MGLL	Thermo Fisher, MA	s22380
MTHFD1	Thermo Fisher, MA	s9032
CDK1	Thermo Fisher, MA	s464
SIRT1	Thermo Fisher, MA	s223591
PSMB5	Thermo Fisher, MA	s11354
TRIO	Dharmacon, CO	L-005047-00-0005
RhoA	Dharmacon, CO	L-003860-00-0005
Rac1	Dharmacon, CO	L-003560-00-0005
LATS1	Sigma-Aldrich, MO	Hs01_00046128
LATS2	Sigma-Aldrich, MO	Hs01_00158803
DNAs		
pCMV-myc-MST1	Addgene	8847

pCMV2-FLAG-SAV1	Addgene	18970
pcDNA3-HA-MOB1	Addgene	32835
pcDNA3-HA-Y26F-MOB1	Generated in-lab	NA
pLENTi-HA-MOB1	Generated in-lab	NA
pLENTi-HA-Y26F-MOB1	Generated in-lab	NA
pGEX-HA-MOB1	Generated in-lab	NA
pGEX-HA-Y26F-MOB1	Generated in-lab	NA
pLVX-TetOne-FLAG-FAK	Generated in-lab	NA
p2xFLAG-CMV2-LATS1	Addgene	18971
8xGTIIC-luciferase	Addgene	34615
REAGENT		
alamarBlue™ Reagent	Grand Island, NY	DAL1100
FAK Kinase Enzyme System	Promega	V1971
YAP1 Recombinant Protein	Abnova	H00010413-P01
Glutathione Sepharose 4B	GE Healthcare	17-0756-01
N/C Extraction Reagents	ThermoFisher	78833
U73122	Sigma-Aldrich, MO	U6756
GF109203X	Sigma-Aldrich, MO	G2911
Clozapine N-oxide (CNO)	Sigma-Aldrich, MO	C0832
VS-4718 (PND-1186)	MedChemExpress	HY-13917
Blebbistatin	Sigma-Aldrich, MO	B0560
Y-27632	Sigma-Aldrich, MO	SCM075
Software and Database		
ISLE	Lee et al 2018	https://www.github.com/jooslee/ISLE
PhosphoSitePlus	Cell signaling technology, MA	
Primers		

Y26F-MOB1-F	Integrated DNA Technologies	CATGTTTTAAGAGTTCAAACTGAT
(For point mutation)		GAGATCCTTCAGGGATATTCTTC
Y26F-MOB1-R	Integrated DNA Technologies	GAAGAATATCCCTGAAGGATCTC
(For point mutation)		ATCAGTTTGAACTCTTAAAACATG
GAPDH-F	Integrated DNA Technologies	GAGTCAACGGATTTGGTCGT
GAPDH-R	Integrated DNA Technologies	TTGATTTTGGAGGGATCTCG
CTGF-F	Integrated DNA Technologies	GTTTGGCCCAGACCCAACTA
CTGF-R	Integrated DNA Technologies	GGCTCTGCTTCTCTAGCCTG
CYR61-F	Integrated DNA Technologies	CAGGACTGTGAAGATGCGGT
CYR61-R	Integrated DNA Technologies	GCCTGTAGAAGGGAAACGCT

EXPERIMENTAL MODEL AND SUBJECT DETAILS

Human tumors xenografts and VS-4718 in vivo treatment

All animal studies were carried out according the University of California San Diego (UCSD) Institutional Animal Care and Use Committee (IACUC)-approved protocol (S15195). Female NOD.Cg-Prkdcscid Il2rgtm1wjl/SzJ mice (commonly known as NOD scid gamma, Jackson Laboratory, Maine), 6 to 8 weeks of age and weighing 18 to 20 g, were used in the study of UM cells, housed in appropriate sterile filter-capped cages, and provided food and water ad libitum. All procedures were essentially as previously described (86,88,107). Briefly, exponentially growing cultures were harvested, washed, resuspended in RPMI 1640, and 2 x 10^6 viable cells were transplanted subcutaneously into the flanks of mice. For tumor growth analysis, tumor volume was assessed as [($LW^2/2$); where L and W represent the length and the width of the tumor]. The animals were monitored twice weekly for tumor development. Results of animal experiments were expressed as mean ± SEM of a total of tumors analyzed. To administer VS-4718 (Verastem Oncology; Needham, MA) to mice, 10 mg/ml VS-4718 was prepared in 0.5% carboxymethyl cellulose (CMC) (C5678, Sigma-Aldrich; St. Louis, MO) 0.1% Tween 80 (P1754,

Sigma Aldrich; St. Louis, MO) in sterile water, 100 mg/kg administered via oral gavage twice daily, control group was treated with vehicle.

Cell lines, culture procedures and chemicals

HEK293 and HEK293T cells were cultured in DMEM (Sigma-Aldrich Inc., MO) containing 10% FBS (Sigma-Aldrich Inc., MO) and 1× antibiotic/antimycotic solution (Sigma-Aldrich Inc., MO). Culture conditions for UM cells (OMM1.3, OMM1.5, MEL202, Mel270 and 92.1) have been described elsewhere (Schmitt et al., 2007; Zuidervaart et al., 2005). SK-MEL-28 cells were purchased from ATCC and cultured following ATCC recommendations in EMEM containing 10% FBS. VS-4718 (PND-1186) was purchased from MedChemExpress (MCE) pre-prepared as a 10mM solution in DMSO. FR900359 (FR) was prepared in the lab of Dr. Evi Kostenis. Clozapine N-oxide (CNO), GF109203X, U73122, Blebbistatin, and Y-27632 were all purchased from Sigma-Aldrich Inc. (MO) and used at concentrations indicated in figure legends.

DNA constructs

Plasmids pCEFL-HA, pCEFL-HA-GαqQL, pCEFL-HA-Gαq-DREADD, pCEFL-3x-Flag-Renilla-luciferase were described previously (129,130). pCEFL-myr-FAK was described previously (131,132). Plasmids pCMV-myc-MST1 (Addgene #8847, originally from Joseph Avruch's lab), pCMV2-FLAG-SAV1 (Addgene #18970, originally from Marius Sudol' lab), pcDNA3-HA-MOB1 (Addgene #32835, originally from Kunliang Guan's lab), p2xFLAG-CMV2-LATS1 (Addgene #18971, originally from Marius Sudol's lab) and 8xGTIIC-luciferase (Addgene #34615, originally from Stefano Piccolo's Lab).

METHOD DETAILS

Bioinformatic analysis (Identifying clinically-relevant Gαq-specific vulnerabilities of UM):

To identify the clinically-relevant vulnerabilities for UM, we performed an analysis that follows the main concepts of our previous work, ISLE (103) with modifications for Gαq-driven UM. We analyzed the cancer genome atlas (TCGA) (23) UM samples with skin cutaneous melanoma (SKCM) samples as control together with the large-scale functional (133-136) and drug response

(137-139) screens. We downloaded the gene expression, copy number alteration, and patient survival and other clinical characteristics of TCGA UM and SKCM cohort from cBioPortal (96) on Feb 1, 2017. We used 80 UM samples and 287 SKCM samples for our analysis. We obtained the data from cBioPortal as it integrates the mutation analysis from different TCGA centers to avoid center specific bias in mutation calls.

We denoted a tumor sample as $G\alpha q^{+}$ if any of the Gαq-family genes (*GNAQ*, *GNA11* and *CYSLTR2*) are either mutated or amplified in the given sample (amplification, if the Gistic score is greater than 0.35), and as $G\alpha q^{-}$ if the sample lacks *GNAQ*, *GNA11* and *CYSLTR2* genes mutation and amplification. First, we selected important genes in UM, that are (i) highly over expressed in $G\alpha q^{+}$ UM (n=77, excluding 3 $G\alpha q^{-}$ cases) with respect to control $G\alpha q^{-}$ SKCM TCGA samples (n=209) using Wilcoxon rank sum test ($p<0.05$). We filtered out (ii) those genes that are overexpressed in UM compared to all SKCM samples irrespective of Gαq status (Wilcoxon rank sum $p>0.05$), leading to 1,146 out of total 18,087 satisfying both conditions. We tested whether these genes show significant overlap with the genes overexpressed in $G\alpha q^{+}$ skin melanoma TCGA samples (n=78, mutation=16, amplification=65, overlap=13) compared to $G\alpha q^{-}$ SKCM samples using hypergeometric test, truncating the hypergeometric p values to 10^{-16}.

Second, we further selected the genes whose inactivation leads to better patient survival in UM, thus potential target of a therapy. We used a stratified Cox proportional hazard model to evaluate the association, while controlling for available potential confounders in the dataset including patients' sex and tumor stage (140). The inactivation of 293 genes (out of 1,146 genes that passed the previous screen) show significant association with improved patient survival.

Third, we used gene essentiality (133-136) and drug response screens (137-139) in a wide panel of cancer cell lines to identify the genes whose knockdown/inhibition specifically reduces $G\alpha q^{+}$ cell viability. We used the mutation and copy number data from the measurements on the cell lines in CCLE collection (138) to determine the status of Gαq-family genes in these cell lines. We performed Wilcoxon rank sum test between the essentiality or drug response values between the

cell lines that are Gαq^{+} *vs.* Gαq-. The essentiality or the drug inhibition identified 72 genes out of 293 genes (that passed the 2nd filter) that satisfy this condition.

Finally, we prioritized the druggable targets. We collected the druggable genome using the drug-to-target mapping curated in DrugBank database (141) and the literature including (96,137-139,142,143). Our collection encompasses 756 targetable genes, including 273 targets of FDA-approved drugs, 10 targets of drugs under clinical trials, and 473 experimental drugs. We further removed the genes that belong to the same chromosomes to the Gαq-family genes to avoid the confounding effect of genomic linkage. This step led to the final set of 7 targets.

Immunoblot assay

Western blot assays were performed as described previously (88). Western blots were developed using Immobilon Western Chemiluminescent HRP substrate (Millipore, MA) according to the manufacturer's instructions.

CRISPR-Cas9-knockout

PTK2-sgRNA-CRISPR/Cas9-all-in-one-lentivector vector was purchased from Applied Biological Materials Inc. (Cat. K1752206). Lentivirus were prepared with HEK293T cells as the packaging cells as previously reported (Basile et al., 2004). To establish *PTK2*-knock out, cells were infected with the corresponding lentiviral supernatants for 16 hours, after which the media was changed to normal growth medium containing puromycin (Sigma-Aldrich Inc., MO) selection.

siRNAs transfection

All cells were transfected using Lipofectamine® RNAiMAX Reagent (Thermo Fisher Scientific) according to manufacturer’s instructions.

MOB1-Y26F point mutation

MOB1-Y26F point mutant was generated using the Quickchange Site-Directed Mutagenesis kit following manufacturer's instructions (Agilent Genomics, CA). pcDNA3-HA-MOB1 was used as the template and see the primers in the Key Resource Table.

Immunofluorescence

Cells cultured on coverslips were washed with PBS, fixed with 3.7% formaldehyde in phosphate-buffered saline (PBS) for 30 min, and permeabilized using 0.05% Triton X-100 for 10 min. Fixed cells were blocked with 3% FBS-containing PBS for 30 min, and incubated with YAP (Cell signaling technology, MI) antibody (in 3% FBS-PBS otherwise stated) for 1 hr at room temperature. The reaction was visualized with Alexa-labeled secondary antibodies (Invitrogen, CA). Samples were mounted in PBS buffer containing Hoechst 33342 (Molecular Probes, OR) for nuclear staining. Images were acquired with an Axio Imager Z1 microscope equipped with ApoTome system controlled by ZEN 2012 software (Carl Zeiss, NY).

Luciferase assays

Cells were co-transfected with pCEFL-3x-Flag-Renilla-luciferase and 8xGTIIC-luciferase (Addgene 34615) in 6-well plates overnight to the detection of the luciferase activity, using a Dual-Glo Luciferase Assay Kit (Promega, WI) and a Microtiter plate luminometer (Dynex Tech., VA).

Immunohistochemistry

The following antibodies were used for immunohistochemistry anti-Ki67 (DAKO) and anti-YAP (CST). Unstained 5 μm paraffin sections were dewaxed in Safeclear II (Fisher Scientific, PA), hydrated through graded alcohols and distilled water, and washed three times with PBS. Antigens were retrieved using or 10 mM citrate buffer boiled in a microwave for 20 min (2 min at 100% power and 18 min at 10% power). The slides were allowed to cool down for 30 min at room temperature, rinsed twice with PBS, incubated in 3% hydrogen peroxide in PBS for 10 min to

quench the endogenous peroxidase. The sections were then sequentially washed in distilled water and PBS, incubated in blocking solution (2.5% bovine serum albumin in PBS) for 30 min at room temperature. Excess solution was discarded and the primary antibodies were applied diluted in blocking solution at 4 °C overnight. After washing with PBS, the slides were sequentially incubated with the biotinylated secondary antibody (1:400) (Vector Laboratories, CA) for 30 min and with the avidin-biotin complex, reconstituted according to the instruction of the manufacturer in PBS (Vector Stain Elite, ABC kit) (Vector Laboratories, CA), for 30 min at room temperature. The slides were developed in 3,3-diaminobenzidine (Sigma FASTDAB tablet) (Sigma Chemical, MO) diluted in distilled water under a microscope.

Immunoprecipitation

Cells were lysed with IP lysis buffer [10 mM Tris-Cl (pH 8.0), 150 mM NaCl, 1 mM EDTA, 0.3% CHAPS, 50 mM NaF, 1.5 mM Na_3VO4, protease inhibitor (Thermo Scientific, CO), 1 mM DTT, 1 mM PMSF], and centrifuged at 16,000 g for 5 min at 4 °C. Supernatants were incubated with first antibody for 1 hr at 4 °C, and protein G or protein A conjugated resin for another 1 hr. Resins were then washed 3 times with lysis buffer and boiled in SDS-loading buffer.

Cell growth assays

Cell growth assays were performed as described previously (144). Cells were cultured in 96-well-plate and treated with drugs for 72 hr. The manufacturer's instructions of Alamar Blue Cell Viability Reagent were followed to complete the assay.

3D cell culture

3-dimensional cultures were performed as described previously (145). Briefly, 10,000 cells were embedded in 1% methylcellulose diluted in growth media and plated onto 6-well poly-hydroxyethyl methacrylic acid (poly-HEMA)-coated plates.

Generation of GST-MOB fusion proteins

GST fusion proteins were prepared engineered, expressed in bacteria, and purified as previously described in (125) using standard procedures.

In vitro FAK kinase assay

Kinase reactions were performed as previously described in Bernard-Trifilo et al. Briefly, 1.5 µg of substrate (MOB1-GST, MOB1-Y26F-GST, GST-only control, or recombinant YAP) was resuspended in 40uL FAK Kinase buffer (20 mM HEPES pH 7.4, 10% glycerol, 10 mM $MgCl_2$, 10 mM $MnCl_2$, and 150 mM NaCl). 5 µL magnesium/ATP cocktail (75 mM $MgCl_2$, 20 mM MOPS pH 7.2, 25 mM β-glycerol phosphate, 5 mM EGTA, 1 mM sodium orthovanadate, 1 mM dithiothreitol) with or without 50 µM ATP was added to appropriate tubes, and placed in 32° water bath for 15 min. Samples were boiled in sample buffer and processed on SDS-PAGE.

Nuclear and Cytoplasm Extraction

Subcellular fractionated lysates were generated using NE-PER Nuclear and Cytoplasmic Extraction Reagents (Thermo Scientific, CO) following manufacturer instructions.

Statistical analysis

All data analysis was performed using GraphPad Prism version 7.03 for Windows (GraphPad Software, CA). The data were analyzed by ANOVA test or t-test (* $p<0.05$, ** $p<0.01$, *** $p< 0.001$).

2.6 Acknowledgements

Chapter 2, in full, has been accepted for publication of the material in “A Platform of Synthetic Lethal Gene Interaction Networks Reveals that the GNAQ Uveal Melanoma Oncogene Controls the Hippo Pathway through FAK”, in *Cancer Cell*, 2019. Feng, Xiaodong; Arang, Nadia; Rigiracciolo, Damiano Cosimo; Lee, Joo Sang; Yeerna, Huwate; Wang, Zhiyong; Lubrano,

Simone; Kishore, Ayush; Pachter, Jonathan; Konig, Gabriele M; Maggiolini, Marcello; Kostenis, Evi, Schlaepfer, David D; Tamayo, Pablo; Chen, Qianming; Ruppin, Eytan; Gutkind, J Silvio. The dissertation author was the primary investigator and author of this paper.

2.7 References

1. Fredriksson, R., Lagerstrom, M. C., Lundin, L. G., and Schioth, H. B. (2003) The G-protein-coupled receptors in the human genome form five main families. Phylogenetic analysis, paralogon groups, and fingerprints. *Mol Pharmacol* **63**, 1256-1272
2. Pierce, K. L., Premont, R. T., and Lefkowitz, R. J. (2002) Seven-transmembrane receptors. *Nat Rev Mol Cell Biol* **3**, 639-650
3. Milligan, G., and Kostenis, E. (2006) Heterotrimeric G-proteins: a short history. *Br J Pharmacol* **147 Suppl 1**, S46-55
4. Dorsam, R. T., and Gutkind, J. S. (2007) G-protein-coupled receptors and cancer. *Nat Rev Cancer* **7**, 79-94
5. Rosenbaum, D. M., Rasmussen, S. G., and Kobilka, B. K. (2009) The structure and function of G-protein-coupled receptors. *Nature* **459**, 356-363
6. Sassone-Corsi, P. (2012) The cyclic AMP pathway. *Cold Spring Harbor perspectives in biology* **4**
7. Howe, A. K. (2011) Cross-talk between calcium and protein kinase A in the regulation of cell migration. *Curr Opin Cell Biol* **23**, 554-561
8. Prevarskaya, N., Skryma, R., and Shuba, Y. (2011) Calcium in tumour metastasis: new roles for known actors. *Nat Rev Cancer* **11**, 609-618
9. Griner, E. M., and Kazanietz, M. G. (2007) Protein kinase C and other diacylglycerol effectors in cancer. *Nat Rev Cancer* **7**, 281-294
10. Newton, A. C. (2010) Protein kinase C: poised to signal. *Am J Physiol Endocrinol Metab* **298**, E395-402
11. Rozengurt, E. (2007) Mitogenic signaling pathways induced by G protein-coupled receptors. *J Cell Physiol* **213**, 589-602
12. Gutkind, J. S. (1998) The pathways connecting G protein-coupled receptors to the nucleus through divergent mitogen-activated protein kinase cascades. *J Biol Chem* **273**, 1839-1842
13. Gutkind, J. S., and Kostenis, E. (2018) Arrestins as rheostats of GPCR signalling. *Nat Rev Mol Cell Biol* **19**, 615-616
14. Weis, W. I., and Kobilka, B. K. (2018) The Molecular Basis of G Protein-Coupled Receptor Activation. *Annual review of biochemistry* **87**, 897-919
15. Hauser, A. S., Chavali, S., Masuho, I., Jahn, L. J., Martemyanov, K. A., Gloriam, D. E., and Babu, M. M. (2018) Pharmacogenomics of GPCR Drug Targets. *Cell* **172**, 41-54 e19
16. Santos, R., Ursu, O., Gaulton, A., Bento, A. P., Donadi, R. S., Bologa, C. G., Karlsson, A., Al-Lazikani, B., Hersey, A., Oprea, T. I., and Overington, J. P. (2017) A comprehensive map of molecular drug targets. *Nat Rev Drug Discov* **16**, 19-34
17. Hauser, A. S., Attwood, M. M., Rask-Andersen, M., Schioth, H. B., and Gloriam, D. E. (2017) Trends in GPCR drug discovery: new agents, targets and indications. *Nat Rev Drug Discov* **16**, 829-842
18. Young, D., Waitches, G., Birchmeier, C., Fasano, O., and Wigler, M. (1986) Isolation and characterization of a new cellular oncogene encoding a protein with multiple potential transmembrane domains. *Cell* **45**, 711-719

19. Julius, D., Livelli, T. J., Jessell, T. M., and Axel, R. (1989) Ectopic expression of the serotonin 1c receptor and the triggering of malignant transformation. *Science* **244**, 1057-1062
20. Gutkind, J. S., Novotny, E. A., Brann, M. R., and Robbins, K. C. (1991) Muscarinic acetylcholine receptor subtypes as agonist-dependent oncogenes. *Proc Natl Acad Sci U S A* **88**, 4703-4707
21. Allen, L. F., Lefkowitz, R. J., Caron, M. G., and Cotecchia, S. (1991) G-protein-coupled receptor genes as protooncogenes: constitutively activating mutation of the alpha 1B-adrenergic receptor enhances mitogenesis and tumorigenicity. *Proc Natl Acad Sci U S A* **88**, 11354-11358
22. O'Hayre, M., Vazquez-Prado, J., Kufareva, I., Stawiski, E. W., Handel, T. M., Seshagiri, S., and Gutkind, J. S. (2013) The emerging mutational landscape of G proteins and G-protein-coupled receptors in cancer. *Nat Rev Cancer* **13**, 412-424
23. Cancer Genome Atlas Research, N., Weinstein, J. N., Collisson, E. A., Mills, G. B., Shaw, K. R., Ozenberger, B. A., Ellrott, K., Shmulevich, I., Sander, C., and Stuart, J. M. (2013) The Cancer Genome Atlas Pan-Cancer analysis project. *Nat Genet* **45**, 1113-1120
24. Tate, J. G., Bamford, S., Jubb, H. C., Sondka, Z., Beare, D. M., Bindal, N., Boutselakis, H., Cole, C. G., Creatore, C., Dawson, E., Fish, P., Harsha, B., Hathaway, C., Jupe, S. C., Kok, C. Y., Noble, K., Ponting, L., Ramshaw, C. C., Rye, C. E., Speedy, H. E., Stefancsik, R., Thompson, S. L., Wang, S., Ward, S., Campbell, P. J., and Forbes, S. A. (2019) COSMIC: the Catalogue Of Somatic Mutations In Cancer. *Nucleic Acids Res* **47**, D941-D947
25. Kan, Z., Jaiswal, B. S., Stinson, J., Janakiraman, V., Bhatt, D., Stern, H. M., Yue, P., Haverty, P. M., Bourgon, R., Zheng, J., Moorhead, M., Chaudhuri, S., Tomsho, L. P., Peters, B. A., Pujara, K., Cordes, S., Davis, D. P., Carlton, V. E., Yuan, W., Li, L., Wang, W., Eigenbrot, C., Kaminker, J. S., Eberhard, D. A., Waring, P., Schuster, S. C., Modrusan, Z., Zhang, Z., Stokoe, D., de Sauvage, F. J., Faham, M., and Seshagiri, S. (2010) Diverse somatic mutation patterns and pathway alterations in human cancers. *Nature* **466**, 869-873
26. Wu, V., Yeerna, H., Nohata, N., Chiou, J., Harismendy, O., Raimondi, F., Inoue, A., Russell, R. B., Tamayo, P., and Gutkind, J. S. (2019) Illuminating the Onco-GPCRome: Novel G protein-coupled receptor-driven oncocrine networks and targets for cancer immunotherapy. *J Biol Chem* **294**, 11062-11086
27. Raimondi, F., Inoue, A., Kadji, F. M. N., Shuai, N., Gonzalez, J. C., Singh, G., de la Vega, A. A., Sotillo, R., Fischer, B., Aoki, J., Gutkind, J. S., and Russell, R. B. (2019) Rare, functional, somatic variants in gene families linked to cancer genes: GPCR signaling as a paradigm. *Oncogene* **38**, 6491-6506
28. Bjarnadottir, T. K., Fredriksson, R., and Schioth, H. B. (2007) The adhesion GPCRs: a unique family of G protein-coupled receptors with important roles in both central and peripheral tissues. *Cell Mol Life Sci* **64**, 2104-2119
29. Gad, A. A., and Balenga, N. (2020) The Emerging Role of Adhesion GPCRs in Cancer. *ACS Pharmacol Transl Sci* **3**, 29-42
30. Aust, G., Zhu, D., Van Meir, E. G., and Xu, L. (2016) Adhesion GPCRs in Tumorigenesis. *Handb Exp Pharmacol* **234**, 369-396
31. Hoang-Vu, C., Bull, K., Schwarz, I., Krause, G., Schmutzler, C., Aust, G., Kohrle, J., and Dralle, H. (1999) Regulation of CD97 protein in thyroid carcinoma. *The Journal of clinical endocrinology and metabolism* **84**, 1104-1109
32. Aust, G., Eichler, W., Laue, S., Lehmann, I., Heldin, N. E., Lotz, O., Scherbaum, W. A., Dralle, H., and Hoang-Vu, C. (1997) CD97: a dedifferentiation marker in human thyroid carcinomas. *Cancer Res* **57**, 1798-1806

33. Aust, G., Steinert, M., Schutz, A., Boltze, C., Wahlbuhl, M., Hamann, J., and Wobus, M. (2002) CD97, but not its closely related EGF-TM7 family member EMR2, is expressed on gastric, pancreatic, and esophageal carcinomas. *Am J Clin Pathol* **118**, 699-707
34. Bayin, N. S., Frenster, J. D., Kane, J. R., Rubenstein, J., Modrek, A. S., Baitalmal, R., Dolgalev, I., Rudzenski, K., Scarabottolo, L., Crespi, D., Redaelli, L., Snuderl, M., Golfinos, J. G., Doyle, W., Pacione, D., Parker, E. C., Chi, A. S., Heguy, A., MacNeil, D. J., Shohdy, N., Zagzag, D., and Placantonakis, D. G. (2016) GPR133 (ADGRD1), an adhesion G-protein-coupled receptor, is necessary for glioblastoma growth. *Oncogenesis* **5**, e263
35. Arrillaga-Romany, I., Chi, A. S., Allen, J. E., Oster, W., Wen, P. Y., and Batchelor, T. T. (2017) A phase 2 study of the first imipridone ONC201, a selective DRD2 antagonist for oncology, administered every three weeks in recurrent glioblastoma. *Oncotarget* **8**, 79298-79304
36. Kline, C. L. B., Ralff, M. D., Lulla, A. R., Wagner, J. M., Abbosh, P. H., Dicker, D. T., Allen, J. E., and El-Deiry, W. S. (2018) Role of Dopamine Receptors in the Anticancer Activity of ONC201. *Neoplasia* **20**, 80-91
37. Teh, J., and Chen, S. (2012) mGlu Receptors and Cancerous Growth. *Wiley Interdiscip Rev Membr Transp Signal* **1**, 211-220
38. Stepulak, A., Luksch, H., Gebhardt, C., Uckermann, O., Marzahn, J., Sifringer, M., Rzeski, W., Staufner, C., Brocke, K. S., Turski, L., and Ikonomidou, C. (2009) Expression of glutamate receptor subunits in human cancers. *Histochem Cell Biol* **132**, 435-445
39. Prickett, T. D., Wei, X., Cardenas-Navia, I., Teer, J. K., Lin, J. C., Walia, V., Gartner, J., Jiang, J., Cherukuri, P. F., Molinolo, A., Davies, M. A., Gershenwald, J. E., Stemke-Hale, K., Rosenberg, S. A., Margulies, E. H., and Samuels, Y. (2011) Exon capture analysis of G protein-coupled receptors identifies activating mutations in GRM3 in melanoma. *Nat Genet* **43**, 1119-1126
40. Pollock, P. M., Cohen-Solal, K., Sood, R., Namkoong, J., Martino, J. J., Koganti, A., Zhu, H., Robbins, C., Makalowska, I., Shin, S. S., Marin, Y., Roberts, K. G., Yudt, L. M., Chen, A., Cheng, J., Incao, A., Pinkett, H. W., Graham, C. L., Dunn, K., Crespo-Carbone, S. M., Mackason, K. R., Ryan, K. B., Sinsimer, D., Goydos, J., Reuhl, K. R., Eckhaus, M., Meltzer, P. S., Pavan, W. J., Trent, J. M., and Chen, S. (2003) Melanoma mouse model implicates metabotropic glutamate signaling in melanocytic neoplasia. *Nat Genet* **34**, 108-112
41. Choi, K. Y., Chang, K., Pickel, J. M., Badger, J. D., 2nd, and Roche, K. W. (2011) Expression of the metabotropic glutamate receptor 5 (mGluR5) induces melanoma in transgenic mice. *Proc Natl Acad Sci U S A* **108**, 15219-15224
42. Shin, S. S., Namkoong, J., Wall, B. A., Gleason, R., Lee, H. J., and Chen, S. (2008) Oncogenic activities of metabotropic glutamate receptor 1 (Grm1) in melanocyte transformation. *Pigment Cell Melanoma Res* **21**, 368-378
43. Brown, T. P., and Ganapathy, V. (2020) Lactate/GPR81 signaling and proton motive force in cancer: Role in angiogenesis, immune escape, nutrition, and Warburg phenomenon. *Pharmacology & therapeutics* **206**, 107451
44. Roland, C. L., Arumugam, T., Deng, D., Liu, S. H., Philip, B., Gomez, S., Burns, W. R., Ramachandran, V., Wang, H., Cruz-Monserrate, Z., and Logsdon, C. D. (2014) Cell surface lactate receptor GPR81 is crucial for cancer cell survival. *Cancer Res* **74**, 5301-5310
45. Mu, X., Zhao, T., Xu, C., Shi, W., Geng, B., Shen, J., Zhang, C., Pan, J., Yang, J., Hu, S., Lv, Y., Wen, H., and You, Q. (2017) Oncometabolite succinate promotes angiogenesis by upregulating VEGF expression through GPR91-mediated STAT3 and ERK activation. *Oncotarget* **8**, 13174-13185

46. Ryan, D. G., Murphy, M. P., Frezza, C., Prag, H. A., Chouchani, E. T., O'Neill, L. A., and Mills, E. L. (2019) Coupling Krebs cycle metabolites to signalling in immunity and cancer. *Nat Metab* **1**, 16-33
47. Wu, J. Y., Huang, T. W., Hsieh, Y. T., Wang, Y. F., Yen, C. C., Lee, G. L., Yeh, C. C., Peng, Y. J., Kuo, Y. Y., Wen, H. T., Lin, H. C., Hsiao, C. W., Wu, K. K., Kung, H. J., Hsu, Y. J., and Kuo, C. C. (2020) Cancer-Derived Succinate Promotes Macrophage Polarization and Cancer Metastasis via Succinate Receptor. *Mol Cell* **77**, 213-227 e215
48. Kleinau, G., Neumann, S., Gruters, A., Krude, H., and Biebermann, H. (2013) Novel insights on thyroid-stimulating hormone receptor signal transduction. *Endocr Rev* **34**, 691-724
49. Parma, J., Duprez, L., Van Sande, J., Cochaux, P., Gervy, C., Mockel, J., Dumont, J., and Vassart, G. (1993) Somatic mutations in the thyrotropin receptor gene cause hyperfunctioning thyroid adenomas *Nature* **365**, 649-651
50. Rodien, P., Ho, S. C., Vlaeminck, V., Vassart, G., and Costagliola, S. (2003) Activating mutations of TSH receptor. *Ann Endocrinol (Paris)* **64**, 12-16
51. Kleinau, G., and Biebermann, H. (2014) Constitutive activities in the thyrotropin receptor: regulation and significance. *Adv Pharmacol* **70**, 81-119
52. Russo, D., Arturi, F., Schlumberger, M., Caillou, B., Monier, R., Filetti, S., and Suarez, H. G. (1995) Activating mutations of the TSH receptor in differentiated thyroid carcinomas. *Oncogene* **11**, 1907-1911
53. Tong, G. X., Mody, K., Wang, Z., Hamele-Bena, D., Nikiforova, M. N., and Nikiforov, Y. E. (2015) Mutations of TSHR and TP53 Genes in an Aggressive Clear Cell Follicular Carcinoma of the Thyroid. *Endocr Pathol* **26**, 315-319
54. Lee, R. T., Zhao, Z., and Ingham, P. W. (2016) Hedgehog signalling. *Development* **143**, 367-372
55. Lum, L., and Beachy, P. A. (2004) The Hedgehog response network: sensors, switches, and routers. *Science* **304**, 1755-1759
56. Iglesias-Bartolome, R., Torres, D., Marone, R., Feng, X., Martin, D., Simaan, M., Chen, M., Weinstein, L. S., Taylor, S. S., Molinolo, A. A., and Gutkind, J. S. (2015) Inactivation of a Galpha(s)-PKA tumour suppressor pathway in skin stem cells initiates basal-cell carcinogenesis. *Nature cell biology* **17**, 793-803
57. Xie, J., Murone, M., Luoh, S. M., Ryan, A., Gu, Q., Zhang, C., Bonifas, J. M., Lam, C. W., Hynes, M., Goddard, A., Rosenthal, A., Epstein, E. H., Jr., and de Sauvage, F. J. (1998) Activating Smoothened mutations in sporadic basal-cell carcinoma. *Nature* **391**, 90-92
58. Kasai, K., Takahashi, M., Osumi, N., Sinnarajah, S., Takeo, T., Ikeda, H., Kehrl, J. H., Itoh, G., and Arnheiter, H. (2004) The G12 family of heterotrimeric G proteins and Rho GTPase mediate Sonic hedgehog signalling. *Genes Cells* **9**, 49-58
59. Riobo, N. A., Saucy, B., Dilizio, C., and Manning, D. R. (2006) Activation of heterotrimeric G proteins by Smoothened. *Proc Natl Acad Sci U S A* **103**, 12607-12612
60. Villanueva, H., Visbal, A. P., Obeid, N. F., Ta, A. Q., Faruki, A. A., Wu, M. F., Hilsenbeck, S. G., Shaw, C. A., Yu, P., Plummer, N. W., Birnbaumer, L., and Lewis, M. T. (2015) An essential role for Galpha(i2) in Smoothened-stimulated epithelial cell proliferation in the mammary gland. *Science signaling* **8**, ra92
61. Nusse, R., and Clevers, H. (2017) Wnt/beta-Catenin Signaling, Disease, and Emerging Therapeutic Modalities. *Cell* **169**, 985-999
62. Segditsas, S., and Tomlinson, I. (2006) Colorectal cancer and genetic alterations in the Wnt pathway. *Oncogene* **25**, 7531-7537
63. Schulte, G., and Wright, S. C. (2018) Frizzleds as GPCRs - More Conventional Than We Thought! *Trends Pharmacol Sci* **39**, 828-842

64. Liu, X., Rubin, J. S., and Kimmel, A. R. (2005) Rapid, Wnt-induced changes in GSK3beta associations that regulate beta-catenin stabilization are mediated by Galpha proteins. *Curr Biol* **15**, 1989-1997
65. Arthofer, E., Hot, B., Petersen, J., Strakova, K., Jager, S., Grundmann, M., Kostenis, E., Gutkind, J. S., and Schulte, G. (2016) WNT Stimulation Dissociates a Frizzled 4 Inactive-State Complex with Galpha12/13. *Mol Pharmacol* **90**, 447-459
66. Liu, T., Liu, X., Wang, H., Moon, R. T., and Malbon, C. C. (1999) Activation of rat frizzled-1 promotes Wnt signaling and differentiation of mouse F9 teratocarcinoma cells via pathways that require Galpha(q) and Galpha(o) function. *J Biol Chem* **274**, 33539-33544
67. Green, J. A., Suzuki, K., Cho, B., Willison, L. D., Palmer, D., Allen, C. D., Schmidt, T. H., Xu, Y., Proia, R. L., Coughlin, S. R., and Cyster, J. G. (2011) The sphingosine 1-phosphate receptor S1P(2) maintains the homeostasis of germinal center B cells and promotes niche confinement. *Nat Immunol* **12**, 672-680
68. Mitra, D., Luo, X., Morgan, A., Wang, J., Hoang, M. P., Lo, J., Guerrero, C. R., Lennerz, J. K., Mihm, M. C., Wargo, J. A., Robinson, K. C., Devi, S. P., Vanover, J. C., D'Orazio, J. A., McMahon, M., Bosenberg, M. W., Haigis, K. M., Haber, D. A., Wang, Y., and Fisher, D. E. (2012) An ultraviolet-radiation-independent pathway to melanoma carcinogenesis in the red hair/fair skin background. *Nature* **491**, 449-453
69. Lee, J. H., Miele, M. E., Hicks, D. J., Phillips, K. K., Trent, J. M., Weissman, B. E., and Welch, D. R. (1996) KiSS-1, a novel human malignant melanoma metastasis-suppressor gene. *J Natl Cancer Inst* **88**, 1731-1737
70. Ohtaki, T., Shintani, Y., Honda, S., Matsumoto, H., Hori, A., Kanehashi, K., Terao, Y., Kumano, S., Takatsu, Y., Masuda, Y., Ishibashi, Y., Watanabe, T., Asada, M., Yamada, T., Suenaga, M., Kitada, C., Usuki, S., Kurokawa, T., Onda, H., Nishimura, O., and Fujino, M. (2001) Metastasis suppressor gene KiSS-1 encodes peptide ligand of a G-protein-coupled receptor. *Nature* **411**, 613-617
71. Singh, L. S., Berk, M., Oates, R., Zhao, Z., Tan, H., Jiang, Y., Zhou, A., Kirmani, K., Steinmetz, R., Lindner, D., and Xu, Y. (2007) Ovarian cancer G protein-coupled receptor 1, a new metastasis suppressor gene in prostate cancer. *J Natl Cancer Inst* **99**, 1313-1327
72. LaTulippe, E., Satagopan, J., Smith, A., Scher, H., Scardino, P., Reuter, V., and Gerald, W. L. (2002) Comprehensive gene expression analysis of prostate cancer reveals distinct transcriptional programs associated with metastatic disease. *Cancer Res* **62**, 4499-4506
73. Zhu, D., Hunter, S. B., Vertino, P. M., and Van Meir, E. G. (2011) Overexpression of MBD2 in glioblastoma maintains epigenetic silencing and inhibits the antiangiogenic function of the tumor suppressor gene BAI1. *Cancer Res* **71**, 5859-5870
74. Zhu, D., Osuka, S., Zhang, Z., Reichert, Z. R., Yang, L., Kanemura, Y., Jiang, Y., You, S., Zhang, H., Devi, N. S., Bhattacharya, D., Takano, S., Gillespie, G. Y., Macdonald, T., Tan, C., Nishikawa, R., Nelson, W. G., Olson, J. J., and Van Meir, E. G. (2018) BAI1 Suppresses Medulloblastoma Formation by Protecting p53 from Mdm2-Mediated Degradation. *Cancer Cell* **33**, 1004-1016 e1005
75. van Biesen, T., Luttrell, L. M., Hawes, B. E., and Lefkowitz, R. J. (1996) Mitogenic signaling via G protein-coupled receptors. *Endocr Rev* **17**, 698-714
76. Kalinec, G., Nazarali, A. J., Hermouet, S., Xu, N., and Gutkind, J. S. (1992) Mutated alpha subunit of the Gq protein induces malignant transformation in NIH 3T3 cells. *Mol Cell Biol* **12**, 4687-4693
77. Van Raamsdonk, C. D., Bezrookove, V., Green, G., Bauer, J., Gaugler, L., O'Brien, J. M., Simpson, E. M., Barsh, G. S., and Bastian, B. C. (2009) Frequent somatic mutations of GNAQ in uveal melanoma and blue naevi. *Nature* **457**, 599-602
78. Van Raamsdonk, C. D., Griewank, K. G., Crosby, M. B., Garrido, M. C., Vemula, S., Wiesner, T., Obenauf, A. C., Wackernagel, W., Green, G., Bouvier, N., Sozen, M. M.,

Baimukanova, G., Roy, R., Heguy, A., Dolgalev, I., Khanin, R., Busam, K., Speicher, M. R., O'Brien, J., and Bastian, B. C. (2010) Mutations in GNA11 in uveal melanoma. *The New England journal of medicine* **363**, 2191-2199

79. Ayturk, U. M., Couto, J. A., Hann, S., Mulliken, J. B., Williams, K. L., Huang, A. Y., Fishman, S. J., Boyd, T. K., Kozakewich, H. P., Bischoff, J., Greene, A. K., and Warman, M. L. (2016) Somatic Activating Mutations in GNAQ and GNA11 Are Associated with Congenital Hemangioma. *Am J Hum Genet* **98**, 789-795
80. Shirley, M. D., Tang, H., Gallione, C. J., Baugher, J. D., Frelin, L. P., Cohen, B., North, P. E., Marchuk, D. A., Comi, A. M., and Pevsner, J. (2013) Sturge-Weber syndrome and port-wine stains caused by somatic mutation in GNAQ. *The New England journal of medicine* **368**, 1971-1979
81. Kusters-Vandevelde, H. V., van Engen-van Grunsven, I. A., Kusters, B., van Dijk, M. R., Groenen, P. J., Wesseling, P., and Blokx, W. A. (2010) Improved discrimination of melanotic schwannoma from melanocytic lesions by combined morphological and GNAQ mutational analysis. *Acta Neuropathol* **120**, 755-764
82. Helgadottir, H., and Höiom, V. (2016) The genetics of uveal melanoma: current insights. in *Appl Clin Genet*. pp 147-155
83. Robertson, A. G., Shih, J., Yau, C., Gibb, E. A., Oba, J., Mungall, K. L., Hess, J. M., Uzunangelov, V., Walter, V., Danilova, L., Lichtenberg, T. M., Kucherlapati, M., Kimes, P. K., Tang, M., Penson, A., Babur, O., Akbani, R., Bristow, C. A., Hoadley, K. A., Iype, L., Chang, M. T., Network, T. R., Cherniack, A. D., Benz, C., Mills, G. B., Verhaak, R. G. W., Griewank, K. G., Felau, I., Zenklusen, J. C., Gershenwald, J. E., Schoenfield, L., Lazar, A. J., Abdel-Rahman, M. H., Roman-Roman, S., Stern, M. H., Cebulla, C. M., Williams, M. D., Jager, M. J., Coupland, S. E., Esmaeli, B., Kandoth, C., and Woodman, S. E. (2017) Integrative Analysis Identifies Four Molecular and Clinical Subsets in Uveal Melanoma. *Cancer Cell* **32**, 204-220 e215
84. Johansson, P., Aoude, L. G., Wadt, K., Glasson, W. J., Warrier, S. K., Hewitt, A. W., Kiilgaard, J. F., Heegaard, S., Isaacs, T., Franchina, M., Ingvar, C., Vermeulen, T., Whitehead, K. J., Schmidt, C. W., Palmer, J. M., Symmons, J., Gerdes, A. M., Jonsson, G., and Hayward, N. K. (2016) Deep sequencing of uveal melanoma identifies a recurrent mutation in PLCB4. *Oncotarget* **7**, 4624-4631
85. Moore, A. R., Ceraudo, E., Sher, J. J., Guan, Y., Shoushtari, A. N., Chang, M. T., Zhang, J. Q., Walczak, E. G., Kazmi, M. A., Taylor, B. S., Huber, T., Chi, P., Sakmar, T. P., and Chen, Y. (2016) Recurrent activating mutations of G-protein-coupled receptor CYSLTR2 in uveal melanoma. *Nature Genetics* **48**, 675-680
86. Vaque, J. P., Dorsam, R. T., Feng, X., Iglesias-Bartolome, R., Forsthoefel, D. J., Chen, Q., Debant, A., Seeger, M. A., Ksander, B. R., Teramoto, H., and Gutkind, J. S. (2013) A genome-wide RNAi screen reveals a Trio-regulated Rho GTPase circuitry transducing mitogenic signals initiated by G protein-coupled receptors. *Molecular cell* **49**, 94-108
87. Pan, D. (2010) The hippo signaling pathway in development and cancer. *Dev Cell* **19**, 491-505
88. Feng, X., Degese, M. S., Iglesias-Bartolome, R., Vaque, J. P., Molinolo, A. A., Rodrigues, M., Zaidi, M. R., Ksander, B. R., Merlino, G., Sodhi, A., Chen, Q., and Gutkind, J. S. (2014) Hippo-independent activation of YAP by the GNAQ uveal melanoma oncogene through a trio-regulated rho GTPase signaling circuitry. *Cancer Cell* **25**, 831-845
89. Yu, F. X., Luo, J., Mo, J. S., Liu, G., Kim, Y. C., Meng, Z., Zhao, L., Peyman, G., Ouyang, H., Jiang, W., Zhao, J., Chen, X., Zhang, L., Wang, C. Y., Bastian, B. C., Zhang, K., and Guan, K. L. (2014) Mutant Gq/11 promote uveal melanoma tumorigenesis by activating YAP. *Cancer Cell* **25**, 822-830
90. Feng, X., Arang, N., Rigiracciolo, D. C., Lee, J. S., Yeerna, H., Wang, Z., Lubrano, S., Kishore, A., Pachter, J. A., Konig, G. M., Maggiolini, M., Kostenis, E., Schlaepfer, D. D.,

Tamayo, P., Chen, Q., Ruppin, E., and Gutkind, J. S. (2019) A Platform of Synthetic Lethal Gene Interaction Networks Reveals that the GNAQ Uveal Melanoma Oncogene Controls the Hippo Pathway through FAK. *Cancer Cell* **35**, 457-472 e455

91. Misra, R. S., Shi, G., Moreno-Garcia, M. E., Thankappan, A., Tighe, M., Mousseau, B., Kusser, K., Becker-Herman, S., Hudkins, K. L., Dunn, R., Kehry, M. R., Migone, T. S., Marshak-Rothstein, A., Simon, M., Randall, T. D., Alpers, C. E., Liggitt, D., Rawlings, D. J., and Lund, F. E. (2010) G alpha q-containing G proteins regulate B cell selection and survival and are required to prevent B cell-dependent autoimmunity. *J Exp Med* **207**, 1775-1789
92. He, Y., Yuan, X., Li, Y., Zhong, C., Liu, Y., Qian, H., Xuan, J., Duan, L., and Shi, G. (2018) Loss of Galphaq impairs regulatory B-cell function. *Arthritis Res Ther* **20**, 186
93. Wang, D., Zhang, Y., He, Y., Li, Y., Lund, F. E., and Shi, G. (2014) The deficiency of Galphaq leads to enhanced T-cell survival. *Immunology and cell biology* **92**, 781-790
94. Li, Z., Zhang, X., Xue, W., Zhang, Y., Li, C., Song, Y., Mei, M., Lu, L., Wang, Y., Zhou, Z., Jin, M., Bian, Y., Zhang, L., Wang, X., Li, L., Li, X., Fu, X., Sun, Z., Wu, J., Nan, F., Chang, Y., Yan, J., Yu, H., Feng, X., Wang, G., Zhang, D., Fu, X., Zhang, Y., Young, K. H., Li, W., and Zhang, M. (2019) Recurrent GNAQ mutation encoding T96S in natural killer/T cell lymphoma. *Nature communications* **10**, 4209
95. Cerami, E., Gao, J., Dogrusoz, U., Gross, B. E., Sumer, S. O., Aksoy, B. A., Jacobsen, A., Byrne, C. J., Heuer, M. L., Larsson, E., Antipin, Y., Reva, B., Goldberg, A. P., Sander, C., and Schultz, N. (2012) The cBio cancer genomics portal: an open platform for exploring multidimensional cancer genomics data. *Cancer Discov* **2**, 401-404
96. Gao, J., Aksoy, B. A., Dogrusoz, U., Dresdner, G., Gross, B., Sumer, S. O., Sun, Y., Jacobsen, A., Sinha, R., Larsson, E., Cerami, E., Sander, C., and Schultz, N. (2013) Integrative analysis of complex cancer genomics and clinical profiles using the cBioPortal. *Science signaling* **6**, pl1
97. Moroishi, T., Hansen, C. G., and Guan, K. L. (2015) The emerging roles of YAP and TAZ in cancer. *Nat Rev Cancer* **15**, 73-79
98. Yu, F. X., Zhao, B., and Guan, K. L. (2015) Hippo Pathway in Organ Size Control, Tissue Homeostasis, and Cancer. *Cell* **163**, 811-828
99. Barbazetto, I. A., Lee, T. C., Rollins, I. S., Chang, S., and Abramson, D. H. (2003) Treatment of choroidal melanoma using photodynamic therapy. *Am J Ophthalmol* **135**, 898-899
100. Soucek, P., and Cihelkova, I. (2006) Photodynamic therapy with verteporfin in subfoveal amelanotic choroidal melanoma (A controlled case). *Neuro endocrinology letters* **27**, 145-148
101. Arnold, J. J., Blinder, K. J., Bressler, N. M., Bressler, S. B., Burdan, A., Haynes, L., Lim, J. I., Miller, J. W., Potter, M. J., Reaves, A., Rosenfeld, P. J., Sickenberg, M., Slakter, J. S., Soubrane, G., Strong, H. A., Stur, M., Treatment of Age-Related Macular Degeneration with Photodynamic Therapy Study, G., and Verteporfin in Photodynamic Therapy Study, G. (2004) Acute severe visual acuity decrease after photodynamic therapy with verteporfin: case reports from randomized clinical trials-TAP and VIP report no. 3. *Am J Ophthalmol* **137**, 683-696
102. Azab, M., Benchaboune, M., Blinder, K. J., Bressler, N. M., Bressler, S. B., Gragoudas, E. S., Fish, G. E., Hao, Y., Haynes, L., Lim, J. I., Menchini, U., Miller, J. W., Mones, J., Potter, M. J., Reaves, A., Rosenfeld, P. J., Strong, A., Su, X. Y., Slakter, J. S., Schmidt-Erfurth, U., and Sorenson, J. A. (2004) Verteporfin therapy of subfoveal choroidal neovascularization in age-related macular degeneration: meta-analysis of 2-year safety results in three randomized clinical trials: Treatment Of Age-Related Macular Degeneration With Photodynamic Therapy and Verteporfin In Photodynamic Therapy Study Report no. 4. *Retina* **24**, 1-12

103. Lee, J. S., Das, A., Jerby-Arnon, L., Arafeh, R., Auslander, N., Davidson, M., McGarry, L., James, D., Amzallag, A., Park, S. G., Cheng, K., Robinson, W., Atias, D., Stossel, C., Buzhor, E., Stein, G., Waterfall, J. J., Meltzer, P. S., Golan, T., Hannenhalli, S., Gottlieb, E., Benes, C. H., Samuels, Y., Shanks, E., and Ruppin, E. (2018) Harnessing synthetic lethality to predict the response to cancer treatment. *Nat Commun* **9**, 2546
104. Tsherniak, A., Vazquez, F., Montgomery, P. G., Weir, B. A., Kryukov, G., Cowley, G. S., Gill, S., Harrington, W. F., Pantel, S., Krill-Burger, J. M., Meyers, R. M., Ali, L., Goodale, A., Lee, Y., Jiang, G., Hsiao, J., Gerath, W. F. J., Howell, S., Merkel, E., Ghandi, M., Garraway, L. A., Root, D. E., Golub, T. R., Boehm, J. S., and Hahn, W. C. (2017) Defining a Cancer Dependency Map. *Cell* **170**, 564-576 e516
105. Sulzmaier, F. J., Jean, C., and Schlaepfer, D. D. (2014) FAK in cancer: mechanistic findings and clinical applications. *Nat Rev Cancer* **14**, 598-610
106. Armbruster, B. N., Li, X., Pausch, M. H., Herlitze, S., and Roth, B. L. (2007) Evolving the lock to fit the key to create a family of G protein-coupled receptors potently activated by an inert ligand. *Proc Natl Acad Sci U S A* **104**, 5163-5168
107. Schrage, R., Schmitz, A. L., Gaffal, E., Annala, S., Kehraus, S., Wenzel, D., Bullesbach, K. M., Bald, T., Inoue, A., Shinjo, Y., Galandrin, S., Shridhar, N., Hesse, M., Grundmann, M., Merten, N., Charpentier, T. H., Martz, M., Butcher, A. J., Slodczyk, T., Armando, S., Effern, M., Namkung, Y., Jenkins, L., Horn, V., Stossel, A., Dargatz, H., Tietze, D., Imhof, D., Gales, C., Drewke, C., Muller, C. E., Holzel, M., Milligan, G., Tobin, A. B., Gomeza, J., Dohlman, H. G., Sondek, J., Harden, T. K., Bouvier, M., Laporte, S. A., Aoki, J., Fleischmann, B. K., Mohr, K., Konig, G. M., Tuting, T., and Kostenis, E. (2015) The experimental power of FR900359 to study Gq-regulated biological processes. *Nat Commun* **6**, 10156
108. Hubbard, K. B., and Hepler, J. R. (2006) Cell signalling diversity of the Gqalpha family of heterotrimeric G proteins. *Cell Signal* **18**, 135-150
109. Narumiya, S., Ishizaki, T., and Uehata, M. (2000) Use and properties of ROCK-specific inhibitor Y-27632. *Methods Enzymol* **325**, 273-284
110. Ikeda, F., Terajima, H., Shimahara, Y., Kondo, T., and Yamaoka, Y. (2003) Reduction of hepatic ischemia/reperfusion-induced injury by a specific ROCK/Rho kinase inhibitor Y-27632. *J Surg Res* **109**, 155-160
111. Kovacs, M., Toth, J., Hetenyi, C., Malnasi-Csizmadia, A., and Sellers, J. R. (2004) Mechanism of blebbistatin inhibition of myosin II. *J Biol Chem* **279**, 35557-35563
112. Subramanian, A., Tamayo, P., Mootha, V. K., Mukherjee, S., Ebert, B. L., Gillette, M. A., Paulovich, A., Pomeroy, S. L., Golub, T. R., Lander, E. S., and Mesirov, J. P. (2005) Gene set enrichment analysis: a knowledge-based approach for interpreting genome-wide expression profiles. *Proc Natl Acad Sci U S A* **102**, 15545-15550
113. Liberzon, A., Birger, C., Thorvaldsdottir, H., Ghandi, M., Mesirov, J. P., and Tamayo, P. (2015) The Molecular Signatures Database (MSigDB) hallmark gene set collection. *Cell systems* **1**, 417-425
114. Zhao, B., Ye, X., Yu, J. D., Li, L., Li, W. Q., Li, S. M., Yu, J. J., Lin, J. D., Wang, C. Y., Chinnaiyan, A. M., Lai, Z. C., and Guan, K. L. (2008) TEAD mediates YAP-dependent gene induction and growth control. *Genes Dev* **22**, 1962-1971
115. Yu, F. X., Zhang, K., and Guan, K. L. (2014) YAP as oncotarget in uveal melanoma. *Oncoscience* **1**, 480-481
116. Meng, Z., Moroishi, T., and Guan, K. L. (2016) Mechanisms of Hippo pathway regulation. *Genes Dev* **30**, 1-17
117. Taniguchi, K., Wu, L. W., Grivennikov, S. I., de Jong, P. R., Lian, I., Yu, F. X., Wang, K., Ho, S. B., Boland, B. S., Chang, J. T., Sandborn, W. J., Hardiman, G., Raz, E., Maehara, Y., Yoshimura, A., Zucman-Rossi, J., Guan, K. L., and Karin, M. (2015) A gp130-Src-YAP module links inflammation to epithelial regeneration. *Nature* **519**, 57-62

118. Li, P., Silvis, M. R., Honaker, Y., Lien, W. H., Arron, S. T., and Vasioukhin, V. (2016) alphaE-catenin inhibits a Src-YAP1 oncogenic module that couples tyrosine kinases and the effector of Hippo signaling pathway. *Genes Dev* **30**, 798-811
119. Julius, D., and Nathans, J. (2012) Signaling by sensory receptors. *Cold Spring Harbor perspectives in biology* **4**, a005991
120. Chen, X., Wu, Q., Depeille, P., Chen, P., Thornton, S., Kalirai, H., Coupland, S. E., Roose, J. P., and Bastian, B. C. (2017) RasGRP3 Mediates MAPK Pathway Activation in GNAQ Mutant Uveal Melanoma. *Cancer Cell* **31**, 685-696 e686
121. Carvajal, R. D., Sosman, J. A., Quevedo, J. F., Milhem, M. M., Joshua, A. M., Kudchadkar, R. R., Linette, G. P., Gajewski, T. F., Lutzky, J., Lawson, D. H., Lao, C. D., Flynn, P. J., Albertini, M. R., Sato, T., Lewis, K., Doyle, A., Ancell, K., Panageas, K. S., Bluth, M., Hedvat, C., Erinjeri, J., Ambrosini, G., Marr, B., Abramson, D. H., Dickson, M. A., Wolchok, J. D., Chapman, P. B., and Schwartz, G. K. (2014) Effect of selumetinib vs chemotherapy on progression-free survival in uveal melanoma: a randomized clinical trial. *Jama* **311**, 2397-2405
122. Carvajal, R. D., Piperno-Neumann, S., Kapiteijn, E., Chapman, P. B., Frank, S., Joshua, A. M., Piulats, J. M., Wolter, P., Cocquyt, V., Chmielowski, B., Evans, T. R. J., Gastaud, L., Linette, G., Berking, C., Schachter, J., Rodrigues, M. J., Shoushtari, A. N., Clemett, D., Ghiorghiu, D., Mariani, G., Spratt, S., Lovick, S., Barker, P., Kilgour, E., Lai, Z., Schwartz, G. K., and Nathan, P. (2018) Selumetinib in Combination With Dacarbazine in Patients With Metastatic Uveal Melanoma: A Phase III, Multicenter, Randomized Trial (SUMIT). *J Clin Oncol* **36**, 1232-1239
123. Feng, X., Chen, Q., and Gutkind, J. S. (2014) Oncotargeting G proteins: The Hippo in the room. *Oncotarget* **5**, 10997-10999
124. Bhatt, M., Shah, S., and Shivprakash. (2010) Development of a high-throughput method for the determination of ethosuximide in human plasma by liquid chromatography mass spectrometry. *J Chromatogr B Analyt Technol Biomed Life Sci* **878**, 1605-1610
125. Martin, D., Degese, M. S., Vitale-Cross, L., Iglesias-Bartolome, R., Valera, J. L. C., Wang, Z., Feng, X., Yeerna, H., Vadmal, V., Moroishi, T., Thorne, R. F., Zaida, M., Siegele, B., Cheong, S. C., Molinolo, A. A., Samuels, Y., Tamayo, P., Guan, K. L., Lippman, S. M., Lyons, J. G., and Gutkind, J. S. (2018) Assembly and activation of the Hippo signalome by FAT1 tumor suppressor. *Nat Commun* **9**, 2372
126. Gutkind, J. S., and Robbins, K. C. (1992) Activation of transforming G protein-coupled receptors induces rapid tyrosine phosphorylation of cellular proteins, including p125FAK and the p130 v-src substrate. *Biochem Biophys Res Commun* **188**, 155-161
127. Hu, J. K., Du, W., Shelton, S. J., Oldham, M. C., DiPersio, C. M., and Klein, O. D. (2017) An FAK-YAP-mTOR Signaling Axis Regulates Stem Cell-Based Tissue Renewal in Mice. *Cell stem cell* **21**, 91-106 e106
128. Lachowski, D., Cortes, E., Robinson, B., Rice, A., Rombouts, K., and Del Rio Hernandez, A. E. (2018) FAK controls the mechanical activation of YAP, a transcriptional regulator required for durotaxis. *FASEB J* **32**, 1099-1107
129. Marinissen, M. J., Servitja, J. M., Offermanns, S., Simon, M. I., and Gutkind, J. S. (2003) Thrombin protease-activated receptor-1 signals through Gq- and G13-initiated MAPK cascades regulating c-Jun expression to induce cell transformation. *J Biol Chem* **278**, 46814-46825
130. Teramoto, H., Malek, R. L., Behbahani, B., Castellone, M. D., Lee, N. H., and Gutkind, J. S. (2003) Identification of H-Ras, RhoA, Rac1 and Cdc42 responsive genes. *Oncogene* **22**, 2689-2697
131. Igishi, T., Fukuhara, S., Patel, V., Katz, B. Z., Yamada, K. M., and Gutkind, J. S. (1999) Divergent signaling pathways link focal adhesion kinase to mitogen-activated protein

kinase cascades. Evidence for a role of paxillin in c-Jun NH(2)-terminal kinase activation. *J Biol Chem* **274**, 30738-30746

132. Chikumi, H., Fukuhara, S., and Gutkind, J. S. (2002) Regulation of G protein-linked guanine nucleotide exchange factors for Rho, PDZ-RhoGEF, and LARG by tyrosine phosphorylation: evidence of a role for focal adhesion kinase. *J Biol Chem* **277**, 12463-12473
133. Marcotte, R., Brown, K. R., Suarez, F., Sayad, A., Karamboulas, K., Krzyzanowski, P. M., Sircoulomb, F., Medrano, M., Fedyshyn, Y., Koh, J. L., van Dyk, D., Fedyshyn, B., Luhova, M., Brito, G. C., Vizeacoumar, F. J., Vizeacoumar, F. S., Datti, A., Kasimer, D., Buzina, A., Mero, P., Misquitta, C., Normand, J., Haider, M., Ketela, T., Wrana, J. L., Rottapel, R., Neel, B. G., and Moffat, J. (2012) Essential gene profiles in breast, pancreatic, and ovarian cancer cells. *Cancer discovery* **2**, 172-189
134. Marcotte, R., Sayad, A., Brown, K. R., Sanchez-Garcia, F., Reimand, J., Haider, M., Virtanen, C., Bradner, J. E., Bader, G. D., Mills, G. B., Pe'er, D., Moffat, J., and Neel, B. G. (2016) Functional Genomic Landscape of Human Breast Cancer Drivers, Vulnerabilities, and Resistance. *Cell* **164**, 293-309
135. Cheung, H. W., Cowley, G. S., Weir, B. A., Boehm, J. S., Rusin, S., Scott, J. A., East, A., Ali, L. D., Lizotte, P. H., Wong, T. C., Jiang, G., Hsiao, J., Mermel, C. H., Getz, G., Barretina, J., Gopal, S., Tamayo, P., Gould, J., Tsherniak, A., Stransky, N., Luo, B., Ren, Y., Drapkin, R., Bhatia, S. N., Mesirov, J. P., Garraway, L. A., Meyerson, M., Lander, E. S., Root, D. E., and Hahn, W. C. (2011) Systematic investigation of genetic vulnerabilities across cancer cell lines reveals lineage-specific dependencies in ovarian cancer. *Proc Natl Acad Sci U S A* **108**, 12372-12377
136. Cowley, G. S., Weir, B. A., Vazquez, F., Tamayo, P., Scott, J. A., Rusin, S., East-Seletsky, A., Ali, L. D., Gerath, W. F., Pantel, S. E., Lizotte, P. H., Jiang, G., Hsiao, J., Tsherniak, A., Dwinell, E., Aoyama, S., Okamoto, M., Harrington, W., Gelfand, E., Green, T. M., Tomko, M. J., Gopal, S., Wong, T. C., Li, H., Howell, S., Stransky, N., Liefeld, T., Jang, D., Bistline, J., Hill Meyers, B., Armstrong, S. A., Anderson, K. C., Stegmaier, K., Reich, M., Pellman, D., Boehm, J. S., Mesirov, J. P., Golub, T. R., Root, D. E., and Hahn, W. C. (2014) Parallel genome-scale loss of function screens in 216 cancer cell lines for the identification of context-specific genetic dependencies. *Scientific data* **1**, 140035
137. Iorio, F., Knijnenburg, T. A., Vis, D. J., Bignell, G. R., Menden, M. P., Schubert, M., Aben, N., Goncalves, E., Barthorpe, S., Lightfoot, H., Cokelaer, T., Greninger, P., van Dyk, E., Chang, H., de Silva, H., Heyn, H., Deng, X., Egan, R. K., Liu, Q., Mironenko, T., Mitropoulos, X., Richardson, L., Wang, J., Zhang, T., Moran, S., Sayols, S., Soleimani, M., Tamborero, D., Lopez-Bigas, N., Ross-Macdonald, P., Esteller, M., Gray, N. S., Haber, D. A., Stratton, M. R., Benes, C. H., Wessels, L. F., Saez-Rodriguez, J., McDermott, U., and Garnett, M. J. (2016) A Landscape of Pharmacogenomic Interactions in Cancer. *Cell* **166**, 740-754
138. Barretina, J., Caponigro, G., Stransky, N., Venkatesan, K., Margolin, A. A., Kim, S., Wilson, C. J., Lehar, J., Kryukov, G. V., Sonkin, D., Reddy, A., Liu, M., Murray, L., Berger, M. F., Monahan, J. E., Morais, P., Meltzer, J., Korejwa, A., Jane-Valbuena, J., Mapa, F. A., Thibault, J., Bric-Furlong, E., Raman, P., Shipway, A., Engels, I. H., Cheng, J., Yu, G. K., Yu, J., Aspesi, P., Jr., de Silva, M., Jagtap, K., Jones, M. D., Wang, L., Hatton, C., Palescandolo, E., Gupta, S., Mahan, S., Sougnez, C., Onofrio, R. C., Liefeld, T., MacConaill, L., Winckler, W., Reich, M., Li, N., Mesirov, J. P., Gabriel, S. B., Getz, G., Ardlie, K., Chan, V., Myer, V. E., Weber, B. L., Porter, J., Warmuth, M., Finan, P., Harris, J. L., Meyerson, M., Golub, T. R., Morrissey, M. P., Sellers, W. R., Schlegel, R., and Garraway, L. A. (2012) The Cancer Cell Line Encyclopedia enables predictive modelling of anticancer drug sensitivity. *Nature* **483**, 603-607

139. Friedman, A. A., Amzallag, A., Pruteanu-Malinici, I., Baniya, S., Cooper, Z. A., Piris, A., Hargreaves, L., Igras, V., Frederick, D. T., Lawrence, D. P., Haber, D. A., Flaherty, K. T., Wargo, J. A., Ramaswamy, S., Benes, C. H., and Fisher, D. E. (2015) Landscape of Targeted Anti-Cancer Drug Synergies in Melanoma Identifies a Novel BRAF-VEGFR/PDGFR Combination Treatment. *PLoS One* **10**, e0140310
140. Therneau, T. M., and Grambsch, P. M. (2000) *Modeling survival data : extending the Cox model*, Springer, New York
141. Law, V., Knox, C., Djoumbou, Y., Jewison, T., Guo, A. C., Liu, Y., Maciejewski, A., Arndt, D., Wilson, M., Neveu, V., Tang, A., Gabriel, G., Ly, C., Adamjee, S., Dame, Z. T., Han, B., Zhou, Y., and Wishart, D. S. (2014) DrugBank 4.0: shedding new light on drug metabolism. *Nucleic Acids Res* **42**, D1091-1097
142. Garnett, M. J., Edelman, E. J., Heidorn, S. J., Greenman, C. D., Dastur, A., Lau, K. W., Greninger, P., Thompson, I. R., Luo, X., Soares, J., Liu, Q. S., Iorio, F., Surdez, D., Chen, L., Milano, R. J., Bignell, G. R., Tam, A. T., Davies, H., Stevenson, J. A., Barthorpe, S., Lutz, S. R., Kogera, F., Lawrence, K., McLaren-Douglas, A., Mitropoulos, X., Mironenko, T., Thi, H., Richardson, L., Zhou, W. J., Jewitt, F., Zhang, T. H., O'Brien, P., Boisvert, J. L., Price, S., Hur, W., Yang, W. J., Deng, X. M., Butler, A., Choi, H. G., Chang, J., Baselga, J., Stamenkovic, I., Engelman, J. A., Sharma, S. V., Delattre, O., Saez-Rodriguez, J., Gray, N. S., Settleman, J., Futreal, P. A., Haber, D. A., Stratton, M. R., Ramaswamy, S., McDermott, U., and Benes, C. H. (2012) Systematic identification of genomic markers of drug sensitivity in cancer cells. *Nature* **483**, 570-U587
143. Basu, A., Bodycombe, N. E., Cheah, J. H., Price, E. V., Liu, K., Schaefer, G. I., Ebright, R. Y., Stewart, M. L., Ito, D., Wang, S., Bracha, A. L., Liefeld, T., Wawer, M., Gilbert, J. C., Wilson, A. J., Stransky, N., Kryukov, G. V., Dancik, V., Barretina, J., Garraway, L. A., Hon, C. S. Y., Munoz, B., Bittker, J. A., Stockwell, B. R., Khabele, D., Stern, A. M., Clemons, P. A., Shamji, A. F., and Schreiber, S. L. (2013) An Interactive Resource to Identify Cancer Genetic and Lineage Dependencies Targeted by Small Molecules. *Cell* **154**, 1151-1161
144. Yamaguchi, K., Iglesias-Bartolome, R., Wang, Z., Callejas-Valera, J. L., Amornphimoltham, P., Molinolo, A. A., Cohen, E. E., Califano, J. A., Lippman, S. M., Luo, J., and Gutkind, J. S. (2016) A synthetic-lethality RNAi screen reveals an ERK-mTOR co-targeting pro-apoptotic switch in PIK3CA+ oral cancers. *Oncotarget* **7**, 10696-10709
145. Tancioni, I., Miller, N. L., Uryu, S., Lawson, C., Jean, C., Chen, X. L., Kleinschmidt, E. G., and Schlaepfer, D. D. (2015) FAK activity protects nucleostemin in facilitating breast cancer spheroid and tumor growth. *Breast Cancer Res* **17**, 47
146. Arang, N., and Gutkind, J. S. (2020) G Protein-Coupled receptors and heterotrimeric G proteins as cancer drivers. *FEBS Lett* **594**, 4201-4232
147. Van Raamsdonk, C. D., Bezrookove, V., Green, G., Bauer, J., Gaugler, L., O'Brien, J. M., Simpson, E. M., Barsh, G. S., and Bastian, B. C. (2009) Frequent somatic mutations of GNAQ in uveal melanoma and blue nevi. *Nature* **457**, 599-602
148. Singh, A. D., Turell, M. E., and Topham, A. K. (2011) Uveal melanoma: trends in incidence, treatment, and survival. *Ophthalmology* **118**, 1881-1885
149. Luke, J. J., USA, H. M. S. D. F. C. I. B. M., Triozzi, P. L., USA, M. C. B. W. F. U. C. C. W. S. N., McKenna, K. C., USA, U. o. P. C. I. P. P., Van Meir, E. G., USA, T. W. C. I. o. E. U. S. o. M. A. G., Gershenwald, J. E., USA, U. o. T. M. A. C. C. H. T., Bastian, B. C., USA, U. o. C. S. F. H. D. C. C. C. S. F. C., Gutkind, J. S., USA, N. I. o. D. a. C. R. B. M., Bowcock, A. M., UK, N. H. L. I. I. C. L., Streicher, H. Z., USA, N. C. I. B. M., Patel, P. M., UK, U. o. N. N., Sato, T., USA, T. J. U. T. K. C. C. P. P., Sossman, J. A., USA, V. U. V. I. C. C. N. T., Sznol, M., USA, Y. U. Y. C. C. N. H. C., Welch, J., USA, N. C. I. B. M., Thurin, M., USA, N. C. I. B. M., Selig, S., USA, B. a. W. s. H. a. t. M. R. F. C. O. W. D., Flaherty, K. T., USA, H. M. S. M. G. H. C. C. B. M., Carvajal, R. D., and USA, M. S. K. C. C. N. Y.

N. (2016) Biology of advanced uveal melanoma and next steps for clinical therapeutics. *Pigment Cell & Melanoma Research* **28**, 135-147

150. Falchook, G. S., Lewis, K. D., Infante, J. R., Gordon, M. S., Vogelzang, N. J., DeMarini, D. J., Sun, P., Moy, C., Szabo, S. A., Roadcap, L. T., Peddareddigari, V. G., Lebowitz, P. F., Le, N. T., Burris, H. A., 3rd, Messersmith, W. A., O'Dwyer, P. J., Kim, K. B., Flaherty, K., Bendell, J. C., Gonzalez, R., Kurzrock, R., and Fecher, L. A. (2012) Activity of the oral MEK inhibitor trametinib in patients with advanced melanoma: a phase 1 dose-escalation trial. *Lancet Oncol* **13**, 782-789
151. Nathan, P., Hassel, J. C., Rutkowski, P., Baurain, J. F., Butler, M. O., Schlaak, M., Sullivan, R. J., Ochsenreither, S., Dummer, R., Kirkwood, J. M., Joshua, A. M., Sacco, J. J., Shoushtari, A. N., Orloff, M., Piulats, J. M., Milhem, M., Salama, A. K. S., Curti, B., Demidov, L., Gastaud, L., Mauch, C., Yushak, M., Carvajal, R. D., Hamid, O., Abdullah, S. E., Holland, C., Goodall, H., Piperno-Neumann, S., and Investigators, I. M.-. (2021) Overall Survival Benefit with Tebentafusp in Metastatic Uveal Melanoma. *The New England journal of medicine* **385**, 1196-1206
152. Middleton, M. R., McAlpine, C., Woodcock, V. K., Corrie, P., Infante, J. R., Steven, N. M., Evans, T. R. J., Anthoney, A., Shoushtari, A. N., Hamid, O., Gupta, A., Vardeu, A., Leach, E., Naidoo, R., Stanhope, S., Lewis, S., Hurst, J., O'Kelly, I., and Sznol, M. (2020) Tebentafusp, A TCR/Anti-CD3 Bispecific Fusion Protein Targeting gp100, Potently Activated Antitumor Immune Responses in Patients with Metastatic Melanoma. *Clin Cancer Res* **26**, 5869-5878
153. Smrcka, A. V., Brown, J. H., and Holz, G. G. (2012) Role of phospholipase Cepsilon in physiological phosphoinositide signaling networks. *Cell Signal* **24**, 1333-1343
154. Sanchez-Fernandez, G., Cabezudo, S., Garcia-Hoz, C., Beninca, C., Aragay, A. M., Mayor, F., Jr., and Ribas, C. (2014) Galphaq signalling: the new and the old. *Cell Signal* **26**, 833-848

CHAPTER 3: Whole genome CRISPR screening identifies PI3K/AKT as a downstream component of the oncogenic GNAQ-FAK signaling circuitry

3.1 Introduction

G protein coupled receptors (GPCRs) and their associated G proteins are the largest family of cell surface proteins involved in signal transduction. As a result, they are central mediators of numerous cellular and physiological processes (1,2). Most GPCRs activate one or multiple Gα protein families: Gαi, Gα12, Gαs, and Gαq, each activating distinct signaling pathways (3). Remarkably, recent analyses have revealed that G proteins and GPCRs are mutated in nearly 30% of all human cancers (4,5). In particular, hotspot mutations in *GNAQ* and *GNA11*, referred to as *GNAQ* oncogenes, encoding GTPase deficient and constitutively active Gαq proteins, have been identified in ~93% of uveal melanoma (UM) and 4% of skin cutaneous melanoma (SKCM), where they act as driver oncogenes (6-10).

UM is the most common primary cancer of the eye in adults, and is the second most common melanoma subtype after SKCM (11). Approximately 50% of UM patients develop metastatic UM (mUM), most of which are refractory to current therapies, leading to patient death within a year (12). The MEK inhibitors (MEKi) selumetinib and trametinib have been extensively evaluated for mUM treatment; however, MEK inhibition with these agents has nearly no impact on the overall survival of mUM patients (13-15). Recent studies exploring the use of tebentafusp, a bispecific fusion antibody, have shown significant yet limited increases in patient overall survival, leading to FDA approval in unresectable or mUM patients (16,17). Despite this, there is still an urgent need for novel and effective therapeutic strategies for advanced and mUM. This prompted renewed interest in investigating the mechanisms by which prolonged Gαq signaling controls cancer cell growth, towards identifying novel pharmacological targets for therapeutic intervention in UM.

The precise molecular mechanisms by which oncogenic Gαq transduce sustained proliferative signals is not yet fully defined. This is primarily due to the large number of second messenger generating systems and signaling events perturbed upon Gαq activation (18,19). Recent findings support that mutant Gαq activates PLCβ/PKC, leading to the activation of ERK/MAPK, while concomitantly stimulating an exchange factor TRIO, thereby activating a Rho GTPase signaling circuitry (8,20,21). The latter activates YAP, a transcriptional co-activator regulated by the Hippo pathway (9). Of interest, synthetic lethal gene interactions of Gαq revealed that Focal Adhesion Kinase (FAK), a non-receptor tyrosine kinase, is a central mediator of non-canonical Gαq-driven signaling and a druggable signaling node downstream of the *GNAQ* oncogene (22).

Collectively, these studies provided a direct link between Gαq-FAK driven tyrosine phosphorylation networks and YAP activation and raise the possibility of the existence of additional signaling circuitries that may be central to the ability of Gαq to drive cell growth. As targeting FAK in UM is now being advanced to the clinic, we hypothesize that elucidation of the Gαq-FAK-regulated signaling networks may help identify novel downstream targets of Gαq, some of which, may represent mechanisms that should be targeted to optimize therapeutic responses to FAKi. Towards this end, we aimed at investigating additional Gαq-FAK-regulated signaling circuitries that may be critical to promote growth in UM, and other Gαq-driven malignancies.

3.2 Results

3.2.1 PI3K/AKT pathway activation drives resistance to FAKi in GNAQ-mutant UM

In order to profile the genetic interactome of Gαq-FAK signaling in UM, we performed a genome-wide CRISPR knock-out screen in *GNAQ*-mutant UM cells in the context of FAK

inhibition (Fig 3.1A). Using Cas9-expressing 92.1 uveal melanoma cells (92.1^{Cas9}), infected with the Brunello Human Genome pooled sgRNA library, cells were passaged under 0.1μM VS-4718 (FAK inhibitor, FAKi) treatment, or vehicle for a total of 19 cell doublings. In order to evaluate pathways that when modulated, resulted in resistance to inhibition of FAK, we examined sgRNAs enriched in FAKi treatment condition. Among the top hits were PTEN and TSC2, which are canonical negative regulators of the PI3K/AKT pathway (23) suggesting that enhanced PI3K/AKT signaling could drive resistance to FAKi (Fig 3.1B). Aligned with this, genes involved in the PI3K/AKT/MTOR signaling pathway were enriched targets of the sgRNAs yielding the most resistance (Fig 3.1C, Fig S3.1A). We also observed enrichment of cells with AMOTL2 sgRNAs in the FAKi conditions, which is a negative regulator of the Hippo/YAP pathway, and is aligned with the role of YAP as a downstream target of FAK in UM (22). Conversely, we observed depletion of sgRNAs for PRKCE, which we have demonstrated to be synthetic lethal with FAK (24). Interestingly, increased expression of PI3K/AKT/MTOR gene signature was associated with poor overall survival in TCGA UM patients (Logrank pvalue = 0.03) (Fig 3.1D). To validate the findings of our CRISPR screen, we performed siRNA mediated knockdown of the top two PI3K/AKT pathway hits from our screen, PTEN and TSC2, and evaluated the effect on cell viability in response to FAK inhibition (Fig 3.1E). We found that knockdown of PTEN and TSC2 both resulted in decreased sensitivity to FAKi in UM cells. We next evaluated the effect on PI3K and FAK signaling caused by PTEN and TSC2 loss (Fig 3.1F). In both cases, while siRNA mediated knockdown of PTEN and TSC2 resulted in increase in phosphorylation of downstream pathway members, AKT and S6, the latter often used to monitor mTOR activity (23), it did not lead to a change in phosphorylation of FAK. This suggests that increased PI3K/AKT signaling does not confer resistance to FAKi through FAK reactivation, and instead raises the possibility that PI3K/AKT may represent a critical signaling pathway activated by Gαq through FAK.

3.2.2 GNAQ is a regulator of PI3K/AKT signaling

In this case, however, whether Gαq activates or inhibits PI3K/AKT is not clear, and the overall underlying mechanisms involved are poorly understood (25-28). Based on these findings, we asked whether the PI3K pathway acts downstream of Gαq-FAK, or if it represents a parallel signaling axis. Inhibiting Gαq with siRNA mediated knockdown and by pharmacological inhibition with FR900359 (FR), resulted in sustained inhibition of canonical (ERK), and non-canonical (FAK) Gαq-driven signaling, as previously reported (24), concomitant with a decreased phosphorylation of the PI3K signaling targets, AKT and S6 (Fig. 3.2A, B). This suggests that Gαq controls PI3K signaling in UM cells harboring active Gαq. As an orthogonal approach, we found that GαqQL, the active Gαq mutant found in UM, promoted the accumulation of the phosphorylated forms of ERK, FAK, AKT, and S6 in HEK293 cells, demonstrating the direct ability of Gαq to promote PI3K/AKT signaling (Fig 3.2C,D). We also challenged our observations using the expression of a synthetic Gαq-coupled receptor, termed Gαq-DREADD, which can only be activated by addition of a pharmacologically inert ligand, clozapine-N-oxide (CNO) (29,30). Expression of Gαq-DREADD in HEK293 cells, and stimulation with CNO revealed a rapid and sustained increase pERK, and pFAK, in addition to an increase in pAKT and pS6 (Fig 3.2E). We validated the specificity of this approach by expressing Gαq-DREADD in Gαq/11 knockout (KO) cells and stimulating with CNO; however, we did not observe an increase in the phosphorylation state of any of the proteins tested (Fig 3.2F). Challenging both HEK293 and HEK293 Gαq/11 KO cell lines with EGF treatment revealed an increase in phosphorylation of all tested proteins in both cases, demonstrating the signaling competence in both models (Fig 3.2G). Collectively, these results indicated that Gαq promotes PI3K/AKT signaling when activated by GPCRs or as part of constitutive Gαq signaling, such as in UM.

3.3.3 FAK mediates PI3K/AKT pathway activation through p85 phosphorylation.

Based on these findings linking Gαq to enhanced PI3K/AKT activity, we then asked whether Gαq controls PI3K/AKT signaling via FAK. To test this, we expressed GαqQL in HEK293 cells alone, or in combination with pharmacological inhibition of FAK (Fig 3.3A). Indeed, inhibition of FAK in the context of Gαq activation was sufficient to block an increase in pAKT and pS6, while no change in pERK was observed. Likewise, activation of Gαq using Gαq-DREADD and stimulation with CNO, in combination with FAK inhibition abrogated an increase in pAKT and pS6 (Fig 3.3B). Based on these findings, we tested the ability of FAK expression to drive PI3K/AKT signaling. Overexpression of FAK in HEK293 cells led to a potent increase in pAKT and pS6 (Fig 3.3C). Conversely, blockade of FAK in UM cells with high basal Gαq-FAK activity, using siRNA mediated knockdown, or by a pharmacological inhibition led to a decrease in pAKT and pS6 levels (Fig 3.3D, E). These data suggest that in UM cells, persistent Gαq-driven signaling promotes PI3K pathway signaling via FAK.

The p110 catalytic subunit of the PI3K heterodimer is comprised of 4 different isoforms, PI3Kα, PI3Kβ, PI3Kγ, and PI3Kδ. The Class IA PI3Ks (α, β, and δ) consist of heterodimers of a catalytic p110 subunit and regulatory p85 subunit (31). In response to stimuli, inhibition of p110 by p85 can be relieved by direct tyrosine phosphorylation of p85, or by recruitment of p85 to tyrosine phosphorylated motifs on other proteins (31). This prompted us to ask if FAK could associate with and tyrosine phosphorylate p85 directly. By performing co-immunoprecipitation of FAK and p85 in UM cells, we observed strong binding of FAK to p85 under basal conditions that was diminished with FAKi treatment (Fig 3.3F). The reverse could also be observed, where under basal conditions, co-immunoprecipitation of p85 revealed strong association with FAK that was relieved upon FAKi treatment (Fig 3.3G). We also observed strong basal tyrosine phosphorylation of p85 that was diminished concomitant with a dissociation from FAK by FAKi treatment. We validated our findings by global immunoprecipitation of tyrosine-phosphorylated proteins using

pTyr antibodies in UM cells (Fig 3.3H). Aligned with our previous results, immunoprecipitation of total pTyr resulted in pulldown of p85 and FAK. Inhibition of FAK activity with FAKi similarly reduced the levels of tyrosine phosphorylated FAK and p85 available to be extracted by pTyr. Taken together these findings suggest that Gαq signaling promotes PI3K/AKT pathway activity through FAK-dependent tyrosine phosphorylation and association with PI3K-p85 (Fig 3.3I).

3.3.4 UM cells are dependent on PI3K/AKT signaling for growth and survival

While expression patterns of each PI3K catalytic subunit isoforms varies across tissues, the expression and isoform usage of PI3K is not currently known in UM. We first screened expression of each PI3K-p110 isoform in a number of UM cell lines on the Depmap Portal, and found that with the exception of PI3Kγ, all p110 isoforms were expressed (Fig 3.4A). We next performed siRNA-mediated knockdown of the major UM-associated p110 isoforms alone, and in combination, and assessed levels PI3K pathway activity by measuring pAKT and pS6 (Fig 3.4B). We found that in UM cells, PI3Kα and PI3Kβ were major drivers of PI3K signaling, with the strongest reduction in the context of triple p110 isoform knockdown. To complement our genetic knockdown approach, we tested the ability of p110 isoform-specific, as well as a pan-PI3K pharmacological inhibitor to inhibit AKT/S6. Aligned with our knockdown data, only BKM120, the pan-PI3K inhibitor that we tested was able to reduce both pAKT and pS6 in a potent and sustained manner, in comparison to inhibitors targeting individual p110 isoforms (Fig 3.4C) (31). Finally, testing cell viability of UM cells in response to our panel of PI3K inhibitors revealed the strongest inhibition in viability with the pan-PI3K inhibitor, indicating that UM cells are reliant on PI3K signaling for growth and survival (Fig 3.4D, Fig S3.2A). Ultimately, these results expand the repertoire of Gαq-FAK regulated signaling circuitries and establish a direct connection between Gαq and PI3K/AKT via FAK (Fig 3.4E).

3.3 Discussion

The *GNAQ* oncogene is the major oncogenic driver for UM, a cancer type characterized by limited additional genetic aberrancies. As a result, UM serves as a unique model to interrogate and profile the diversity of signaling mechanisms initiated by Gαq and Gαq-coupled GPCRs to promote cell proliferation. Coupled with this, a deeper understanding of Gαq-initiated mitogenic networks provide an opportunity for the identification of novel signal transduction based targeted therapies against UM. Our dissection of the signaling networks regulated by Gαq led to the finding that activation of Gαq is sufficient to promote PI3K pathway. Further interrogation into the underlying mechanisms revealed that Gαq controls PI3K activation through FAK mediated association and phosphorylation of the p85 regulatory subunit of PI3K. Finally, we demonstrate that UM cells are sensitive to genetic and pharmacological inhibition of PI3K signaling. Taken together these findings revealed a novel signaling axis by which Gαq controls cell growth and survival by regulating the PI3K/AKT/mTOR pathway through FAK.

In this regard, Gαq has been previously linked to AKT/mTOR signaling; however prior studies have reported varying and even paradoxical roles, suggesting that the role of Gαq in mediating PI3K/AKT signaling could be dependent on distinct cellular contexts. In exogenous overexpression systems, Gαq has been suggested to bind to and inhibit PI3K p110α, and in other settings, binding to mTOR directly and promoting the activity of mTORC1; however, the precise structural basis of these proposed mechanisms have yet to be uncovered (25-28). Similarly, activity of mTOR inhibitors have been explored in *in vitro* and preclinical models of UM, but the molecular basis for these findings, as well as whether *GNAQ* activates the mTOR pathway have not been fully investigated (32).

In general, GPCRs have been shown to signal to PI3K through the Gβγ dimers of the heterotrimeric G protein, by direct binding and activation of the p110γ/p101 heterodimer that is typically restricted to myeloid cell populations, or PI3Kβ in cells lacking p110γ (33-37). Our interrogation into the underlying mechanisms of Gαq oncogenic signaling network prompted us to focus our studies on endogenous contexts, enabling us to reveal key signaling components that we validated in a more generalizable, HEK293-based system. In particular, focusing on UM, a cell context with persistent aberrant Gαq signaling and high FAK activity, our data support that oncogenic Gαq promotes the activation of PI3K/AKT signaling by a tyrosine phosphorylation-dependent mechanism, thereby converging with the best understood growth factor receptor tyrosine kinase (RTK) signaling network. In this regard, our findings suggest that inhibition of all p85-associated PI3Ks may be necessary to achieve full blockade of PI3K signaling rather than individual PI3K catalytic isoforms. Indeed, this may explain why PI3Kα-specific inhibition has not been able to demonstrate significant clinical activity in UM (38). Extending this further, our findings suggest that pharmacological targeting of the pan-PI3K pathway may represent an attractive therapeutic strategy in UM, alone or as an approach to abrogate resistance to FAK inhibition, or as a part of multimodal targeting strategies downstream of Gαq.

Taken together, our current findings in the context of a prior body of literature, underscore the complex and cell context dependent molecular events underlying Gαq-driven oncogenic signaling. The duality between canonical PLCβ/PKC/ERK driven signaling and the non-canonical RhoA dependent activation of YAP and FAK poises Gαq to the direct regulation of both transient second messenger systems, as well as growth promoting transcriptional programs and tyrosine kinase regulated phosphorylation networks (9,22,39). Within this framework, the activation of PI3K/AKT through Gαq may represent a novel pro-survival mechanism by which oncogenic Gαq drives cell growth and proliferation when aberrantly activated.

3.4 Figures

Figure 3.1 PI3K/AKT pathway activation drives resistance to FAKi in GNAQ-mutant UM.

A, Schematic of whole-genome CRISPR screen experimental design. Created with Biorender.com. ***B***, Cell viability represented by beta score where a positive beta score indicates positive selection (resistance) (beta > 0.5, indicated by dotted line), and a negative beta score indicates negative selection (sensitivity) (beta < -0.5, indicated by dotted line) under FAK inhibitor treatment. **C**, Overrepresentation analysis of top sgRNAs (FDR < 0.015) with positive beta score using KEGG and Biocarta gene sets. Color intensity of bars fade by decreasing -Log_{10}p-value. ***D***, Overall survival analysis of UM TCGA patient cohort with high (top 25%) or low (bottom 25%) expression of PI3K/AKT/mTOR Hallmark gene signature. Dotted lines indicate 95% confidence interval. ***E***, Cell viability of 92.1 UM cells after siRNA knockdown of PTEN or TSC2 compared to Control siRNA in response to VS-4718 (FAKi) treatment for 72hrs, percent viability is normalized to vehicle treatment (mean ± SEM, n = 3). ***F***, Phosphorylation of FAK, AKT and S6 after siRNA mediated knockdown of CRISPR top hits (PTEN and TSC2) in 92.1 UM cells.

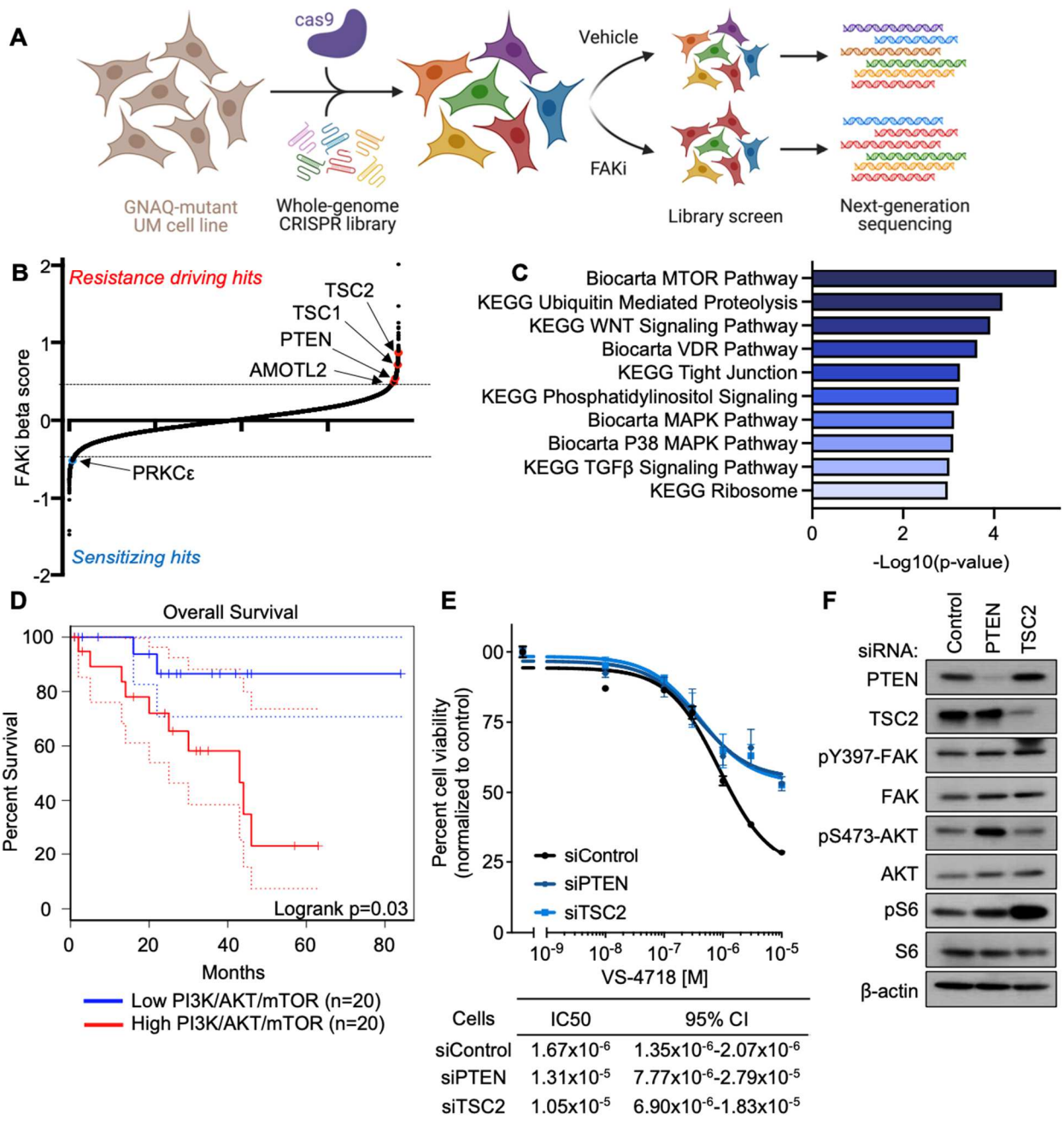
A
cas9
Vehicle
FAKi
GNAQ-mutant UM cell line
Whole-genome CRISPR library
Library screen
Next-generation sequencing
B
Resistance driving hits
TSC2
TSC1
PTEN
AMOTL2
PRKCε
Sensitizing hits
FAKi beta score
C
Biocarta MTOR Pathway
KEGG Ubiquitin Mediated Proteolysis
KEGG WNT Signaling Pathway
Biocarta VDR Pathway
KEGG Tight Junction
KEGG Phosphatidylinositol Signaling
Biocarta MAPK Pathway
Biocarta P38 MAPK Pathway
KEGG TGFβ Signaling Pathway
KEGG Ribosome
-Log10(p-value)
D
Overall Survival
Percent Survival
Months
Logrank p=0.03
Low PI3K/AKT/mTOR (n=20)
High PI3K/AKT/mTOR (n=20)
E
Percent cell viability (normalized to control)
VS-4718 [M]
siControl
siPTEN
siTSC2
Cells | IC50 | 95% CI
siControl | 1.67x10-6 | 1.35x10-6-2.07x10-6
siPTEN | 1.31x10-5 | 7.77x10-6-2.79x10-5
siTSC2 | 1.05x10-5 | 6.90x10-6-1.83x10-5
F
siRNA: Control PTEN TSC2
PTEN
TSC2
pY397-FAK
FAK
pS473-AKT
AKT
pS6
S6
β-actin

Figure 3.2 GNAQ is a regulator of PI3K/AKT signaling.

Phosphorylation of canonical (ERK) and non-canonical (FAK) Gαq-regulated pathways, and PI3K/AKT pathway (AKT and S6) in response to A, siRNA mediated knockdown of GNAQ in 92.1 UM cells. B, 500nM FR900359 (Gαq inhibitor) treatment over a timecourse. C, Expression of GαqQL in HEK293 cells. D, Schematic of Gαq regulated signaling. Created with Biorender.com. E, Stimulation of Gαq signaling using 1μM CNO over a timecourse, after expression of Gαq-DREADD in HEK293 cells or F, in Gαq/11 KO HEK293 cells. G, Phosphorylation of canonical (ERK) and non-canonical (FAK) Gαq-regulated pathways, and PI3K/AKT pathway (AKT and S6) in response to 20nM EGF treatment for 1hr in HEK293 and HEK293 Gαq/11 KO cells.

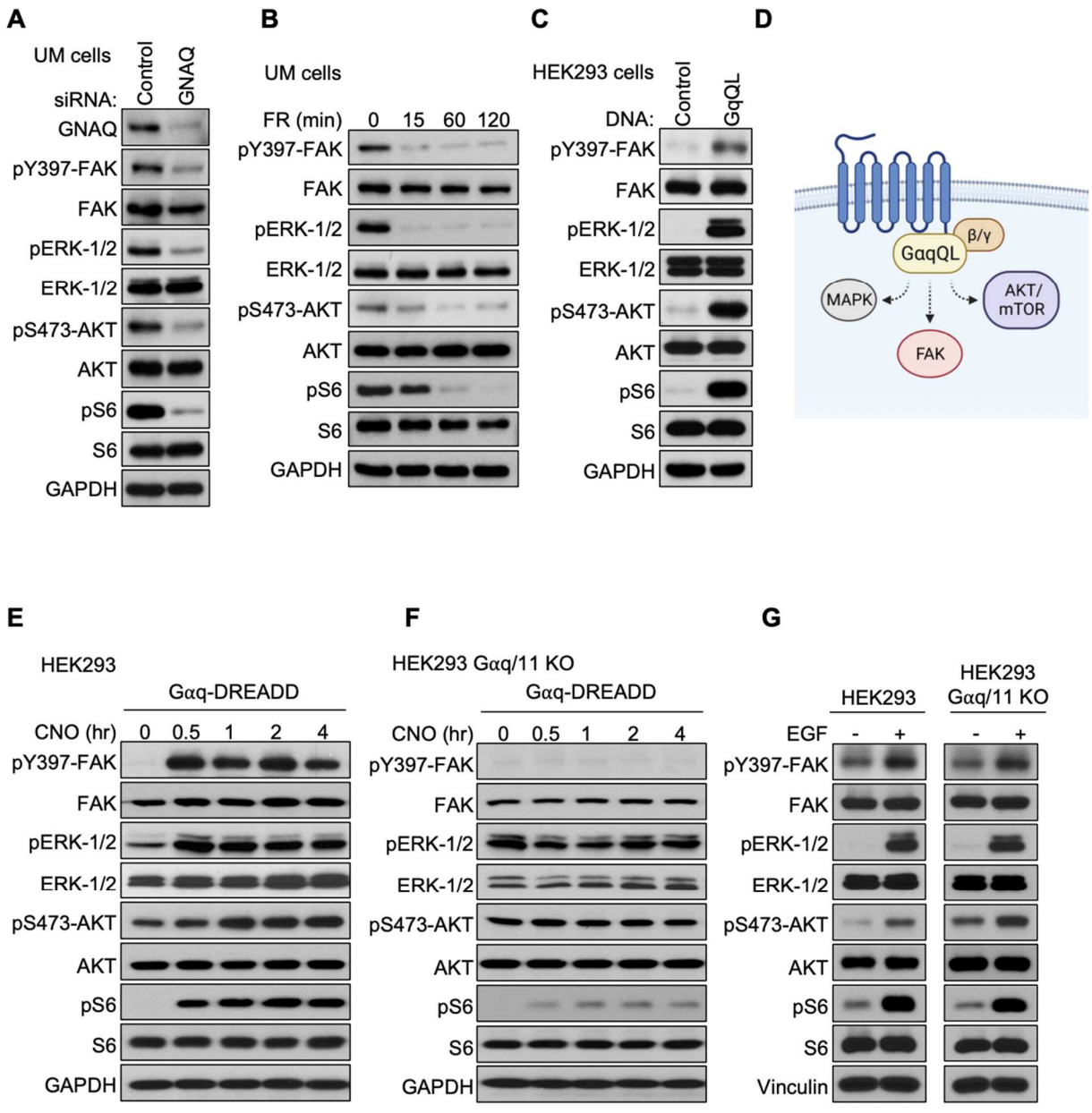
A
UM cells
siRNA:
Control
GNAQ
GNAQ
pY397-FAK
FAK
pERK-1/2
ERK-1/2
pS473-AKT
AKT
pS6
S6
GAPDH
B
UM cells
FR (min)
0
15
60
120
pY397-FAK
FAK
pERK-1/2
ERK-1/2
pS473-AKT
AKT
pS6
S6
GAPDH
C
HEK293 cells
DNA:
Control
GqQL
pY397-FAK
FAK
pERK-1/2
ERK-1/2
pS473-AKT
AKT
pS6
S6
GAPDH
D
GαqQL
β/γ
MAPK
AKT/
mTOR
FAK
E
HEK293
Gαq-DREADD
CNO (hr)
0
0.5
1
2
4
pY397-FAK
FAK
pERK-1/2
ERK-1/2
pS473-AKT
AKT
pS6
S6
GAPDH
F
HEK293 Gαq/11 KO
Gαq-DREADD
CNO (hr)
0
0.5
1
2
4
pY397-FAK
FAK
pERK-1/2
ERK-1/2
pS473-AKT
AKT
pS6
S6
GAPDH
G
HEK293
HEK293
Gαq/11 KO
EGF
-
+
-
+
pY397-FAK
FAK
pERK-1/2
ERK-1/2
pS473-AKT
AKT
pS6
S6
Vinculin

Figure 3.3 FAK mediates PI3K/AKT pathway activation through p85 phosphorylation.

Phosphorylation of canonical (ERK) and non-canonical (FAK) Gαq-regulated pathways, and PI3K/AKT pathway (AKT and S6) in response to ***A***, Expression of GαqQL alone, or in combination with 1μM VS-4718 treatment for 15hrs in HEK293 cells. ***B***, Stimulation of Gαq signaling using 1μM M CNO for 1hr after expression of Gαq-DREADD, in combination with 2μM VS-4718. ***C***, Expression of FAK-GFP in HEK293 cells. ***D***, siRNA mediated knockdown of FAK in OMM1.3 UM cells. ***E***, Timecourse of 1μM VS-4817 treatment in OMM1.3 UM cells. ***F***, Association of p85 with FAK after FAK immunoprecipitation with or without 1μM VS-4718 treatment for 15hrs in OMM1.3 UM cells. ***G***, Association of p85 with FAK and tyrosine phosphorylation after p85 immunoprecipitation and treatment with or without 1μM VS-4718 treatment for 15hrs in OMM1.3 UM cells. ***H***, Association of p85 and FAK after pY immunoprecipitation with or without 1μM VS-4817 treatment for 15hrs in OMM1.3 UM cells. ***I***, Schematic of signaling mechanisms regulated by Gαq and FAK mediated control of PI3K. Created with Biorender.com.

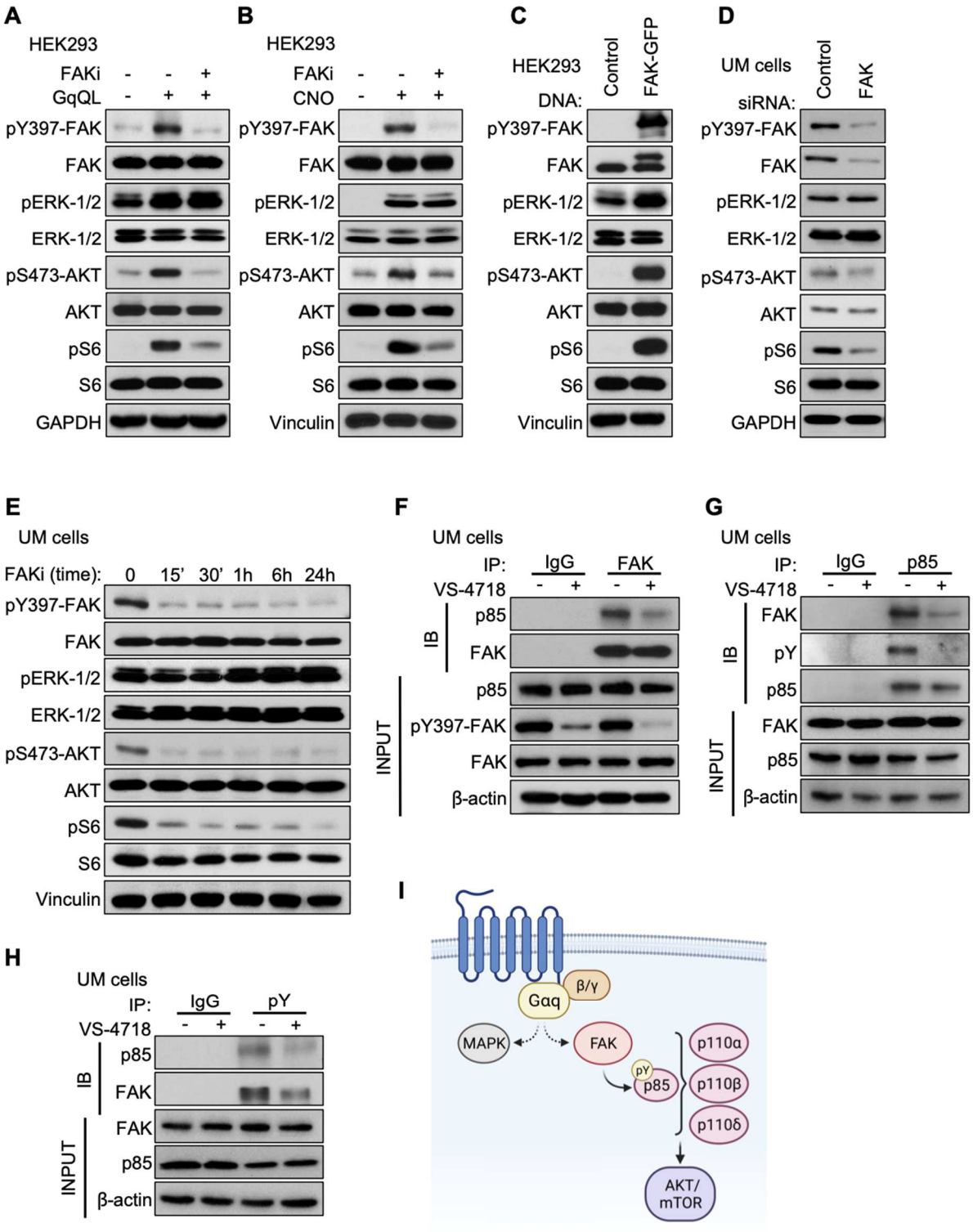
A
HEK293
FAKi - - +
GqQL - + +
pY397-FAK
FAK
pERK-1/2
ERK-1/2
pS473-AKT
AKT
pS6
S6
GAPDH
B
HEK293
FAKi - - +
CNO - + +
pY397-FAK
FAK
pERK-1/2
ERK-1/2
pS473-AKT
AKT
pS6
S6
Vinculin
C
HEK293
DNA: Control FAK-GFP
pY397-FAK
FAK
pERK-1/2
ERK-1/2
pS473-AKT
AKT
pS6
S6
Vinculin
D
UM cells
siRNA: Control FAK
pY397-FAK
FAK
pERK-1/2
ERK-1/2
pS473-AKT
AKT
pS6
S6
GAPDH
E
UM cells
FAKi (time): 0 15' 30' 1h 6h 24h
pY397-FAK
FAK
pERK-1/2
ERK-1/2
pS473-AKT
AKT
pS6
S6
Vinculin
F
UM cells
IP: IgG FAK
VS-4718 - + - +
IB
p85
FAK
INPUT
p85
pY397-FAK
FAK
β-actin
G
UM cells
IP: IgG p85
VS-4718 - + - +
IB
FAK
pY
p85
INPUT
FAK
p85
β-actin
H
UM cells
IP: IgG pY
VS-4718 - + - +
IB
p85
FAK
INPUT
FAK
p85
β-actin
I
Gαq
β/γ
MAPK
FAK
pY
p85
p110α
p110β
p110δ
AKT/
mTOR

Figure 3.4 UM cells are dependent on PI3K/AKT signaling for growth and survival.

A, mRNA expression of PI3K-p110 isoforms from UM cell lines in Depmap Portal, Expression Public 2Q22 (mean ± SEM, n = 9 cell lines). ***B***, Phosphorylation of AKT and S6 after single and combination siRNA mediated PI3K-p110 knockdown in OMM1.3 UM cells. ***C***, Phosphorylation of AKT and S6 after treatment with 1μM BYL719, TGX221, CAL101 and BKM120 for the indicated timepoints. ***D***, Cell viability of 92.1 UM cells after 72hrs treatment with BYL719, TGX221, CAL101 and BKM120, percent viability is normalized to vehicle treatment (mean ± SEM, n = 3). ***E***, Schematic of signaling mechanisms controlled by Gαq. Created with Biorender.com.

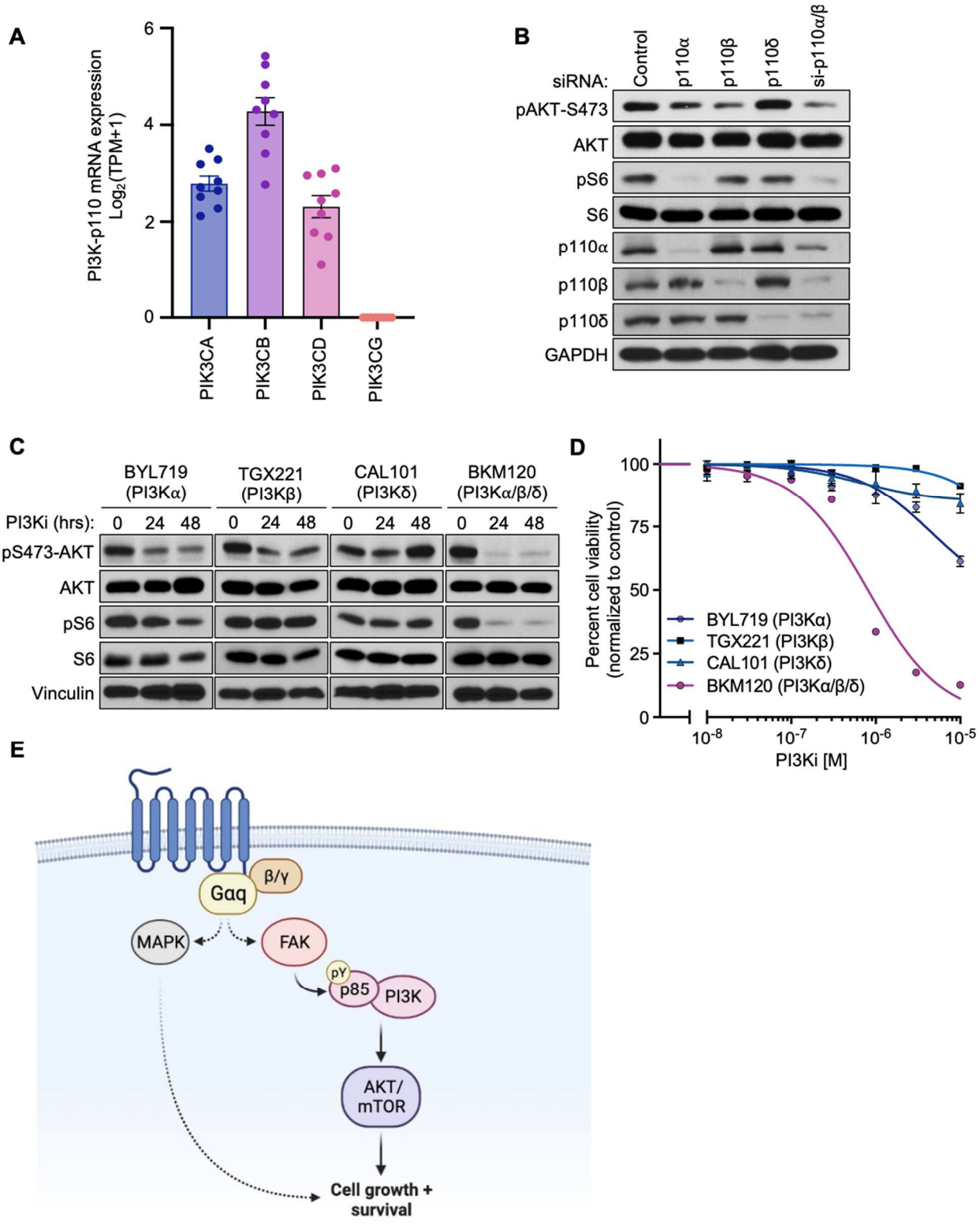
A
PI3K-p110 mRNA expression
Log2(TPM+1)
6
4
2
0
PIK3CA
PIK3CB
PIK3CD
PIK3CG
B
siRNA:
Control
p110α
p110β
p110δ
si-p110α/β
pAKT-S473
AKT
pS6
S6
p110α
p110β
p110δ
GAPDH
C
BYL719 (PI3Kα)
TGX221 (PI3Kβ)
CAL101 (PI3Kδ)
BKM120 (PI3Kα/β/δ)
PI3Ki (hrs):
0 24 48 0 24 48 0 24 48 0 24 48
pS473-AKT
AKT
pS6
S6
Vinculin
D
Percent cell viability
(normalized to control)
100
75
50
25
0
BYL719 (PI3Kα)
TGX221 (PI3Kβ)
CAL101 (PI3Kδ)
BKM120 (PI3Kα/β/δ)
10-8
10-7
10-6
10-5
PI3Ki [M]
E
Gαq
β/γ
MAPK
FAK
pY
p85
PI3K
AKT/
mTOR
Cell growth +
survival

A

Gene Set Name	p-value	FDR
Biocarta MTOR Pathway	4.22 e^{-6}	2.02 e^{-3}
KEGG Ubiquitin Mediated Proteolysis	6.57 e^{-5}	1.57 e^{-2}
KEGG WNT Signaling Pathway	1.22 e^{-4}	1.94 e^{-2}
Biocarta VDR Pathway	2.34 e^{-4}	2.8 e^{-2}
KEGG Tight Junction	5.64 e^{-4}	4.72 e^{-2}
KEGG Phosphatidylinositol Signaling System	5.99 e^{-4}	4.72 e^{-2}
Biocarta MAPK Pathway	7.62 e^{-4}	4.72 e^{-2}
Biocarta P38 MAPK Pathway	7.91 e^{-4}	4.72 e^{-2}
KEGG TGFβ Signaling Pathway	9.54 e^{-4}	4.97 e^{-2}
KEGG Ribosome	1.04 e^{-3}	4.97 e^{-2}

Figure S3.1

A, Overrepresentation analysis of top sgRNAs (FDR < 0.015) with positive beta score using KEGG and Biocarta gene sets, including p-value and FDR.

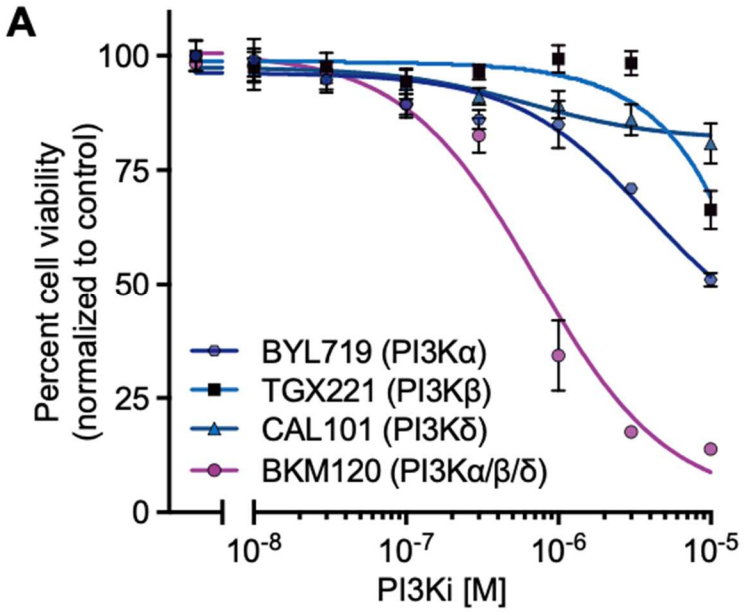

Figure S3.2

***A*,** Cell viability of OMM1.3 UM cells after 72hrs treatment with BYL719, TGX221, CAL101 and BKM120, percent viability is normalized to vehicle treatment (mean ± SEM, n = 3).

3.5 Materials and Methods

Cell Lines, Culture Procedures and Chemicals: HEK293 cells were cultured in DMEM (D6429, Sigma-Aldrich Inc.) containing 10% FBS (F2442, Sigma-Aldrich Inc.), 1X antibiotic/antimycotic solution (A5955, Sigma-Aldrich Inc.), and 1X Plasmocin prophylactic (ant-mpp, InvivoGen). HEK293 Gαq/11 KO cells were cultured using the same conditions described previously and were a kind gift from Dr. Asuka Inoue (40). Uveal melanoma cells (92.1, OMM1.3) were cultured in RPMI-1640 (R8758, Sigma Aldrich Inc.) containing 10% FBS (F2442, Sigma-Aldrich Inc.), 1X antibiotic/antimycotic solution (A5955, Sigma-Aldrich Inc.), and 1X Plasmocin prophylactic (ant-mpp, InvivoGen). All cell lines were routinely tested free of mycoplasma contamination. VS-4718 (S7653), BYL719 (S2814), TGX221 (S1169), CAL101 (S2226) and BKM120 (S2247) were purchased from SelleckChem. FR900359 (FR) was prepared in the lab of Dr. Evi Kostenis. Clozapine N-oxide (CNO) (4936), was purchased from Tocris Inc. EGF (E9644) was purchased from Sigma-Aldrich Inc. All compounds were used at concentrations indicated in figure legends.

Plasmids and Transfections: Plasmids pCEFL-HA, pCEFL-HA-GαqQL, and pCEFL-HA-Gαq-DREADD, were described previously (8). pEGFP-C1-FAK plasmid was a kind gift from Dr. David Schlaepfer (41). For overexpression experiments, HEK293 cells were transfected with Turbofect (R0531, Thermofisher Scientific, CA) according to manufacturer instructions. All knockdown experiments were performed using siRNAs purchased from Horizon Discovery Biosciences (Non-targeting Control: D-001810-10-05, PTEN: L-003023-00-0005, TSC2: L-003029-00-0005, GNAQ: L-008562-00-0005, FAK: L-003164-00-0005, PIK3CA: L-003018-00-0005, PIK3CB: L-003019-00-0005, PIK3CD: L-006775-00-0005), and Lipofectamine RNAiMAX Reagent (13778150, Thermofisher Scientific, CA) according to manufacturer's instructions.

CRISPR Screen and analysis: Genome wide CRISPR-KO screen was performed using the methods described in (24). Briefly, LentiCas9-Blast plasmid was a gift from Feng Zhang (Addgene plasmid #52962) and was used to generate Cas9-expressing 92.1 UM cell line (92.1^{Cas9}). The human Brunello whole genome CRISPR pooled library was a gift from David Root and John Doench (Addgene #73178). The library contains 76,441 sgRNAs targeting 19,114 genes (4 sgRNA per gene) and 1000 non-targeting sgRNAs as the negative control.

The screen was performed by seeding 92.1^{Cas9} cells into 2 245 mm x 245 mm tissue culture dishes plates (12 x 10^6 cells/plate) divided into two treatment arms: 3 replicate plates for either vehicle/DMSO or VS-4718 treatments. A total of 24 x 10^6 cells were passaged into new plates containing DMSO or 0.1μM VS-4718 until the population doubling level reached 19. A total of 24 x 10^6 cells were aliquoted from each plate at the end of the screen and stored at 80°C for genomic DNA extraction, and subsequent sgRNA quantification. The entirety of isolated genomic DNA was used for subsequent PCR, to ensure capturing the full representation of the libraries. PCR products were sequenced on a HiSeq4000 instrument (Illumina) (350M Reads).

NGS read counts were processed, aligned, using PinAPL-Py (v2.9.2) (42). Read counts were analyzed using Mageck-MLE (0.5.9.5) (43,44) to identify enrichment or depletion of sgRNAs in treatment vs control samples. Overrepresentation analysis of top resistance driving hits against KEGG (45) and Biocarta (46) pathways was performed by computing statistical overlap (hypergeometric test) of all sgRNA with positive beta score and FDR < 0.015 using MSigDB (v7.5.1) (47,48). P-value is derived from hypergeometric distribution, FDR q-value was corrected for multiple hypothesis testing according to Benjamini-Hochberg method.

Cell viability assay: Cells were seeded at a density of 8000 cells/well in 96-well white plates. Eight dilutions of each inhibitor were assayed in technical triplicates for 72 hours. Cell viability was measured with the AquaBluer Cell Viability Reagent on a Spark microplate reader (Tecan).

Using the GraphPad Prism v8.2.0 software, the half-maximal inhibitor concentration values (GI_{50}) were determined from the curve using the nonlinear log (inhibitor) versus response–variable slope (three parameters) equation. GI_{50} values were only determined for compounds that inhibited growth by more than 50%.

Immunoblotting and Immunoprecipitations: Cells were serum starved overnight, and then treated according to the conditions in the figure legend. For cell lysis, cells were washed 2X in cold PBS and lysed in 1XCell Lysis buffer (Cell Signaling Technologies, 9803) supplemented with HaltTM Protease and Phosphatase Inhibitor Cocktail (#78440, ThermoFisher Scientific) and 1mM Sodium Orthovanadate (P0758S, New England Biolabs). Lysates were centrifuged at max speed at 4°C, concentrations were measured using DC Protein Assay (BioRad Laboratories, 5000111) and lysates were prepared with addition of 4x Laemmli Sample Buffer (#1610747, BioRad Laboratories), and boiled for 5min at 98°C.

For immunoprecipitations, cells were lysed with IP lysis buffer [10 mM Tris-Cl (pH 8.0), 150 mM NaCl, 1 mM EDTA, 0.3% CHAPS, 50 mM NaF, 1.5 mM Na3VO4, protease/phosphatase inhibitor (Thermo Scientific, CO), 1 mM DTT, 1 mM PMSF], and centrifuged at 16,000 g for 5 min at 4°C. Supernatants were incubated with primary antibody overnight at 4°C, and protein A conjugated Sepharose beads for 1 hr at 4°C. Beads were washed 3 times with lysis buffer and prepared with addition of 4x Laemmli Sample Buffer (#1610747, BioRad Laboratories), and boiled for 5min at 98°C.

For immunoblotting, cell lysates were subjected to SDS/PAGE on 10% acrylamide gels and electroblotted to PVDF membranes. Blocking and primary and secondary antibody incubations of immunoblots were performed in Tris-buffered saline + 0.1% Tween 20 supplemented with 5%

(w/v) BSA or 5% w/v skim milk. Primary antibodies were all purchased from Cell Signaling Technologies and used at 1:1000. FAK (71433), pY397-FAK (8556), PTEN (9188), TSC2 (4308), AKT (4691), pS473-AKT (4060), S6 (2317), pS235/236 S6 (4858), ERK1/2 (9102), pT202/Y204-ERK1/2 (4370), GAPDH (5174), Beta-actin (4970), Vinculin (13901), p-Tyrosine (8954), p85 (4257), p110α (4249), p110β (3011), p110δ (34050). HRP-conjugated goat anti-rabbit and anti-mouse IgGs (Southern Biotech, AL) were used at a dilution of 1:30,000, and immunoreactive bands were detected using Immobilon Western Chemiluminescent HRP substrate (Millipore, MA) according to the manufacturer's instructions.

3.6 Acknowledgements

Chapter 3, in full, is under review for publication of the material in "Whole genome CRISPR screening identifies PI3K/AKT as a downstream component of the oncogenic GNAQ-FAK signaling circuitry" in the *Journal of Biological Sciences*. Arang, Nadia; Lubrano, Simone; Rigiracciolo, Damiano Cosimo; Nachmanson, Daniela; Mali, Prashant; Harismendy, Olivier; Gutkind, J Silvio. The dissertation author was the primary investigator and author of this paper.

3.7 References

1. Pierce, K. L., Premont, R. T., and Lefkowitz, R. J. (2002) Seven-transmembrane receptors. *Nat Rev Mol Cell Biol* **3**, 639-650
2. Arang, N., and Gutkind, J. S. (2020) G Protein-Coupled receptors and heterotrimeric G proteins as cancer drivers. *FEBS Lett* **594**, 4201-4232
3. Dorsam, R. T., and Gutkind, J. S. (2007) G-protein-coupled receptors and cancer. *Nat Rev Cancer* **7**, 79-94
4. O'Hayre, M., Vazquez-Prado, J., Kufareva, I., Stawiski, E. W., Handel, T. M., Seshagiri, S., and Gutkind, J. S. (2013) The emerging mutational landscape of G proteins and G-protein-coupled receptors in cancer. *Nat Rev Cancer* **13**, 412-424
5. Wu, V., Yeerna, H., Nohata, N., Chiou, J., Harismendy, O., Raimondi, F., Inoue, A., Russell, R. B., Tamayo, P., and Gutkind, J. S. (2019) Illuminating the Onco-GPCRome: Novel G protein-coupled receptor-driven oncocrine networks and targets for cancer immunotherapy. *J Biol Chem* **294**, 11062-11086

6. Van Raamsdonk, C. D., Bezrookove, V., Green, G., Bauer, J., Gaugler, L., O'Brien, J. M., Simpson, E. M., Barsh, G. S., and Bastian, B. C. (2009) Frequent somatic mutations of GNAQ in uveal melanoma and blue nevi. *Nature* **457**, 599-602
7. Van Raamsdonk, C. D., Griewank, K. G., Crosby, M. B., Garrido, M. C., Vemula, S., Wiesner, T., Obenauf, A. C., Wackernagel, W., Green, G., Bouvier, N., Sozen, M. M., Baimukanova, G., Roy, R., Heguy, A., Dolgalev, I., Khanin, R., Busam, K., Speicher, M. R., O'Brien, J., and Bastian, B. C. (2010) Mutations in GNA11 in uveal melanoma. *The New England journal of medicine* **363**, 2191-2199
8. Vaque, J. P., Dorsam, R. T., Feng, X., Iglesias-Bartolome, R., Forsthoefel, D. J., Chen, Q., Debant, A., Seeger, M. A., Ksander, B. R., Teramoto, H., and Gutkind, J. S. (2013) A genome-wide RNAi screen reveals a Trio-regulated Rho GTPase circuitry transducing mitogenic signals initiated by G protein-coupled receptors. *Molecular cell* **49**, 94-108
9. Feng, X., Degese, M. S., Iglesias-Bartolome, R., Vaque, J. P., Molinolo, A. A., Rodrigues, M., Zaidi, M. R., Ksander, B. R., Merlino, G., Sodhi, A., Chen, Q., and Gutkind, J. S. (2014) Hippo-independent activation of YAP by the GNAQ uveal melanoma oncogene through a trio-regulated rho GTPase signaling circuitry. *Cancer Cell* **25**, 831-845
10. Robertson, A. G., Shih, J., Yau, C., Gibb, E. A., Oba, J., Mungall, K. L., Hess, J. M., Uzunangelov, V., Walter, V., Danilova, L., Lichtenberg, T. M., Kucherlapati, M., Kimes, P. K., Tang, M., Penson, A., Babur, O., Akbani, R., Bristow, C. A., Hoadley, K. A., Iype, L., Chang, M. T., Network, T. R., Cherniack, A. D., Benz, C., Mills, G. B., Verhaak, R. G. W., Griewank, K. G., Felau, I., Zenklusen, J. C., Gershenwald, J. E., Schoenfield, L., Lazar, A. J., Abdel-Rahman, M. H., Roman-Roman, S., Stern, M. H., Cebulla, C. M., Williams, M. D., Jager, M. J., Coupland, S. E., Esmaeli, B., Kandoth, C., and Woodman, S. E. (2017) Integrative Analysis Identifies Four Molecular and Clinical Subsets in Uveal Melanoma. *Cancer Cell* **32**, 204-220 e215
11. Singh, A. D., Turell, M. E., and Topham, A. K. (2011) Uveal melanoma: trends in incidence, treatment, and survival. *Ophthalmology* **118**, 1881-1885
12. Luke, J. J., USA, H. M. S. D. F. C. I. B. M., Triozzi, P. L., USA, M. C. B. W. F. U. C. C. W. S. N., McKenna, K. C., USA, U. o. P. C. I. P. P., Van Meir, E. G., USA, T. W. C. I. o. E. U. S. o. M. A. G., Gershenwald, J. E., USA, U. o. T. M. A. C. C. H. T., Bastian, B. C., USA, U. o. C. S. F. H. D. C. C. C. S. F. C., Gutkind, J. S., USA, N. I. o. D. a. C. R. B. M., Bowcock, A. M., UK, N. H. L. I. I. C. L., Streicher, H. Z., USA, N. C. I. B. M., Patel, P. M., UK, U. o. N. N., Sato, T., USA, T. J. U. T. K. C. C. P. P., Sossman, J. A., USA, V. U. V. I. C. C. N. T., Sznol, M., USA, Y. U. Y. C. C. N. H. C., Welch, J., USA, N. C. I. B. M., Thurin, M., USA, N. C. I. B. M., Selig, S., USA, B. a. W. s. H. a. t. M. R. F. C. O. W. D., Flaherty, K. T., USA, H. M. S. M. G. H. C. C. B. M., Carvajal, R. D., and USA, M. S. K. C. C. N. Y. N. (2016) Biology of advanced uveal melanoma and next steps for clinical therapeutics. *Pigment Cell & Melanoma Research* **28**, 135-147
13. Falchook, G. S., Lewis, K. D., Infante, J. R., Gordon, M. S., Vogelzang, N. J., DeMarini, D. J., Sun, P., Moy, C., Szabo, S. A., Roadcap, L. T., Peddareddigari, V. G., Lebowitz, P. F., Le, N. T., Burris, H. A., 3rd, Messersmith, W. A., O'Dwyer, P. J., Kim, K. B., Flaherty, K., Bendell, J. C., Gonzalez, R., Kurzrock, R., and Fecher, L. A. (2012) Activity of the oral MEK inhibitor trametinib in patients with advanced melanoma: a phase 1 dose-escalation trial. *Lancet Oncol* **13**, 782-789
14. Carvajal, R. D., Sosman, J. A., Quevedo, J. F., Milhem, M. M., Joshua, A. M., Kudchadkar, R. R., Linette, G. P., Gajewski, T. F., Lutzky, J., Lawson, D. H., Lao, C. D., Flynn, P. J., Albertini, M. R., Sato, T., Lewis, K., Doyle, A., Ancell, K., Panageas, K. S., Bluth, M., Hedvat, C., Erinjeri, J., Ambrosini, G., Marr, B., Abramson, D. H., Dickson, M. A., Wolchok, J. D., Chapman, P. B., and Schwartz, G. K. (2014) Effect of selumetinib vs chemotherapy on progression-free survival in uveal melanoma: a randomized clinical trial. *Jama* **311**, 2397-2405

15. Carvajal, R. D., Piperno-Neumann, S., Kapiteijn, E., Chapman, P. B., Frank, S., Joshua, A. M., Piulats, J. M., Wolter, P., Cocquyt, V., Chmielowski, B., Evans, T. R. J., Gastaud, L., Linette, G., Berking, C., Schachter, J., Rodrigues, M. J., Shoushtari, A. N., Clemett, D., Ghiorghiu, D., Mariani, G., Spratt, S., Lovick, S., Barker, P., Kilgour, E., Lai, Z., Schwartz, G. K., and Nathan, P. (2018) Selumetinib in Combination With Dacarbazine in Patients With Metastatic Uveal Melanoma: A Phase III, Multicenter, Randomized Trial (SUMIT). *J Clin Oncol* **36**, 1232-1239
16. Nathan, P., Hassel, J. C., Rutkowski, P., Baurain, J. F., Butler, M. O., Schlaak, M., Sullivan, R. J., Ochsenreither, S., Dummer, R., Kirkwood, J. M., Joshua, A. M., Sacco, J. J., Shoushtari, A. N., Orloff, M., Piulats, J. M., Milhem, M., Salama, A. K. S., Curti, B., Demidov, L., Gastaud, L., Mauch, C., Yushak, M., Carvajal, R. D., Hamid, O., Abdullah, S. E., Holland, C., Goodall, H., Piperno-Neumann, S., and Investigators, I. M.-. (2021) Overall Survival Benefit with Tebentafusp in Metastatic Uveal Melanoma. *The New England journal of medicine* **385**, 1196-1206
17. Middleton, M. R., McAlpine, C., Woodcock, V. K., Corrie, P., Infante, J. R., Steven, N. M., Evans, T. R. J., Anthoney, A., Shoushtari, A. N., Hamid, O., Gupta, A., Vardeu, A., Leach, E., Naidoo, R., Stanhope, S., Lewis, S., Hurst, J., O'Kelly, I., and Sznol, M. (2020) Tebentafusp, A TCR/Anti-CD3 Bispecific Fusion Protein Targeting gp100, Potently Activated Antitumor Immune Responses in Patients with Metastatic Melanoma. *Clin Cancer Res* **26**, 5869-5878
18. Rozengurt, E. (2007) Mitogenic signaling pathways induced by G protein-coupled receptors. *J Cell Physiol* **213**, 589-602
19. Hubbard, K. B., and Hepler, J. R. (2006) Cell signalling diversity of the Gqalpha family of heterotrimeric G proteins. *Cell Signal* **18**, 135-150
20. Smrcka, A. V., Brown, J. H., and Holz, G. G. (2012) Role of phospholipase Cepsilon in physiological phosphoinositide signaling networks. *Cell Signal* **24**, 1333-1343
21. Sanchez-Fernandez, G., Cabezudo, S., Garcia-Hoz, C., Beninca, C., Aragay, A. M., Mayor, F., Jr., and Ribas, C. (2014) Galphaq signalling: the new and the old. *Cell Signal* **26**, 833-848
22. Feng, X., Arang, N., Rigiracciolo, D. C., Lee, J. S., Yeerna, H., Wang, Z., Lubrano, S., Kishore, A., Pachter, J. A., Konig, G. M., Maggiolini, M., Kostenis, E., Schlaepfer, D. D., Tamayo, P., Chen, Q., Ruppin, E., and Gutkind, J. S. (2019) A Platform of Synthetic Lethal Gene Interaction Networks Reveals that the GNAQ Uveal Melanoma Oncogene Controls the Hippo Pathway through FAK. *Cancer Cell* **35**, 457-472 e455
23. Liu, G. Y., and Sabatini, D. M. (2020) mTOR at the nexus of nutrition, growth, ageing and disease. *Nat Rev Mol Cell Biol* **21**, 183-203
24. Paradis, J. S., Acosta, M., Saddawi-Konefka, R., Kishore, A., Gomes, F., Arang, N., Tiago, M., Coma, S., Lubrano, S., Wu, X., Ford, K., Day, C. P., Merlino, G., Mali, P., Pachter, J. A., Sato, T., Aplin, A. E., and Gutkind, J. S. (2021) Synthetic Lethal Screens Reveal Cotargeting FAK and MEK as a Multimodal Precision Therapy for GNAQ-Driven Uveal Melanoma. *Clin Cancer Res* **27**, 3190-3200
25. Ballou, L. M., Lin, H. Y., Fan, G., Jiang, Y. P., and Lin, R. Z. (2003) Activated G alpha q inhibits p110 alpha phosphatidylinositol 3-kinase and Akt. *J Biol Chem* **278**, 23472-23479
26. Ballou, L. M., Chattopadhyay, M., Li, Y., Scarlata, S., and Lin, R. Z. (2006) Galphaq binds to p110alpha/p85alpha phosphoinositide 3-kinase and displaces Ras. *Biochem J* **394**, 557-562
27. Wu, E. H., Tam, B. H., and Wong, Y. H. (2006) Constitutively active alpha subunits of G(q/11) and G(12/13) families inhibit activation of the pro-survival Akt signaling cascade. *FEBS J* **273**, 2388-2398

28. Cabezudo, S., Sanz-Flores, M., Caballero, A., Tasset, I., Rebollo, E., Diaz, A., Aragay, A. M., Cuervo, A. M., Mayor, F., Jr., and Ribas, C. (2021) Galphaq activation modulates autophagy by promoting mTORC1 signaling. *Nat Commun* **12**, 4540
29. Guettier, J. M., Gautam, D., Scarselli, M., Ruiz de Azua, I., Li, J. H., Rosemond, E., Ma, X., Gonzalez, F. J., Armbruster, B. N., Lu, H., Roth, B. L., and Wess, J. (2009) A chemical-genetic approach to study G protein regulation of beta cell function in vivo. *Proc Natl Acad Sci U S A* **106**, 19197-19202
30. Armbruster, B. N., Li, X., Pausch, M. H., Herlitze, S., and Roth, B. L. (2007) Evolving the lock to fit the key to create a family of G protein-coupled receptors potently activated by an inert ligand. *Proc Natl Acad Sci U S A* **104**, 5163-5168
31. Vanhaesebroeck, B., Perry, M. W. D., Brown, J. R., Andre, F., and Okkenhaug, K. (2021) PI3K inhibitors are finally coming of age. *Nat Rev Drug Discov* **20**, 741-769
32. Amirouchene-Angelozzi, N., Nemati, F., Gentien, D., Nicolas, A., Dumont, A., Carita, G., Camonis, J., Desjardins, L., Cassoux, N., Piperno-Neumann, S., Mariani, P., Sastre, X., Decaudin, D., and Roman-Roman, S. (2014) Establishment of novel cell lines recapitulating the genetic landscape of uveal melanoma and preclinical validation of mTOR as a therapeutic target. *Molecular oncology* **8**, 1508-1520
33. Lopez-Ilasaca, M., Crespo, P., Pellici, P. G., Gutkind, J. S., and Wetzker, R. (1997) Linkage of G protein-coupled receptors to the MAPK signaling pathway through PI 3-kinase gamma. *Science* **275**, 394-397
34. Dbouk, H. A., Vadas, O., Shymanets, A., Burke, J. E., Salamon, R. S., Khalil, B. D., Barrett, M. O., Waldo, G. L., Surve, C., Hsueh, C., Perisic, O., Harteneck, C., Shepherd, P. R., Harden, T. K., Smrcka, A. V., Taussig, R., Bresnick, A. R., Nurnberg, B., Williams, R. L., and Backer, J. M. (2012) G protein-coupled receptor-mediated activation of p110beta by Gbetagamma is required for cellular transformation and invasiveness. *Science signaling* **5**, ra89
35. Vadas, O., Dbouk, H. A., Shymanets, A., Perisic, O., Burke, J. E., Abi Saab, W. F., Khalil, B. D., Harteneck, C., Bresnick, A. R., Nurnberg, B., Backer, J. M., and Williams, R. L. (2013) Molecular determinants of PI3Kgamma-mediated activation downstream of G-protein-coupled receptors (GPCRs). *Proc Natl Acad Sci U S A* **110**, 18862-18867
36. Khalil, B. D., Hsueh, C., Cao, Y., Abi Saab, W. F., Wang, Y., Condeelis, J. S., Bresnick, A. R., and Backer, J. M. (2016) GPCR Signaling Mediates Tumor Metastasis via PI3Kbeta. *Cancer Res* **76**, 2944-2953
37. Guzman-Hernandez, M. L., Vazquez-Macias, A., Carretero-Ortega, J., Hernandez-Garcia, R., Garcia-Regalado, A., Hernandez-Negrete, I., Reyes-Cruz, G., Gutkind, J. S., and Vazquez-Prado, J. (2009) Differential inhibitor of Gbetagamma signaling to AKT and ERK derived from phosducin-like protein: effect on sphingosine 1-phosphate-induced endothelial cell migration and in vitro angiogenesis. *J Biol Chem* **284**, 18334-18346
38. Shoushtari, A. N., Khan, S., Komatsubara, K., Feun, L., Acquavella, N., Singh-Kandah, S., Negri, T., Nesson, A., Abbate, K., Cremers, S., Musi, E., Ambrosini, G., Lee, S., Schwartz, G. K., and Carvajal, R. D. (2021) A Phase Ib Study of Sotrastaurin, a PKC Inhibitor, and Alpelisib, a PI3Kalpha Inhibitor, in Patients with Metastatic Uveal Melanoma. *Cancers (Basel)* **13**
39. Yu, F. X., Luo, J., Mo, J. S., Liu, G., Kim, Y. C., Meng, Z., Zhao, L., Peyman, G., Ouyang, H., Jiang, W., Zhao, J., Chen, X., Zhang, L., Wang, C. Y., Bastian, B. C., Zhang, K., and Guan, K. L. (2014) Mutant Gq/11 promote uveal melanoma tumorigenesis by activating YAP. *Cancer Cell* **25**, 822-830
40. Inoue, A., Raimondi, F., Kadji, F. M. N., Singh, G., Kishi, T., Uwamizu, A., Ono, Y., Shinjo, Y., Ishida, S., Arang, N., Kawakami, K., Gutkind, J. S., Aoki, J., and Russell, R. B. (2019) Illuminating G-Protein-Coupling Selectivity of GPCRs. *Cell* **177**, 1933-1947 e1925

41. Lawson, C., Lim, S. T., Uryu, S., Chen, X. L., Calderwood, D. A., and Schlaepfer, D. D. (2012) FAK promotes recruitment of talin to nascent adhesions to control cell motility. *J Cell Biol* **196**, 223-232
42. Spahn, P. N., Bath, T., Weiss, R. J., Kim, J., Esko, J. D., Lewis, N. E., and Harismendy, O. (2017) PinAPL-Py: A comprehensive web-application for the analysis of CRISPR/Cas9 screens. *Sci Rep* **7**, 15854
43. Li, W., Xu, H., Xiao, T., Cong, L., Love, M. I., Zhang, F., Irizarry, R. A., Liu, J. S., Brown, M., and Liu, X. S. (2014) MAGeCK enables robust identification of essential genes from genome-scale CRISPR/Cas9 knockout screens. *Genome Biol* **15**, 554
44. Li, W., Koster, J., Xu, H., Chen, C. H., Xiao, T., Liu, J. S., Brown, M., and Liu, X. S. (2015) Quality control, modeling, and visualization of CRISPR screens with MAGeCK-VISPR. *Genome Biol* **16**, 281
45. Kanehisa, M., Sato, Y., Kawashima, M., Furumichi, M., and Tanabe, M. (2016) KEGG as a reference resource for gene and protein annotation. *Nucleic Acids Res* **44**, D457-462
46. Nishimura, D. (2001) BioCarta. *Biotech Software & Internet Report: The Computer Software Journal for Scientists* **2**, 117–120
47. Subramanian, A., Tamayo, P., Mootha, V. K., Mukherjee, S., Ebert, B. L., Gillette, M. A., Paulovich, A., Pomeroy, S. L., Golub, T. R., Lander, E. S., and Mesirov, J. P. (2005) Gene set enrichment analysis: a knowledge-based approach for interpreting genome-wide expression profiles. *Proc Natl Acad Sci U S A* **102**, 15545-15550
48. Liberzon, A., Subramanian, A., Pinchback, R., Thorvaldsdottir, H., Tamayo, P., and Mesirov, J. P. (2011) Molecular signatures database (MSigDB) 3.0. *Bioinformatics* **27**, 1739-1740

CHAPTER 4: High throughput chemogenetic drug screening reveals kinase-driven therapeutic vulnerabilities in GNAQ-mutant uveal melanoma

4.1 Introduction

In the current era of precision medicine, targeted therapies have transformed the standard of care and clinical outcomes for numerous cancer types. Examples of success include imatinib for BCR-ABL-driven chronic myeloid leukemia (CML)(1), and trastuzumab against HER2+ breast cancer(2), in both cases this approach takes advantage of cancer-specific oncogene addiction that can serve as actionable therapeutic targets. This paradigm has proven to be particularly true for cancer types with well-defined cancer-driving genetic alterations, in which the integration of genomic data to functional signaling events can be readily translated into targetable molecular vulnerabilities.

However, in spite of their clearly identifiable oncogenic drivers, we still lack effective targeted therapies for many human malignancies. This includes uveal melanoma (UM), the most common intraocular malignancy in adults, and the second most frequent melanoma site after skin cutaneous melanoma (SKCM)(3). UM is unique among adult cancers with one of the lowest mutation burdens across all cancers in The Cancer Genome Atlas (TCGA)(3). Whereas most SKCM typically possess characteristic *BRAF* or *NRAS* mutations, UM is driven by aberrant activation of the Gαq pathway, with >95% of patients harboring gain-of-function mutation of *GNAQ/GNA11*, encoding the Gαq subunit family of heterotrimeric G proteins, and rendering them as driver oncogenes(3-5). Patients lacking *GNAQ/11* mutations typically possess mutation and subsequent aberrant activation of *CYSLTR2*, a Gαq-coupled GPCR(3,6). Roughly 50% of UM patients progress to metastatic UM (mUM), which is associated with loss of function in BAP1 and is highly refractory to current therapies with a median survival of approximately 1 year(7-10).

Gαq and Gαq-coupled GPCRs have been long implicated as drivers of neoplastic growth, involved in numerous human malignancies, including UM(4,11-14). Canonically, Gαq signals through PLCβ, initiating the generation of second messenger systems that lead to the activation of PKCs, and the MEK/ERK MAPK cascade via RasGEFs such as RASGRP3(15-20). However despite the clean genetic landscape, there are limited targeted therapies available for UM. Clinical efforts aimed towards inhibition of MAPK signaling using agents including trametinib and selumetinib have not demonstrated a significant clinical benefit or improvement in overall patient survival(21-23). Tebentafusp, a bispecific fusion antibody, has been recently approved in unresectable or mUM patients; however, only 50% of the patient population is eligible based on HLA haplotype restriction and responses remain limited with a 9% objective response rate(24-26). Moreover, while we and others have shown that targeted inhibition of Gαq/11 using agents such as FR900359, a cyclic desipeptide, effectively block Gαq function and decrease UM growth, the centrality of Gαq to essential physiological processes including neurotransmission, cardiac function, and vasculogenesis, pose a significant challenge towards the development of safe agents targeting Gαq for the treatment of UM and other Gαq-driven malignancies in the clinic(27,28). Taken together, there is a critical and urgent need for novel therapeutic strategies against mUM and advanced primary UM cases.

In this regard, functional genetics approaches have served as highly valuable tools for the identification of molecular targets for multiple cancer types. However, our ability to translate cancer cell dependencies to the clinic is often not limited to the discovery of novel gene candidates, but rather restricted by the toolbox of approved, or soon-to-be approved pharmacological agents at our disposal. The limited genetic aberrancies in UM and its defined oncogenic signaling drivers, coupled with the lack of FDA-approved targeted therapies provided

a unique opportunity to use a network chemical biology-based approach to identify pharmacologically tractable UM-specific vulnerabilities that can be readily translated to the clinic.

4.2 Results

4.2.1 A chemogenetic screen defines the druggable landscape of UM

To comprehensively characterize the cell-intrinsic vulnerabilities of GNAQ-mutant UM, we performed a high throughput chemogenetic screen using a library of highly annotated, oncology-focused agents that have been prioritized for their clinical relevance while maintaining high mechanistic and biological target diversity (Fig 4.1A). Screening 4 genetically distinct GNAQ-mutant UM and 3 BRAF-mutant SKCM cell lines against ~2500 agents, we performed full 11-point dose response curves for each agent, generating nearly 20,000 dose-response signatures that could be used to generate area-under-the-curve (AUC) scores. Using Z-transformed AUC scores, we ranked compound activities and classify hits. Unsupervised hierarchical clustering of drug-activity profiles resulted in separation of UM and SKCM cell clusters demonstrating strong genotype-driven compound sensitivities (Fig 4.1B). We took advantage of differences in AUCs in order to extract drugs with preferential activity against UM identifying 70 uveal-specific hits, and 84 cutaneous-specific hits (Fig 4.1C). Using an approach we developed termed Drug Set Enrichment Analysis (DSEA), we further interrogated the dataset in order to classify the most highly enriched drug targets. Our approach revealed a number of target classes that have not yet been explored in the context of UM, including XPO1, CHEK1, and MCL1, and a high representation of epigenetic modifiers including agents targeting HDAC1,6 and BRD2,4 (Fig 4.1D, Fig S4.1A,B). PKC targeting drugs also emerged amongst the top hits (Fig 4.1D, E, Fig S4.1A). As PKC inhibitors (PKCi). Given the relevance of PKC to canonical Gαq signaling, we chose to further investigate the subset of agents targeting PKC from our screen[14]. Among them, LXS-196, a PKCi under current clinical investigation for the treatment of UM, exhibited the most highly differential Z-AUC score, and lowest IC50 across all PKCi tested (Fig 4.1E, 4.1F)[15]. Aligned with

the basis of our screen, dose response curves of LXS-196 demonstrated strong UM-specific activity in comparison to SKCM cell viability (Fig 4.1G). As an independent target validation, PKCε (PRKCε) is among the top cell essential genes in UM, with a significantly stronger cell-dependency score in UM compared to SKCM, and all other cell lines in the Cancer Cell Line Encyclopedia (CCLE) as determined by whole genome wide CRISPR screening efforts (Fig 4.1H,I). Taken together, this convergence of genetic and pharmacological data establishing PKC as a critical survival node in UM. However, PKC inhibition has been tested in mUM in the clinic, with limited responses[16]. In this regard, we noticed that LXS-196 was more effective than classical PKC inhibitors, which raised the possibility that this agent may be more potent regarding target inhibition, or harbor other yet to be identified properties increasing its response in UM cells.

4.2.2 LXS-196 is a multitargeted kinase inhibitor blocking PKC and PKN.

We next investigated whether LXS-196 exerts unique activities that may help explain its increased activity in UM as compared to all other PKCi in our screen. We first examined the signaling inhibition profile of LXS-196 against the two major described signaling axes downstream of Gαq, using pERK as a surrogate of inhibition of canonical Gαq-driven signaling through PLCβ, and pFAK as a measure of inhibition of non-canonical signaling downstream of Gαq through TRIO and RhoA(34-36). We compared the activity of LXS-196 against Go6983, a broad-spectrum highly selective PKC inhibitor, and VS-4718, a highly specific FAK inhibitor (Fig 4.2A). We observed that both PKCi tested inhibit pERK at similar levels. However, we discovered that in contrast to Go6983, LXS-196 partially diminished pFAK, whereas Go6983 treatment had no effect on pFAK (Fig 4.2A). As a control, FR900359 (FR), an inhibitor of Gαq potently abrogated all Gαq-driven signaling (Fig S4.2A). This distinct activity of LXS-196 led us to ask whether this agent may help us identify a new mechanism whereby PKC could control FAK activity. To test this, we performed siRNA mediated knockdown (KD) of PKCδ and PKCε, the primary PKC isoforms described to be critical in UM(15). Aligned with our gene-essentiality data. We found that while PKC KD led to a

potent decrease in pERK, it did not affect pFAK (Fig 4.2B). This suggested that the ability of LXS-196 to reduce pFAK is not concordant with inhibition of PKC, but that instead it may involve additional yet to be elucidated mechanisms.

To explore this possibility, we performed a kinome-wide screen, testing the capacity of LXS-196 to inhibit enzymatic activity against the most commonly targeted kinases (Fig 4.2C). Among the top kinases with greater than 75% activity control included PKC isosymes, as expected (Fig 4.2C, D). However, of interest, the top kinase inhibited was PKN2, a member of the PKN (also known as PRK) kinase subfamily (Fig 4.2C, D). While they belong to the same kinase superfamily, PKCs and PKNs consisting of three members (PKN1, 2 and 3) have distinct N-terminal regulatory regions and diverge in their activation mechanisms(37). Namely, in contrast to the PKCs, the PKNs are a family of Rho-responsive kinases, and have been shown to be involved in numerous functions, including actin cytoskeleton remodeling, cell migration, and cell cycle regulation(37-42). To complement our kinome selectivity screen, we next performed a detailed analysis of LXS-196 activity against a selection of AGC family kinases using recombinant proteins and found strong activity against novel and conventional classes of PKCs in addition to PKN1 (Fig 4.2E). Aligned with the results of our screen, we found that LXS-196 treatment potently decreased the accumulation of the phosphorylated, active form of PKN (pPKN); however, treatment with Go-6983 or Sotrastaurin, the latter a clinical PKCi that failed to demonstrate significant clinical benefit in mUM patients(33) did not result in a change in pPKN levels (Fig 4.2F).

4.2.3 PKN converges with ROCK to control FAK downstream of the Gαq-RhoA signaling axis.

We next sought to determine the mechanism by which PKN controls FAK activity. We have previously shown that FAK acts as a central mediator of oncogenic signaling in UM by transducing signaling that is driven by mutant Gαq through the RhoA-ROCK signaling

pathway(36). To first understand the impact of a parallel RhoA-PKN signaling axis on controlling FAK activity, we expressed constitutively active mutants of Gαq (GαqQL) and RhoA (RhoAQL) in HEK293 cells as a widely used experimental cellular system. Immunoblotting against total and phosphorylated forms of FAK and PKN revealed that activation of Gαq or its downstream RhoA-initiated signaling mechanisms led to an increase in active phosphorylated FAK and PKN (Fig 4.3A). PKN has also been shown to be activated in response to binding to RhoA. To test this in an unbiased manner, and in the context of Gαq-driven signaling, we performed affinity-purification mass spectrometry (AP/MS) after doxycycline-inducible expression of a FLAG-tagged RhoA in Gαq-expressing HEK293 cells (Fig 4.3B). Indeed, upon expression of RhoA-FLAG, we observed robust binding of RhoA to Rhotekin, a canonical RhoA-activated protein, as well as PKN2 and PKN3 (Fig 4.3C)(43). Aligned with this, blockade of RhoA activity using C3 toxin, a potent and specific inhibitor of RhoA, abrogated the increase of pFAK, and phosphorylated forms of PKN in response to pathway activation by GαqQL (Fig 4.3D, left). Similarly, treatment of UM cells harboring Gαq mutations endogenously with C3 toxin decreased pFAK and pPKN (Fig 4.3D, right).

We next assessed the impact of PKN on FAK activity, and found in both HEK293 cells transfected with GαqQL as well as in UM cells, that knockdown of PKN isoforms, which are broadly expressed in UM cells resulted in a significant decrease in pFAK levels (Fig 4.3E, F, G, Fig S4.3A). Based on these results, we hypothesized that Gαq non-canonical signaling branches at the level of RhoA into ROCK and PKN-mediated signaling, converging on the promotion of FAK activity. To test this, we examined pFAK levels in response to the combination of PKN and ROCK inhibition. Independently, inhibition of PKN either using siRNA mediated knockdown (Fig 4.3H), or by LXS-196 (Fig 4.3I) resulted in a partial decrease in pFAK levels. In contrast, inhibition of PKN concomitant with ROCK inhibition potently decreased pFAK with similar efficiency as VS-4718, suggesting that RhoA controls FAK via two distinct ROCK and PKN-mediated signaling

axes (Fig 4.3H, I). Finally, to assess if PKN can directly promote the activity of FAK, we overexpressed PKN2 in HEK293 cells, and observed a marked increase in pFAK (Fig 4.3J). These results suggest that PKN is a component of the Gαq-regulated signaling circuitry in UM, and that together with ROCK, PKN converges on the promotion of FAK activity. This may in turn suggest that LXS-196 inhibits FAK activity by blocking PKN, independently of its activity on PKC.

4.2.4 LXS-196 transiently blocks Gαq signaling to YAP.

FAK has been shown to play a significant functional role in promoting tumor growth in UM by controlling YAP activity(36). Thus, we asked if the indirect inhibition of FAK through PKN by LXS-196 could control YAP as potently as direct FAK inhibition. As a tumor promoter, YAP is under negative regulation by the Hippo kinase cascade, namely by its phosphorylation on multiple sites, including S127 by the LATS1/2 kinases, which promotes its cytoplasmic retention and subsequent degradation(44,45). As YAP activity is tightly controlled by its phosphorylation state, we first assessed levels of YAP pS127 in response to FAK inhibition directly or via LXS-196 inhibition of PKN. Notably, while direct inhibition of FAK by VS-7418 promoted a potent and sustained increase in pS127 YAP, LXS-196 transiently increased YAP phosphorylation that reverted to baseline by 24hrs (Fig 4.4A). YAP is a transcriptional co-activator, which together with the TEAD family of transcription factors controls complex pro-growth transcriptional programs(45). To profile the functional impact of LXS-196 on YAP activity, we first assessed YAP transcriptional activity using a YAP/TEAD luciferase reporter. We found that aligned with our prior observations, while VS-4718 and LXS-196 both had early effects on inhibiting YAP/TEAD activity, the observed inhibition was lost in the LXS-196 condition over time (Fig 4.4B). To complement this, we assessed YAP nuclear localization by immunofluorescence in UM cells, which express high levels of nuclear YAP at baseline conditions. Aligned with the sustained increase in pS127 YAP after direct FAK inhibition, we observed significant reduction in nuclear-localized YAP, indicative of its suppression (Fig 4.4C). In contrast, LXS-196 treatment resulted in a partial reduction in YAP

nuclear localization (Fig 4.4C). Finally, we assessed levels of canonical YAP transcriptional targets. While VS4718 treatment led to a decrease in mRNA levels of CTGF, CYR61 and AMOTL2 as previously reported(36), LXS-196 treatment did not result in a decrease of gene expression, similar to treatment with Go6983 (Fig 4.4E). While these data suggest that LXS-196 interferes with Gαq-driven signaling by dual inhibition of PKC and PKN, it is insufficient to control FAK/YAP signaling fully (Fig 4.4F), which led us to explore the effect of combining them *in vitro* and in *in vivo* UM models of disease (see below).

4.2.5 High throughput combinatorial screening reveal that FAKi and PKCi are synergistic in UM *in vitro*

Based on our emerging results, we first examined the effect of co-targeting FAK- and PKC-regulated signaling axes. We found that the combination of FAKi using VS-4718 and LXS-196 synergistically inhibited cell viability and promoted apoptosis in UM cells (Fig 4.5A). We expanded our analysis to include a number of UM cell lines with distinct genetic BAP1 status and found strong synergistic profiles across all UM cell lines tested, suggesting that co-targeting FAK and PKC/PKN may be active in mUM (Fig 4.5B). We also observed that the combination of VS-4718 and LXS-196 was able to synergistically inhibit growth under 3D growth conditions (Fig S4.4A, B). We further interrogated multiple clinically relevant FAKi versus PKCi (LXS-196 and Go6983) in three UM cell lines. We observed synergistic antiproliferative effects in UM cells with the combination of FAKi with LXS-196 as well as Go6983, albeit the synergistic score was more significant for LXS-196 (Fig 4.5C). However, synergism was not observed in UM cells with the combination of BRAF and PKC inhibitors as a specificity control (Fig 4.5C). We next tested the ability of VS-4718 and LXS-196 to induce apoptotic cell death. Using a CaspaseGlo sensor for capase-3/7 cleavage as a measure of apoptosis, we observed significant induction of apoptosis aligned with our synergism results (Fig 4.5D). Complementing this, we assessed the ability of FAK and LXS-196 to induce apoptosis measuring levels of cleaved-PARP, a major substrate of

caspases. In most systems, FAKi have been shown to be primarily cytostatic in nature as single agents. In line with this, we observed minimal apoptotic effects using VS-4718 as a single agent; however, the combination of LXS-196 and FAKi potently induced apoptosis in several UM cell lines, including a BAP1 mutant cell line, emphasizing the potential of this combination in the context of mUM (Fig 4.5E). Interestingly, one cell line in our panel, OMM1.3, demonstrated greater sensitivity to single-agent LXS-196 treatment. Despite this, the majority of cell lines required both FAK and LXS-196 in order to promote apoptosis, supporting the use of the combination as a robust therapy against UM.

4.2.6 FAKi and LXS-196 are synergistic in UM preclinical *in vivo* models.

To further evaluate the anticancer activity of FAKi/LXS-196, we used two independent *in vivo* uveal melanoma models capturing clinically relevant stages of UM disease. First, we used a UM xenograft model using a human primary UM cell line 92.1, in NSG mice. Tumor bearing mice were randomized into 4 groups: vehicle control, VS-4718, LXS-196, and the VS-4718+LXS-196 combination and administered drugs at doses comparable to those used in humans in the clinic. Over the course of treatment, while single agent FAK and PKC/PKN inhibition were sufficient to induce partial control of tumor growth, only the combination was able to achieve and sustain tumor regression (Fig 4.6A, B). No significant changes in body weight of treated mice were observed, suggesting that treatments were well-tolerated by mice with minimal adverse events (Fig 4.6C). To monitor the signaling pathways in the xenograft tumors, we assessed levels of key MEK/ERK, FAK/YAP, and apoptotic pathway proteins by immunohistochemistry. As anticipated, treatment groups with FAKi resulted in nuclear exclusion of YAP (Fig 4.6D, E, Fig S4.5)(36). LXS-196 treated groups demonstrated a significant decrease in pERK, which is aligned with PKC control of canonical Gαq-driven signaling to MAPK (Fig 4.6D, E). Only the combination of VS-4718+LXS-196 resulted in a significant decrease in proliferating Ki67+ cells concomitant with a significant increase in cleaved-caspase 3 as a marker of apoptosis (Fig 4.6D, E). We finally interrogated the

efficacy of the VS-4718+LXS-196 combination treatment on a metastatic UM model. This model takes advantage of GFP-Luciferase expressing UM cells that exhibit a highly specific hepatotropism, which is aligned with clinical presentation of mUM in humans (Fig 4.6F)(46). Using this model, we observed a significant reduction in metastatic burden with the combination of VS-4718+LXS-196 (Fig 4.6 G, H). Similar to the tumor response observed in our xenograft model, VS-4718 and LXS-196 alone were predominantly cytostatic, whereas the combination induced potent and sustained tumor regression (Fig 4.6G, H). Taken together, our findings demonstrate that the combination of VS-4718+LXS-196 induces cytotoxic activity *in vitro* and *in vivo*, which cannot be achieved by administration of each single agent alone and support the future investigation evaluating the efficacy of this combination in the clinical setting.

4.3 Discussion

Although Gαq is the oncogenic driver in UM, a cancer type with limited additional genetic aberrancies, Gαq itself is not directly druggable with clinically ready compounds. Hence, targeting its downstream pro-proliferative signaling circuits may provide a precision therapy approach for mUM and other *GNAQ*-driven malignancies. However, there are no currently available targeted therapies for mUM, and in spite of the recent approval of Tebentafusp, a bispecific fusion antibody engaging T cells in eligible, HLA matched patients, responses remain limited. Coupled with the prior failure of MAPK inhibitors in clinical trials, the survival of mUM patients is still dismal(22,23). In this context, we have shown that parallel to the MAPK-mediated canonical signaling axis, Gαq controls a non-canonical oncogenic signaling axis through the RhoGEF TRIO and RhoA(34). This leads to the activation of FAK, which then promotes the aberrant activation of YAP to drive tumor growth, highlighting the complexity of the mechanisms by which Gαq and Gαq-coupled GPCRs promote aberrant cell proliferation(35,36,47).

Here, we took advantage of a clinically-oriented, oncology-focused compound library and performed high throughput single-agent and combinatorial chemogenetic drug screens to broadly interrogate the druggable landscapes of *BRAF*-mutant SKCM and *GNAQ*-mutant UM(29). In the context of SKCM, we identified enrichment of drug classes targeting mechanistic underpinnings of SKCM, including BRAF and MEK drug sets, and targets that have not yet been extensively investigated in SKCM, including GSK3B and HSP90AB1. Our focal effort in identifying molecular targets that may demonstrate synthetic lethality with oncogenic *GNAQ* also revealed a number of targets, including epigenetic modifiers, such as HDAC and BRD-targeting drug sets, which are being recently explored in UM. Among the UM-enriched drug targets, we also identified PKC inhibitors as a mechanistic class of compounds with high selective activity against UM. Guided by our finding that one PKC inhibitor, LXS-196, demonstrated superior performance compared to all other agents in our screen, and the proximity of PKC as a signal transducer of Gαq signaling, we further investigated PKC inhibition by LXS-196 as a precision therapeutic target in UM.

Our investigation interrogating the enhanced activity of LXS-196 as compared to other PKCi in UM revealed that it acts as a dual inhibitor of both PKC and PKN, the latter a closely related group of kinases in the AGC family of serine/threonine kinases. Compared to PKCs, PKNs are relatively poorly investigated, and PKN family members are considered part of the “dark kinome”, thus presenting an exciting opportunity to expand our understanding of their regulation mechanisms, downstream substrates, and role in the context of larger signaling networks(48). We find here that PKNs are activated downstream of Gq/RhoA. In addition, although there has been a recently proposed a role of PKC regulating FAK in UM, we show that blockade of PKN, but not PKC decreases FAK activity, and that in turn, PKN can further activate FAK(49). The latter is aligned with recent site-recognition screens of PKN-family kinases, which revealed FAK as a PKN substrate, thus suggesting that PKN may directly regulate FAK activity in UM(50). Taken together, these findings support that RhoA acts as a central signaling node for the non-canonical

Gαq signaling, coordinating an axis that bifurcates into ROCK and PKN-mediated control of FAK activity. This establishes PKN as a novel element of the multicomponent signaling network driven by Gαq. Moreover, our finding that LXS-196 acts as a multi-targeted inhibitor of both canonical and non-canonical Gαq-driven signaling pathways (e.g., PKC and FAK, respectively), defines the mechanism underlying the unique potency of LXS-196 as compared to other PKCi in UM. Indeed, while previous PKCi tested in UM patients have failed to demonstrate significant clinical responses, our observations revealing the multi-targeted activity of LXS-196 may explain its more promising clinical activity in ongoing trials(33,51).

Remarkably, our recently reported kinome-wide CRISPR/Cas9 sgRNA screen investigating compensatory resistance mechanisms to FAKi revealed the MAPK pathway and PRKCδ and PRKCε as top hits driving resistance to FAKi in UM(46). The blockade of these PKCs by LXS-196, thus disrupts the co-compensatory nature of these Gαq-driven signaling axes, and therefore enhance the response to FAKi. However, LXS-196 alone is insufficient to promote a sustained inhibition of YAP activity downstream of FAK. This is aligned with recent work demonstrating that PKC inhibitor monotherapy is not sufficient to suppress the multiple Gαq-regulated growth-promoting pathways in UM(52). Instead the partial reduction of FAK activation by LXS-196 may sensitize FAK for its further inhibition by direct ATP-competitive kinase inhibitors. This possibility is supported by the potent synergism we observe by co-targeting PKC/PKN and FAK mediated signaling pathways *in vitro* and *in vivo* xenograft and metastatic UM models. Within this framework, our findings, in the context of emerging studies investigating the complex signaling circuits underlying Gαq-driven UM, substantiate the usage of rational signal transduction-based combination therapies to control primary UM and mUM. Ongoing clinical trials using both LXS-196 (NCT03947385) and FAKi (NCT04109456) as single agents and other combinations, may enhance the clinical translatability of this approach. Specifically for the latter, our initial studies led to the initiation of a phase II clinical trial investigating the efficacy of co-

targeting of FAK and MEK-regulated pathways in mUM patients (NCT04720417). While this trial is ongoing, there remains an urgent need to identify additional treatment options for mUM patients(53). Our current study supports the combination of LXS-196 with FAKi as a potentially powerful precision medicine strategy for UM patients.

In this regard, as the field of precision medicine evolves to encompass the numerous molecular drivers of cancer, integrating the use of rational combination therapies will be key to compete with dynamic signaling crosstalk and feedback loops that often hamper durable clinical responses. Indeed, the failure of most clinical strategies against mUM are likely due in part to the complexity of the growth-driving and compensatory feedback mechanisms underlying the ability of persistent Gαq signaling to drive aberrant cell proliferation(30,31). Specifically, we have shown that canonical (PLCβ-PKC) and non-canonical (TRIO-Rho-FAK) signaling by Gαq are inherently co-compensatory in nature, thus reinforcing a multipronged pharmacology paradigm that ultimately requires co-targeting both Gαq-regulated signaling axes to achieve a durable clinical benefit(46). Taken together, our findings also clearly demonstrate the utility of chemogenetic drug screens and network-based approaches to identify new targetable signaling hubs, thereby strengthening the clinical toolbox against primary and mUM and working towards filling a large therapeutic gap for this *GNAQ*-driven malignancy

4.4 Figures

Figure 4.1 High throughput drug screening reveals PKC as a precision target in the druggable landscape of UM

A) Schematic of screening pipeline in GNAQ-mutant and BRAF-mutant cell lines. **B**) Heatmap depicting Z-transformed Area Under the Curve (AUC) scores for all cell lines versus MIPE 5.0 compound library. Compounds (rows) were sorted based on the difference in average Z-AUC (ΔZ-AUC) between UM and SKCM cell contexts. Unsupervised hierarchical clustering was performed on cell lines (columns). **C**) Average Z-AUCs for UM plotted against SKCM. Hits identified in the uveal context are highlighted in blue and SKCM hits are highlighted in red. **D**) Enrichment plot for PKC targeting drugs in uveal cell lines. **E**) Top 20 most selective drugs ranked by Z-AUC score. PKC-targeting drugs are shaded in darker blue, and BRAF-targeting drugs are shaded in darker red. **F**) IC_{50} values for all PKCi in UM cell lines. **G**) Cell viability curves across doses of LXS-196 in all cell lines screened. Data are the percent viability normalized to vehicle treatment. **H**) CRISPR gene effect plotted against -log10Pvalue for gene essentiality for all UM cell lines in Depmap. *I*) Gene effect for PRKCE in UM and SKCM cell lines in CCLE.

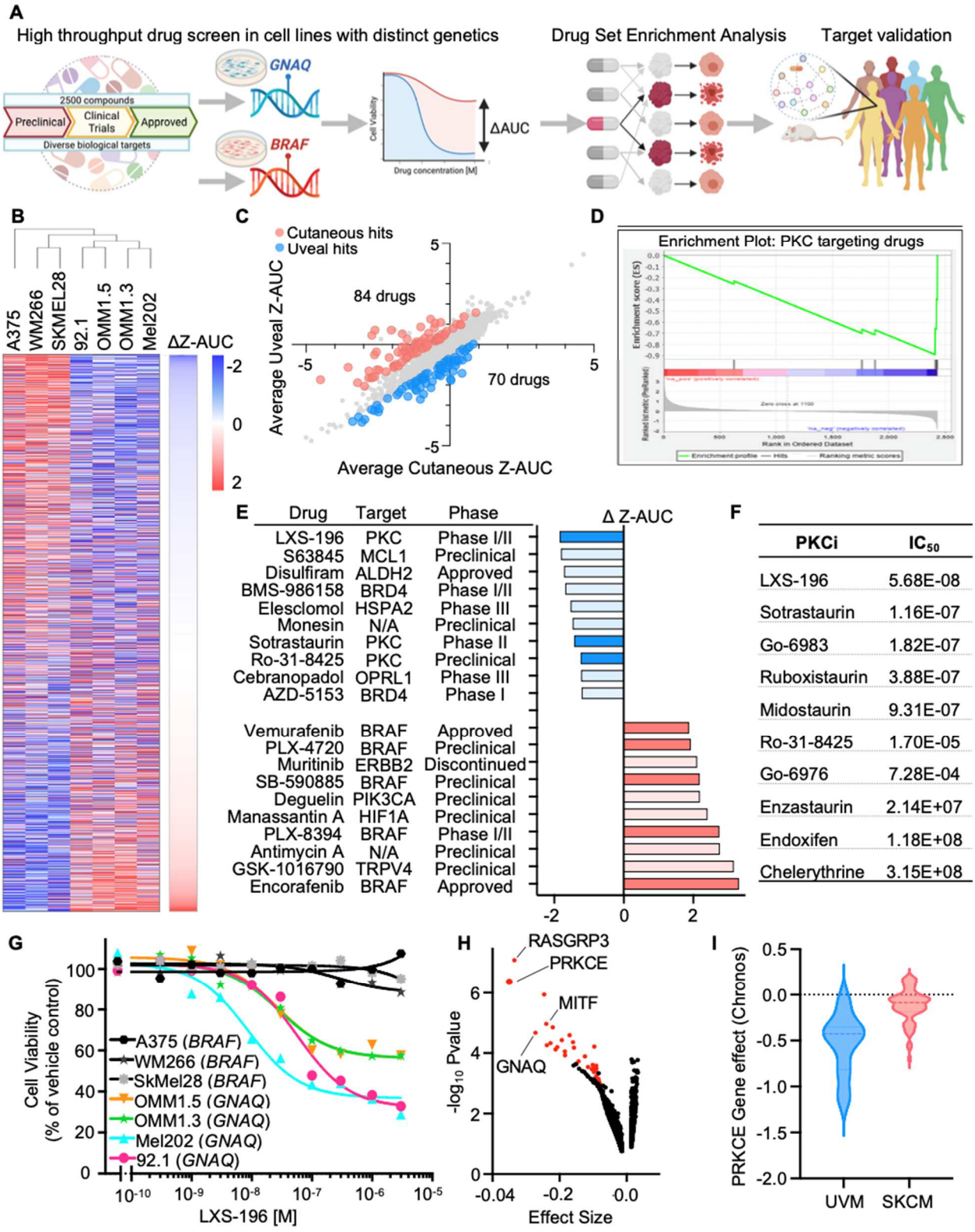
A
High throughput drug screen in cell lines with distinct genetics
Drug Set Enrichment Analysis
Target validation
2500 compounds
Preclinical
Clinical Trials
Approved
Diverse biological targets
GNAQ
BRAF
Cell Viability
Drug concentration [M]
ΔAUC
B
A375
WM266
SKMEL28
92.1
OMM1.5
OMM1.3
Mel202
ΔZ-AUC
-2
0
2
C
Cutaneous hits
Uveal hits
84 drugs
70 drugs
Average Uveal Z-AUC
Average Cutaneous Z-AUC
D
Enrichment Plot: PKC targeting drugs
Enrichment score (ES)
Rank in Ordered Dataset
Enrichment profile
Hits
Ranking metric scores
E
Drug Target Phase
LXS-196 PKC Phase I/II
S63845 MCL1 Preclinical
Disulfiram ALDH2 Approved
BMS-986158 BRD4 Phase I/II
Elesclomol HSPA2 Phase III
Monesin N/A Preclinical
Sotrastaurin PKC Phase II
Ro-31-8425 PKC Preclinical
Cebranopadol OPRL1 Phase III
AZD-5153 BRD4 Phase I
Vemurafenib BRAF Approved
PLX-4720 BRAF Preclinical
Muritinib ERBB2 Discontinued
SB-590885 BRAF Preclinical
Deguelin PIK3CA Preclinical
Manassantin A HIF1A Preclinical
PLX-8394 BRAF Phase I/II
Antimycin A N/A Preclinical
GSK-1016790 TRPV4 Preclinical
Encorafenib BRAF Approved
Δ Z-AUC
F
PKCi IC50
LXS-196 5.68E-08
Sotrastaurin 1.16E-07
Go-6983 1.82E-07
Ruboxistaurin 3.88E-07
Midostaurin 9.31E-07
Ro-31-8425 1.70E-05
Go-6976 7.28E-04
Enzastaurin 2.14E+07
Endoxifen 1.18E+08
Chelerythrine 3.15E+08
G
Cell Viability (% of vehicle control)
A375 (BRAF)
WM266 (BRAF)
SkMel28 (BRAF)
OMM1.5 (GNAQ)
OMM1.3 (GNAQ)
Mel202 (GNAQ)
92.1 (GNAQ)
LXS-196 [M]
H
RASGRP3
PRKCE
MITF
GNAQ
-log10 Pvalue
Effect Size
I
PRKCE Gene effect (Chronos)
UVM
SKCM

Figure 4.2 LXS-196 is a multitargeted inhibitor of PKC and PKN

A) Dose-dependent effects on phosphorylated FAK and ERK in UM cells in response to treatment with VS-4718, LXS-196 and Go6983 for 2hrs. **B**) Impact of siRNA mediated knockdown of PKCδ+ε on phosphorylated FAK, ERK and MEK in UM cells. **C**) Kinome profiling of LXS-196. Node size and color indicate degree of kinase inhibition in response to 1μM LXS-196. **D**) Percent kinase activity remaining after treatment with 1μM LXS-196 for top 15 kinases with highest inhibition. **E**) IC50 of LXS-196 on recombinant enzymes for a sub-panel of AGC kinases. **F**) Phosphorylation of PKNs and ERK in response to treatment with a panel of PKCi: 1μM LXS-196, Sotrastaurin and Go-6983 for 1hr.

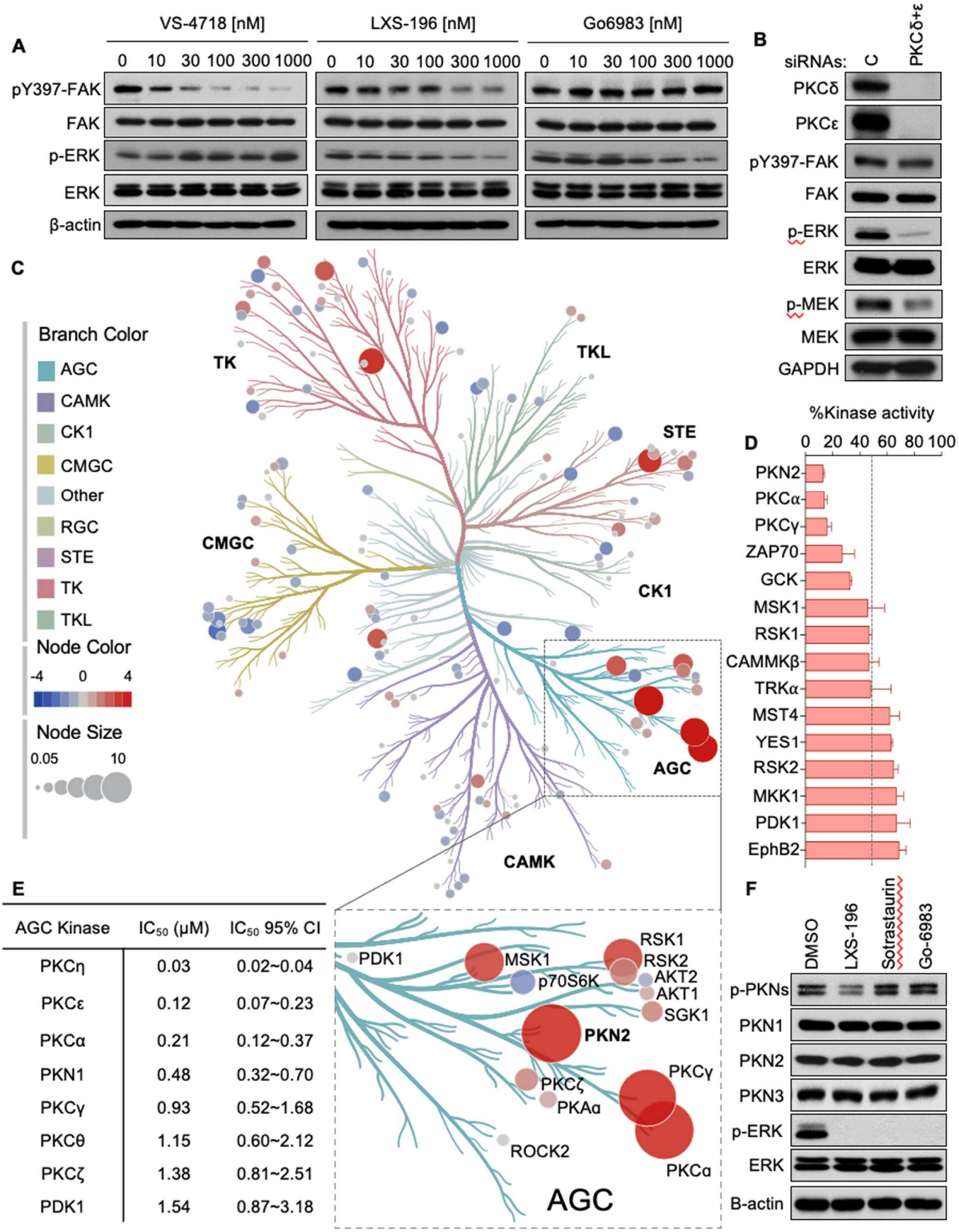

AGC Kinase	IC_{50} (μM)	IC_{50} 95% CI
PKCη	0.03	0.02~0.04
PKCε	0.12	0.07~0.23
PKCα	0.21	0.12~0.37
PKN1	0.48	0.32~0.70
PKCγ	0.93	0.52~1.68
PKCθ	1.15	0.60~2.12
PKCζ	1.38	0.81~2.51
PDK1	1.54	0.87~3.18

Figure 4.3 PKN is a component of the Gαq-regulated signalome to control FAK

A) Phosphorylation of FAK and PKNs in HEK293 cells transfected with empty vector, Gαq-QL or RhoA-QL active mutants. **B**) Schematic of AP-MS pipeline used to identify protein protein interactions. Doxycycline inducible FLAG-tagged RhoA was expressed in HEK293 cells with stable overexpression of Gαq. Using FLAG antibody, RhoA and its associated protein binding partners were extracted and identified using mass spectrometry. **C**) Spectral counts of RhoA binding to Rhotekin as a positive control, PKN2 and PKN3 when expressed induced by 1μM doxycycline treatment for 42hrs. **D**) Phosphorylation of FAK and PKNs HEK293 cells in response to expression of Gαq-QL alone or in combination with RhoA blockade using 2μg/mL C3 toxin for 16hrs (left). Phosphorylation of FAK and PKNs in response to RhoA blockade using 2μg/mL C3 toxin for 16hrs in UM cells (right). **E**) Phosphorylation of FAK in response to expression of Gαq-QL alone or in combination with siRNA mediated knockdown of PKNs in HEK293 cells. **F**) Phosphorylation of FAK in UM cells in response to siRNA mediated knockdown of PKNs. **G**) Quantification of phospho-FAK signal normalized to total FAK levels (mean ± SEM, n = 3). **H**) Phosphorylation of FAK in UM cells in response to siRNA mediated knockdown of PKNs, alone or in combination with ROCK inhibition using 10μM ROCKi (Y-27632) 1hr. **I**) Phosphorylation of FAK in UM cells in response to a panel of inhibitors, all used at 1uM for 1hr. **J**) FAK phosphorylation in response to overexpression of PKN2 in HEK293 cells.

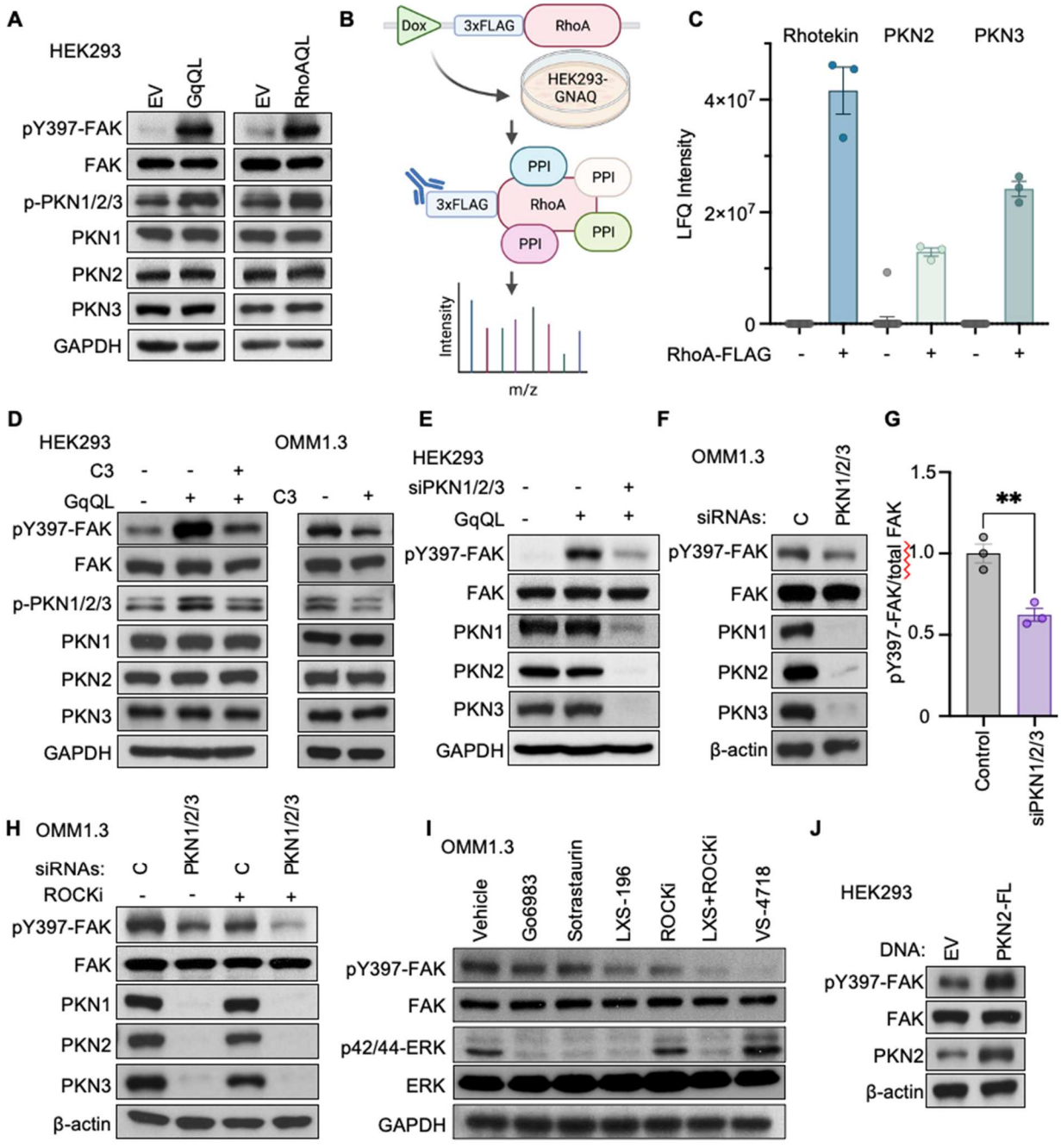
A
HEK293
EV
GqQL
EV
RhoAQL
pY397-FAK
FAK
p-PKN1/2/3
PKN1
PKN2
PKN3
GAPDH
B
Dox
3xFLAG
RhoA
HEK293-GNAQ
PPI
PPI
3xFLAG
RhoA
PPI
PPI
Intensity
m/z
C
Rhotekin
PKN2
PKN3
LFQ Intensity
4×10^7
2×10^7
0
RhoA-FLAG - + - + - +
D
HEK293
OMM1.3
C3 - - +
GqQL - + +
C3 - +
pY397-FAK
FAK
p-PKN1/2/3
PKN1
PKN2
PKN3
GAPDH
E
HEK293
siPKN1/2/3 - - +
GqQL - + +
pY397-FAK
FAK
PKN1
PKN2
PKN3
GAPDH
F
OMM1.3
siRNAs: C PKN1/2/3
pY397-FAK
FAK
PKN1
PKN2
PKN3
β-actin
G
pY397-FAK/total FAK
1.5
1.0
0.5
0
**
Control
siPKN1/2/3
H
OMM1.3
siRNAs: C PKN1/2/3 C PKN1/2/3
ROCKi - - + +
pY397-FAK
FAK
PKN1
PKN2
PKN3
β-actin
I
OMM1.3
Vehicle
Go6983
Sotrastaurin
LXS-196
ROCKi
LXS+ROCKi
VS-4718
pY397-FAK
FAK
p42/44-ERK
ERK
GAPDH
J
HEK293
DNA: EV PKN2-FL
pY397-FAK
FAK
PKN2
β-actin

Figure 4.4 LXS-196 primes UM cells for blockade of Gαq signaling to YAP with FAKi

A) YAP and FAK phosphorylation in response to 1μM VS-4718 or 1μM LXS-196 over a time course. **B**) YAP/TAZ luciferase reporter assay after 1μM VS-4718 or 1μM LXS-196 treatment for 2 or 24hrs in UM cells (mean ± SEM, n = 3). **C**) Monitoring of endogenous YAP subcellular localization by immunofluorescent staining (green), and DAPI staining for nuclear DNA (blue) in UM cells after 1μM VS-4817 or 1μM LXS-196 treatment for 24hrs, vehicle treatment was used as a control. **D**) Quantification of (C) showing fraction of cells with nuclear YAP localization in grey, and cytoplasmic fraction in color (vehicle as black, VS-4718 as gold, LXS-196 as blue) (mean ± SEM, n = 3). mRNA expression of YAP target genes (CTGF, CYR61, AMOTL2) in response to 1μM VS-4718, 1μM LXS-196, and 1μM Go6983. **F**) Schematic depicting the non-canonical signaling pathway regulating FAK activation by Gαq. Signaling downstream of RhoA is co-regulated by ROCK and PKN, converging on FAK activity.

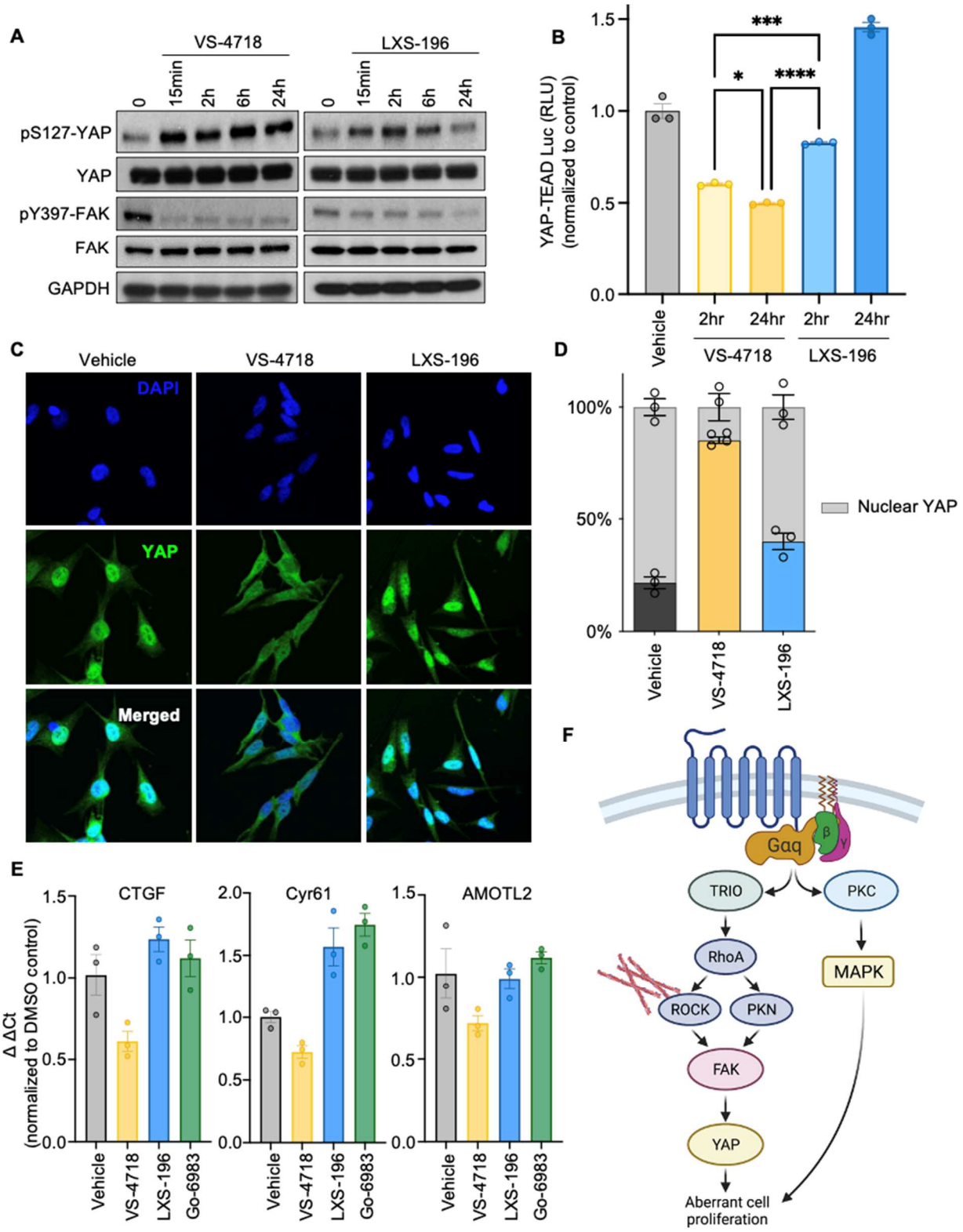
A
VS-4718
LXS-196
0
15min
2h
6h
24h
pS127-YAP
YAP
pY397-FAK
FAK
GAPDH
B
YAP-TEAD Luc (RLU)
(normalized to control)
***
*
****
Vehicle
2hr
24hr
VS-4718
LXS-196
C
Vehicle
VS-4718
LXS-196
DAPI
YAP
Merged
D
100%
50%
0%
Nuclear YAP
E
CTGF
Cyr61
AMOTL2
Δ ΔCt
(normalized to DMSO control)
Vehicle
VS-4718
LXS-196
Go-6983
F
Gαq
β
γ
TRIO
PKC
RhoA
MAPK
ROCK
PKN
FAK
YAP
Aberrant cell
proliferation

Figure 4.5 High throughput combinatorial screening reveal that co-targeting FAK and PKC/PKN is synergistic in UM *in vitro*

A) Assessment of synergy in UM cells treated with a combination of VS-4718 and LXS-196. Cell viability was measured using CellTiter Glo assay 48hrs after treatment (left). Combination index (CI) determined using ΔBliss method (CI <1 synergism, CI=1 additivity, CI>1 antagonism (middle). Apoptosis measured by CaspaseGlo assay, 18hrs after treatment (right). **B**) Distribution of CI in a diverse panel of UM and mUM cells with distinct BAP1 status. CI was determined using HSA method, (CI >10 synergism, 0<CI<10 additivity, CI<0 antagonism). **C**) CI in a panel of UM cells combining LXS-196 or Go6983 to various FAKi in OMM1.3, OMM1.5 and Mel202 cells. CI of PKCi combined with BRAFi (dabrafenib, vemurafenib) used as a comparison. **D**) Apoptosis of UM cells measured by CaspaseGlo assay, in response to vehicle, 1μM VS-4718, 1μM LXS-196, or 1μM VS-4718+1μM LXS-196 for 24hrs. **E**) Immunoblot showing cleaved-PARP, pFAK and pERK in response to treatment with 1μM VS-4718, 1μM LXS-196, or 1μM VS-4718+1μM LXS-196 for 24hrs in UM cells.

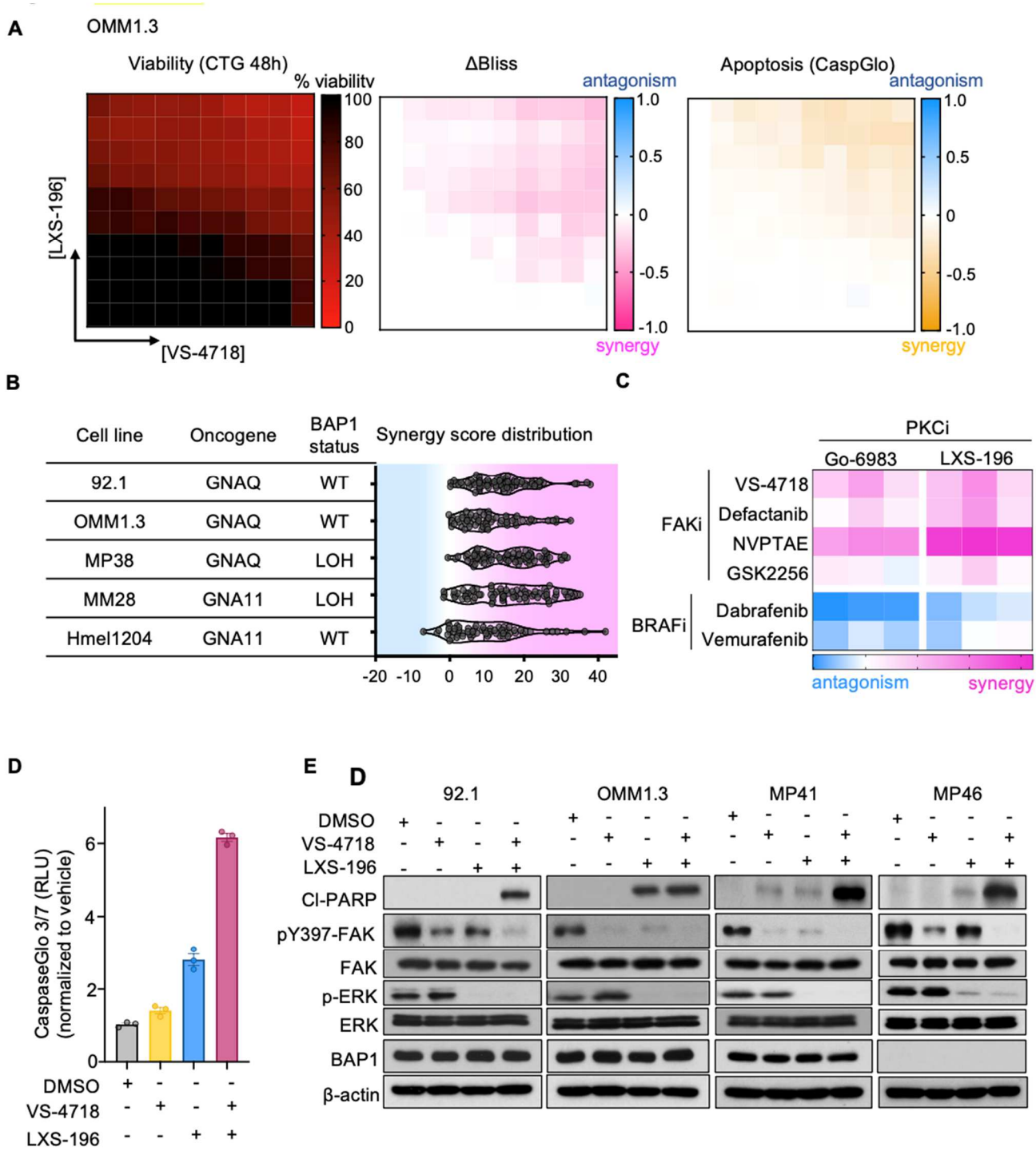
A
OMM1.3
Viability (CTG 48h)
% viability
100
80
60
40
20
0
[LXS-196]
[VS-4718]
ΔBliss
antagonism
1.0
0.5
0
-0.5
-1.0
synergy
Apoptosis (CaspGlo)
antagonism
1.0
0.5
0
-0.5
-1.0
synergy
B
Cell line
Oncogene
BAP1 status
Synergy score distribution
92.1 GNAQ WT
OMM1.3 GNAQ WT
MP38 GNAQ LOH
MM28 GNA11 LOH
Hmel1204 GNA11 WT
-20 -10 0 10 20 30 40
C
PKCi
Go-6983
LXS-196
FAKi
VS-4718
Defactanib
NVPTAE
GSK2256
BRAFi
Dabrafenib
Vemurafenib
antagonism
synergy
D
CaspaseGlo 3/7 (RLU)
(normalized to vehicle)
6
4
2
0
DMSO + - - -
VS-4718 - + - +
LXS-196 - - + +
E
D
92.1
OMM1.3
MP41
MP46
DMSO
VS-4718
LXS-196
Cl-PARP
pY397-FAK
FAK
p-ERK
ERK
BAP1
β-actin

Figure 4.6 Combination of VS-4718 and LXS-196 is synergistic in UM *in vivo* xenograft and metastatic models

A) UM tumor xenograft volume in SCID/NOD mice treated with vehicle (control), VS-4718 50mg/kg BID PO, LXS-196 50mg/kg BID PO, or VS-4718+LXS-196. Data are mean ± SEM (>5 mice/group). ***, $P < 0.001$; n.s., not significant. **B,** H&E staining of representative xenograft tumor sections from (A) after 25 days of treatment. **C**) Violin plot depicting changes in body weight of mice between day 0 and day 25 with respect to the indicated treatment groups from (A). **D**) Representative IHC staining tumor sections for Ki67, pERK, YAP, and cleaved caspase-3 (cl-Casp3). Scale bar is 100 μm. **E**) Quantification of IHC-stained tumor sections in (D). Control is in grey, VS-4718 is in gold, LXS-196 is in blue, and VS-4718+LXS-196 combination is in magenta. **F**) Schematic of UM metastatic model. Splenic injection of 92.1 GFP-luc cells is followed by a short period of hematogenous dissemination, splenectomy, and subsequent monitoring of hepatic metastasis. **G**) Hepatic tumor burden measured by IVIS imaging after injection of 92.1 GFP luc UM cells in SCID/NOD mice. Mice were treated with vehicle (control) VS-4718 50mg/kg BID PO, LXS-196 50mg/kg BID PO, or VS-4718+LXS-196. Data are mean ± SEM (>5 mice/group). ***, $P < 0.001$. **H**) IVIS imaging of representative mice from (G).

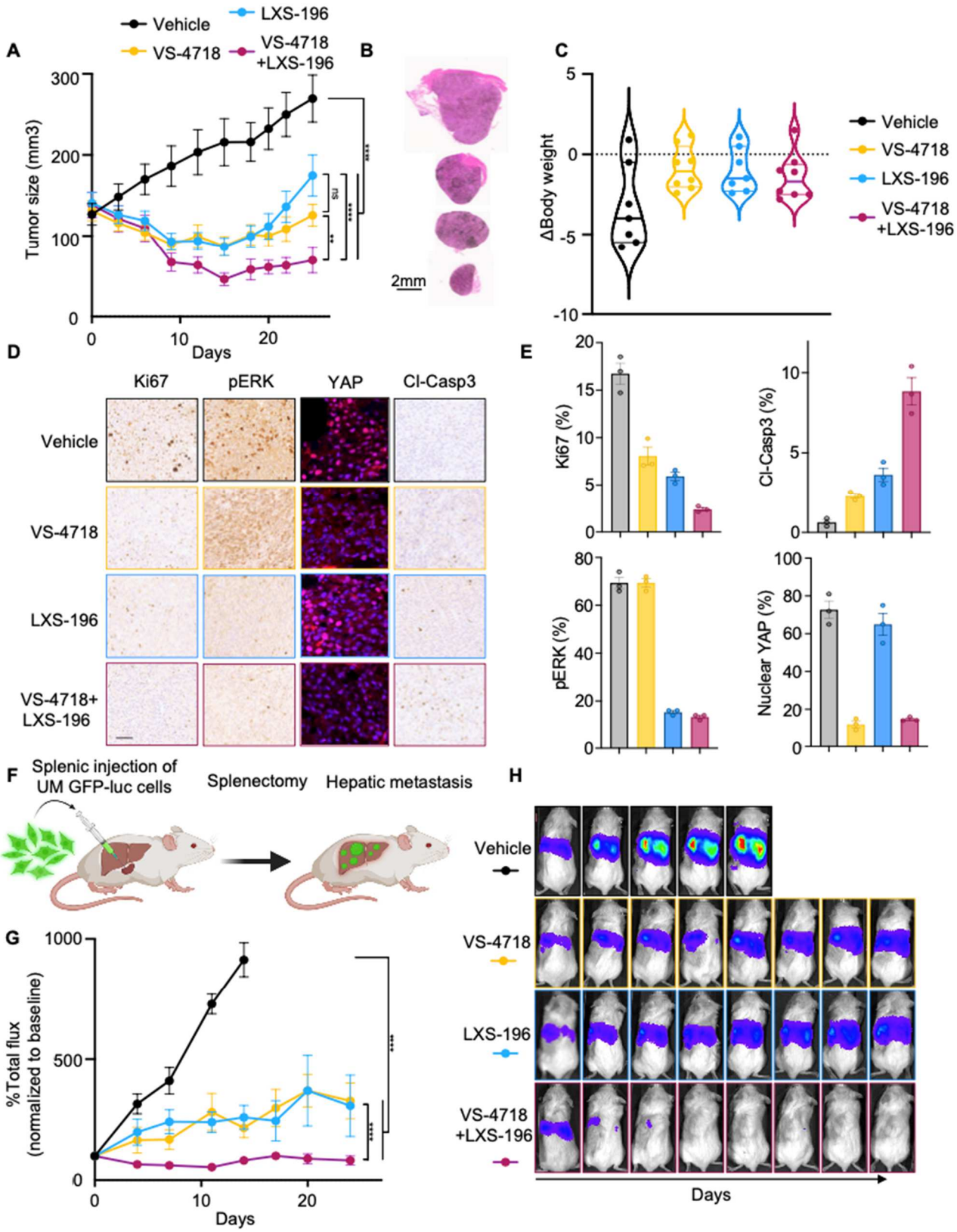
A
Vehicle
VS-4718
LXS-196
VS-4718 +LXS-196
Tumor size (mm3)
Days
B
2mm
C
ΔBody weight
D
Ki67
pERK
YAP
Cl-Casp3
Vehicle
VS-4718
LXS-196
VS-4718+ LXS-196
E
Ki67 (%)
Cl-Casp3 (%)
pERK (%)
Nuclear YAP (%)
F
Splenic injection of UM GFP-luc cells
Splenectomy
Hepatic metastasis
G
%Total flux (normalized to baseline)
Days
H
Vehicle
VS-4718
LXS-196
VS-4718 +LXS-196
Days

A

Drug set	Enriched Subtype	Size	Enrich Score (ES)	Normalized ES (NES)	NOM p-val	FDR q-val	FWER p-val
TUBB	UVM	37	-0.7393	-2.33548	0	0	0
BRD2-4	UVM	17	-0.88968	-2.29194	0	0	0
HDAC1	UVM	18	-0.75078	-2.02309	0	0.000466	0.002
BRD4	UVM	13	-0.87078	-2.10563	0	0.000621	0.002
PRKCs	UVM	8	-0.90261	-1.92185	0	0.001818	0.009
HDAC6	UVM	10	-0.79031	-1.78519	0	0.016091	0.096
CDK1	UVM	13	-0.71079	-1.73603	0.002028	0.023504	0.203
BRD2	UVM	4	-0.95931	-1.73674	0	0.0262	0.201
MCL1	UVM	4	-0.95411	-1.69547	0	0.036792	0.324
XPO1	UVM	5	-0.90122	-1.67745	0.001923	0.043458	0.388
CHEK1	UVM	13	-0.6936	-1.65213	0.010965	0.057668	0.504
EP300	UVM	6	-0.81932	-1.61649	0.003953	0.081759	0.666
CDK4	UVM	11	-0.68555	-1.61076	0.026374	0.081844	0.691

B

Drug set	Enriched Subtype	Size	Enrich Score (ES)	Normalized ES (NES)	NOM p-val	FDR q-val	FWER p-val
BRAF	SKCM	18	0.893223	2.239835	0	0	0
HSP90AB1	SKCM	18	0.832443	2.142556	0	0	0
MAP2K1	SKCM	16	0.864533	2.071136	0	0	0
GSK3B	SKCM	10	0.852684	1.855847	0	0.015604	0.059
MAPK3	SKCM	6	0.887301	1.723525	0.003984	0.068169	0.33
LCK	SKCM	4	0.936616	1.727005	0.006186	0.076648	0.313
NAMPT	SKCM	4	0.978784	1.688923	0	0.097679	0.489
PIK3CB	SKCM	13	0.70094	1.611222	0.026616	0.180722	0.863
PIK3CA	SKCM	43	0.538217	1.603144	0.010204	0.183028	0.885
AURKB	SKCM	7	0.805964	1.621923	0.015564	0.190283	0.811
ADRB2	SKCM	3	0.980832	1.629087	0.001957	0.194295	0.78
CDC7	SKCM	4	0.904913	1.612	0.010288	0.196192	0.857

Figure S4.1

Drug set enrichment (DSEA) scores and significance values for drug sets enriched in UM (**A)** and SKCM (**B**) subtypes.

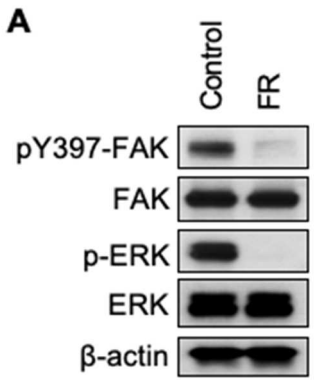

Figure S4.2

Changes in phosphorylation of FAK and ERK in UM cells in response to 500nM FR900359 treatment for 2hrs.

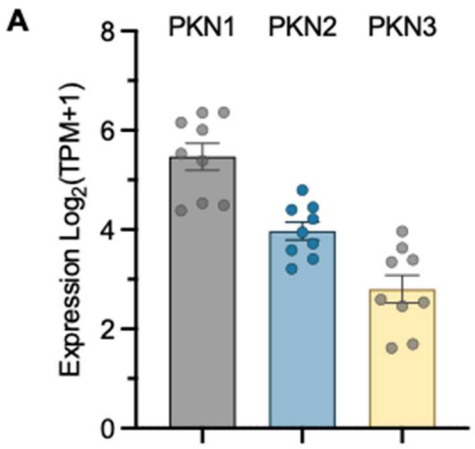

Figure S4.3

mRNA expression of PKN isoforms in UM cells from Depmap portal.

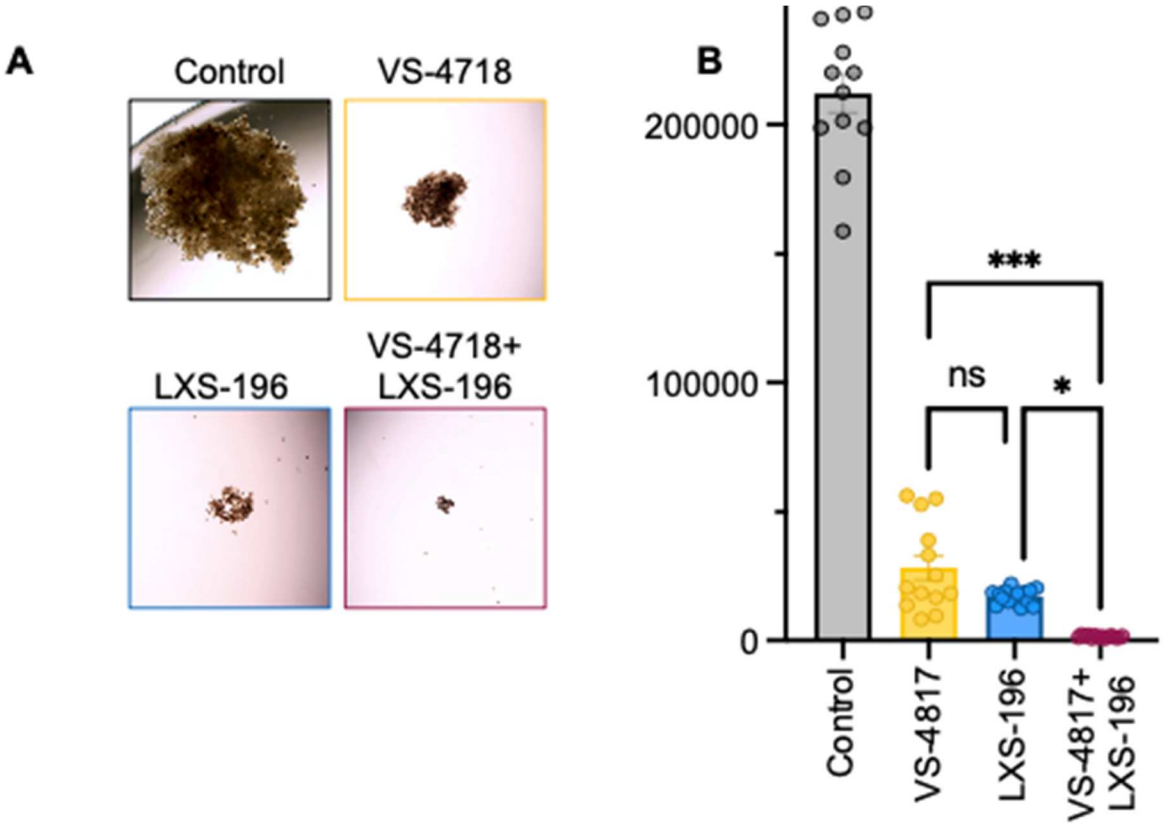

Figure S4.4

Inhibition of UM proliferation in 3D growth conditions in response to 1μM VS-4718, 1μM LXS-196, or 1μM VS-4718+1μM LXS-196 for 24hrs in 92.1 UM cells for 20 days. Representative images in (**A**) and quantification of sphere area in (**B**).

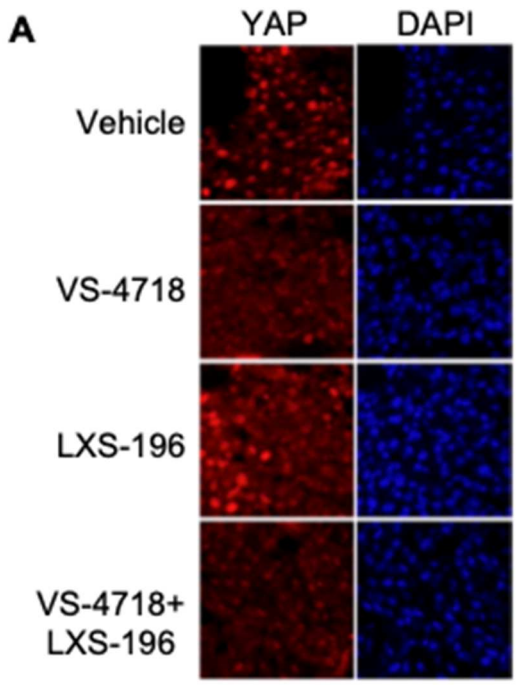

Figure S4.5

A) Single channel YAP and DAPI (nuclear) staining of 92.1 xenograft tumors treated with VS-4718, LXS-196 or VS-4718+LXS-196 combination, corresponding to Fig. 4.6D

4.4 Materials and Methods:

Cell Lines, Culture Procedures and Chemicals: HEK293, A375, WM266 and SKMEL28 cells were cultured in DMEM (D6429, Sigma-Aldrich Inc.) containing 10% FBS (F2442, Sigma-Aldrich Inc.), 1X antibiotic/antimycotic solution (A5955, Sigma-Aldrich Inc.), and 1X Plasmocin prophylactic (ant-mpp, InvivoGen). Uveal melanoma cells (92.1, OMM1.3, OMM1.5, and Mel202) and mouse melanoma cells (Hmel1204) were cultured in RPMI-1640 (R8758, Sigma Aldrich Inc.) containing 10% FBS (F2442, Sigma-Aldrich Inc.), 1X antibiotic/antimycotic solution (A5955, Sigma-Aldrich Inc.), and 1X Plasmocin prophylactic (ant-mpp, InvivoGen). MP46, MP38, MM28, and MP41 were cultured in RPMI-1640 (R8758, Sigma Aldrich Inc.) containing 20% FBS (F2442, Sigma-Aldrich Inc.), 1X antibiotic/antimycotic solution (A5955, Sigma-Aldrich Inc.), and 1X Plasmocin prophylactic (ant-mpp, InvivoGen). All cell lines were routinely tested free of mycoplasma contamination. VS-4718 (S7653), LXS-196 (S6723), Go6983 (S2911), Sotrastaurin (S2791) and ROCKi (Y-27632) (S6390) were purchased from SelleckChem. C3 toxin (CT04-A) was purchased from Cytoskeleton Inc.

Plasmids and Transfections: Plasmids pCEFL-EV, pCEFL-GαqQL, pCEFL-RhoA-QL, and pCEFL-PKN2-FL were described previously [42]. For overexpression experiments, HEK293 cells were transfected with Turbofect (R0531, Thermofisher Scientific, CA) according to manufacturer instructions. All knockdown experiments were performed using siRNAs purchased from Horizon Discovery Biosciences (Non-targeting Control: D-001810-10-05, PRKCD: L-003524-00-0005, PRKCE: L-004653-00-0005, PKN1: L-004175-00-0005, PKN2: L-004612-00-0005, PKN3: L-004647-00-0005), and Lipofectamine RNAiMAX Reagent (13778150, Thermofisher Scientific, CA) according to manufacturer's instructions.

Drug screening and drug combination studies: High throughput single agent and combinatorial drug screen was performed as described previously[48]. Cells were seeded at a density of 5×10^3 to 1×10^4 cells/well in 96-well white plates. Eight different dilutions of each inhibitor were assayed in technical triplicates for 72 hours in each experiment. Cell viability was measured with the AquaBluer Cell Viability Reagent on a Spark microplate reader (Tecan). Using the GraphPad Prism v8.2.0 software, the half-maximal inhibitor concentration values (GI_{50}) were determined from the curve using the nonlinear log (inhibitor) versus response–variable slope (three parameters) equation. GI_{50} values were only determined for compounds that inhibited growth by more than 50%.

Protein interaction studies: Affinity purification and downstream mass spectroscopic analysis was performed as previously described[49].

Kinome profiling: The principal method utilized for kinome profiling is a radioactive filter binding assay using 33P ATP, described previously[50,51].

Melanosphere assay: Cells were seeded in 96-well ultra-low attachment plate (#CLS3474, Corning, Tewksbury, MA) at 50 cells/well with sphere medium consisted of DMEM/F12 Glutamax (#10565042, Thermo Fisher Scientific), 20 ng/mL basic fibroblast growth factor (#13256029, Thermo Fisher Scientific), 20 ng/mL epithelial growth factor (#PHG0313, Thermo Fisher Scientific), B-27 (#17504044, Thermo Fisher Scientific), and N2 Supplement (#17502-048, Thermo Fisher Scientific). Drug was added the day after cells were seeded. After 20 days, images were acquired, and size of spheres were quantified using ImageJ.

Immunoblotting and Immunoprecipitations: Cells were serum starved overnight, and then treated according to the conditions in the figure legend. For cell lysis, cells were washed 2X in

cold PBS and lysed in 1XCell Lysis buffer (Cell Signaling Technologies, 9803) supplemented with HaltTM Protease and Phosphatase Inhibitor Cocktail (#78440, ThermoFisher Scientific) and 1mM Sodium Orthovanadate (P0758S, New England Biolabs). Lysates were centrifuged at max speed at 4°C, concentrations were measured using DC Protein Assay (BioRad Laboratories, 5000111) and lysates were prepared with addition of 4x Laemmli Sample Buffer (#1610747, BioRad Laboratories), and boiled for 5min at 98°C.

For immunoblotting, cell lysates were subjected to SDS/PAGE on 10% acrylamide gels and electroblotted to PVDF membranes. Blocking and primary and secondary antibody incubations of immunoblots were performed in Tris-buffered saline + 0.1% Tween 20 supplemented with 5% (w/v) BSA or 5% w/v skim milk. The following primary antibodies were all purchased from Cell Signaling Technologies and used at 1:1000. FAK (71433), pY397-FAK (8556), ERK1/2 (9102), pT202/Y204-ERK1/2 (4370), GAPDH (5174), PKN2 (2612), PKCε (2683), PKCδ (9616), MEK1/2 (9126), pS217/221 MEK1/2 (9154), Cl-PARP (5625), YAP (14074), pS127 YAP (13008), BAP1 (13271), Beta-actin (4970), and Vinculin (13901). PKN1 (MA5-19703) was purchased from ThermoFisher Scientific. pPKN (ab187660) was purchased from Abcam. PKN3 (NBP1-30102) was purchased from Novus Biologicals. HRP-conjugated goat anti-rabbit and anti-mouse IgGs (Southern Biotech, AL) were used at a dilution of 1:30,000, and immunoreactive bands were detected using Immobilon Western Chemiluminescent HRP substrate (Millipore, MA) according to the manufacturer's instructions.

Human xenograft tumor models: All animal studies were approved by the Institutional Animal Care and Use Committee of University of California, San Diego (San Diego, CA) with protocol S15195. Female 4- to 6-week-old NOD.Cg-Prkdcscid Il2rgtm1Wjl/SzJ (SCID-NOD) mice were purchased from the UCSD in-house breeding program. Mice were injected subcutaneously in

both flanks with 1 × 10^6 or 2.5 × 10^6 92.1 cells. Mice were monitored twice weekly for tumor development. Tumor growth analysis was assessed as $LW^2/2$, where *L* and *W* represent length and width of the tumor. VS-4718 and LXS-196 were prepared in 0.5% CMC (Sigma-Aldrich) and 0.1% Tween 80 (Sigma-Aldrich) in sterile water. Mice were administered 50 mg/kg VS-4718 (Verastem Oncology) and 50 mg/kg LXS-196 twice daily by oral gavage; control group was treated with vehicle. Mice were euthanized at the indicated time points and tumors were isolated for sequencing, histologic, and IHC evaluation. Results of mice experiments were expressed as mean ± SEM of a total of tumors analyzed.

Splenic injection

Mice were injected with 1 × 10^6 92.1 GFP-Luc cells in the spleen, followed by removal of the spleen at 2 minutes postinjection. Tumor implantation by bioluminescence was assessed twice weekly by bioluminescence images captured using the In Vivo Imaging System (IVIS) Spectrum (PerkinElmer). To this end, mice received an intraperitoneal injection of 200 mg/kg D-luciferin firefly potassium salt diluted in PBS 15 minutes before imaging (GoldBio). Total bioluminescence was determined upon subtracting the background from the region of interest. Vehicle, VS-4718, LXS-196, or VS-4718/LXS-196 were administered, starting 10 days postsurgery, with the abovementioned dosing.

Immunohistochemistry and Immunofluoresence: For IHC and IF, all tissue samples were processed and stained as described previously[52]. Slides were scanned using a Zeiss Axioscan Z1 slide scanner equipped with a 20×/0.8 NA objective.

4.6 Acknowledgements

Chapter 4 in full, is currently being prepared for submission for publication of the material in “High throughput chemogenetic drug screening reveals kinase-driven therapeutic vulnerabilities in *GNAQ*-mutant uveal melanoma”. Arang, Nadia; Ceribelli, Michele; Rigiracciolo, Damiano Cosimo; Lubrano, Simone; Saddawi-Konefka, Robert; Wang, Zhiyong; Kim, Daewhan; Molinolo, Alfredo; Coma, Silvia; Pachter, Jon; Yang, Jing; Swaney, Danielle L; Krogan, Nevan J; Alessi, Dario; Thomas, Craig; Gutkind, J Silvio. The dissertation author was the primary investigator and author of this paper.

4.6 References

1. Druker, B. J., Tamura, S., Buchdunger, E., Ohno, S., Segal, G. M., Fanning, S., Zimmermann, J., and Lydon, N. B. (1996) Effects of a selective inhibitor of the Abl tyrosine kinase on the growth of Bcr-Abl positive cells. *Nat Med* **2**, 561-566
2. Baselga, J., Tripathy, D., Mendelsohn, J., Baughman, S., Benz, C. C., Dantis, L., Sklarin, N. T., Seidman, A. D., Hudis, C. A., Moore, J., Rosen, P. P., Twaddell, T., Henderson, I. C., and Norton, L. (1999) Phase II study of weekly intravenous trastuzumab (Herceptin) in patients with HER2/neu-overexpressing metastatic breast cancer. *Semin Oncol* **26**, 78-83
3. Robertson, A. G., Shih, J., Yau, C., Gibb, E. A., Oba, J., Mungall, K. L., Hess, J. M., Uzunangelov, V., Walter, V., Danilova, L., Lichtenberg, T. M., Kucherlapati, M., Kimes, P. K., Tang, M., Penson, A., Babur, O., Akbani, R., Bristow, C. A., Hoadley, K. A., Iype, L., Chang, M. T., Network, T. R., Cherniack, A. D., Benz, C., Mills, G. B., Verhaak, R. G. W., Griewank, K. G., Felau, I., Zenklusen, J. C., Gershenwald, J. E., Schoenfield, L., Lazar, A. J., Abdel-Rahman, M. H., Roman-Roman, S., Stern, M. H., Cebulla, C. M., Williams, M. D., Jager, M. J., Coupland, S. E., Esmaeli, B., Kandoth, C., and Woodman, S. E. (2017) Integrative Analysis Identifies Four Molecular and Clinical Subsets in Uveal Melanoma. *Cancer Cell* **32**, 204-220 e215
4. Van Raamsdonk, C. D., Griewank, K. G., Crosby, M. B., Garrido, M. C., Vemula, S., Wiesner, T., Obenauf, A. C., Wackernagel, W., Green, G., Bouvier, N., Sozen, M. M., Baimukanova, G., Roy, R., Heguy, A., Dolgalev, I., Khanin, R., Busam, K., Speicher, M. R., O'Brien, J., and Bastian, B. C. (2010) Mutations in GNA11 in uveal melanoma. *The New England journal of medicine* **363**, 2191-2199
5. Van Raamsdonk, C. D., Bezrookove, V., Green, G., Bauer, J., Gaugler, L., O’Brien, J. M., Simpson, E. M., Barsh, G. S., and Bastian, B. C. (2009) Frequent somatic mutations of GNAQ in uveal melanoma and blue nevi. *Nature* **457**, 599-602

6. Moore, A. R., Ceraudo, E., Sher, J. J., Guan, Y., Shoushtari, A. N., Chang, M. T., Zhang, J. Q., Walczak, E. G., Kazmi, M. A., Taylor, B. S., Huber, T., Chi, P., Sakmar, T. P., and Chen, Y. (2016) Recurrent activating mutations of G-protein-coupled receptor CYSLTR2 in uveal melanoma. *Nat Genet* **48**, 675-680
7. Harbour, J. W., Onken, M. D., Roberson, E. D., Duan, S., Cao, L., Worley, L. A., Council, M. L., Matatall, K. A., Helms, C., and Bowcock, A. M. (2010) Frequent mutation of BAP1 in metastasizing uveal melanomas. *Science* **330**, 1410-1413
8. Rantala, E. S., Hernberg, M., and Kivela, T. T. (2019) Overall survival after treatment for metastatic uveal melanoma: a systematic review and meta-analysis. *Melanoma Res* **29**, 561-568
9. Khoja, L., Atenafu, E. G., Suciu, S., Leyvraz, S., Sato, T., Marshall, E., Keilholz, U., Zimmer, L., Patel, S. P., Piperno-Neumann, S., Piulats, J., Kivela, T. T., Pfoehler, C., Bhatia, S., Huppert, P., Van Iersel, L. B. J., De Vries, I. J. M., Penel, N., Vogl, T., Cheng, T., Fiorentini, G., Mouriaux, F., Tarhini, A., Patel, P. M., Carvajal, R., and Joshua, A. M. (2019) Meta-analysis in metastatic uveal melanoma to determine progression free and overall survival benchmarks: an international rare cancers initiative (IRCI) ocular melanoma study. *Ann Oncol* **30**, 1370-1380
10. Carvajal, R. D., Schwartz, G. K., Tezel, T., Marr, B., Francis, J. H., and Nathan, P. D. (2017) Metastatic disease from uveal melanoma: treatment options and future prospects. *Br J Ophthalmol* **101**, 38-44
11. Arang, N., and Gutkind, J. S. (2020) G Protein-Coupled receptors and heterotrimeric G proteins as cancer drivers. *FEBS Lett* **594**, 4201-4232
12. Van Raamsdonk, C. D., Bezrookove, V., Green, G., Bauer, J., Gaugler, L., O'Brien, J. M., Simpson, E. M., Barsh, G. S., and Bastian, B. C. (2009) Frequent somatic mutations of GNAQ in uveal melanoma and blue naevi. *Nature* **457**, 599-602
13. Gutkind, J. S., Novotny, E. A., Brann, M. R., and Robbins, K. C. (1991) Muscarinic acetylcholine receptor subtypes as agonist-dependent oncogenes. *Proc Natl Acad Sci U S A* **88**, 4703-4707
14. Kalinec, G., Nazarali, A. J., Hermouet, S., Xu, N., and Gutkind, J. S. (1992) Mutated alpha subunit of the Gq protein induces malignant transformation in NIH 3T3 cells. *Mol Cell Biol* **12**, 4687-4693
15. Chen, X., Wu, Q., Depeille, P., Chen, P., Thornton, S., Kalirai, H., Coupland, S. E., Roose, J. P., and Bastian, B. C. (2017) RasGRP3 Mediates MAPK Pathway Activation in GNAQ Mutant Uveal Melanoma. *Cancer Cell* **31**, 685-696 e686
16. Griner, E. M., and Kazanietz, M. G. (2007) Protein kinase C and other diacylglycerol effectors in cancer. *Nat Rev Cancer* **7**, 281-294
17. Newton, A. C. (2010) Protein kinase C: poised to signal. *Am J Physiol Endocrinol Metab* **298**, E395-402
18. Julius, D., and Nathans, J. (2012) Signaling by sensory receptors. *Cold Spring Harbor perspectives in biology* **4**, a005991
19. Prevarskaya, N., Skryma, R., and Shuba, Y. (2011) Calcium in tumour metastasis: new roles for known actors. *Nat Rev Cancer* **11**, 609-618
20. Howe, A. K. (2011) Cross-talk between calcium and protein kinase A in the regulation of cell migration. *Curr Opin Cell Biol* **23**, 554-561
21. Falchook, G. S., Lewis, K. D., Infante, J. R., Gordon, M. S., Vogelzang, N. J., DeMarini, D. J., Sun, P., Moy, C., Szabo, S. A., Roadcap, L. T., Peddareddigari, V. G., Lebowitz, P. F., Le, N. T., Burris, H. A., 3rd, Messersmith, W. A., O'Dwyer, P. J., Kim, K. B., Flaherty, K., Bendell, J. C., Gonzalez, R., Kurzrock, R., and Fecher, L. A. (2012) Activity of the oral MEK inhibitor trametinib in patients with advanced melanoma: a phase 1 dose-escalation trial. *Lancet Oncol* **13**, 782-789

22. Carvajal, R. D., Sosman, J. A., Quevedo, J. F., Milhem, M. M., Joshua, A. M., Kudchadkar, R. R., Linette, G. P., Gajewski, T. F., Lutzky, J., Lawson, D. H., Lao, C. D., Flynn, P. J., Albertini, M. R., Sato, T., Lewis, K., Doyle, A., Ancell, K., Panageas, K. S., Bluth, M., Hedvat, C., Erinjeri, J., Ambrosini, G., Marr, B., Abramson, D. H., Dickson, M. A., Wolchok, J. D., Chapman, P. B., and Schwartz, G. K. (2014) Effect of selumetinib vs chemotherapy on progression-free survival in uveal melanoma: a randomized clinical trial. *Jama* **311**, 2397-2405
23. Carvajal, R. D., Piperno-Neumann, S., Kapiteijn, E., Chapman, P. B., Frank, S., Joshua, A. M., Piulats, J. M., Wolter, P., Cocquyt, V., Chmielowski, B., Evans, T. R. J., Gastaud, L., Linette, G., Berking, C., Schachter, J., Rodrigues, M. J., Shoushtari, A. N., Clemett, D., Ghiorghiu, D., Mariani, G., Spratt, S., Lovick, S., Barker, P., Kilgour, E., Lai, Z., Schwartz, G. K., and Nathan, P. (2018) Selumetinib in Combination With Dacarbazine in Patients With Metastatic Uveal Melanoma: A Phase III, Multicenter, Randomized Trial (SUMIT). *J Clin Oncol* **36**, 1232-1239
24. Liu, A. W., Wei, A. Z., Maniar, A. B., and Carvajal, R. D. (2022) Tebentafusp in advanced uveal melanoma: proof of principle for the efficacy of T-cell receptor therapeutics and bispecifics in solid tumors. *Expert Opin Biol Ther*, 1-8
25. Middleton, M. R., McAlpine, C., Woodcock, V. K., Corrie, P., Infante, J. R., Steven, N. M., Evans, T. R. J., Anthoney, A., Shoushtari, A. N., Hamid, O., Gupta, A., Vardeu, A., Leach, E., Naidoo, R., Stanhope, S., Lewis, S., Hurst, J., O'Kelly, I., and Sznol, M. (2020) Tebentafusp, A TCR/Anti-CD3 Bispecific Fusion Protein Targeting gp100, Potently Activated Antitumor Immune Responses in Patients with Metastatic Melanoma. *Clin Cancer Res* **26**, 5869-5878
26. Nathan, P., Hassel, J. C., Rutkowski, P., Baurain, J. F., Butler, M. O., Schlaak, M., Sullivan, R. J., Ochsenreither, S., Dummer, R., Kirkwood, J. M., Joshua, A. M., Sacco, J. J., Shoushtari, A. N., Orloff, M., Piulats, J. M., Milhem, M., Salama, A. K. S., Curti, B., Demidov, L., Gastaud, L., Mauch, C., Yushak, M., Carvajal, R. D., Hamid, O., Abdullah, S. E., Holland, C., Goodall, H., Piperno-Neumann, S., and Investigators, I. M.-. (2021) Overall Survival Benefit with Tebentafusp in Metastatic Uveal Melanoma. *The New England journal of medicine* **385**, 1196-1206
27. Annala, S., Feng, X., Shridhar, N., Eryilmaz, F., Patt, J., Yang, J., Pfeil, E. M., Cervantes-Villagrana, R. D., Inoue, A., Haberlein, F., Slodczyk, T., Reher, R., Kehraus, S., Monteleone, S., Schrage, R., Heycke, N., Rick, U., Engel, S., Pfeifer, A., Kolb, P., Konig, G., Bunemann, M., Tuting, T., Vazquez-Prado, J., Gutkind, J. S., Gaffal, E., and Kostenis, E. (2019) Direct targeting of Galphaq and Galpha11 oncoproteins in cancer cells. *Science signaling* **12**
28. Schrage, R., Schmitz, A. L., Gaffal, E., Annala, S., Kehraus, S., Wenzel, D., Bullesbach, K. M., Bald, T., Inoue, A., Shinjo, Y., Galandrin, S., Shridhar, N., Hesse, M., Grundmann, M., Merten, N., Charpentier, T. H., Martz, M., Butcher, A. J., Slodczyk, T., Armando, S., Effern, M., Namkung, Y., Jenkins, L., Horn, V., Stossel, A., Dargatz, H., Tietze, D., Imhof, D., Gales, C., Drewke, C., Muller, C. E., Holzel, M., Milligan, G., Tobin, A. B., Gomeza, J., Dohlman, H. G., Sondek, J., Harden, T. K., Bouvier, M., Laporte, S. A., Aoki, J., Fleischmann, B. K., Mohr, K., Konig, G. M., Tuting, T., and Kostenis, E. (2015) The experimental power of FR900359 to study Gq-regulated biological processes. *Nat Commun* **6**, 10156
29. Lin, G. L., Wilson, K. M., Ceribelli, M., Stanton, B. Z., Woo, P. J., Kreimer, S., Qin, E. Y., Zhang, X., Lennon, J., Nagaraja, S., Morris, P. J., Quezada, M., Gillespie, S. M., Duveau, D. Y., Michalowski, A. M., Shinn, P., Guha, R., Ferrer, M., Klumpp-Thomas, C., Michael, S., McKnight, C., Minhas, P., Itkin, Z., Raabe, E. H., Chen, L., Ghanem, R., Geraghty, A. C., Ni, L., Andreasson, K. I., Vitanza, N. A., Warren, K. E., Thomas, C. J., and Monje, M.

(2019) Therapeutic strategies for diffuse midline glioma from high-throughput combination drug screening. *Science translational medicine* **11**

30. Rozengurt, E. (2007) Mitogenic signaling pathways induced by G protein-coupled receptors. *J Cell Physiol* **213**, 589-602
31. Hubbard, K. B., and Hepler, J. R. (2006) Cell signalling diversity of the Gqalpha family of heterotrimeric G proteins. *Cell Signal* **18**, 135-150
32. Ellen Kapiteijn, M. C., Valentina Boni, Delphine Loirat, Frank Speetjens, John Park, Emiliano Calvo, Richard Carvajal, Marta Nyakas, Juan Gonzalez-Maffe, Xu Zhu, Ramu Thiruvamoor, Padmaja Yerramilli-Rao Sophie Piperno-Neumann. (2019) Abstract CT068: A Phase I trial of LXS196, a novel PKC inhibitor for metastatic uveal melanoma. *Cancer Research* **79**
33. Piperno-Neumann, S., Larkin, J., Carvajal, R. D., Luke, J. J., Schwartz, G. K., Hodi, F. S., Sablin, M. P., Shoushtari, A. N., Szpakowski, S., Chowdhury, N. R., Brannon, A. R., Ramkumar, T., de Koning, L., Derti, A., Emery, C., Yerramilli-Rao, P., and Kapiteijn, E. (2020) Genomic Profiling of Metastatic Uveal Melanoma and Clinical Results of a Phase I Study of the Protein Kinase C Inhibitor AEB071. *Mol Cancer Ther* **19**, 1031-1039
34. Vaque, J. P., Dorsam, R. T., Feng, X., Iglesias-Bartolome, R., Forsthoefel, D. J., Chen, Q., Debant, A., Seeger, M. A., Ksander, B. R., Teramoto, H., and Gutkind, J. S. (2013) A genome-wide RNAi screen reveals a Trio-regulated Rho GTPase circuitry transducing mitogenic signals initiated by G protein-coupled receptors. *Molecular cell* **49**, 94-108
35. Feng, X., Degese, M. S., Iglesias-Bartolome, R., Vaque, J. P., Molinolo, A. A., Rodrigues, M., Zaidi, M. R., Ksander, B. R., Merlino, G., Sodhi, A., Chen, Q., and Gutkind, J. S. (2014) Hippo-independent activation of YAP by the GNAQ uveal melanoma oncogene through a trio-regulated rho GTPase signaling circuitry. *Cancer Cell* **25**, 831-845
36. Feng, X., Arang, N., Rigiracciolo, D. C., Lee, J. S., Yeerna, H., Wang, Z., Lubrano, S., Kishore, A., Pachter, J. A., Konig, G. M., Maggiolini, M., Kostenis, E., Schlaepfer, D. D., Tamayo, P., Chen, Q., Ruppin, E., and Gutkind, J. S. (2019) A Platform of Synthetic Lethal Gene Interaction Networks Reveals that the GNAQ Uveal Melanoma Oncogene Controls the Hippo Pathway through FAK. *Cancer Cell* **35**, 457-472 e455
37. Mukai, H. (2003) The structure and function of PKN, a protein kinase having a catalytic domain homologous to that of PKC. *J Biochem* **133**, 17-27
38. Vincent, S., and Settleman, J. (1997) The PRK2 kinase is a potential effector target of both Rho and Rac GTPases and regulates actin cytoskeletal organization. *Mol Cell Biol* **17**, 2247-2256
39. Flynn, P., Mellor, H., Palmer, R., Panayotou, G., and Parker, P. J. (1998) Multiple interactions of PRK1 with RhoA. Functional assignment of the Hr1 repeat motif. *J Biol Chem* **273**, 2698-2705
40. Maesaki, R., Ihara, K., Shimizu, T., Kuroda, S., Kaibuchi, K., and Hakoshima, T. (1999) The structural basis of Rho effector recognition revealed by the crystal structure of human RhoA complexed with the effector domain of PKN/PRK1. *Molecular cell* **4**, 793-803
41. Marinissen, M. J., Chiariello, M., and Gutkind, J. S. (2001) Regulation of gene expression by the small GTPase Rho through the ERK6 (p38 gamma) MAP kinase pathway. *Genes Dev* **15**, 535-553
42. Quetier, I., Marshall, J. J. T., Spencer-Dene, B., Lachmann, S., Casamassima, A., Franco, C., Escuin, S., Worrall, J. T., Baskaran, P., Rajeeve, V., Howell, M., Copp, A. J., Stamp, G., Rosewell, I., Cutillas, P., Gerhardt, H., Parker, P. J., and Cameron, A. J. M. (2016) Knockout of the PKN Family of Rho Effector Kinases Reveals a Non-redundant Role for PKN2 in Developmental Mesoderm Expansion. *Cell reports* **14**, 440-448
43. Reid, T., Furuyashiki, T., Ishizaki, T., Watanabe, G., Watanabe, N., Fujisawa, K., Morii, N., Madaule, P., and Narumiya, S. (1996) Rhotekin, a new putative target for Rho bearing

homology to a serine/threonine kinase, PKN, and rhophilin in the rho-binding domain. *J Biol Chem* **271**, 13556-13560
44. Avruch, J., Zhou, D., Fitamant, J., Bardeesy, N., Mou, F., and Barrufet, L. R. (2012) Protein kinases of the Hippo pathway: regulation and substrates. *Semin Cell Dev Biol* **23**, 770-784
45. Meng, Z., Moroishi, T., and Guan, K. L. (2016) Mechanisms of Hippo pathway regulation. *Genes Dev* **30**, 1-17
46. Paradis, J. S., Acosta, M., Saddawi-Konefka, R., Kishore, A., Gomes, F., Arang, N., Tiago, M., Coma, S., Lubrano, S., Wu, X., Ford, K., Day, C. P., Merlino, G., Mali, P., Pachter, J. A., Sato, T., Aplin, A. E., and Gutkind, J. S. (2021) Synthetic Lethal Screens Reveal Cotargeting FAK and MEK as a Multimodal Precision Therapy for GNAQ-Driven Uveal Melanoma. *Clin Cancer Res* **27**, 3190-3200
47. Yu, F. X., Luo, J., Mo, J. S., Liu, G., Kim, Y. C., Meng, Z., Zhao, L., Peyman, G., Ouyang, H., Jiang, W., Zhao, J., Chen, X., Zhang, L., Wang, C. Y., Bastian, B. C., Zhang, K., and Guan, K. L. (2014) Mutant Gq/11 promote uveal melanoma tumorigenesis by activating YAP. *Cancer Cell* **25**, 822-830
48. Berginski, M. E., Moret, N., Liu, C., Goldfarb, D., Sorger, P. K., and Gomez, S. M. (2021) The Dark Kinase Knowledgebase: an online compendium of knowledge and experimental results of understudied kinases. *Nucleic Acids Res* **49**, D529-D535
49. Ma, J., Weng, L., Bastian, B. C., and Chen, X. (2021) Functional characterization of uveal melanoma oncogenes. *Oncogene* **40**, 806-820
50. Collazos, A., Michael, N., Whelan, R. D., Kelly, G., Mellor, H., Pang, L. C., Totty, N., and Parker, P. J. (2011) Site recognition and substrate screens for PKN family proteins. *Biochem J* **438**, 535-543
51. Kapiteijn, E., Carlino, M., Boni, V., Loirat, D., Speetjens, F., Park, J., Calvo, E., Carvajal, R., Nyakas, M., Gonzalez-Maffe, J., Zhu, X., Thiruvamoor, R., Yerramilli-Rao, P., and Piperno-Neumann, S. (2019) Abstract CT068: A Phase I trial of LXS196, a novel PKC inhibitor for metastatic uveal melanoma. *Cancer Research* **79**, CT068-CT068
52. Park, J. J., Stewart, A., Irvine, M., Pedersen, B., Ming, Z., Carlino, M. S., Diefenbach, R. J., and Rizos, H. (2022) Protein kinase inhibitor responses in uveal melanoma reflects a diminished dependency on PKC-MAPK signaling. *Cancer Gene Ther*
53. Rino S. Seedor, M. O., Gutkind, A. J. S., Aplin, A. A. E., Terai, A. M., Sharpe-Mills, A. E., Klose, A. H., Mastrangelo, A. M. J., and Sato, A. T. (2021) Clinical trial in progress: Phase II trial of defactinib (VS-6063) combined with VS-6766 (CH5126766) in patients with metastatic uveal melanoma. *Journal of Clinical Oncology* **39**, TPS9588-TPS9588
54. Metz, K. S., Deoudes, E. M., Berginski, M. E., Jimenez-Ruiz, I., Aksoy, B. A., Hammerbacher, J., Gomez, S. M., and Phanstiel, D. H. (2018) Coral: Clear and Customizable Visualization of Human Kinome Data. *Cell systems* **7**, 347-350 e341
55. Mathews Griner, L. A., Guha, R., Shinn, P., Young, R. M., Keller, J. M., Liu, D., Goldlust, I. S., Yasgar, A., McKnight, C., Boxer, M. B., Duveau, D. Y., Jiang, J. K., Michael, S., Mierzwa, T., Huang, W., Walsh, M. J., Mott, B. T., Patel, P., Leister, W., Maloney, D. J., Leclair, C. A., Rai, G., Jadhav, A., Peyser, B. D., Austin, C. P., Martin, S. E., Simeonov, A., Ferrer, M., Staudt, L. M., and Thomas, C. J. (2014) High-throughput combinatorial screening identifies drugs that cooperate with ibrutinib to kill activated B-cell-like diffuse large B-cell lymphoma cells. *Proc Natl Acad Sci U S A* **111**, 2349-2354
56. Kim, M., Park, J., Bouhaddou, M., Kim, K., Rojc, A., Modak, M., Soucheray, M., McGregor, M. J., O'Leary, P., Wolf, D., Stevenson, E., Foo, T. K., Mitchell, D., Herrington, K. A., Munoz, D. P., Tutuncuoglu, B., Chen, K. H., Zheng, F., Kreisberg, J. F., Diolaiti, M. E., Gordan, J. D., Coppe, J. P., Swaney, D. L., Xia, B., van 't Veer, L., Ashworth, A., Ideker, T., and Krogan, N. J. (2021) A protein interaction landscape of breast cancer. *Science* **374**, eabf3066

57. Hastie, C. J., McLauchlan, H. J., and Cohen, P. (2006) Assay of protein kinases using radiolabeled ATP: a protocol. *Nat Protoc* **1**, 968-971
58. Bain, J., Plater, L., Elliott, M., Shpiro, N., Hastie, C. J., McLauchlan, H., Klevernic, I., Arthur, J. S., Alessi, D. R., and Cohen, P. (2007) The selectivity of protein kinase inhibitors: a further update. *Biochem J* **408**, 297-315
59. Madera, D., Vitale-Cross, L., Martin, D., Schneider, A., Molinolo, A. A., Gangane, N., Carey, T. E., McHugh, J. B., Komarck, C. M., Walline, H. M., William, W. N., Jr., Seethala, R. R., Ferris, R. L., and Gutkind, J. S. (2015) Prevention of tumor growth driven by PIK3CA and HPV oncogenes by targeting mTOR signaling with metformin in oral squamous carcinomas expressing OCT3. *Cancer Prev Res (Phila)* **8**, 197-207

CHAPTER 5: Future Directions and Perspectives

5.1 GPCRs in cancer

GPCRs and their coupled heterotrimeric G proteins are central to a diverse array of cellular processes, including the activation of numerous signaling and transcriptional networks. Since the original discovery that G protein-mediated signaling has the potential to induce cell transformation, dysfunctional G protein-mediated signaling has been increasingly tied to cancer initiation and progression. Both mutation and aberrant expression are molecular mechanisms that contribute to subverting the normal function of GPCRs and heterotrimeric G proteins to conferring pro-oncogenic capabilities on them. However, given that GPCR signaling is centrally embedded in normal physiology, cancer cells can also modulate the function of GPCRs to promote an immune suppressive and a pro-oncogenic state through dysregulated paracrine and autocrine (endocrine) or even compensatory signaling mechanisms.

While hyperactive GPCR and heterotrimeric G protein-driven signaling has often been found to be pro-oncogenic, a growing body of literature is supporting a paradigm of the cell context-specific nature of such signaling pathways. LOF mutations or copy number loss of genes GPCRs and heterotrimeric G proteins have unveiled the tumor-suppressive roles that these protein families play in certain cancer types, highlighting the complexity of G protein-driven signaling and the significant impact of cellular states in the integration and output of these signaling events. Further insight into the relationship between cell type lineage and the functional duality of GPCR signaling outcomes will likely reveal unanticipated mechanisms driving cancer, and potentially novel vulnerabilities that can be targeted therapeutically. Moreover, while GPCRs and their coupled heterotrimeric G proteins have been primarily studied from a signaling perspective, their central role in diverse cellular functions strongly suggests their involvement in broader processes such as the regulation of epigenetic networks. Future work defining these nodes of connectivity will likely expand our understanding of GPCRs in cancer even further.

Within the complex network of cancer signaling, numerous opportunities arise for GPCRs to be used for therapeutic intervention. Interfering with GPCR activity using both pharmacological inhibitors and biologics, encompassing antagonists, inverse agonists, allosteric modulators, in addition to antibody-based therapies, can inform novel therapeutic strategies. Specifically, positive and negative allosteric modulators will likely emerge as pharmacological avenues for cancer prevention and treatment, as they may dial up or down the signaling capacity of GPCRs that are aberrantly modulated in cancer rather than directly stimulating or inhibiting them, or competing for their natural ligands. Guided towards the development of precision therapeutic approaches, more comprehensive characterization of dysregulated GPCR expression and signaling coupled with the diverse modes of action of these inhibitors will likely reveal context-specific dependencies that can provide opportunities to rationally target GPCRs for cancer therapies.

Recent studies investigating the range and depth of biased GPCR signaling, and the potential impact of GPCR mutations in G protein-coupling selectivity, will likely also enable the development of novel approaches exploiting the tremendous potential of GPCRs as signal transducers to modulate signaling in cancer and other diseases. Moreover, advances and emerging techniques in the field of gene editing may also add to the repertoire of mechanisms by which we can modulate GPCR activity.

Given the large proportion of FDA-approved drugs that target GPCRs, there is mounting evidence supporting the utility of repurposing existing drugs to block or modulate GPCR-mediated oncogenic signaling circuitries, either alone or as adjuvant therapies. Regarding the latter, drug resistance has remained a major challenge in the era of precision medicine. GPCR modulators administered along with conventional anticancer agents may allow abrogating the initiation of compensatory signaling mechanisms and resultant drug resistance. Similarly, the dynamic influx of immune cells to the tumor, which leads to a highly infiltrative ‘hot’ tumor or a poorly infiltrative ‘cold’ tumor, is in part dependent on the chemokine gene signature of the tumor itself, which may

provide a powerful prognostic tool to predict therapeutic response rates in the clinic. Harnessing the immunomodulatory power of GPCRs or their ability to regulate tumor-immune interactions could revolutionize current immunotherapies and result in durable clinical responses while preventing tumor relapse. Investigation exploring combining GPCR-targeted therapies with existing chemo- and immunotherapies either for the treatment of cancer, or as cancer preventative strategies are currently ongoing. Ultimately, just as we gain a clearer understanding of the complex mechanisms underlying cancer initiation and progression, so too will the role of GPCRs as cancer drivers and therapeutic targets become more important.

5.2 Targeting oncogenic Gαq-driven signaling circuitries for the treatment of uveal melanoma

Taken together, the discoveries made in this thesis have illuminated our understanding of the molecular mechanisms underlying the ability of Gαq and Gαq-coupled receptors to drive aberrant cell growth in Gαq-regulated pathophysiologies, including uveal melanoma (UM) (Fig 5.1). Importantly, in cases such as UM, where precision targeting of the driver oncogene is unfeasible, either due to lack of clinically available compounds, or due to unmanageable toxicities, a comprehensive understanding of the most critical signaling nodes at which to target signal transduction-based therapies will be the key to revolutionizing the standard of care.

Within this framework, oncogenic drivers are part of highly complex and interconnected signaling pathways and identification of synthetic lethal interactions embedded within these networks can provide the molecular basis upon which to design targeted combination therapies. Towards this end, the work compiled in this thesis demonstrate how the remarkable convergence of bioinformatic, genetic, and biochemical data can highlight systems vulnerabilities in a given cancer type and how that can lead to breakthrough discoveries for cancers with unmet therapeutic needs. Our discovery that FAK is a central mediator of non-canonical Gαq-regulated signaling,

and that it represents a viable therapeutic target for UM, has opened new doors for strategies to treat UM. Aligned with this, based in-part on this body of work, multiple clinical trials have been initiated investigating the efficacy of targeting FAK alone, or as part of combination therapies in UM patients [NCT04720417, NCT04109456], representing a true “bench-to-bedside” story.

Indeed, these ongoing studies represent one of the few precision medicine-based targeted therapies in the field of UM. Given that UM clinical trials in the past decades have been largely unsuccessful, this is a major advance in the field as a new clinical strategy for the treatment and management of UM and metastatic UM (mUM). We are hopeful regarding the significant and positive impact that the usage of FAK co-targeting therapies may have for UM patients. In particular, strategies co-targeting canonical (MEK or PKC) and non-canonical (FAK) Gαq-regulated signaling mechanisms are highly promising due to the specific blockade of core survival signaling mechanisms underlying UM growth, and ability to abrogate compensatory mechanisms of resistance.

Despite this, there still remain critical therapeutic gaps for UM and mUM patients, who will greatly benefit from novel strategies to improve clinical outcomes. Identification of additional agents whose activity may further synergize with FAK/MEK or FAK/PKC combinatorial therapies, or alone, through independent mechanisms of action have the potential to significantly shape the future of UM therapies. In this regard, the additional enriched drug targets discovered in AIM 3, warrant further investigation into the mechanism of how they participate in the GNAQ-regulated signalome, and how they may fit into the framework of targeted therapies in UM. These are the focus of our ongoing efforts in this aspect. Going forward, we hope to continue taking advantage of cutting-edge systems biology and bioinformatic approaches, through a lens of signal transduction to further detangle G-protein regulated signaling networks and precision therapeutic approaches against UM and other cancers.

5.2 Figures

Figure 5.1 Summary of findings

Schematic depicting the major findings of the thesis in elucidating the oncogenic Gαq-regulated signaling circuitries. Novel discoveries are in labeled in color, and previously described signaling axes are in labeled in grey. Discoveries in the present thesis have uncovered novel components of Gαq-driven signaling, including a RhoA-mediated axis that bifurcates into ROCK and PKN-regulated signaling mechanisms that converge on the control of FAK. FAK was discovered as a therapeutically targetable central mediator of the non-canonical Gαq signaling axis. FAK regulates YAP through two distinct mechanisms that promote YAP activity. FAK also controls PI3K/AKT signaling, thereby promoting two core survival signaling mechanisms in uveal melanoma (UM). Importantly, several aspects of the signaling mechanisms uncovered in this thesis shed light on targetable signaling hubs for the treatment of UM patients. Specifically, lateral inhibition of Gαq-regulated signaling mechanisms represents a promising signal-transduction based precision therapy against UM. The multi-target kinase activity of LXS-196 prime it to act on specific Gαq-regulated growth promoting signaling networks and in combination with FAKi, target essential survival mechanisms in UM.

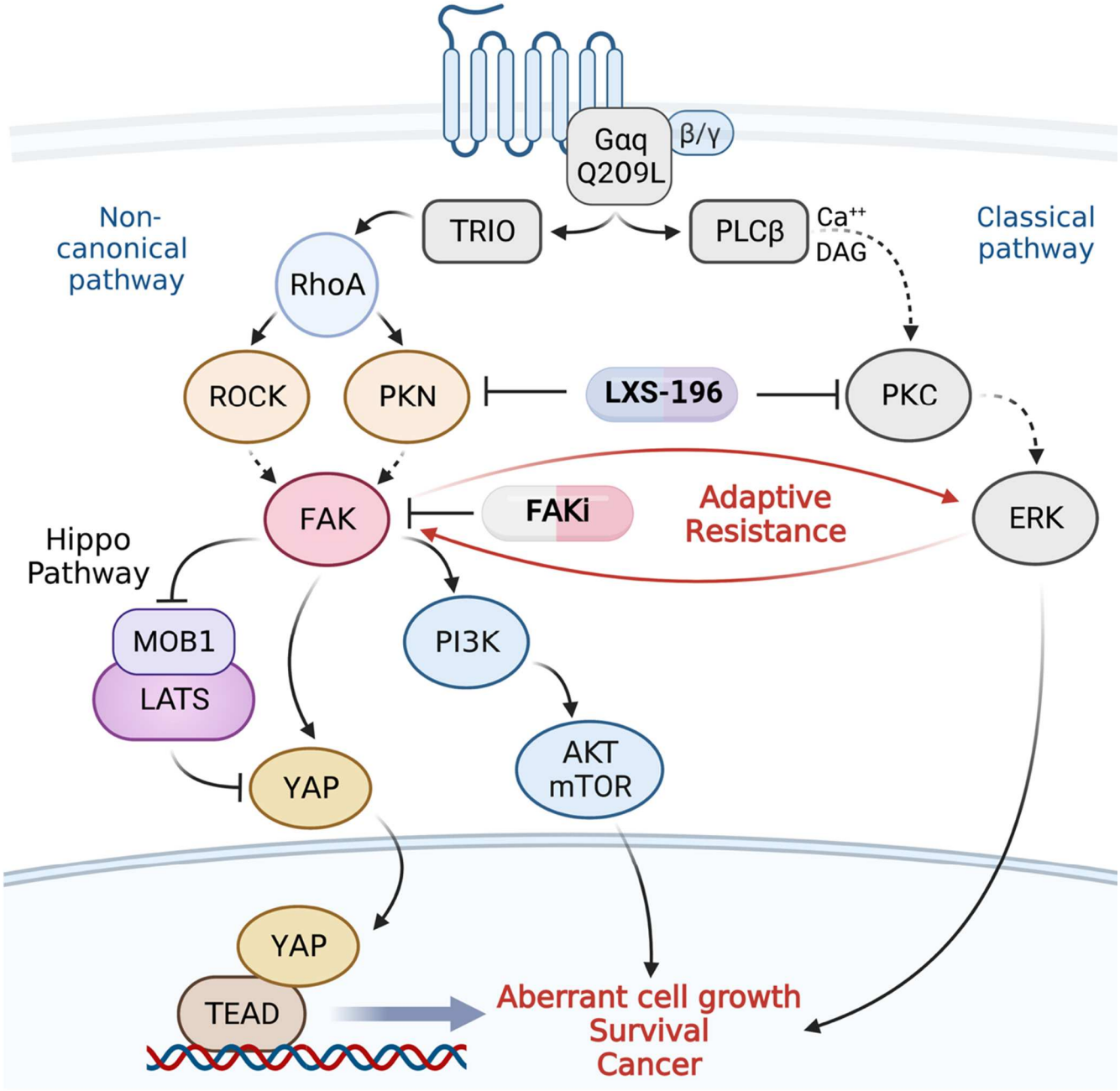
Gαq
Q209L
β/γ
Non-
canonical
pathway
TRIO
PLCβ
Ca++
DAG
Classical
pathway
RhoA
ROCK
PKN
LXS-196
PKC
FAK
FAKi
Adaptive
Resistance
ERK
Hippo
Pathway
MOB1
LATS
PI3K
AKT
mTOR
YAP
YAP
TEAD
Aberrant cell growth
Survival
Cancer

5.3 Acknowledgements

Chapter 5, in part, has been accepted for publication of the material in “G Protein-Coupled receptors and heterotrimeric G proteins as cancer drivers”, in *FEBS Letters*, 2020. Arang, Nadia; Gutkind, J Silvio. The dissertation author was the primary investigator and author of this paper.